BREAKUP OF A LAMINAR CAPILLARY JET OF A NON-NEWTONIAN FLUID

by

MICHAEL GOLDIN

A dissertation submitted to the
Graduate Faculty in Engineering in partial
fulfillment of the requirement for the
degree of Doctor of Philosophy,
The City University of New York.

1970

This manuscript has been read and accepted for the Graduate Faculty in Engineering in satisfaction of the dissertation requirement for the degree of Doctor of Philosophy.

May 18 1970
date

Reuel Shinnar
Chairman of Examining Committee

18 May 1970
date

Executive Officer

Reuel Shinnar (Chairman)

Robert Pfeffer

Stanley Katz

Raymond Parnes

Supervisory Committee

The City University of New York

To my wife for her encouragement and

boundless patience

ACKNOWLEDGEMENTS

I would like to express my appreciation to Professor Reuel Shinnar, who directed this research, for his continual guidance and for his many contributions.

I am appreciative of the encouragment received from Professor Aloix X. Schmidt, Chairman of the Chemical Engineering Department, and for his confidence which enabled me to teach in the Chemical Engineering Department during the course of my Graduate studies.

I gratefully acknowledge the valuable discussions held with Professors Robert Pfeffer, the co-mentor in this research, and Stanley Katz.

I would like to thank my colleague Joseph Yerushalmi for permission to present his stability analysis of viscoelastic jet breakup for comparison with the experimental results presented here. I would also like to acknowledge the helpful suggestions of my fellow graduate student Marvin Gordon.

The shop personnel under John Bodnaruk aided considerably in the construction of the experimental equipment and their assistance is appreciated.

This research has been supported by the National Aeronautics and Space Administration under Grant No. NGR-33-013-009 and also by the National Science Foundation under Grant No. GK 11374. During the fall term of 1966, I received financial support from the City College Graduate Assistance Fund. This support is gratefully acknowledged.

TABLE OF CONTENTS

TABLE OF CONTENTS (continued)

TABLE OF CONTENTS (concluded)

LIST OF FIGURES

LIST OF FIGURES (continued)

LIST OF FIGURES (continued)

LIST OF FIGURES (continued)

LIST OF FIGURES(continued)

LIST OF FIGURES (concluded)

LIST OF TABLES

NOMENCLATURE

The major notation used in this thesis are listed below. Those symbols which have only a temporary significance are not shown but are clearly defined in the text.

a ..... Radius of jet

a_o ..... Radius of nozzle

a_∞ ..... Radius of relaxed jet

C_r ..... Coefficient of complex viscosity defined in equation (6.10)

D ..... Linear operator defined in equation (6.16)

Deb ..... Deborah number= $\lambda V/a$

D_g ..... Geometric mean droplet diameter defined in equation (6.36)

D_i ..... Droplet diameter

D_L ..... Length mean droplet diameter

D_s ..... Sauter mean diameter defined by equation (6.33)

D_w ..... Weight mean droplet diameter defined by equation (6.34)

E ..... Elastic modulus

g_c ..... Gravitational constant

h ..... Damping coefficient

H ..... Height of rotor

H_o ..... End correction on rotor

I_n ..... Bessel function of imaginary arguement and order n

J_n ..... Bessel function of order n

k ..... Wave number = $2\pi/\delta$

k_o ..... Wave number for a Newtonian jet

K ..... Power law parameter defined in equation (1.14) or Ellis model parameter defined in equation (1.16)

K' ..... Power law parameter for capillary tube flow defined by equation (1.15)

K_n ..... Modified Bessel function of order n

ℓ ..... Capillary tube length

L ..... Breakup length of a capillary jet

M ..... Torque applied to rotor

n ..... Power law exponent defined in equation (1.14) or Ellis model exponent defined in equation (1.16)

p ..... Pressure

q ..... slope of (d ln shear rate)/(d ln shear stress)

Q ..... Volumetric flow rate

r ..... Radial coordinate in cylindrical coordinate system

r_y ..... Critical radius for flow of fluid with a yield stress

R_b ..... Radius of bob

R_c ..... Radius of cup

Re_o ..... Reynolds number based on capillary diameter $=2a_oV_o/\upsilon$ for a Newtonian liquid

Re_∞ ..... Reynolds number based on relaxed jet diameter $=2a_\infty V_\infty/\upsilon$ for a Newtonian liquid

Re_o' ..... Generalized non-Newtonian Reynolds number for power law fluids defined by equation (6.32)

s ..... Ratio of bob radius to cup radius

S ..... Surface tension parameter defined by equation (5.22)

t ..... Time

V_i ..... Component of velocity

V_o ..... Average velocity of fluid in capillary

V_∞ ..... Average velocity of relaxed jet

W ..... Weight applied to rotor in Stormer viscometer

We_o ..... Weber number based on capillary diameter $=2a_o V_o^2 \rho / \sigma$

We_∞ ..... Weber number based on relaxed jet diameter $=2a_\infty V_\infty^2 \rho / \sigma$

x_i ..... Space coordinate

Y_n ..... Modified Bessel function of order n

z ..... Axial coordinate in cylindrical coordinate system

Greek symbols

α ..... Growth rate of disturbance wave or transform variable

α_o ..... Growth rate of disturbance wave in a Newtonian jet

γ ..... Deformation or strain

$\dot{\gamma}$ ..... Constant deformation rate

δ ..... Wavelength of disturbance wave

Δ ..... Rate of deformation

ϵ ..... Perturbation parameter

η ..... Apparent viscosity

η_o ..... Zero shear viscosity

η_∞ ..... Infinite shear viscosity

λ_1 ..... Relaxation time

μ_1 ..... Retardation time

NOMENCLATURE (concluded)

ν ..... Kinematic viscosity

ξ ..... Displacement of the free surface from the unperturbed radius of the jet

ρ ..... Fluid density

σ ..... Coefficient of surface tension

τ ..... Dynamic stress on fluid

ϕ_n ..... Relaxation function defined in equation (1.20)

ϕ_r ..... Relaxation function defined in equation (6.7)

χ ..... Diameter ratio=a_∞ / a_o

ψ ..... Stream function

ω ..... Angular velocity

Ω ..... Angular velocity of rotor

Other symbols

$\mathcal{D}/\mathcal{D}t$ ..... Convected derivative operator such as the Oldroyd or Jaumann derivative- equation (1.18)

$\partial/\partial t$ ..... Partial derivative

$\tilde{(\,)}$ ..... Denotes a perturbation quantity

$\hat{(\,)}$ ..... Denotes a Laplace transform

$\mathcal{F}_{t=-\infty}^{t=0}$ ..... Functional

ABSTRACT

The behavior of capillary jets of non-Newtonian inelastic liquids and of viscoelastic fluids was investigated experimentally. Data were obtained through high speed still photographs and motion pictures taken along the length of the liquid column. The program concentrated on profile decay measurements, which refers to the change in jet diameter with axial distance due to stress relaxation, and on jet breakup studies.

The viscoinelastic liquids all possessed yield stresses and were comprised of a wide variety of organic and inorganic materials. The less gellified fluids formed capillary jets which propagated disturbances in the same manner as for a Newtonian jet, that is, as an exponentially growing wave of constant wave length. Even the most highly gellified fluids could be readily atomized. The behavior of this class of non-Newtonian liquids could be explained if it was assumed that the time required to reform the gel structure outside the capillary was large compared to the jet breakup time. Thus, the apparent viscosity possessed at the nozzle exit is substantially maintained throughout the lifetime of the jet. Using this model, the wavelength and breakup length data for the viscoinelastic jets were in fair agreement with that predicted for a Newtonian jet of the same apparent viscosity.

The viscoelastic test liquids were composed of aqueous solutions of 'drag reducing' polymers. These formed capillary jets which differed considerably in appearance from Newtonian and non-Newtonian inelastic jets. Disturbances were propagated as a non-linear series of droplets connected by threads which thinned with distance and ultimately broke. Even in the most dilute systems studied, the initial linear wave propagation was arrested and gradually evolved into the droplet-thread configuration which characterizes these fluids. Within the linear range of wave propagation, the data for dilute solutions confirms the prediction of stability theory that a viscoelastic jet without structure is less stable than a Newtonian jet of the same zero shear viscosity.

High speed motion pictures taken along the length of viscoelastic jets show that large scale axial deformations occur continually. This shows the jet to be under tension since these strains require the existence of axial normal forces for their continuance.

CHAPTER 1

INTRODUCTION

1.1 PRELIMINARY REMARKS

The atomization of a liquid is a phenomena of considerable practical importance and examples of it may be found in such diverse fields as spray drying, fuel combustion and liquid-liquid extraction. It usually occurs under turbulent flow conditions and is one of the most difficult problems in fluid dynamics to treat analytically. Test data are correlated empirically. For this reason, the low speed breakup of a capillary jet of liquid is often studied as an aid towards understanding atomization. Newtonian jet breakup is one of the few flow geometries where linear stability theory has been able to accurately predict observed results.

Newtonian jets have been studied extensively, both experimentally and theoretically. In recent years, the use of non-Newtonian additives has substantially increased and yet there is very little published information available on the behavior of non-Newtonian jets. This research represents an introduction to this important area.

The term 'non-Newtonian liquid' encompasses fluids with a wide range of properties. Though their classification into groups of similar characteristics is somewhat arbitrary, two categories may be broadly identified- 1. those materials which, when in the melt state or in solution, are found to

exhibit both viscous and elastic properties, commonly known as viscoelastic fluids, and 2. those materials which are non-Newtonian but do not possess measureable elastic effects. These subdivisions will be used in discussing the experimental results for capillary jets of non-Newtonian liquids.

A natural question arises as to whether a viscoelastic jet is more or less stable as compared to a Newtonian jet. In other geometries, the question remains unresolved as data are available to support both conclusions. A theoretical analysis by Middleman (58) using a linearized, three constant Oldroyd model (66) shows a viscoelastic jet to have a higher growth rate of axisymmetric disturbances than a Newtonian fluid of the same zero shear viscosity. If the growth rate is assumed inversely proportional to the breakup length, an assumption which is satisfactory with Newtonian liquids, then it can be concluded that a viscoelastic jet will exhibit a shorter breakup length. Kroesser and Middleman (39) confirmed this result for capillary jets of polyisobutylene in tetralin.

1.2 AIM AND SCOPE OF THESIS

Because of the lack of published experimental data on the behavior of non-Newtonian jets, there is a need to broadly define the breakup characteristics of capillary jets produced by various classes of non-Newtonian fluids.

The research presented in this thesis has attempted to provide this comparison for several viscoelastic polymer solutions and for several non-Newtonian inelastic fluids. The particular polymeric additives chosen are known as drag reducing fluids because of their unique ability to lower turbulent pressure drop by as much as 50% in concentrations as low as 10-50 parts per million.

Two explanatory sections are included in the introduction to acquaint the reader with some of the concepts and terminology to be used in the main body of the thesis. Section 1.3 discusses the physical causes for the onset of secondary flows by disturbances and outlines the small perturbation method of analysis. The introduction continues in section 1.4 with a classification of fluid behavior and a detailed discussion of non-Newtonian properties. Section 1.5 concludes this chapter with a description of Newtonian jet breakup.

Chapter 2 surveys the state of the art in the area of Newtonian and non-Newtonian jets. The mathematical treatment of the problem to predict the breakup length is presented and the validity of each of the simplifying assumptions involved in the analysis is examined by comparison to available experimental data. Prior investigations into the hydrodynamic stability of non-Newtonian fluids in other geometries are reviewed to provide some insight into their behavior.

A complete description of the experimental apparatus and procedures used in this research is given in chapter 3. Each chapter presenting the test results also includes an abbreviated version of the techniques used.

Some pertinent physical properties and shear stress-shear rate measurements of the test fluids are presented in chapter 4. The available rheological instruments also determined yield stresses (the minimum shear stress required for flow) on the viscoinelastic liquids but could not obtain normal stresses with the viscoelastic fluids.

Chapter 5 considers the rate of relaxation of stresses in an unconfined liquid column due to the abrupt removal of the capillary wall. This phenomena occurs in the region immediately outside of the nozzle. The problem is solved for the case of a dilute viscoelastic fluid and the predictions are compared to experimental data taken with Newtonian, non-Newtonian inelastic and viscoelastic liquids.

The sixth chapter investigates the breakup of a laminar capillary jet of a non-Newtonian fluid. High speed still and motion picture photographs vividly illustrate the different characteristics of Newtonian, viscoinelastic and viscoelastic jets. A theoretical analysis due to my colleague, Dr. J. Yerushalmi (29,94) is included for comparision with experimental data.

Chapter 7 closes this work with a summary of the results and the conclusions drawn from them.

Experimental data, which cannot be obtained from the tables and figures in the main text of the thesis, are included in the appendix. The computer programs used for data reduction are straightforward and have been omitted.

1.3 THE NOTION OF HYDRODYNAMIC STABILITY

A fluid flowing in a given geometry is subject to a variety of natural disturbances arising from sources such as burrs on the walls of the container or external vibrations from the environment. No matter how carefully the flow system is isolated, there will always be disorders on a microscopic level. The question arises as to whether these small perturbations will dampen with time or will amplify in such a way as to create a new disturbed flow pattern. Such patterns are known to exist, the most familiar being the transition from laminar to turbulent flow. If the disturbance dampens with time, as in laminar flow, the system is stable; if it amplifies, the flow is unstable.

Since a given set of flow conditions defines a stable regime, while another set can produce an unstable state, some criteria must exist that provide a condition of neutral or marginal stability. The theory of hydrodynamic stability is concerned with the location of

this locus. Results are often stated in terms of a dimensionless parameter whose magnitude must be below some critical value to assure stability. Typical examples of disturbed or secondary flows are given in Table 1-1.

Table 1-1. Examples of Secondary Flows

Mode of Flow	Pattern of Instability	Critical Parameter
Natural Convection	Hexagonal Bénard Cells	Rayleigh or Marangoni Number
Cylindrical Couette Flow	Taylor Vortices	Taylor Number
Pipeline Flow	Random Eddies	Reynolds Number

The breakup of a capillary jet is always unstable and, in this instance, stability is spoken of on a relative basis between different fluids.

An elementary example will be chosen to illustrate the small perturbation technique used in analyzing the effects of an infinitesimal disturbance superimposed upon the main flow. In the usual summation notation with Cartesian coordinates, the equations of continuity and motion can be written as

$$\frac{\partial V_k}{\partial x_k} = 0 \qquad (1.1)$$

$$\frac{\partial V_i}{\partial t} + V_j \frac{\partial V_i}{\partial x_j} = -\frac{1}{\rho}\frac{\partial P}{\partial x_i} + \nu \nabla^2 V_i \qquad (1.2)$$

where ν is the kinematic viscosity and ∇ is the Laplacian. Body forces have been assumed to be negligible.

At steady state, in the absence of oscillations, the velocity and pressure are functions of position only.

$$V_i = \bar{V}_i(x_k) \; ; \; p = \bar{p}(x_k) \tag{1.3}$$

For small disturbances superimposed upon the main flow, the velocity and pressure may be expressed as

$$V_i = \bar{V}_i + \epsilon' V_i^{(1)} + \epsilon^2 V_i^{(2)} + \ldots . \tag{1.4}$$

$$P = \bar{P} + \epsilon' P^{(1)} + \epsilon^2 P^{(2)} \ldots . \tag{1.5}$$

where ϵ is a small parameter and

$$V_i = V_i(x_k, t) \; ; \; P = P(x_k, t) \tag{1.6}$$

When equations (1.4) and (1.5) are substituted in the equations of motion and continuity, a partial differential equation results which can be grouped into similar powers of ϵ . The series of equations is expressed as

$$\frac{\partial \bar{V}_i}{\partial x_i} = 0 \; ; \quad \frac{\partial \bar{V}_i}{\partial t} + \bar{V}_j \frac{\partial \bar{V}_i}{\partial x_j} = -\frac{1}{\rho} \frac{\partial \bar{P}}{\partial x_i} + \nu \nabla^2 \bar{V}_i \tag{1.7}$$

$$\frac{\partial V_i^{(1)}}{\partial x_i} = 0; \quad \frac{\partial V_i^{(1)}}{\partial t} + \bar{V}_j \frac{\partial V_i^{(1)}}{\partial x_j} + V_j^{(1)} \frac{\partial \bar{V}_i}{\partial x_j} = -\frac{1}{\rho} \frac{\partial P^{(1)}}{\partial x_i} + \nu \nabla^2 V_i^{(1)} \tag{1.8}$$

etc.

If infinitesimally small disturbances are assumed, it is usual to neglect terms of ϵ^N beyond ϵ' and also to omit product terms which are second order in the disturbance. With these simplifications, the series (1.8) reduces to

$$\frac{\partial V^{(1)}}{\partial x_i} = 0; \quad \frac{\partial V_i^{(1)}}{\partial t} + \bar{V}_j \frac{\partial V_i^{(1)}}{\partial x_j} + V_j^{(1)} \frac{\partial \bar{V}_i}{\partial x_j} = -\frac{1}{\rho} \frac{\partial P}{\partial x_i} + \nu \nabla V_i^{(1)} \tag{1.9}$$

This equation is often put into dimensionless form in order to more clearly display the controlling parameters. By choosing a form of the stream function-Ψ it may be possible to reduce the partial differential equation to an ordinary differential equation. Equation (1.9) admits solutions which are exponential in time: the dependence on the space variables- x_1, x_2 and x_3 comes from the physical knowledge of the problem. Thus the disturbance can be written as

$$\Psi(x_1, x_2, x_3, t) = \varphi(x_1, x_2, x_3)\, e^{\alpha t} \qquad (1.10)$$

The governing equations together with the boundary conditions define a characteristic value problem with α as parameter. If all the characteristic values of α have negative real parts, the disturbances will dampen with time and the flow is stable. If just one of the characteristic values is positive and real, the flow is unstable.

Extensive treatments of the linearized theory of hydrodynamic stability may be found in the monographs of Lin (42) and Chandresakar (8).

The disturbances cannot continue to grow exponentially without bound and the problem must be treated on the basis of non-linear stability theory once the disturbances are finite. Early contributions have come from Meksyn and Stuart (47), and Stuart (82). More recently, Eckhaus (18) has summarized his research in a monograph.

1.4 PROPERTIES OF NON-NEWTONIAN FLUIDS

A detailed discussion of the classification and properties of non-Newtonian fluids is presented and is intended to aid the reader who may not be familiar with this area of fluid dynamics. In examining the behavior of non-Newtonian fluids, it is useful to group together fluids of similar rheological properties as a means of achieving some sort of order. The classification given in table 1-2 was adopted from that given by Metzner (51). Examples of typical flow curves exhibited by each of the fluid categories are shown in figure 1-1.

Table 1-2. Classification of fluid behavior.

A. Purely viscous fluids-the shear rate depends only upon imposed shear stress.

$\tau = \eta \Delta$ where τ, η and Δ are the shear stress, the apparent viscosity and the rate of deformation respectively.

1. Newtonian: η = constant
2. Non-Newtonian: $\eta = \eta(I, II, III)$ or $\Delta = \Delta(\tau)$ where I, II, III are the principal invariants of the rate of deformation tensor (22). This category includes pseudoplastic and Bingham plastic fluids in which η is a decreasing function of the invariants and also embodies dilatant fluids in which η is an increasing function of the invariants.

B. Time dependent inelastic fluids-the shear rate depends upon both the imposed shear stress and the duration of the stress.

$\tau = \eta \Delta$; $\eta = \eta(I, II, III, t)$

This subdivision describes materials which are part of the groups known as thixotropic and rheopectic fluids.

C. Viscoelastic liquids-the shear rate depends upon the imposed shear stress and the extent of the deformation (strain).

$$\tau = \mathcal{F}_{t=-\infty}^{t=0} [\gamma(t)] \quad \text{or} \quad \Delta = \Delta(\tau, \gamma)$$

where γ is the strain or deformation.

D. Complex rheological fluids-these materials exhibit the complexity of categories A,B and C combined.

In Newtonian liquids, the shear stress is directly proportional to the rate of deformation, the constant of proportionality being the viscosity- η_0 .

$$\tau = \eta_0 \Delta \tag{1.11}$$

Non-Newtonian fluids are distinguished by an apparent viscosity which is a function of the flow conditions and is defined as

$$\eta = \tau/\Delta \tag{1.12}$$

The particular variables which η depends upon identify the class of non-Newtonian behavior. Many non-Newtonian fluids are found to approach Newtonian behavior at sufficiently low shear rates and this limiting viscosity is termed its viscosity at zero shear or, more simply, its zero shear viscosity- η_0 . Similarly, at very high shear rates, Newtonian behavior may also be displayed and the viscosity corresponding to this region is known as the viscosity at infinite shear rate or the infinite shear viscosity- η_∞ .

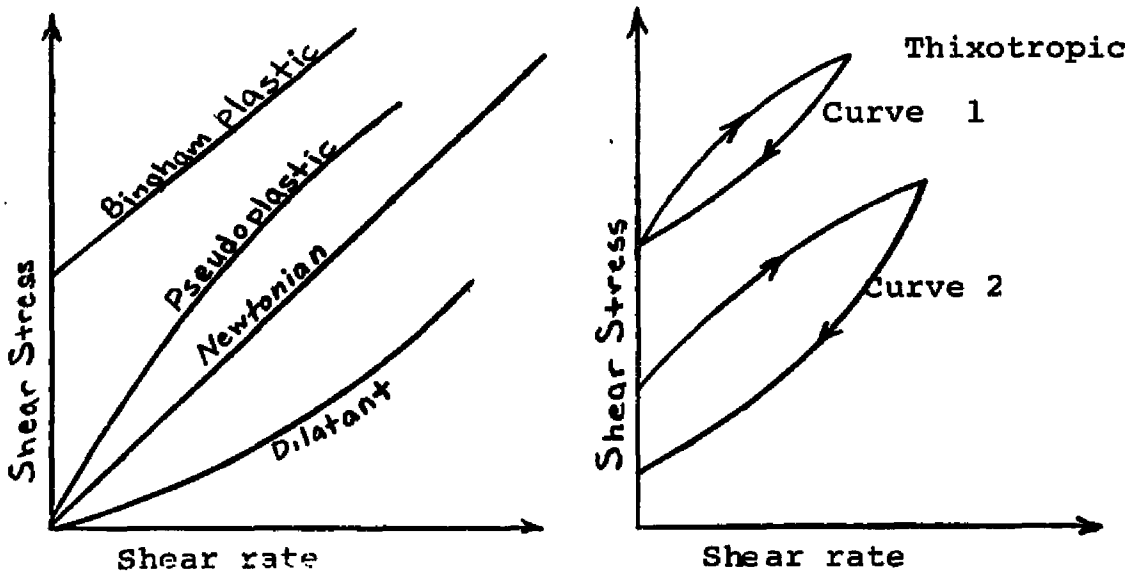

Figure 1-1. Fluid flow curves (arithmetic coordinates)

Pseudoplastic fluids exhibit a decreasing slope as the shear rate is increased which is synonymous with a decreasing apparent viscosity while dilatant liquids show the opposite effect. Bingham plastics do not flow until the yield stress is exceeded and then display the linear relation between shear stress and shear rate that is common to Newtonian liquids. Viscometer measurements on a thixotropic fluid would reveal hysteresis loops of the type shown in figure 1-1. Curve 1 illustrates the response of a fluid whose yield stress is unaffected by the shear history while curve 2 depicts a liquid in which the recovery is slower and the yield value is not constant. This effect

is reversible in that sufficient rest brings about a recovery of structure. Rheopectic fluids would also exhibit hysteresis loops of similar form but with the arrows drawn opposite to that shown.

The following subsections summarize the more commonly accepted microscopic explanations for the macroscopic behavior of non-Newtonian liquids. The constitutive equations given relate to simple shear in which there is only one non-zero velocity component. which varies in a direction perpendicular to the velocity vector.

1.4-1 BINGHAM PLASTICS

A Bingham plastic is assumed to possess a three dimensional structure which has sufficient rigidity to resist shearing stresses that are less than the yield stress. Once the yield value is exceeded, the structure breaks down and flows as a Newtonian liquid. It obeys the following relationships :

$$\Delta_{12} = 0 \qquad \tau_{12} < \tau_y \tag{1.13}$$

$$\tau_{12} - \tau_y = \eta_0 \Delta_{12} \qquad \tau_{12} > \tau_y \tag{1.13a}$$

$$\eta = \frac{\tau_y}{\Delta_{12}} + \eta_0 \qquad \tau_{12} > \tau_y \tag{1.13b}$$

where τ_y is the yield stress and Δ_{12} is the constant shear rate for a fluid subjected to the shearing stress-τ_{12}.

While no real fluid behaves in exactly the manner described, many materials do approximate Bingham plastic behavior. Some of the more common examples are drilling mud, chalk suspensions and sewer sludge.

1.4-2 PSEUDOPLASTIC FLUIDS

This important category describes the behavior of many commonly used non-Newtonian fluids. Pseudoplasticity occurs in solutions of asymmetric particles which are loosely bound to one another by secondary forces to form a randomly entangled network. Under shear, the particles tend to orient themselves so that their major axes are parallel to the direction of shear. This behavior would also be displayed by systems of solvated particles whose degree of solvation was a function of the rate of shear. The apparent viscosity decreases with increasing rate of shear. At very low shear rates, there is little alignment and the structure exhibits Newtonian behavior with a zero shear viscosity- η_o . When the shear rate is very high, the particles are fully extended and Newtonian behavior is again evidenced with an infinite shear viscosity- η_∞ .

The change in particle configuration with shearing stress cannot occur instantly and pseudoplastic fluids must be regarded as those in which the time for structural rearrangement is small with regard to the time constant of the experiment.

The following three constitutive equations for

pseudoplastic flow represent the more popular ones of the many purely viscous relations proposed (3). None of them are able to describe stress relaxation or normal stress phenomena, two types of behavior common to viscoelastic fluids.

1. Power law

a. $\tau_{12} = K \Delta_{12}^{n}$ (1.14)

$\eta = K / \Delta_{12}^{1-n}$ (1.14a)

b. $\tau_w = \frac{a_o \Delta P}{2 \ell} = K' \left(\frac{4 V_o}{a_o}\right)^{n}$ for tubular flow (1.15)

where τ_w is the wall shear stress in a tube of diameter-$2a_o$ and length-ℓ for a fluid flowing with an average velocity-V_o under an imposed pressure gradient-ΔP.

The power law is a two constant empirical equation which many fluids obey over moderate ranges of shear rates. It fails to describe observed behavior at low shear rates in that it predicts an infinite viscosity at zero shear rate.

2. Ellis model

$$\Delta_{12} = \frac{\tau_{12}}{\eta_o}\left[1 + \left(\frac{\tau_{12}}{K}\right)^{\frac{1-n}{n}}\right] \qquad (1.16)$$

$$\eta = \eta_o / \left[1 + \left(\frac{\tau_{12}}{K}\right)^{\frac{1-n}{n}}\right] \qquad (1.16a)$$

This three constant empirical model reduces to Newtonian behavior with constant viscosity-η_o at low shear rates and approaches power law behavior at high shear rates.

3. Eyring-Powell model

$$\eta = \eta_\infty + (\eta_o - \eta_\infty) \frac{\sinh^{-1} B\Delta_{12}}{B\Delta_{12}} \qquad (1.17)$$

The Eyring-Powell fluid, a three constant semi-theoretical model, reduces to Newtonian behavior at both low and high shear rates while predicting pseudoplastic behavior at intermediate shear rates. Its use has been limited because it results in forms that are difficult to solve analytically.

1.4-3 DILATANT FLUIDS

Dilatant fluids display an apparent viscosity which increases with increasing shear rate. This behavior usually occurs in concentrated slurries in which there is insufficient liquid present to enable the particles to flow freely past one another. Metzner and Whitlock (56) have compiled a number of systems which exhibit dilatancy.

1.4-4 TIME DEPENDENT NON-NEWTONIAN FLUIDS

In materials exhibiting time dependent behavior, the shear stress (at a given shear rate) changes with the duration of the shear. Those fluids in which the shear stress increases with time are called rheopectic and those in which a decrease occurs are called thixotropic.

The mechanism responsible for thixotropy is possibly similar to pseudoplasticity. In any unsteady flow, from a Lagrangian viewpoint, the orientation of asymmetrical molecules and particles or the breakdown of solvated masses cannot occur instantaneously with respect to time. Pseudoplastic behavior may be considered as a form of thixotropy which has a time constant much smaller than the

time scale of the experiment. Carver and Van Wazer (7) have shown that certain fluids may require times of several minutes or hours before the structure is completely regained. Several authors, including Fischer, Bauer and Wiberly (21) present evidence that this formation time is also proportional to the level of shear to which the material was previously subjected. Thixotropy occurs in many practical materials such as paints, food products and some polymeric solutions.

Rheopexy may be considered as being caused by the same phenomena as dilatancy but with time dependent effects large enough to be detected. It is a relatively rare occurrence but has been observed in certain sols and bentonite clay suspensions.

1.4-5 VISCOELASTIC FLUIDS

High molecular weight polymers dissolved in solution or alone as a melt form a class of non-Newtonian behavior known as viscoelasticity. These materials differ from elastic solids in that they flow under an imposed pressure gradient and, unlike purely viscous fluids, they display elastic properties such as recoil and stress relaxation. Such responses are related to the ability of the polymer chain to assume different spatial configurations under shear flow. A description of some characteristic viscoelastic phenomena follows.

A. RECOIL

If the shearing stresses imposed upon a viscoelastic fluid under flow are rapidly removed, the fluid will undergo a partial recovery of strain. This may be observed experimentally by following the movement of tracer particles in the solution (40) or the deflection of an unconstrained rotor in a concentric cylinder apparatus (7).

The viscoelastic fluid may be said to possess a 'partial memory' of its rest state. An elastic solid has a 'perfect memory' and returns completely to its rest state when the deforming stress is removed.

B. JET SWELLING

An unconfined liquid jet emerging from a cylindrical tube can expand to a diameter considerably larger than the nozzle diameter, as shown in figure 1-2.

Moderate shear rates High shear rates

Figure 1-2. Jet swelling for a viscoelastic fluid.

The magnitude of the effect is dependent upon the particular

fluid, the L/D of the capillary (9,69) and the shear rate (52,61). At sufficiently high shear rates, contraction always occurs due to the rearrangement of the velocity profile (35).

C. WEISSENBERG ROD CLIMBING EFFECT (90)

When a rod is rotated in a Newtonian liquid, the free surface is depressed in the neighborhood of the rod and elevated on the walls of the container. This is a consequence of the centrifugal forces accompanying the flow. In viscoelastic liquids, there is a tendency for the fluid to climb the rod. This phenomena, shown in figure 1-3, arises from normal stresses in the flow field of a form radically different from that occuring in a Newtonian liquid. A quantitative description of the distribution of normal tractions may be obtained from pressure measurements in a rotating parallel plate or cone and plate system (11). A typical distribution of normal stresses is shown in figure 1-4.

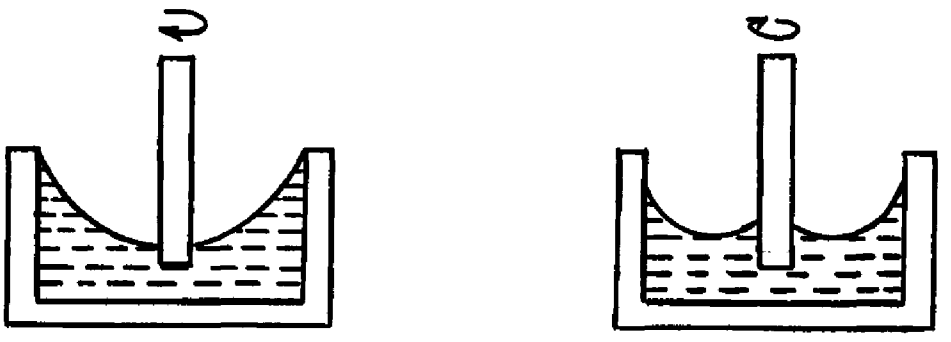

Newtonian liquid Viscoelastic liquid

Figure 1-3. The Weissenberg rod climbing effect.

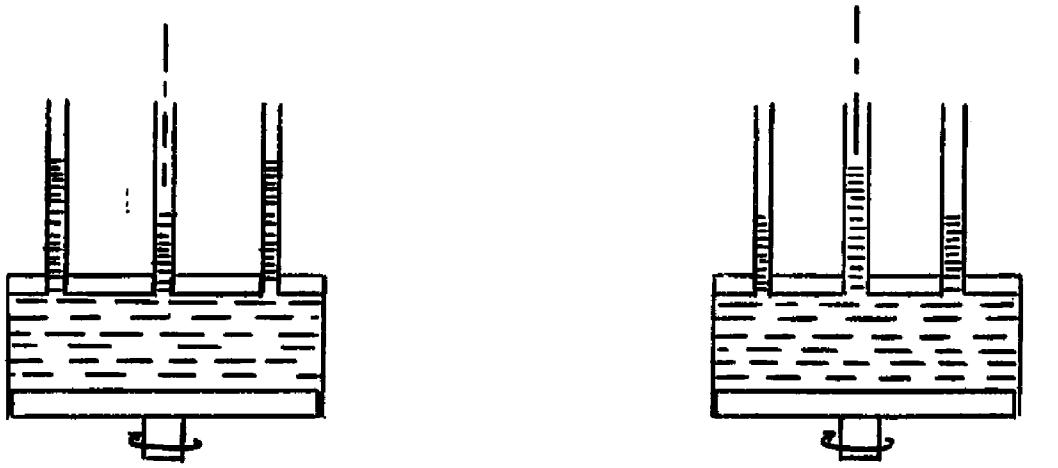

Figure 1-4. Pressure distribution in a parallel plate shear field.

D. STRESS RELAXATION

If a Newtonian liquid is subjected to a flow history and then held at constant deformation, the shearing stresses will be observed to relax instantaneously, even though the strain persists. In a perfectly elastic solid, the stress caused by the deformation does not relax at all. Between these two extremes are viscoelastic fluids which undergo stress relaxation at a finite rate.

Stress relaxation experiments have been used to evaluate the constants and predictions of proposed constitutive equations (20).

E. DRAG REDUCTION

The addition of certain polymeric additives in concentrations as low as 10-50 parts per million can reduce

turbulent pressure drop by as much as 50% (23,36,76,84). Seyer and Metzner (78) report that for solutions exhibiting drag reduction, the flow may be transitional up to Reynolds numbers of about 10^5.

F. ELONGATIONAL VISCOSITY

Viscoelastic theories predict that, under tension, a viscoelastic fluid will exhibit an elongational viscosity which increases with shear rate (10,43,92). This is in contrast to the shear viscosity which is a decreasing function of shear rate. Experimental data are sparse but Ballman (1) reported a constant elongational viscosity for polystyrene. The ability of polymers to be drawn into long fibers has been related to this predicted property (44,64,95).

1.4-6 CONSTITUTIVE RELATIONS FOR VISCOELASTIC FLUIDS

Ideally, the constitutive equation for a viscoelastic fluid should be complete enough to describe all of the previously described phenomena yet be of such a form as to yield tractable solutions from the equations of motion. It must obey certain invariance principles (22) since natural laws are independent of any coordinate transformation. In addition, the response of the material to a given set of causes must be indifferent to the coordinate system chosen. Both requirements may be satisfied by casting the constitutive equation in a tensorial form and formulating the relation in a coordinate system that moves and deforms

with the continuum (65).

Some general statements can be made concerning what the constitutive relation for a viscoelastic fluid should contain if it is to predict observed phenomena.

a) Experimental data show that in the limit of zero velocity gradient, the shear dependent viscosity tends towards a limiting value. The viscous part of the complex viscosity, determined from transient response experiments also approaches the same limiting value. Therefore, the constitutive equation should also contain a zero shear viscosity- η_0 .

b) The constitutive equation should contain a characteristic time(s) which can be identified with stress relaxation phenomena.

c) The constitutive equation should correlate steady shear as well as oscillatory data.

d) Normal stresses in steady shear should be predictable from the model.

e) The shear viscosity, shearing stress and normal stress should be functions of the shear rate and, in simple shear, be of the experimentally observed form shown in figure 1-5. The slope $\frac{d \log \tau_{12}}{d \log \Delta_{12}}$ should be unity at low shear rates, and less than one at intermediate to high shear rates. Similarly, the slope $\frac{d \log (\tau_{11} - \tau_{22})}{d \log \Delta_{12}}$ is initially two and is reduced below that value at higher shear rates.

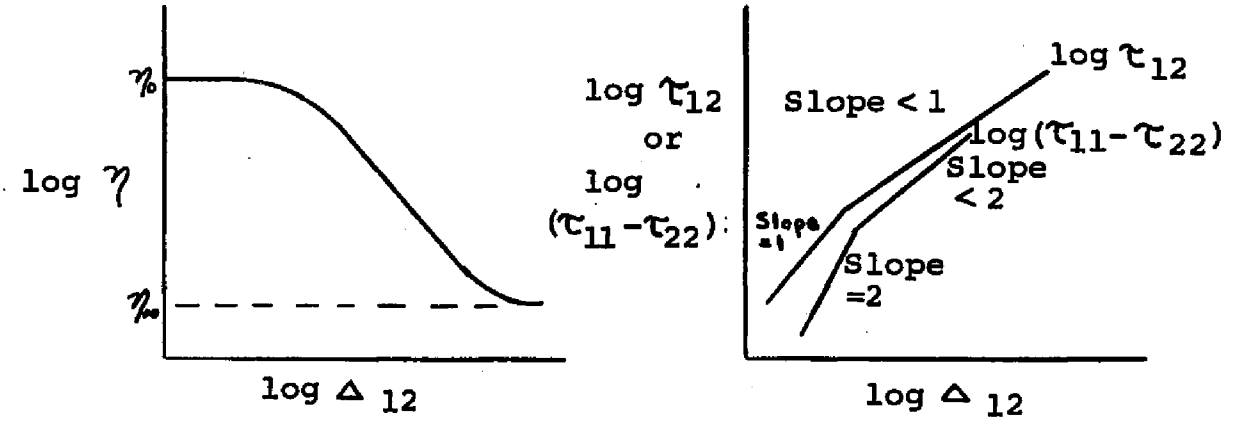

Figure 1-5. Experimentally observed response of viscoelastic fluids.

Constitutive equations for viscoelastic fluids may be classified as being either of the 'rate' type or of the 'integral' type.

Rate equations are characterized by time derivatives of the stress and deformation. Linear relations may be written in the form

$$P\tau = Q\Delta \tag{1.18}$$

where $$P = 1 + \lambda_1 \frac{\mathcal{D}}{\mathcal{D}t} + \lambda_2 \frac{\mathcal{D}^2}{\mathcal{D}t^2} + \cdots + \lambda_N \frac{\mathcal{D}^N}{\mathcal{D}t^N} \tag{1.18a}$$

and $$Q = \eta_0 \left(1 + \mu_1 \frac{\mathcal{D}}{\mathcal{D}t} + \mu_2 \frac{\mathcal{D}^2}{\mathcal{D}t^2} + \cdots + \mu_M \frac{\mathcal{D}^M}{\mathcal{D}t^M}\right) \tag{1.18b}$$

P and Q are linear, time differential operators which satisfy the principle of material objectivity, while λ_i and μ_i are relaxation and retardation times, respectively. $\frac{\mathcal{D}(\,)}{\mathcal{D}t}$ is a convected time derivative such as the Oldroyd (65) or Jaumann (67) derivative. The published experimental evidence does not favor a particular derivative over another.

Linear rate equations such as (1.18) are capable of predicting normal stresses in steady shear and stress relaxation but do not exhibit a shear dependent viscosity.

By the addition of product terms in Δ , τ , and $\Delta\cdot\tau$ to (1.18), Oldroyd (66) formulated a non-linear rate equation which qualitatively reproduced observed properties. It is mentioned briefly that many other non-linear rate equations have appeared in the literature and the interested reader can find several summarized in Fredrickson (22).

Integral constitutive equations have the advantage of being explicit in stress and may be represented by the following form.

$$\tau(t) = \int_{-\infty}^{t} (\text{relaxation function})(\text{strain history})\, dt' \quad (1.19)$$

The basis for linear, integral representations originates from the Boltzman superposition principle. For small departures from equilibrium, the total stress acting on a viscoelastic material at time t may be obtained by summing the stresses due to individual strains- γ which originated at time-t_n, with each strain weighted by a relaxation function.

$$\tau_{ij}(t) = \sum_{n=0} \phi_n(t - t_n)\, \gamma_{ij}(t_n) \quad (1.20)$$

If the individual strains are replaced by a continuous strain history- $\gamma(t')$, the summation sign may be replaced by the integral representation.

$$\tau_{ij}(t) = \int_{-\infty}^{t} \phi(t-t')\, d\gamma_{ij}(t') \qquad (1.21)$$

$$\text{or} \quad \tau_{ij} = \int_{-\infty}^{t} \phi(t-t')\,\Delta_{ij}\, dt' \qquad (1.22)$$

where $\Delta_{ij} = \frac{d\gamma_{ij}}{dt'}$

Equation (1.22), being a linear formulation, possesses the same limitations as do linear rate equations. While it is able to predict normal stresses and stress relaxation phenomena, the viscosity is constant. If the relaxation function is taken to be dependent upon the rate of deformation tensor, a shear dependent viscosity will be obtained. Several non-linear integral theories are summarized in Middleman (59).

Metzner, White and Denn (54,55) have considered criteria for selecting viscoelastic constitutive equations which are applicable to solving practical engineering problems. The Deborah number, defined as the ratio of the fluid's relaxation time to the deformation time, is used as a natural ordering parameter to determine the appropriate type of relation.

Several review articles are available (5,45,81) which compare the predictive ability of rate and integral constitutive equations with experimental data. The comparison does not argue for either rate or integral constitutive equations. However, Spriggs, Huppler and Bird conclude that selected constitutive equations from each type show considerable promise as rheological equations of state for

use in fluid dynamical calculations.

While the preceding theories have treated the material as a continuum, molecular models have been successfully developed which predict non-Newtonian behavior as a function of shear rate in terms of known molecular parameters. A comprehensive review of several molecular theories and comparisons with experimental data may be found in Middleman (59).

1.5 A DESCRIPTION OF NEWTONIAN JET BREAKUP

When liquid flows within a capillary, the confining walls serve to retard the fluid movement and thereby give rise to shearing stresses. For Newtonian liquids in fully developed flow, this results in the well known parabolic velocity profile. Upon emerging from the nozzle into ambient air, the liquid column is no longer confined and undergoes a stress relaxation at a rate determined by the flow velocity and the rheological properties of the fluid. At low velocities, the surroundings exert no influence on the liquid column. The appearance of an unconfined, laminar Newtonian jet is represented in figure 1-6. It is assumed in this representation that the fluid velocity is sufficient to render gravity effects negligible and that the time required for relaxation is short compared to the lifetime of the jet.

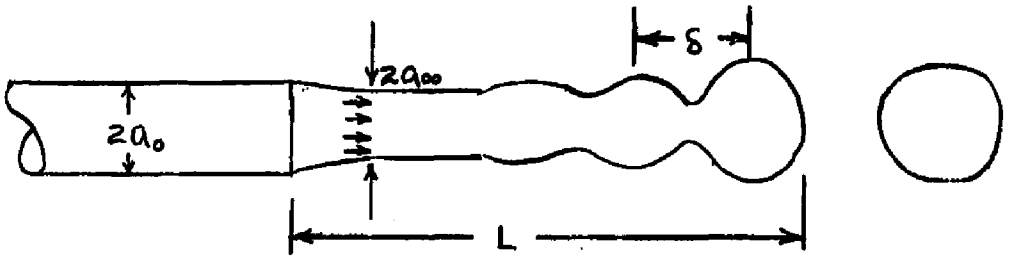

Nozzle diameter = $2a_o$ Breakup length-L
Relaxed diameter = $2a_\infty$ Wave length- δ

Figure 1-6. Breakup of a laminar capillary jet of a Newtonian liquid.

Superimposed upon the liquid column are small disturbances from sources such as microscopic burrs within the capillary or external vibrations transmitted through the nozzle. Surface tension forces alone act to return the locally disturbed surface to its equilibrium position but overshoot the mark. A larger restorative force results from the overshoot which then produces an even greater deviation from equilibrium. The disturbance thus propagates as an axially symmetric wave of increasing amplitude and fixed wavelength until surface tension forces pinch off the column to form individual droplets. The intact portion of the liquid column is known as the breakup length.

The breakup length of a capillary jet of a Newtonian liquid as a function of velocity has the form shown in figure 1-7.

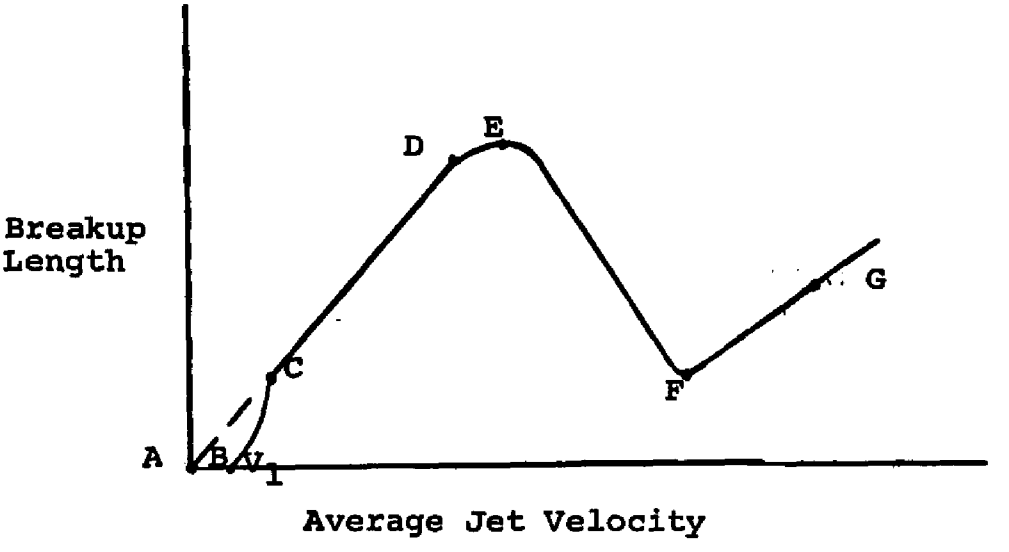

Figure 1-7. Breakup length of a capillary jet of a Newtonian liquid as a function of velocity.

At very low flow rates (velocities lower than V_1) , the fluid drips out of the nozzle and does not form a jet with any defineable breakup length. It follows the path (BC) but, for all practical purposes, this small section may easily be ignored and the L vs. V curve can be assumed to follow the extrapolated line segment (AC). When the jet velocity is sufficiently low so that the ambient air exerts no influence, the breakup length is linear with velocity (ACD). As the velocity is increased past that corresponding to point D, frictional drag by the air results in a departure from linearity (DE) and a maximum breakup length is reached. Further increases in jet velocity cause a decrease in breakup length (EF). Over the region (FG), the jet is turbulent

and the breakup length again increases. This should not be interperted that turbulence enhances stability since, as shown in figure 1-8, the breakup time past point D is a decreasing function of jet velocity.

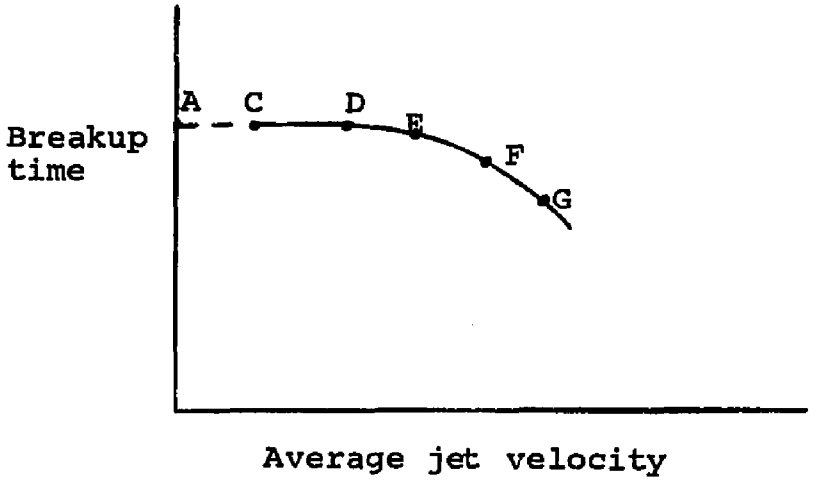

Figure 1-8. Breakup time of a Newtonian capillary jet as a function of jet velocity (points correspond to figure 1-7).

CHAPTER 2

STATE OF THE ART

This chapter will review the published literature dealing with the breakup of a low speed, capillary jet of liquid moving through ambient air. In order to keep this survey to a reasonable size, the related stability topics of a liquid jet in liquid surroundings and the breakup of a turbulent jet have been omitted. When background material is needed for completeness, efforts were made to cite a recent review article rather than list the numerous original contributors.

2.1 STRESS RELAXATION

A fluid which emerges from a capillary into ambient air suffers an abrupt removal of the confining wall. This results in a relaxation of all prior stresses. If the relaxation is complete within the lifetime of the jet, the velocity profile rearranges from the original, radially varying shape to a flat profile. Continuity arguements show that these changes must also cause the jet diameter-$2a_\infty$ to differ from the nozzle diameter-$2a_o$ and the ratio is termed $\chi = a_\infty/a_o$.

For capillary jets of Newtonian liquids, it has been found experimentally that the diameter ratio is a function of the capillary Reynolds number-Re_o alone for fully developed flow (26,32,60,62). Gavis and Modan (26) report

that a nozzle length to diameter ratio- $\ell/2a_o$ greater than 32 is needed to produce consistent results for χ . At Reynolds numbers below 16, Newtonian jets expand due to viscous forces ($\chi > 1$) while at $Re_o < 16$ contraction occurs because of inertial forces. Gavis (25) summarized the data of Middleman and Gavis (60) as

$$\chi = 1.10 - 0.23e^{-60/(Re_o)^{3/2}} \qquad (2.1)$$

Goren and Wronski (32) did not find any upper limit to the diameter ratio at the lower Reynolds number range. Only at Reynolds numbers greater than 300 was the lower theoretical limit of $\chi = \sqrt{3}/2$ approached (35).

Goren (30) considered the rate at which the stresses relax in a Newtonian jet. He used a boundary layer approach, valid for small axial distances where the periphery of the liquid column does not interact with the core, and showed that the jet diameter varies as the cube root of the axial distance.

$$(a_o - a)/a_o = 0.703(z/a_o Re_o)^{1/3} \qquad (2.2)$$

At large axial distances, where the boundary layer assumptions are invalid, Goren and Wronski employ a linear perturbation technique and show that the relaxation follows an exponential decay of the form

$$a = a_\infty + \sum_1^\infty A_n e^{-h_n z/a_\infty} \qquad (2.3)$$

The decay rate-h is a function of the jet Reynolds number and a surface tension parameter.

They experimentally verified the predicted dependence for small and large axial distances. For capillary Reynolds numbers below 100, the jet diameter reached 99% of its final value within 1.5 jet diameters. Middleman (57) obtained similar data and found that, at Reynolds numbers up to 1000, relaxation is 99% complete within 3 jet diameters. Thus, for Newtonian liquids, the relaxation length may be neglected in comparison to the breakup length over the usual range of Reynolds numbers encountered.

The relaxation of stresses outside the capillary for a non-Newtonian jet involves considerations of the effect of a shear dependent viscosity and, in the case of viscoelastic liquids, the presence of normal stresses. Powell (69) and Middleman and Gavis (61,62) investigated stress relaxation in capillary jets of viscoelastic liquids. They found that a nozzle length to diameter ratio of $\ell/2a_0$ = 40-50 produced consistent results for χ, which is similar to the Newtonian value. However, Metzner et. al.(52) measured a small but definite effect on χ when $\ell/2a_0$ was increased to 126 from 97. These conflicting conclusions regarding the entrance length required for fully developed flow remain to be resolved. The data from all investigators show that, at low shear rates an expansion is obtained, $\chi > 1$, but as the shear rate is increased contraction always occurs.

No experiments have been reported on the direct measurement of the rate of stress relaxation in non-Newtonian jets. In the experiments just reviewed for the effect of shear rate on the diameter ratio, the authors make no comment on the axial distance required to achieve constant values for χ . This may be construed as meaning that the axial distance was of the same order as for Newtonian liquids. However, the data of other investigators with capillary jets of viscoelastic liquids indicate that the relaxation length may be considerable. Gill and Gavis (27) imposed artifical disturbances upon the motion of carboxymethyl cellulose jets and measured the nodal lengths of the resulting transverse wave. Starting from a model of a wave propagating on a string of slowly varying tension they obtained, after considerable linearization, an expression which permitted the calculation of the fluid's relaxation time from their data. Values of 0.32 seconds and 0.27 seconds were calculated for solutions of 1.4% SCMC and 1.7% SCMC, respectively. This means that a slowly decaying axial tension exists over the lifetime of the jet. Goren and Gavis (31) have developed a theoretical analysis for this geometry. By assuming an exponential decay of the axial normal stress, a solution was obtained for the nodal points of the wave as a function of the axial distance. Middleman (59) summarizes experimental results obtained by Middleman and Rautenbach for artificially disturbed SCMC jets. Relaxation

times on the order of 10^{-2} seconds were calculated and, while this value differs by an order of magnitude from those reported by Gill and Gavis, it also shows that the relaxation length is considerably longer than for Newtonian jets. Additional evidence in this direction comes from Gaskins and Phillipoff (24) who measured the ratio of the jet velocity to the average capillary velocity-V_∞/V_o and found it to be less for viscoelastic jets than for Newtonian jets. They attribute this to the presence of accumulated elastic energy which absorbs some of the kinetic energy. Further experiments appear to be necessary to clarify the phenomena of stress relaxation with capillary jets of non-Newtonian liquids.

Mass and momentum balances have been used (22,25,26, 60,62,79) to relate the change in jet diameter from that of the capillary to the forces causing the change, i.e. the velocity profile rearrangement, the normal stress relaxation and surface tension forces. Control surfaces are taken at the capillary exit and at a point far enough downstream for the jet to be completely relaxed except for an everpresent axial surface tension force. A properly formulated balance must reproduce the experimentally observed facts that, for Newtonian jets, the diameter ratio is a strong function of the Reynolds number and the Weber number has little, if any, effect. Contraction results for $Re_o < 16$; expansion occurs for $Re_o > 16$ and, at Reynolds numbers greater than 300, the diameter ratio approaches the limit $\chi = \sqrt{3}/2$.

Even for Newtonian liquids, it has not been possible to predict the observed diameter ratio from a knowledge of the flow velocity and the physical properties of the fluid. This is due to the lack of a quantitative expression for the axial normal stress at the capillary exit. Oliver (68) has measured the thrust exerted by Newtonian and non-Newtonian jets and has shown that Newtonian liquids also display an axial normal stress under the circumstances of a relaxing velocity profile. The usual practice has been to calculate this tensile stress from the momentum balance and the experimentally determined diameter ratio.

2.2 BREAKUP OF A LAMINAR CAPILLARY JET

Considerable theoretical and experimental efforts have been made in investigating the laminar breakup of a capillary jet of a Newtonian liquid. The major analytical contributions have come from the pioneering works of Lord Rayleigh (70-73) and Weber (89).

Lord Rayleigh (70,71) developed the first understanding of the causes of jet instability through a consideration of potential and kinetic energies of an inviscid jet moving through a non-interacting medium. He showed that if the wavelength of the propagating disturbance exceeded the circumference of the jet, the surface tension forces were not at a minimum. This condition is unstable and results in the breakup of the coherent liquid column

into spherical droplets, each separated by the disturbance wavelength. Through a numerical solution of the characteristic equation, the growth rate of the most rapidly growing disturbance was obtained as

$$\alpha_{max} = \frac{1}{2}\sqrt{\frac{\sigma}{2\rho(a_\infty)^3}} \qquad (2.4)$$

where α_{max} is the growth rate for a jet of radius-a_∞, surface tension-σ and density-ρ . The wavelength-δ of the disturbance wave corresponding to the maximum growth rate is given by

$$\delta = 9.02 a_\infty \qquad (2.5)$$

If the breakup length is assumed inversely proportional to the growth rate, the intact length of the liquid column-L is obtained as

$$L/2a_\infty = C\sqrt{\frac{2a_\infty V_\infty^2 \rho}{\sigma}} \qquad (2.6)$$

where V_∞ is the average jet velocity and C is an experimentally determined constant.

Rayleigh's predictions for the breakup length of a Newtonian liquid have been confirmed by many investigators (75,80,85). His later attempts (72) to include the effects of fluid viscosity and interactions with the surroundings

resulted in analytical expressions containing Bessel function ratios which were not solvable in any convenient form. It was possible to conclude, however, that in the limit of very high viscosities, the jet would be completely stable.

In 1931, Weber (89) considered the same equations as did Rayleigh, but was able to show that, when the disturbance wavelength was much larger than the jet radius, the Bessel functions could be approximated by their leading term. With this simplification, the growth rate of the fastest growing disturbance may be written as

$$\alpha_0^* = \frac{\sqrt{\frac{\sigma}{2\rho a_\infty^3}}}{2 + \frac{3\eta_0}{\rho}\sqrt{\frac{2\rho}{\sigma a_\infty}}} \qquad (2.7)$$

The presence of viscosity- η_0 is seen to stabilize the jet. Corresponding to this maximum growth rate is the wavelength of the propagating disturbance which is expressed as

$$\frac{\lambda}{2a_\infty} = \pi\sqrt{2}\left[1 + \frac{3\eta_0}{\sqrt{2\rho a_\infty \sigma}}\right]^{1/2} \qquad (2.8)$$

The length of the intact column prior to breakup is given by

$$\frac{L}{2a_\infty} = C\,\frac{V_\infty}{\alpha_0^*} = C\left[We_\infty^{1/2} + \frac{3We_\infty}{Re_\infty}\right] \qquad (2.9)$$

where We_∞ is the jet Weber number, $We_\infty = \frac{2a_\infty V_\infty^2 \rho}{\sigma}$, and Re_∞ is the jet Reynolds number $Re_\infty = \frac{2a_\infty V_\infty}{\nu}$. All quantities

in equation (2.9) are based on the jet diameter rather than the nozzle diameter. The two are usually different due to the velocity profile rearrangement. Weber's predictions for low speed breakup have been verified by many investigators (19,33,34,39,50,86,87).

The assumptions of the derivation are as follows:

1. Upon ejection from the capillary, all stresses generated by the previous shear flow relax in a distance which may be neglected in comparision to the breakup length and the jet then moves with a uniform axial velocity-V_∞ (apart from small perturbations).

2. The disturbance propagates as a wave which is periodic in the axial direction and exponential in time.

3. There is no interaction with the ambient air.

4. The disturbance wave is axisymmetric.

5. The fluid is incompressible.

In the following paragraphs, detailed comments will be made regarding experimental verification of the first four assumptions.

The relaxation of all stresses due to the capillary shear flow is accompanied by changes in the jet diameter and is considered complete when the jet diameter remains constant with increasing distance from the nozzle exit. Section 2.1 has previously detailed the ample experimental evidence (32,57) proving that, over the normal range of Reynolds numbers encountered, the relaxation

length in a laminar, Newtonian jet may be neglected in comparison to the breakup length.

Donnelly and Glaberson (16) imposed audio frequency disturbances on the motion of the jet and confirmed the exponential growth rate of the propagating wave.

Fenn and Middleman (19) established that the surroundings exert no influence on the jet for Weber numbers less than $We_\infty = 5.3$ but, above this, a frictional interaction does occur which results in a maximum in the breakup length vs. fluid velocity curve. The location of this maximum is dependent on the ambient pressure.

Grant and Middleman (33) found that laminar jets do propagate disturbances as an axisymmetric wave, in agreement with assumption 4. Beyond the maximum, transverse waves appear close to the nozzle but the jet still persists in being destroyed by the growth of an axisymmetric wave. The nozzle length did not exert any influence on the breakup length for $\ell/2a_o$ ratios greater than 26. Their breakup length data for laminar, Newtonian jets are correlated by the expression.

$$L/2a_o = 19.5\left(We_o^{\frac{1}{2}} + 3We_o/Re_o\right)^{0.85} \qquad (2.10)$$

where all dimensionless groups are based on the nozzle diameter.

As previously noted, profile relaxation results in a change of the jet diameter from that of the capillary bore. Kroesser and Middleman used the relaxed diameter instead of the capillary diameter to correlate their Newtonian jet breakup data and recalculated the measurements of Grant and Middleman. The resulting correlation is given by

$$L/2a_\infty = 18\left(We_\infty^{\frac{1}{2}} + 3We_\infty/Re_\infty \right)^{0.87} \qquad (2.11)$$

The departure from the unit slope prediction of Weber is claimed to be statistically valid.

Weber's analysis assumes the amplitude of the initial disturbance to be constant and predicts a uniform droplet diameter after breakup. When the disturbance is initiated as a result of naturally occurring noise, the initial amplitude is a function of time and this periodicity produces a droplet size distribution. Duffie and Marshall (17) investigated the droplet size distribution to be expected from laminar, low viscosity Newtonian jets. Their data fit the relation

$$D_g = 36(2a_o)^{0.56}(Re_o)^{-0.10} \qquad (2.12)$$

where D_g, the geometric mean diameter, and a_o are in microns. For a sample of N droplets, the geometric mean diameter is defined as

$$\ln D_g = \sum(\ln D_i)/N \qquad (2.12a)$$

In a second analysis, Weber modified the boundary conditions to include the external pressure of the gas. His solution predicts the experimentally observed maximum in the L vs. V curve but is only in qualitative agreement with the data beyond the maximum (19,33).

Borodin and Dityakin (6) also attempted to evaluate the effect of air interaction by writing the equations of motion for both the jet and the surroundings. Common boundary conditions were imposed which resulted in an 18th degree equation with complex coefficients that was not evaluated because of its complexity.

For completeness, the paper of Lee and Spencer (41) is recommended for its extensive collection of photographs showing the effects of injection pressure, air density and orifice roughness. A good introductory review of investigations into jet stability up to 1955 is found in Miesse (63). The empirical techniques used to correlate turbulent atomization data are summarized by Marshall (46).

In recent years, considerable theoretical and experimental efforts have been directed towards understanding the unusual behavior of viscoelastic fluids. This research has been spawned by the rapid growth of the polymer and polymer related industries.

A fundamental question concerning viscoelastic liquids is whether the ability to store elastic energy enhances or retards their hydrodynamic stability in a given

flow geometry, relative to a Newtonian fluid. For non-Newtonian liquids, the basis for comparison must be in terms of its apparent viscosity at the shear rate of the experiment. The available evidence is inconclusive as data exist to support both conclusions. However, there is no reason to believe that viscoelasticity is only stabilizing or only destabilizing. It may depend upon the magnitude and the algebraic sign of the elastic parameters comprising the particular fluid.

Wilcox et. al. (93) found that droplets of viscoelastic fluids resisted breakup in a high velocity air stream compared to Newtonian liquids of the same zero shear viscosity. Davies (12) also noted a stabilizing effect by viscoelastic additives on the atomization of fluids.

Dombrowsky, Eisenklam and Fraser (15) studied the behavior of a highly elastic Napalm solution in an expanding sheet formed by a fan jet. Instead of breaking up into droplets as Newtonian liquids do, the Napalm sheet formed a large number of filaments.

Many investigators have studied the onset of secondary motions between rotating concentric cylinders as their relative velocity is increased for both Newtonian and viscoelastic liquids. The instability appears as a series of rolls whose onset can be detected visually by the use of dyes or mechanically through torque measurements.

A review of the extensive results in this geometry is considered useful towards appreciating the behavior of viscoelastic jets in the capillary jet geometry.

In 1923, G.I. Taylor (83) presented a linearized analysis for a Newtonian fluid contained between concentric, rotating cylinders and showed that instabilities occur whenever the critical value of a certain parameter, since named in his honor, was exceeded. His experimental results were in excellent agreement with the theoretical predictions. Most of the available studies with Newtonian liquids for the onset of secondary motions are summarized in the books of Lin and Chandresakar. When the disturbances become finite, the problem must be treated on the basis of non-linear stability theory.

Many analytical treatments of rotational stability with viscoelastic fluids are available using linear and non-linear constitutive relations. Ginn and Denn (28) cite or review several of these models in their recent paper. The results show that the critical Taylor number is dependent upon the magnitude and, in the case of some models, the algebraic sign of the fluid's elastic parameters. Thus, the question of whether viscoelasticity enhances or retards the hydrodynamic stability, relative to a Newtonian fluid of the same apparent viscosity, cannot be answered inclusively but is specific to the particular viscoelastic fluid. These conclusions are, of

course, dependent upon the ability of the constitutive equation to describe the real behavior of viscoelastic fluids.

Merrill, Mickley and Ram (49) investigated the rotational stability of polystyrene, polyisobutylene and polymethylmethacrylate dissolved in various organic solvents and found little deviation from Newtonian results for liquids of the same apparent viscosity. However, for two samples of ultrahigh molecular weight polyisobutylene, significantly lower Taylor numbers were obtained. Rubin and Elata (74) reported substantial stabilization for solutions of polyethylene oxide, polyacrylamide and a natural polysaccharide. However, viscosity data presented for the non-Newtonian solutions is at variance with many published measurements. Low zero shear viscosities are reported, on the order of 1-6 centipoise for concentrations up to 0.2% and the fluids are claimed to exhibit Newtonian behavior except at high shear rates. It is suspected that degradation has occurred either in the initial preparation or by exposure to the surroundings.

Denn and Roisman (13) used polyethylene oxide, polyacrylamide, hydroxyethylcellulose, carboxymethylcellulose and polyisobutylene solutions in their investigation of rotational stability. The experimentally determined Taylor numbers showed a general trend towards flow stabilization, particularly in the narrowest annular gap. In many cases though, there was little difference from Newtonian values

and there was some evidence of destabilization for polyisobutylene in the widest gap.

The results of the various experimental investigations just described have shown that for selected viscoelastic fluids some stabilization or destabilization may occur, but, for most of the liquids employed, little deviation from Newtonian measurements were found. It is difficult to obtain a quantitative comparison between experimental data and analytical predictions because the elastic parameters in the viscoelastic constitutive equations cannot be reliably determined for the dilute solutions of these investigations.

Only limited attention has been given to the breakup of a capillary jet of a viscoelastic liquid. Middleman (58) presented an analysis for a viscoelastic fluid whose behavior is described by a linearized, three constant Oldroyd model. The constitutive equation for this material is given by

$$\left(1 + \lambda_1 \frac{\partial}{\partial t}\right) \tau_{ij} = \eta_0 \left(1 + \mu_1 \frac{\partial}{\partial t}\right) \Delta_{ij} \qquad (2.13)$$

where λ_1 and μ_1 are the relaxation times and retardation times, respectively, with $\lambda_1 > \mu_1$. Any variable $f(r,z,t)$ was assumed to have the general form

$$f(r,z,t) = F(r)e^{ikz + \alpha t} \qquad (2.14)$$

where k, the wave number, is defined as $k=2\pi/\delta$.
Equation (2.13) with the aid of equation (2.14) can be written as

$$\tau = \eta_0 \frac{1+\mu_1\alpha}{1+\lambda_1\alpha}\,\Delta \qquad (2.15)$$

This result can be regarded as the constitutive equation for a Newtonian fluid having the viscosity

$$\eta(\alpha) = \eta_0 \frac{1+\mu_1\alpha}{1+\lambda_1\alpha} \qquad (2.16)$$

The problem is then solved in a manner paralleling the development of Weber.

When λ_1 and μ_1 are very small, Middleman showed that an expression can be obtained for the breakup length of a viscoelastic jet-L_v compared to the breakup length of a Newtonian jet of the same zero shear viscosity-η_0 .

$$\frac{L_v}{L} = 1 - \frac{\lambda_1-\mu_1}{a_\infty} V_\infty \cdot \frac{1}{We_\infty^{1/2} + 3We_\infty/Re_\infty} \qquad (2.17)$$

Since $\lambda_1 > \mu_1$, a capillary jet of a viscoelastic fluid obeying equation (2.13) is less stable than a Newtonian jet of the same zero shear viscosity.

In a recent paper, Kroesser and Middleman have confirmed the predicted decreased stability for capillary jets of polyisobutylene in tetralin. Quantitative comparison with

the prediction of equation (2.17) could not be made without known values for λ_1 and μ_1 .

The analytical result of Middleman assumes that the jet relaxes from all stresses generated during the previous capillary flow in a distance which is short compared to the breakup length and therefore regains its zero shear viscosity 'instantaneously'. He then argues that the shear rates associated with the growth of symmetrical disturbances are sufficiently low that departure from Newtonian behavior would be slight. Thus, the jet propagates disturbances at a rate corresponding to its zero shear viscosity.

As discussed in section 2.1, there have been no published measurements on the rate of stress relaxation in viscoelastic jets. The data of Gill and Gavis as well as that of Middleman and Rautenbach, as reported by Middleman, indicate that a slowly decaying axial tension exists throughout the lifetime of the jet. Such behavior would invalidate an analysis based on an initially relaxed viscoelastic column.

The whole area of stress relaxation and viscosity buildup in a newly emergent, non-Newtonian jet will be examined in the light of the experimental data taken in this investigation. Since the lifetime of a jet is of the order of 10^{-2} seconds, a jet experiment affords the opportunity to witness effects whose existence is of a similar

order of magnitude. Such short time scales are difficult to determine on conventional instruments.

CHAPTER 3

EXPERIMENTAL APPARATUS AND PROCEDURES

3.1 OVERALL DESCRIPTION OF EXPERIMENTS

This chapter provides a detailed description of the experimental apparatus and techniques. When necessary, additional amplification of the procedures will be given in later chapters along with the test results.

A schematic diagram of the apparatus is shown in figure 3-1. Either an Instron mechanical tester or pressurized nitrogen activated the piston of a hydraulic cylinder, which contained the test fluid. The liquid flowed through a section of flexible, reinforced hose and past a 50-125 micron filter. These served to minimize mechanical vibrations from being transmitted along the walls of the stainless steel piping or through the fluid itself and also to trap any contaminant particles. The fluid then entered a cube designed to house a pressure transducer and the capillary. The cube was mounted on a concrete block to dampen vibrations from the surroundings.

Still photographs and high speed motion pictures were taken of the capillary at magnifications ranging from 0.8-25 times the actual size. The jet motion was effectively stopped by the use of microsecond duration flash equipment.

Typical experimental measurements included the jet

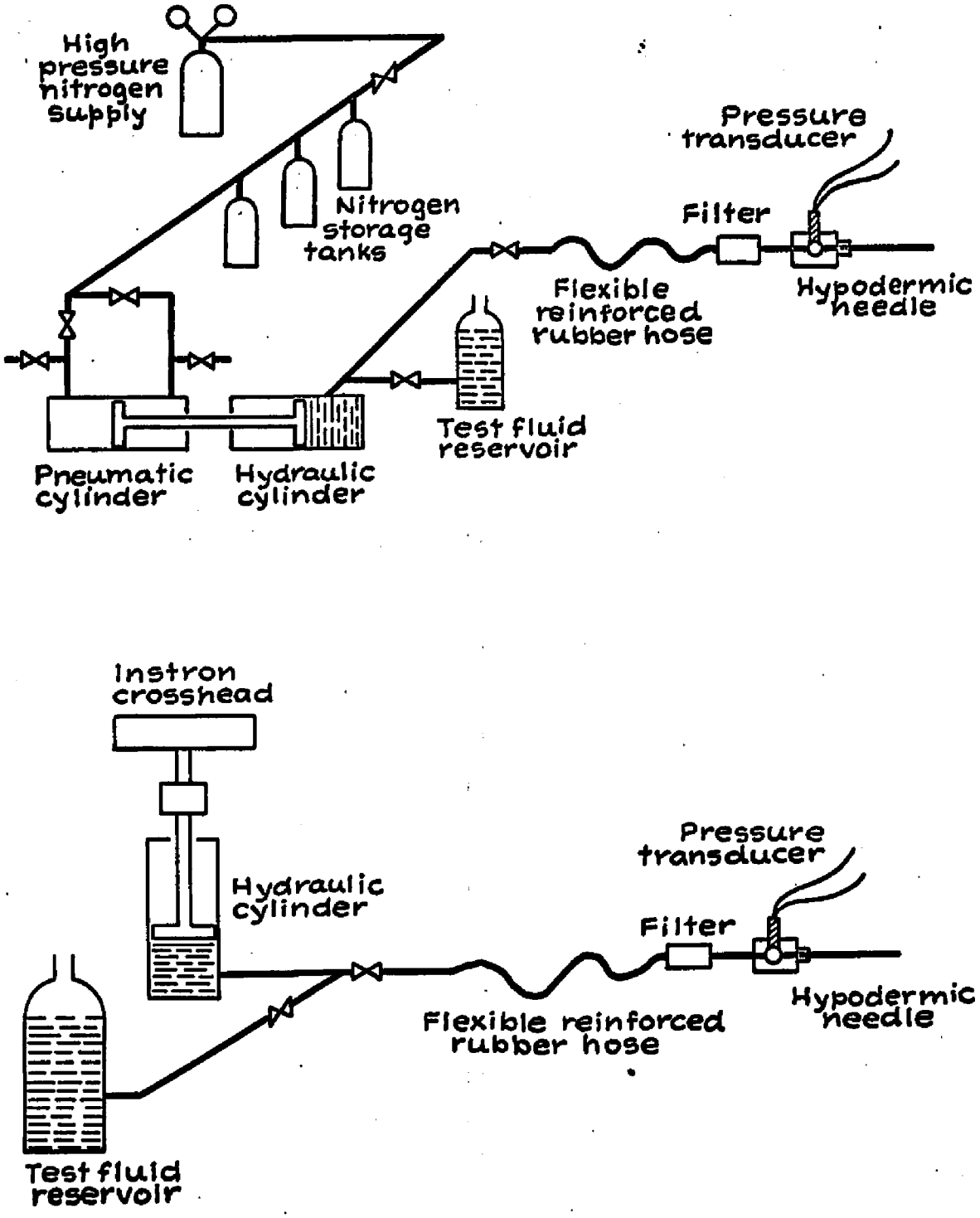

Figure 3-1. Experimental apparatus for studying jet behavior.

breakup length, droplet diameter, disturbance wavelength, volumetric flow rate and pressure drop through the capillary.

3.2 MECHANICAL EQUIPMENT

The Instron mechanical tester is a constant speed device which moves a crosshead at a preset rate and automatically adjusts the force required to do so, up to a maximum of 10,000 lbs. of force for the model used. Thus, with the Instron crosshead acting on the piston of a 4 inch diameter cylinder, containing the test fluid, a maximum pressure of 800 lbs/in^2 is available. This type of instrument is particularly useful in experiments requiring a constant volumetric flow rate in capillaries of varying length. It was used in capillary viscometer experiments and in preliminary tests to determine the effect of capillary length to diameter ratio on the jet breakup length.

When pressurized nitrogen served as the prime mover, Hoke gas regulators were used to reduce the pressure to the desired working value.

Cylinders of differing construction were used to provide low and high pressures. The low pressure set, manufactured by the Parker-Hannafin Co., had a 4 inch diameter piston by 10 inch stroke. Limitations on leakage past the Buna-N piston seals set the maximum operating pressure on the steel pneumatic cylinder at

250 lbs/in^2. The hydraulic cylinder was fabricated from chrome plated brass and used Viton rubber as the piston seal material. It was found that the chrome plating was not durable and the exposed base metal corroded if kept in contact with the test fluid for several hours. This did not pose any problem and only required an initial flushing with fresh test fluid at the beginning of a day's run to cleanse the system. The hydraulic cylinder was rated at 500 lbs/in^2. For high pressure operations up to 3000 lbs/in^2, steel cylinders of 5 inch bore by 12 inch stroke were used. These were fabricated by the W.E. Hennells Co. and employed polyurethane U-cups as piston seals in the pneumatic cylinder and Viton rubber for the same purpose in the hydraulic cylinder. Bronze plating was used on all surfaces in contact with the test fluid. This lowered the corrosion rate compared to chrome plated brass but did not eliminate it.

Special consideration was given to safely mounting the cylinders since the axial force generated on a 5 inch diameter piston by a 2000 psig pressure is about 39,000 lbs. of force. The cylinders were fastened to appropriately sized steel 'I' beams with high tensile strength bolts. In selecting the components, careful attention was given to the shearing stress and bending movements acting under the most severe loading conditions. Plates were welded on either side of the cylinder legs to prevent shifting during any cycling operation.

A Dynisco 0-1000 psig pressure transducer was used to measure the pressure drop of the fluid flowing through the capillary. The millivolt output of the transducer was plotted on a Leeds and Northrup 'Azar' recorder.

Nozzles were fashioned from hypodermic needles or tubing by grinding their ends to a flat face. The bores were examined under 100 power magnification for concentricity and surface imperfections. A stage micrometer was used to determine the inside diameter. The length/diameter ratio of the nozzles were usually greater than 100/1 although, in certain experimental runs, shorter nozzles were used to maintain a safe working pressure.

3.3 PHOTOGRAPHIC EQUIPMENT

Still photographs were taken with either of two 4"x5", triple extension (22") bellows cameras made by the Bausch & Lomb Co. and the Calumet Photographic Co. A 32 mm. f4.5 lens was used for closeup work of high magnification and a 158 mm. f6.3 lens was used for general purpose photography of lower magnification. The cameras were mounted on a specially constructed table which allowed movements along the x,y and z axes.

Both 3"x4" Polaroid roll film and 4"x5" Polaroid sheet film of ASA 3000 rating were used. The high speed film allowed small lens openings to be used with the accompanying advantage of a wide depth of field.

Motion pictures were made with a 400 foot capacity,

16 mm 'Hycam' series camera manufactured by Red Lake Laboratories. It is capable of frame rates between 10-11,000 pictures per second. By means of a timing light, which placed a mark on the edge of the movie film at a frequency of 10,100 or 1000 pulses per second, the instantaneous frame rate could be determined. An accessory event sychronizer fired an electronic flash when the 1/2.5 shutter was fully open.

The microsecond duration, high intensity lighting was provided by electronic single flash and strobe units produced by Edgerton, Germeshausen and Grier, Inc., models 549 and 501 respectively. A General Radio Co. strobe, model 1538, was available for visual measurements under circumstances where photographic determination was difficult.

3.4 GENERAL EXPERIMENTAL PROCEDURES

The experimental procedures used to obtain the test results are generally straightforward and do not require extensive explanations. An overall description of the techniques that were utilized has been given previously in section 3.1 . Some additional details will be furnished in this and the following sections.

When nitrogen gas was used as the prime mover instead of the Instron, two to four holding tanks were first pressurized to the desired working level. The gas regulator was then valved off from the system in order to avoid the

possibility of periodic disturbances produced by the opening and closing of the regulator. The decrease in pressure during an experimental run, due to piston travel, was negligible.

A Dynisco strain gage transducer measured the fluid pressure at the entrance to the capillary. The calibration was checked periodically against a dead weight tester and found to be invariant. A typical plot of the transducer's millivolt output versus applied pressure is shown in figure 3-2.

Volumetric flow rates of the test fluid were determined easily with a graduate cylinder and a stop-watch. When the Instron was used in the experimental system, the crosshead travel could be read to the nearest 0.005 inches. This movement was translated into volumetric flow rates from a knowledge of the hydraulic cylinder and capillary diameters.

3.5 PROCEDURES FOR PROFILE DECAY EXPERIMENTS

Accurate measurements were taken of the jet diameter as a function of the axial distance in the region immediately outside of the capillary. This is related to the rate at which the velocity profile decays.

The electronic flash was placed behind the jet with its light output directed onto a translucent plastic disk. A shadow photograph of the capillary jet was obtained at a magnification of approximately 10/1. In order to

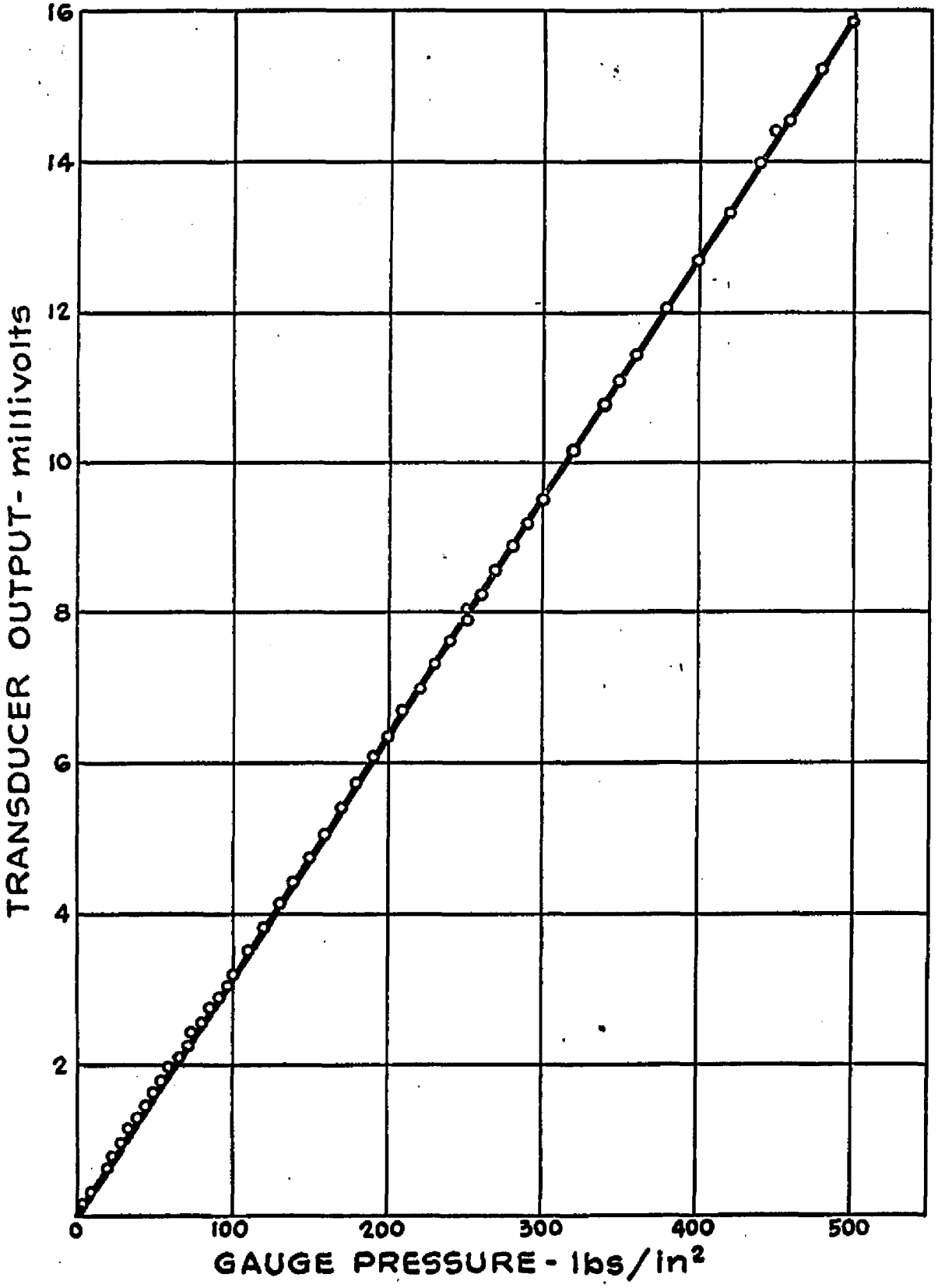

Figure 3-2. Calibration of pressure transducer.

to correct for any distortion from the camera lens or arising from a lack of parallelism between the plane of the film and that of the jet, a rod of known diameter was also photographed at each location. The required measurements were performed on a Nikon profile projector, model 6C, fitted with a 10/1 enlarging lens and a micrometer stage readable to 0.0001 inches. Values reported for the jet diameter are probably accurate to more than three significant figures.

Below a minimum velocity, the jet was either affected by gravity or the fluid wetted the capillary face to form a larger diameter than the bore. These runs were rejected. The temperature of the jet was measured after collection and compared to ambient for evidence of viscous heating. A Brookfield viscometer was used to check the viscosity of Newtonian test fluids after collection. The shear dependent viscosity of the non-Newtonian liquids made a similar check on them impractical.

3.6 PROCEDURES FOR JET BREAKUP EXPERIMENTS

Still photographs were taken of the capillary jet every few centimeters along the liquid column, starting from the nozzle tip and ending after the appearance of free droplets. A white reflector card was placed 6-12 inches behind the jet and the area of interest illuminated by the EG&G electronic flash, placed at a 45^{o} angle to the camera. Figure 3-3 illustrates the photographic arrangement.

Still pictures were taken with the room darkened and the shutter speed set on 'time'. A lens opening of f32 was used for magnifications of 3/1 while at enlargements of 25/1, a lens opening of f4.5 was required.

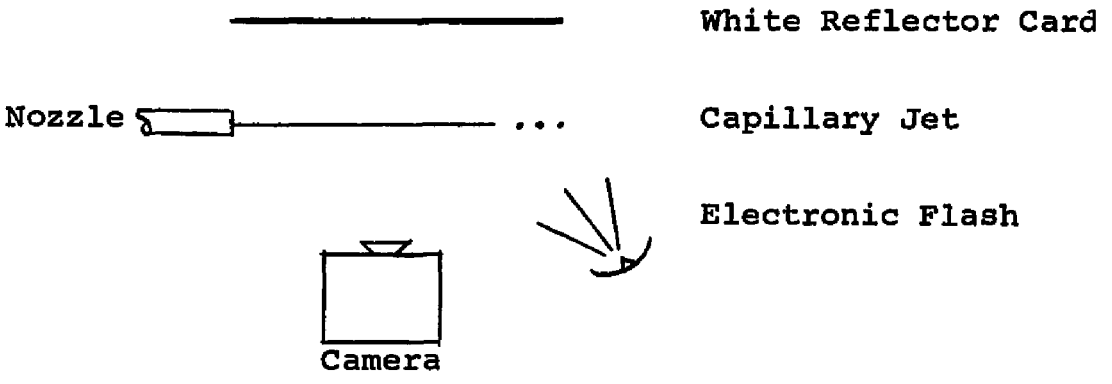

Figure 3-3. Photography of a capillary jet.

By means of a plumb bob suspended from the camera to a millimeter ruler, the distance between individual photographs could be determined, as illustrated in figure 3-4.

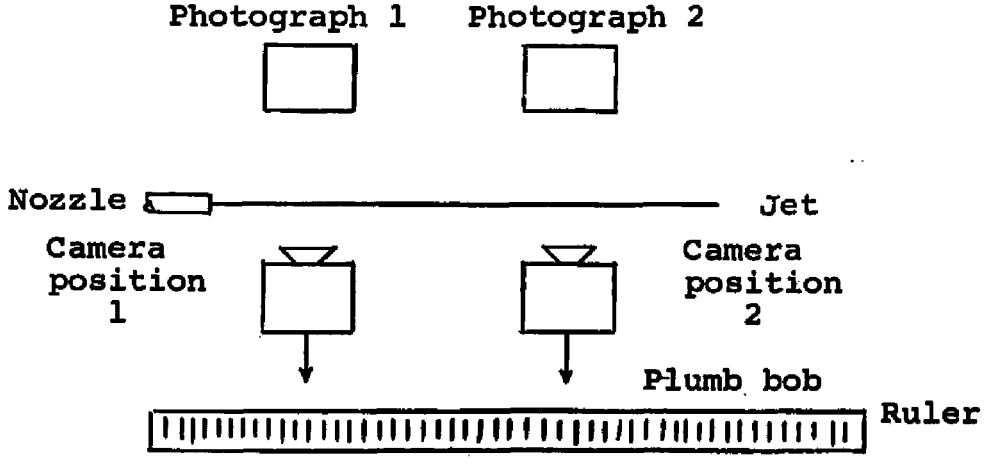

Figure 3-4. Measurement of distances between photographs.

The breakup length of a capillary jet is the distance from the nozzle tip to the point where the liquid column is no longer coherent and forms individual droplets. To determine this quantity from photographs taken at the two locations first requires obtaining the overall distance, as described in the previous paragraph. This length is then adjusted for the increment that the nozzle tip and the breakup point are each offset from the midpoints of their respective photographs. A photograph of a millimeter ruler placed in the same plane as the jet allowed actual distances to be measured on the experimental photographs. Ordinarily, an enlargement of 3-6 times actual size was used.

Moderately concentrated solutions of the visco-elastic additives formed capillary jets which often had breakup lengths larger than the 5-6 foot span that could be conveniently photographed. In these instances, visual measurements were made with the aid of the General Radio strobe.

In order to determine the disturbance wavelengths and the droplet diameters, more accurate techniques were required. The photographs of these subjects were placed in an overhead projector and the resulting image cast upon a screen had an overall magnification of 10-11 times actual size. Lengths were read off the screen with the aid of a dial caliper to an accuracy of 0.001 inches.

CHAPTER 4

TEST FLUIDS

4.1 SELECTION OF TEST FLUIDS

The test fluids used in this research can be broadly classified into three rheological categories:

1. Newtonian
2. Non-Newtonian inelastic
3. Viscoelastic

Newtonian fluids consisted of water, ethylene glycol and glycerin-water solutions. These were included in order to verify the soundness of the experimental apparatus and procedures by comparing the data with published results of other investigators.

The non-Newtonian inelastic fluids were comprised of Carbopol 934-water solutions and dispersions of the following materials- MPA 60 in xylene, MPA 60 in odorless mineral spirits and silica EH-5 in water. Despite their compositional differences, the liquids shared certain similarities from a rheological point of view. All exhibited a yield stress, a shear dependent viscosity and an absence of viscoelastic phenomena,e.g. a Weissenberg effect or recoil upon removal of shearing stresses.

Carbopol is a carboxypolymethylene polymer, thought to be slightly crosslinked (21), and is one of the few organic polymers whose solutions do not display elastic effects. Huppler (37) and Hurd (38) have characterized Carbopol solutions as a non-Newtonian fluid which possesses

very small normal forces. Several investigators, including Dodge and Metzner (14) and Kapoor (40) have demonstrated that Carbopol solutions are not drag reducing nor do they demonstrate any recoil upon removal of shear stress.

MPA 60 is a hydrogenated castor oil derivative which was selected in order to observe the behavior of a capillary jet where the fluid's gellation time clearly exceeded the jet breakup time. They are time dependent fluids whose rheological behavior depends upon the previous shear history. Upon cessation of shear, the consistency of the fluid increases with time and attains a steady state structure after about a day's standing. On the other hand, the Carbopol solutions and the silica dispersion appeared to gell immediately after the shearing stress was discontinued.

The aqueous viscoelastic solutions were prepared from a class of polymeric additives which exhibit drag reducing properties (23,36,76,84) in turbulent flow. These test fluids consisted of Separan AP30- a partially hydrolyzed polyacrylamide, Polyox: coagulant grade- a polyethylene oxide polymer, SCMC 7HS- a high viscosity grade of sodium carboxymethylcellulose and Guar Gum- a naturally occurring polysaccharide.

4.2 PREPARATION OF TEST FLUIDS

All aqueous polymer solutions were prepared by dissolving the additive in distilled water using one minute of

mixing with a laboratory mixer followed by gentle rolling overnight. This procedure was chosen to minimize shear and thermal degradation. Exposure to outside ultraviolet radiation was also avoided as many organic polymers are adversely affected by such treatment. The MPA 60 dispersions were used as supplied by the manufacturer. Silica dispersions require high shear mixing to break up the agglomerates and this was accomplished by batchwise addition to a Waring blendor. A non-ionic surface active agent, Triton X-100, was added to improve the wettability of the silica particles.

Several of the organic polymers required the use of additional additives in order to minimize chemical degradation. In private communications, Dr. B.D. Marsh advised the use of small quantities of glycerin with Separan solutions to offset the effects of carbon dioxide absorption. The manufacturer of Polyox recommends isopropyl alcohol in solutions to prevent chain sission reactions. Formaldehyde was added to SCMC and Guar Gum solutions to avoid biological attack.

4.3 PHYSICAL PROPERTIES OF TEST FLUIDS

Surface tensions of non-Newtonian fluids were determined on a Rossano tensiometer while those of Newtonian fluids were taken from published data. The common static techniques were found to be inadequate for fluids with appreciable yield stresses or those of high viscosity as

the measuring element could not penetrate the liquid surface. For such solutions, a dynamic method taken under flow conditions would appear to be necessary. Surface tension values for the two MPA 60 dispersions were determined by heating a sample to a temperature of approximately 70-90°C, at which point they were substantially inviscid, and extrapolating the data back to room temperature by assuming the same linear temperature dependence as for benzene and toluene. The results are tabulated in table 4-1. This technique was ineffective with 0.6% Carborpol or with the silica dispersion, both of which remained gellified at elevated temperatures.

Table 4-1. Surface tension of MPA 60 dispersions as a function of temperature.

Fluid	Temperature	Surface tension
MPA 60 in xylene	80 C	24.6 dynes/cm.
	75	25.6
	70	27.2
	25(est.)	32.5
MPA 60 in odorless mineral spirits	90	19.0
	85	19.4
	80	19.7
	75	20.2
	25(est.)	26.0

Surface tension measurements on the moderately concentrated viscoelastic solutions were found to depend upon the rate at which the platinum blade was withdrawn from the solution, with slower rates producing lower values. This variation is probably related to relaxation phenomena.

Within the same concentration range as that used here, the density of aqueous solutions of the organic polymers has

been shown by many authors to be equivalent to pure water and this value is accepted.

Table 4-2 is a classification of the test fluids and lists some pertinent physical properties. All Newtonian properties were obtained from published values in the standard handbooks. For the convenience of the reader, the density, surface tension and viscosity of glycerin-water solutions are shown graphically as a function of composition in figure 4-1.

4.4 DEVELOPMENT OF THE COAXIAL CYLINDER EQUATIONS

A coaxial cylinder viscometer was used to obtain shear stress-shear rate data at low to medium rates of shear and was also employed in the determination of yield stresses. The equations of flow for this geometry will be derived in a manner similar to that presented by Middleman (59). A schematic representation of this instrument is shown in figure 4-2.

A torque-M rotates the inner cylinder of radius-R_b and height-H at an angular velocity-Ω. The shear stress at the wall of the bob is given by

$$\tau_b = \frac{M}{2\pi R_b^2 (H+H_o)} \qquad (4.1)$$

where H_o is the end correction of the rotor. The outer stationary cup of radius-R_c is under a shearing stress-which is written as

Table 4-2. Physical properties of the test fluids.

Test fluid	Concentration	Density	Surface tension	Newtonian or zero shear viscosity
Carbopol 934 (carboxypolymethylene:B.F. Goodrich Co.)	0.1% in water[a]	1. gm./cc.	60 dynes/cm.	see table 4-3
	0.2% in water[a]	1.	not measurable	see table 4-3
	0.6% in water[a]	1.	not measurable	see table 4-3
Ethylene glycol	100%	1.116	48	0.178 poise
Glycerin-water	varied	see figure 4-1	see figure 4-1	see figure 4-1
Guar Gum (natural polysaccharide: Stein-Hall Co.)	0.05% in water[b]	1.	72	0.02 poise
MPA 60 (hydrogenated castor oil derivative:Baker Castor Oil Co.)	24% in xylene	0.872	32.5 dynes/cm.	see table 4-3
	24% in odorless mineral spirits	0.816	26.0	see table 4-3
SCMC 7HS (sodium carboxymethylcellulose: Hercules Powder Co)	0.25% in water[c]	1.	72	0.45 poise
	0.7% in water[c]	1.	72	2.3
Separan AP30 (hydrolyzed polyacrylamide: Dow. Chemical Co.)	0.05% in water[d]	1.	72	0.50*
	0.25% in water[d]	1.	63-72 (time dependent)	10.0*

Table 4-2. Physical properties of test fluids (continued).

Test fluid	Concentration	Density	Surface tension	Newtonian or zero shear viscosity
Silica EH-5 (Cabot Co.)	12.4% in water[e]	1.16 gm/cc	not measurable	see table 4-3
Polyox-coagulant (polyethylene oxide: Union Carbide Co.)	0.25% in water[f]	1.		2-5 poise (est.)
Water	100%	0.997	72 dynes/cm.	0.0092

a- neutralized with 0.4 gm. of sodium hydroxide/gm. of Carbopol.

b,c- formaldehyde added to prevent bacterial growth.

d- small quantities of glycerin added for stability.

e- Triton X-100 (Rohm and Haas Co.) wetting agent added.

f- isopropyl alcohol added for stability.

*- data of Schwarz and Bruce (77).

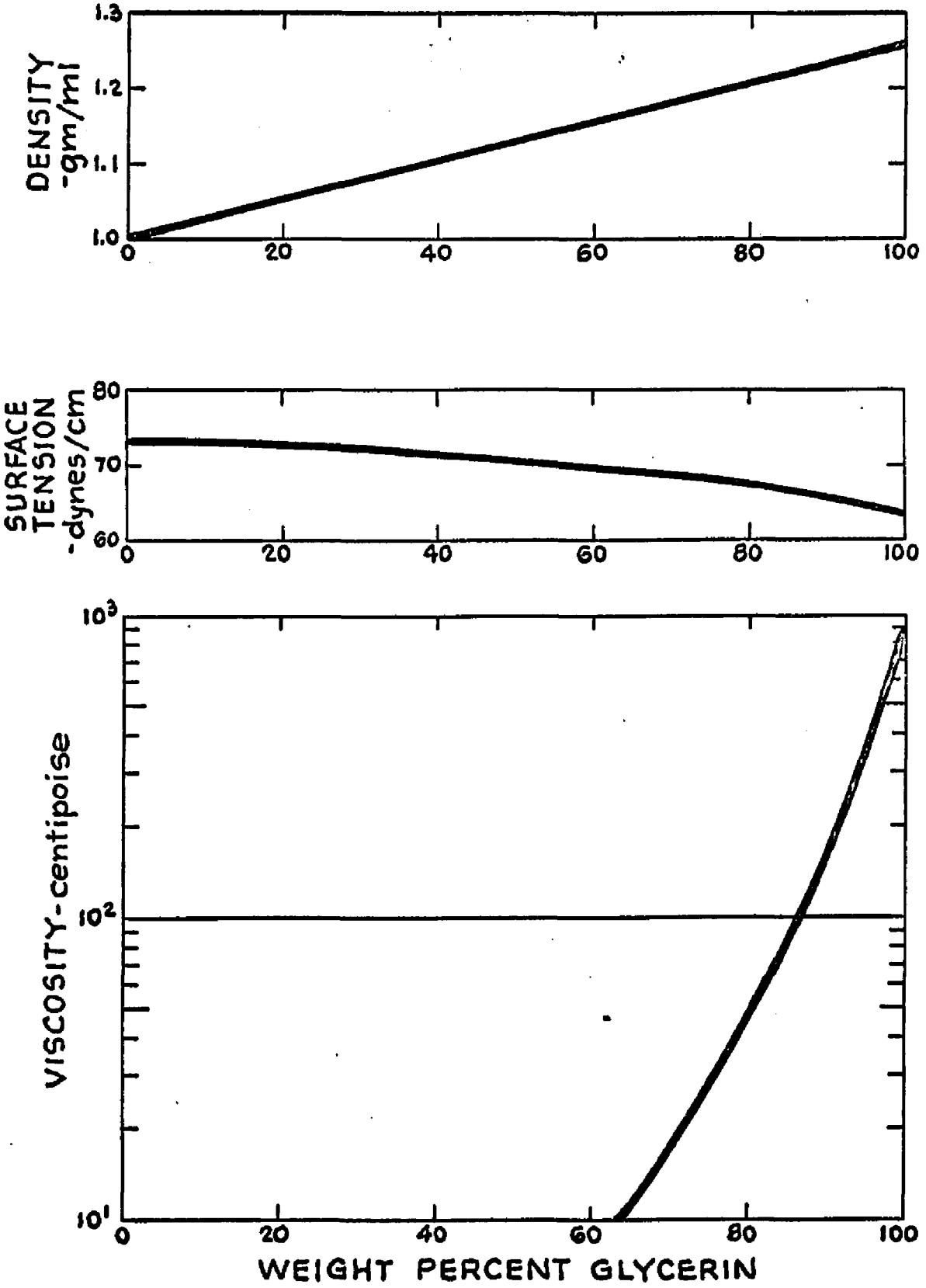

Figure 4-1. Physical properties of glycerin as a function of composition.

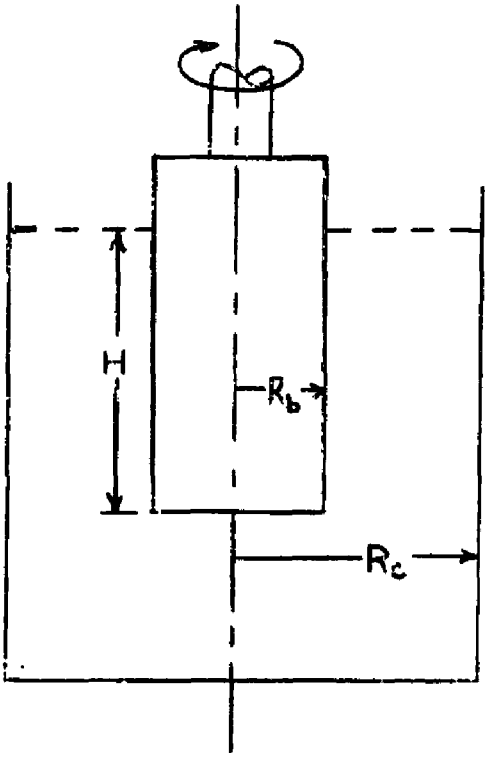

Figure 4-2. Typical coaxial cylinder viscometer.

$$\tau_c = \frac{M}{2\pi R_c^2 (H + H_o)} \tag{4.2}$$

If the fluid has a yield stress- τ_y , there are three possible conditions of flow behavior.

$$\tau_b < \tau_y \tag{4.3a}$$

$$\tau_c < \tau_y < \tau_b \tag{4.3b}$$

$$\tau_y < \tau_c \tag{4.3c}$$

In the condition demanded by (4.3a), there will be no flow in the gap. When inequality (4.3b) holds, the fluid will flow only in that portion of the annular space where the local shear stress exceeds the yield stress and the effective

gap size will be less than that defined by the viscometer walls. The critical radius at which flow occurs is obtained from the relation

$$M = 2\pi R_y^2 (H + H_o) \cdot \tau_y \tag{4.4}$$

which is rearranged to

$$R_y = \sqrt{\frac{M}{2\pi(H + H_o)\tau_y}} \tag{4.5}$$

By virtue of equation (4.1), the critical radius for flow may be written as

$$R_y = R_b \sqrt{\frac{\tau_b}{\tau_y}} \tag{4.6}$$

The minimum shearing stress needed to insure flow across the entire annular space will occur when $\tau_y = \tau_c$. From equations (4.1) and (4.2)

$$\frac{(\tau_b)_{min}}{\tau_c} = \frac{(\tau_b)_{min}}{\tau_y} = \frac{R_c^2}{R_b^2} \tag{4.7}$$

$$\text{or} \quad (\tau_b)_{min.} = \tau_y \left(\frac{R_c}{R_b}\right)^2 \tag{4.8}$$

In a simple shear flow field where the only non-zero velocity component is $V_\theta = V_\theta(r) = r\omega(r)$, the rate of deformation tensor, Δ_{ij} , is given by

$$\Delta_{\theta r} = \dot{\gamma} = r \frac{d\omega}{dr} \tag{4.9}$$

where $\omega(r)$ is the angular velocity.

From the equations of motion

$$r^2 \tau_{\theta r} = \text{constant} \tag{4.10}$$

Taking the total differential of equation (4.10) and dropping the subscripts

$$2r\tau\,dr + r^2\,d\tau = 0 \tag{4.11}$$

$$\text{or} \quad \frac{d}{dr} = -\frac{2\tau}{r}\frac{d}{d\tau} \tag{4.11a}$$

Applying this transformation to equation (4.9)

$$f(\tau) = -\dot{\gamma} = r\frac{dw}{dr} = 2\tau\frac{dw}{d\tau} \tag{4.12}$$

Integrating and applying the boundary conditions that $w=0$ at $r=R_c$ and that $w=\Omega$ at $r=R_b$.

$$\Omega = \frac{1}{2}\int_{\tau_c}^{\tau_b}\frac{f(\tau)}{\tau}\,d\tau \tag{4.13}$$

Equation (4.13) is differentiated with respect to τ_b to yield

$$\frac{d\Omega}{d\tau_b} = \frac{1}{2}\left[\frac{f(\tau_b)}{\tau_b} - \frac{f(\tau_c)}{\tau_c}\frac{d\tau_c}{d\tau_b}\right] \tag{4.14}$$

This result is valid only if the shearing stress at the cup exceeds the yield stress of the fluid

From equations (4.1) and (4.2)

$$\tau_c = \tau_b\left(\frac{R_b}{R_c}\right)^2 \tag{4.15}$$

$$\text{Therefore} \quad \frac{d\tau_c}{d\tau_b} = \left(\frac{R_b}{R_c}\right)^2 = S^2 \tag{4.16}$$

and equation (4.14) becomes

$$2\tau_b\frac{d\Omega}{d\tau_b} = f(\tau_b) - f(S^2\tau_b) \tag{4.17}$$

If $R_c \gg R_b$ or, equivalently, if $s \ll 1$ a closed form solution of equation (4.7) is obtained as

$$f(\tau_b) = 2\tau_b \frac{d\Omega}{d\tau_b} = 2\Omega \frac{d \ln \Omega}{d \ln \tau_b} \tag{4.18}$$

The general case for finite s is treated by an iterative procedure. Equation (4.18) is valid for all values of τ_b, e.g. $\tau_b, s^2\tau_b \ldots$ etc. and may therefore be written as

$$2s^2\tau_b \left.\frac{d\Omega}{d\tau_b}\right|_{s^2\tau_b} = f(s^2\tau_b) - f(s^4\tau_b) \tag{4.19a}$$

$$2s^4\tau_b \left.\frac{d\Omega}{d\tau_b}\right|_{s^4\tau_b} = f(s^4\tau_b) - f(s^6\tau_b) \tag{4.19b}$$

$$\vdots \qquad \vdots \qquad \vdots \qquad \vdots$$

$$2s^{2(N-1)}\tau_b \left.\frac{d\Omega}{d\tau_b}\right|_{s^{2(N-1)}\tau_b} = f(s^{2(N-1)}\tau_b) - f(s^{2N}\tau_b) \tag{4.19c}$$

Adding equations (4.18) and (4.19a)-(4.19c) produces the summation equation

$$f(\tau_b) - f(s^{2N}\tau_b) = 2\tau_b \sum_{i=0}^{N} s^{2i} \left.\frac{d\Omega}{d\tau_b}\right|_{s^{2i}\tau_b} \tag{4.20}$$

As $N \to \infty$, $f(s^{2N}) \longrightarrow 0$. The result obtained is

$$f(\tau_b) = 2\tau_b \sum_{i=0}^{\infty} s^{2i} \left.\frac{d\Omega}{d\tau_b}\right|_{s^{2i}\tau_b} \tag{4.21}$$

or $$f(\tau_b) = 2\Omega \sum_{i=0}^{\infty} s^{2i} \left.\frac{d \ln \Omega}{d \ln \tau_b}\right|_{s^{2i}\tau_b} \tag{4.22}$$

If $q = \frac{d \ln \Omega}{d \ln \tau_b}$ is constant, as it is for a power law fluid, it may be shown that the shear rate at the bob is given by

$$f(\tau_b) = 2\Omega \sum_{i=0}^{\infty} s^{2iq} q \Big|_{s^{2i}\tau_b} \tag{4.23}$$

$$= \frac{2q\Omega}{1 - s^{2q}} \tag{4.23a}$$

4.5 COAXIAL CYLINDER MEASUREMENTS

Shear stress-shear rate data at low to medium rates of shear and yield stress measurements were obtained on the Stormer and Brookfield LVT viscometers, modified so as to provide mathematically treatable results. The Brookfield guard ring was removed and simple adaptions on both instruments permitted the use of the rotors and cup assembly from the MacMichael viscometer.

End corrections for the rotors were established with a Dow Corning 50 cs. silicone oil, which has been shown to be Newtonian up to shear rates of 10^5 sec^{-1} (19). The method outlined by Van Wazer et.al. (88) was used and involves measuring the angular velocity-Ω as a function of the torque applied to the rotor at several values of H, the depth of immersion. Experimental data are plotted as M/Ω vs. H, which is a straight line for Newtonian liquids. The line is extrapolated back to $(M/\Omega)=0$ and the negative intercept-H_o corresponding to this point gives the corrected height of the rotor as $(H+H_o)$. Figure 4-3 is a typical plot of the data taken on a modified Stormer viscometer for a 2 cm. diameter rotor in a 3.5 cm. cup and the extrapolation shows H_o to be 0.38 cm.

The yield stress for a test fluid was determined on the Stormer viscometer by noting the minimum weight required to turn the rotor. From the dimensions of the instrument, the yield stress in $dynes/cm^2$ is given as

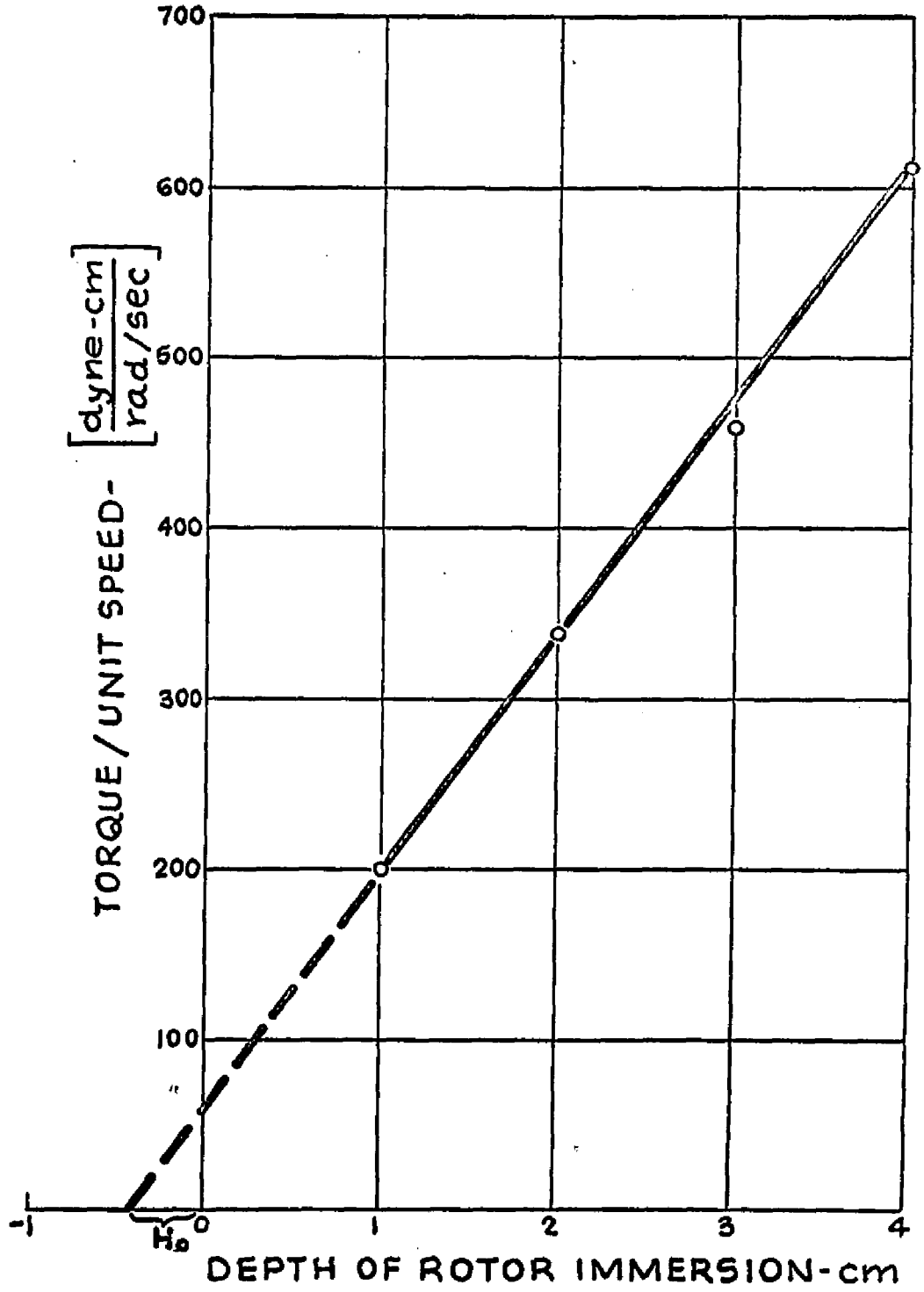

Figure 4-3. Determination of the end correction for a rotor in a modified Stormer viscometer;
test fluid - 50 c.s. silicone oil, bob radius - 1 cm, cup radius - 3.5 cm.

$$\tau_y = \frac{\frac{1.425 \times 980}{11}}{2 R_b^2 (H+H_o)} W_{min} = \frac{20.2\ W_{min}}{R_b^2 (H+H_o)} \qquad (4.24)$$

where $W_{min.}$ is the minimum weight which will turn the rotor. Yield stresses were also obtained on the Brookfield viscometer by twisting the rotor until the dial reading is at full scale and then releasing it. The dial reading where the pointer ultimately stops may be converted to a yield stress by the relation

$$\tau_y = \frac{\text{fraction of full scale reading} \times \text{dyne-cm torque for full scale reading}}{2 \pi R_b^2 (H+H_o)} \qquad (4.25)$$

A final steady state value for the yield stress was considered to be reached when the instrument reading remained constant for several hours. This criteria will not detect any fractional revolution of the rotor at rates slower than this time period.

Table 4-3 lists the yield stress determination for the viscoinelastic test fluids. Fisher et.al. (21) have also measured yield values for Carbopol solutions and their results are plotted along with the current value in figure 4-4. Good agreement is seen between the data points of Fisher and that of this investigation. Since the MPA 60 dispersions have long gelation times, they were prepared for testing by pouring a freshly sheared sample into the

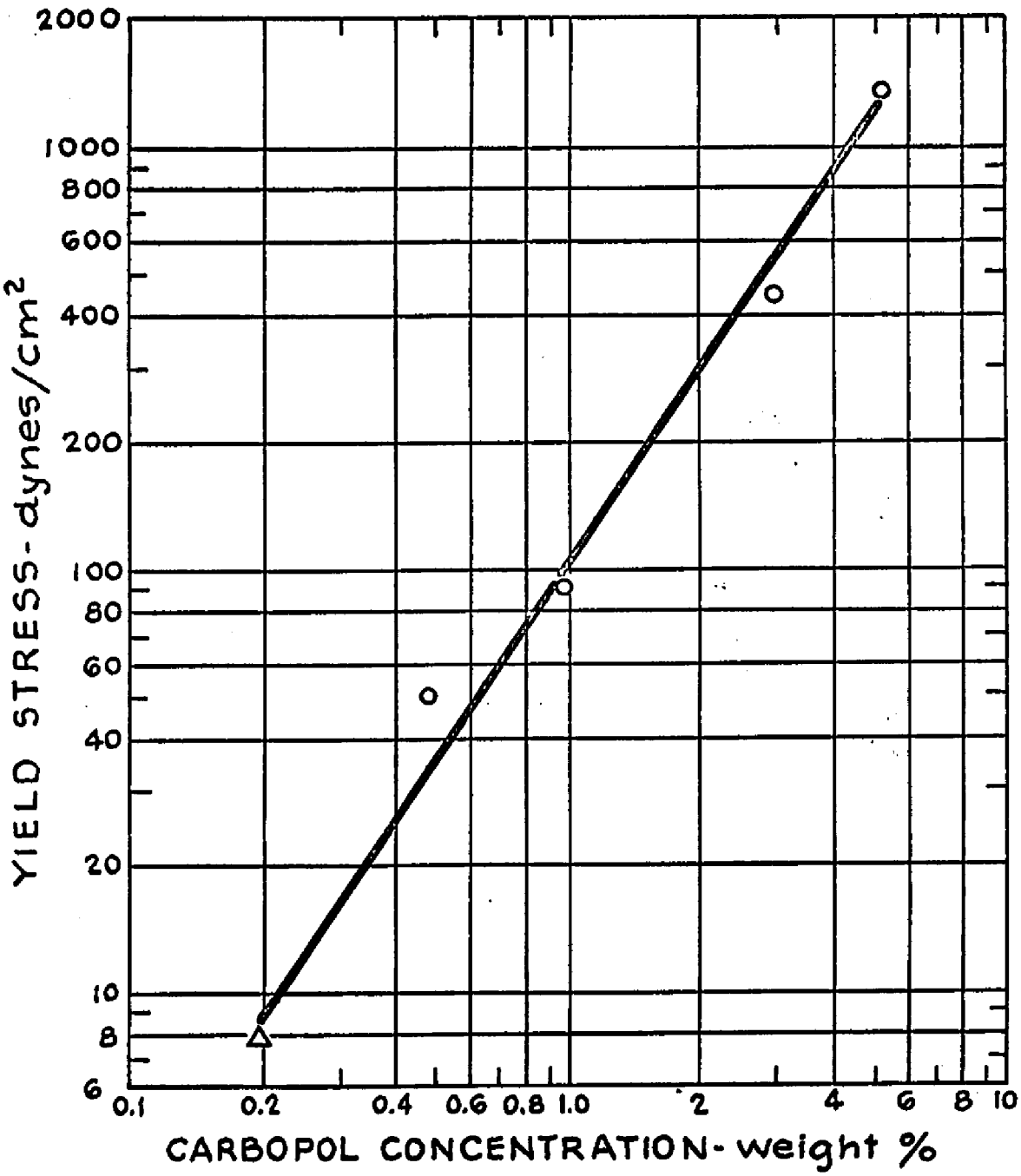

Figure 4-4. Yield stresses of Carbopol solutions; O-data of Fisher et al. (21), Δ- the present work.

annular space between the cup and rotor, then allowing the thixotropic fluid to set for 2-3 days. An appropriate cover was provided to prevent solvent evaporation. The resultant accuracy of the yield stress for these fluids is uncertain because of the tendency of the MPA 60 to separate from the rotor while undergoing gellation.

Table 4-3. Yield stresses of the viscoinelastic test liquids.

Test liquid	Yield stress
0.1% Carbopol	0 dynes/cm^2
0.2% Carbopol	8
0.6% Carbopol	55
24% MPA 60 in xylene	800
24% MPA 60 in mineral spirits	800
12.4% silica in water	2000

Shear stress vs. angular velocity measurements at the rotor were obtained on the Brookfield and Stormer viscometers for 0.1%, 0.2% and 0.6% Carbopol solutions. Similar data could not be acquired with the MPA 60 dispersions because of their thixotropic nature and is also absent for the 12.4% silica dispersion as this highly gellified fluid separated from the rotor, once motion was initiated, and did not flow back. The measurements were plotted in figure 4-5 and show that the fluids exhibit power law behavior. In all cases, the data were examined to insure that the shearing stress at the cup exceeded the yield value, a procedure which guarantees flow across the entire gap. The slope of the lines, $n = d \log \tau_b / d \log \Omega$, is given in table 4-4.

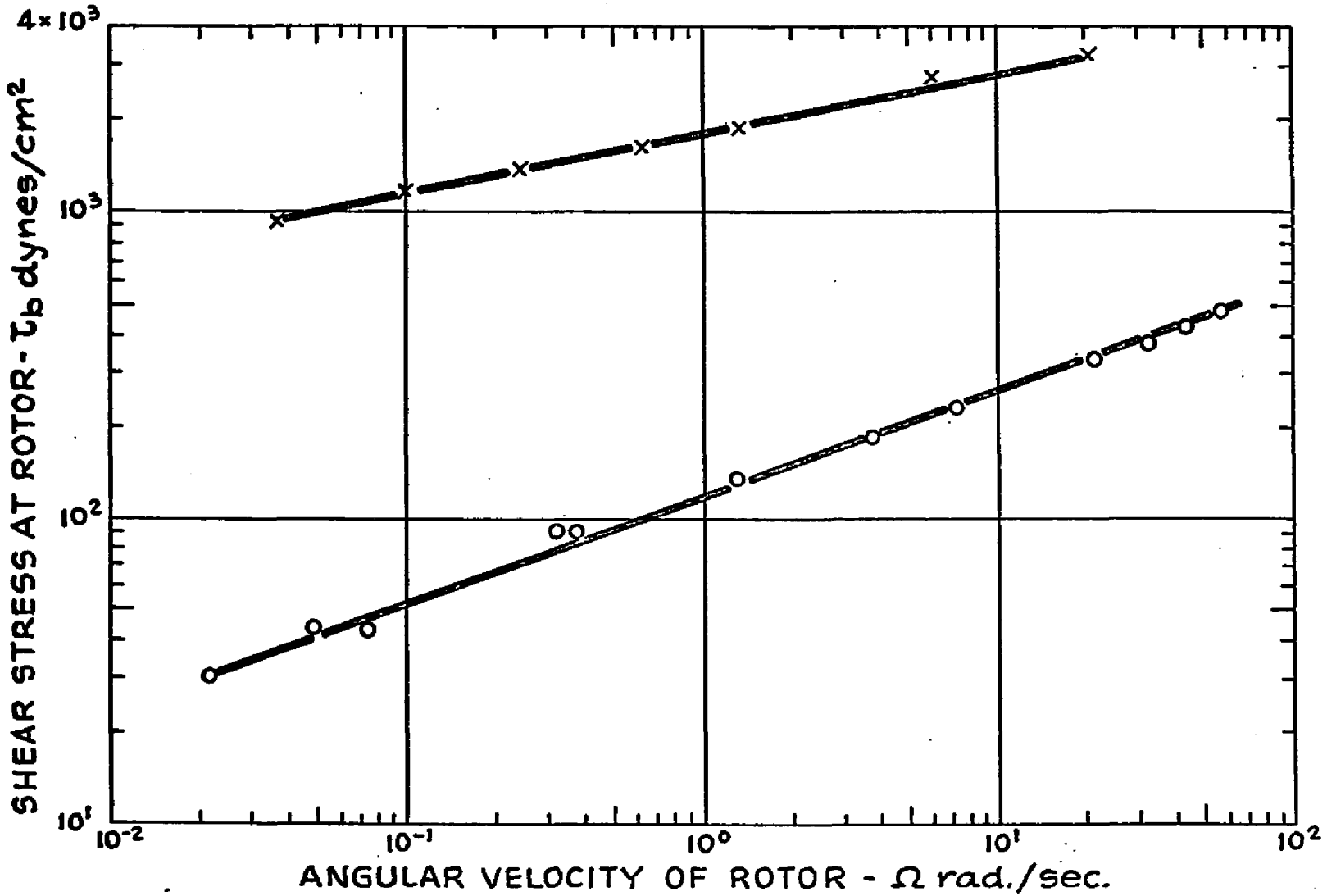

Figure 4-5. Coaxial cylinder measurements in modified Stormer and Brookfield viscometers; X-0.6% Carbopol, O-0.2% Carbopol, □-0.1% Carbopol; continued on next page.

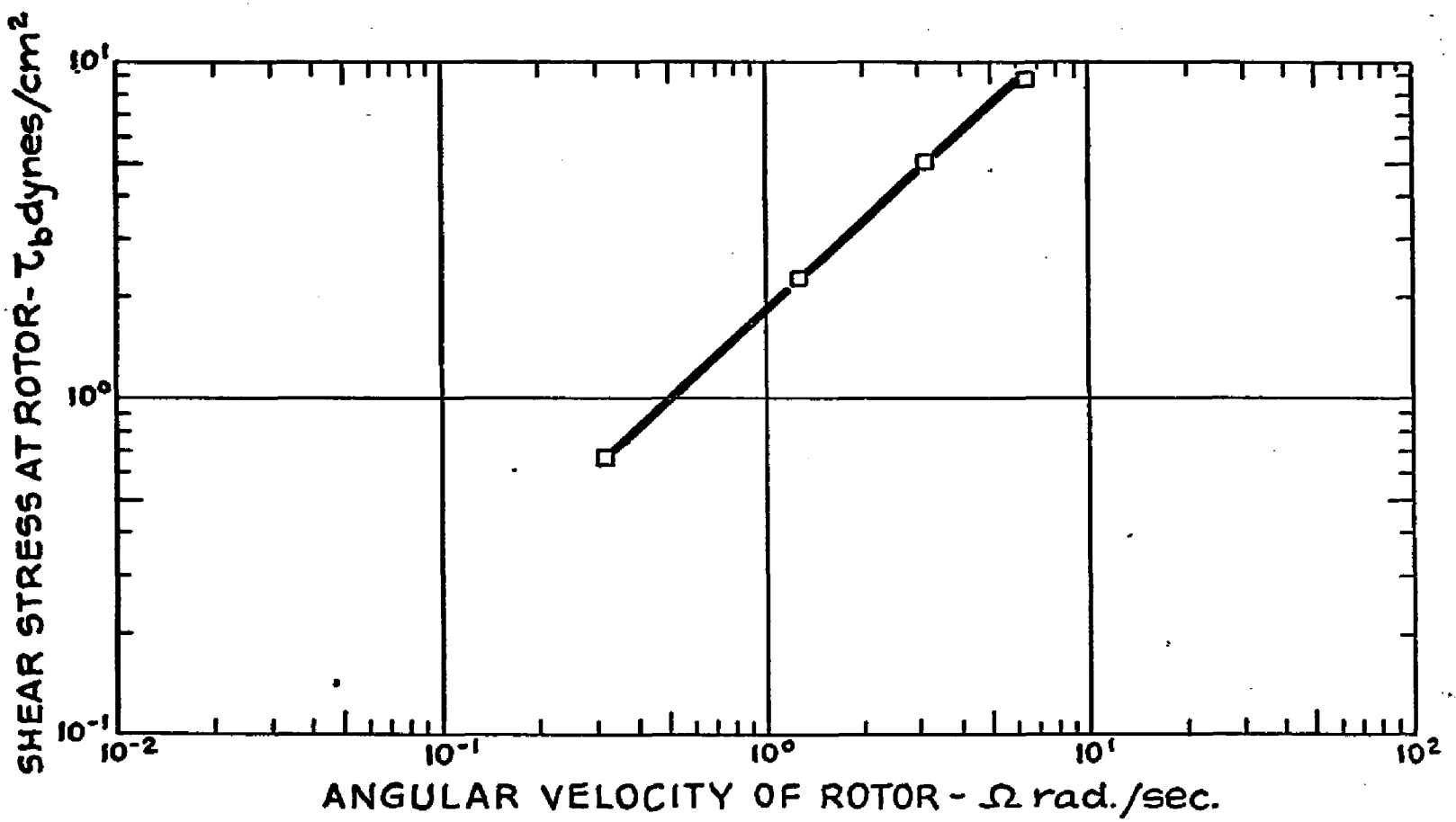

Figure 4-5. continued.

Table 4-4. Power law exponent for Carbopol solutions from coaxial cylinder viscometer measurements.

Fluid	n
0.1% Carbopol	0.88
0.2% Carbopol	0.32
0.6% Carbopol	0.20

Figure 4-5 results will be combined with the high shear rate data from the capillary viscometer in section 4.8 to provide shear stress-shear rate data over a wide range.

4.6 DEVELOPMENT OF THE CAPILLARY FLOW EQUATIONS

Viscometric data at high shear rates were obtained with a capillary viscometer.

The classical Rabinowitsch derivation for the wall shear rate of a general fluid will be modified to show that the existence of a yield stress does not alter the final result. A typical section of a capillary tube is shown in figure 4-6.

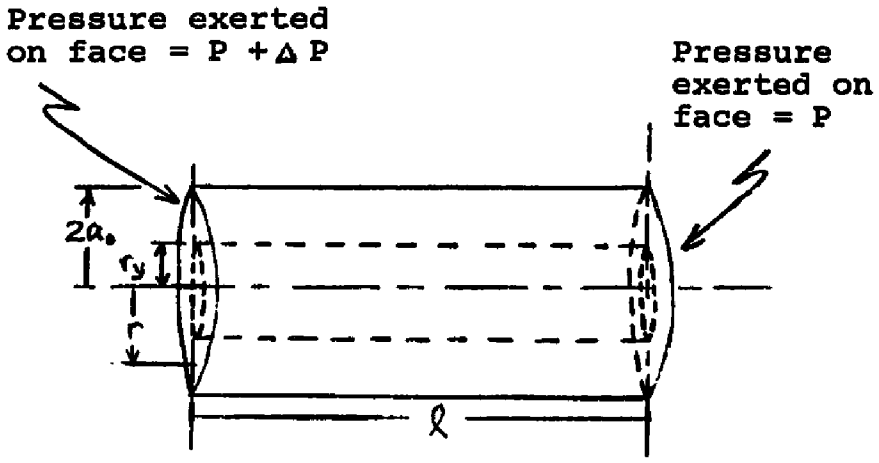

Figure 4-6. Force balance for a capillary viscometer.

The pressure- ΔP acting on the ends of the fluid cylinder exerts a force-F equal to

$$F = \Delta P \cdot \pi r^2 \tag{4.26}$$

If the fluid possesses a yield stress, viscous flow will occur only over that portion of the capillary crossection where the shear stress exceeds the yield value; otherwise, plug flow results. Above the critical radius for flow-r_y, the force arising from the pressure is resisted by the viscous restraining forces

$$F = \tau \cdot 2\pi r l \tag{4.27}$$

where τ is the shearing stress. In steady flow, the two forces are equal

$$\tau = \frac{\Delta P r}{2l} \qquad r > r_y \tag{4.28}$$

At the capillary wall, equation (4.28) may be written as

$$\tau_w = \frac{\Delta P a_o}{2l} \tag{4.29}$$

Dividing equation (4.28) by equation (4.29) gives the linear relation between the shearing stress and the radius.

$$\frac{\tau}{\tau_w} = \frac{r}{a_o} \qquad r > r_y \tag{4.30}$$

As indicated, it is valid for all values of the radius greater than the critical radius.

The flow rate through the capillary tube is given by

$$Q = \int_0^{a_0} 2\pi r V_z(r) dr \tag{4.31}$$

Integrating by parts and invoking the zero slip condition at $r = a_0$

$$Q = \int_0^{a_0} \pi r^2 \left(-\frac{dV_z}{dr}\right) dr \tag{4.32}$$

or $$Q = \int_0^{r_y} \pi r^2 \left(-\frac{dV_z}{dr}\right) dr + \int_{r_y}^{a_0} \pi r^2 \left(-\frac{dV_z}{dr}\right) dr \tag{4.33}$$

But $\left(\frac{dV_z}{dr}\right) = 0$ for $0 < r < r_y$ and equation (4.33) reduces to

$$Q = \int_{r_y}^{a_0} \pi r^2 f(\tau) dr \tag{4.34}$$

where $f(\tau)$ has been defined as $-\frac{dV_z}{dr}$

By virtue of equation (4.30), (4.34) may be written as

$$\frac{4Q}{\pi a_0^3} = \frac{4}{\tau_w^3} \int_{\tau_y}^{\tau_w} f(\tau) \tau^2 d\tau \tag{4.35}$$

Differentiating equation (4.35) with respect to τ_w

$$\frac{d}{d\tau_w}\left(\frac{4Q}{\pi a_0^3}\right) = -\frac{12}{\tau_w^4} \int_{\tau_y}^{\tau_w} f(\tau)\tau^2 d\tau + \frac{4}{\tau_w} f(\tau_w) - \frac{4}{\tau_w^3} f(\tau_y)\tau_y^2 \frac{d\tau_y}{d\tau_w} \tag{4.36}$$

The last term on the right hand side of (4.36) is identically zero since $f(\tau_y) = 0$. Rearranging equation (4.36)

with the aid of (4.35) results in an expression for the wall shear rate for a general fluid in terms of macroscopically measurable variables.

$$\frac{d}{d\tau_w}\left(\frac{4Q}{\pi a_o^3}\right) = -\frac{3}{\tau_w}\left(\frac{4Q}{\pi a_o^3}\right) + \frac{4f(\tau_w)}{\tau_w} \qquad (4.37)$$

$$\text{or } f(\tau_w) = \frac{3+q}{4}\left(\frac{4Q}{\pi a_o^3}\right) \qquad (4.38)$$

$$\text{where } q \text{ is defined as } \quad q = \frac{d\ \ln(4Q/\pi a_o^3)}{d\ \ln \tau_w} \qquad (4.39)$$

It is usual to plot τ_w vs. $\frac{4Q}{\pi a_o^3}$ and to define the slope as $n = 1/q$. Equation (4.38) is alternately written as

$$f(\tau_w) = \frac{3n+1}{4n}\left(\frac{4Q}{\pi a_o^3}\right) \qquad (4.40)$$

Many pseudoplastic fluids are found to obey the relation

$$\tau_w = \frac{\Delta P a_o}{2l} = K'\left(\frac{4Q}{\pi a_o^3}\right)^n \qquad (4.41)$$

This may be put into the standard form for the power law,

$$\tau_w = K\,[f(\tau_w)]^n = K\dot{\gamma}_w^n \qquad (4.42)$$

$$\text{by the relation } \quad K = K'\left(\frac{4n}{3n+1}\right)^n \qquad (4.43)$$

The entrance and exit losses for flow through a capillary may be eliminated by taking pressure drop

measurements with capillaries of two different lengths but at the same flow rate. This method, originally used by Couette, is discussed in Fredrickson (22). Consider a capillary of length- ℓ_L in which the pressure drop is ΔP_L and a short capillary in which the corresponding quantities are ℓ_s and ΔP_s , respectively. The total pressure drop through the capillary may be written as the sum of an entrance loss- ΔP_{ent}, an exit loss - ΔP_{ex} and a pressure drop due to fully developed flow - ΔP_f.

$$\Delta P_L = \Delta P_{ent} + (\Delta P_f)_L + \Delta P_{ex} \tag{4.44}$$

$$\Delta P_s = \Delta P_{ent} + (\Delta P_f)_s + \Delta P_{ex} \tag{4.45}$$

Since the flow rates are identical, the entrance and exit losses are the same for each capillary. Subtracting equation (4.45) from (4.44) gives the corrected pressure drop over the length- $\ell = (\ell_L - \ell_s)$ as

$$\frac{\Delta P}{\ell} = \frac{\Delta P_L - \Delta P_s}{\ell_L - \ell_s} \tag{4.46}$$

4.7 CAPILLARY VISCOMETER MEASUREMENTS

Shear stress-shear rate measurements were obtained with a capillary viscometer. The Couette two capillary method just described was used to eliminate entrance and exit effects. An Instron mechanical tester was used to drive the fluid from the hydraulic storage cylinder through the capillary. The constant speed feature of this instrument makes it highly convenient for this type of

experiment, where it is necessary to achieve a fixed volumetric flow rate in capillaries of varying diameter and length. Pressure drops were measured with a calibrated strain gage transducer while flow rates were accurately known from the Instron crosshead travel. A more detailed discussion of procedures is available in chapter 3. The nozzles were sufficiently long to ensure fully developed flow.

The original test data for the fluids, taken in the capillary viscometer, are tabulated in appendix A . From these measurements, plots were prepared of the wall shear stress as a function of the apparent shear rate and, as seen in figure 4-7, the fluids exhibit power law behavior. Table 4-5 summarizes the power law constants- K' and n from the relation: $a_o \Delta P/2\ell = K'(4V_o/a_o)^n$

Table 4-5 Power law constants from capillary viscometer data

Test fluid	K'	n
24% MPA 60 in xylene	8.9 $\frac{\text{dynes-sec}^n}{\text{cm}^2}$	0.74
24% MPA 60 in mineral spirits	3.8	0.79
12.4% silica-water	22.5	0.60
0.2% Carbopol	11.7	0.59
0.6% Carbopol	504	0.35

In section 4.8, the capillary viscometer measurements and those from the coaxial cylinder will be recalculated to obtain shear stress-shear rate curves.

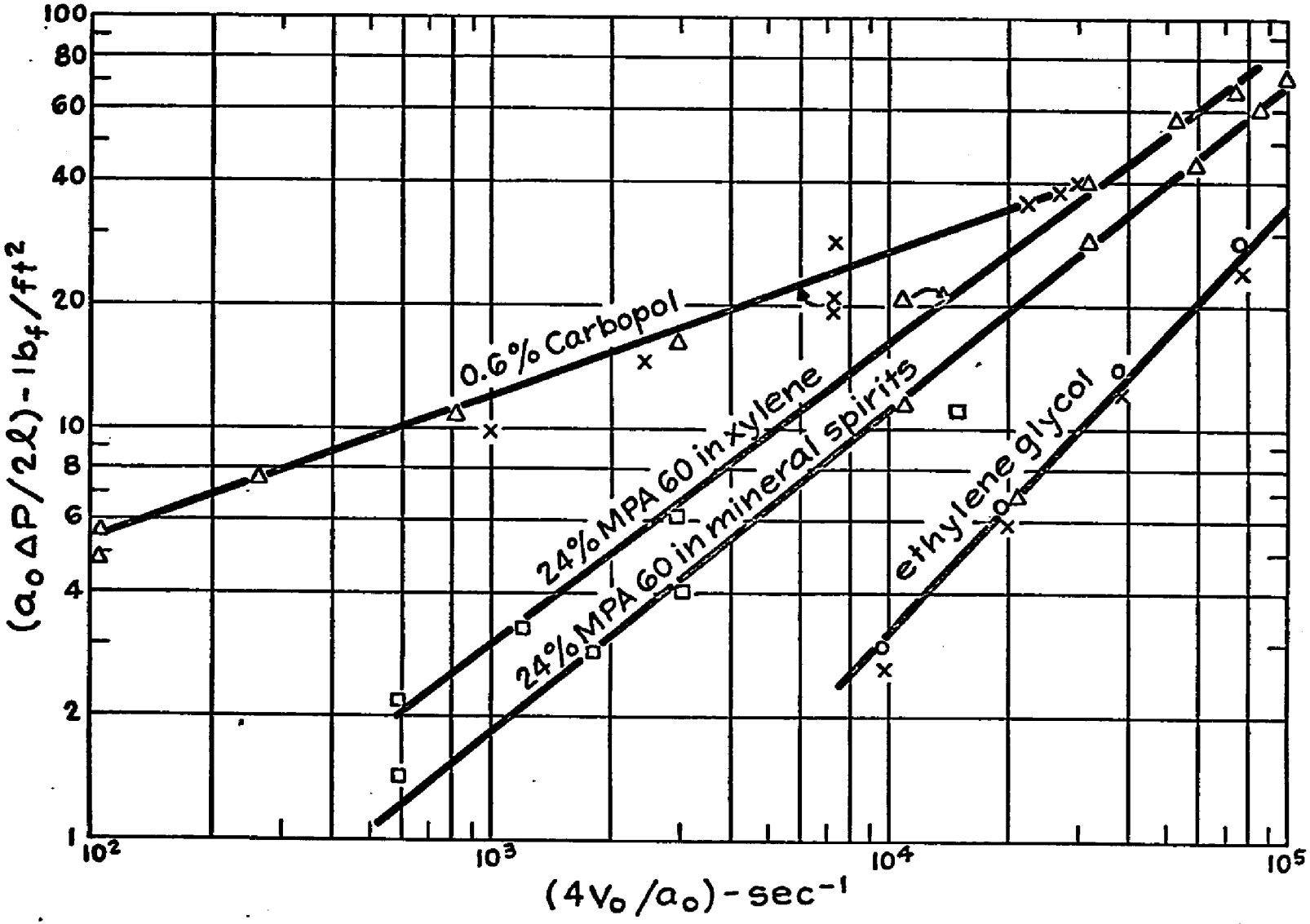

Figure 4-7 Capillary viscometer data for test fluids;
O-0.0263 cm. nozzle, X-0.0414 cm. nozzle, Δ-0.0868 cm. nozzle,
□-0.228 cm. nozzle;
continued on next page.

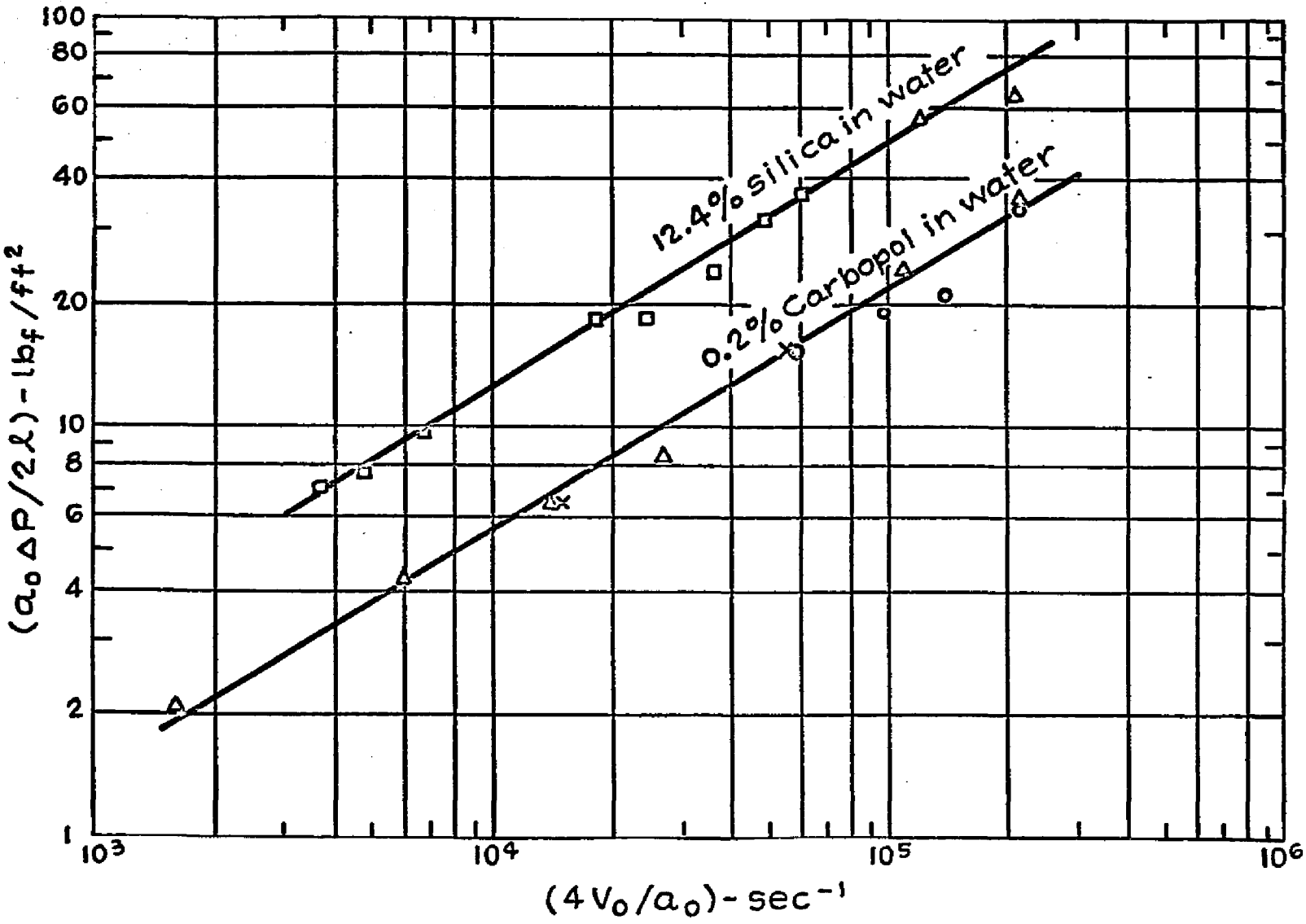

Figure 4-7. continued.

4.8 SHEAR STRESS-SHEAR RATE DATA

The true shear rate for data taken with the coaxial cylinder viscometer was obtained from equation (4.23a). This requires the angular velocity of the rotor- Ω , the ratio of the bob radius to the cup radius- s and the slope of the double logarithmic plot: $\log \Omega$ vs. $\log \tau_b$. The shear stress at the rotor is given by equation (4.1). For fluids with a yield stress, the data should be trimmed to exclude any measurements where $\tau_y > \tau_c$.

In a similar manner, equation (4.40) gives the true shear rate for data taken with the capillary viscometer. The input required for this equation is the flow rate-Q, the capillary radius- a_o and the slope of the double logarithmic plot: $\log \tau_w$ vs. $\log 4V_o/a_o$. Equation (4.29) is used to obtain the wall shear stress.

The shear stress-shear rate curves obtained for the test fluids are given in figure 4-8. Data for 0.2 % Carbopol and 0.6% Carbopol show a 'flattening' of the curve at low shear rates as the yield stress becomes a significant portion of the total applied stress. At higher shear rates, the usual power law behavior is indicated.

Shear stress-shear rate measurements are available in the published literature for most of the viscoelastic fluids used in this investigation- 0.05% and 0.25% Separan (77,78), 0.25% SCMC (48), 0.7% SCMC (52) and 0.05% Guar Gum (91).

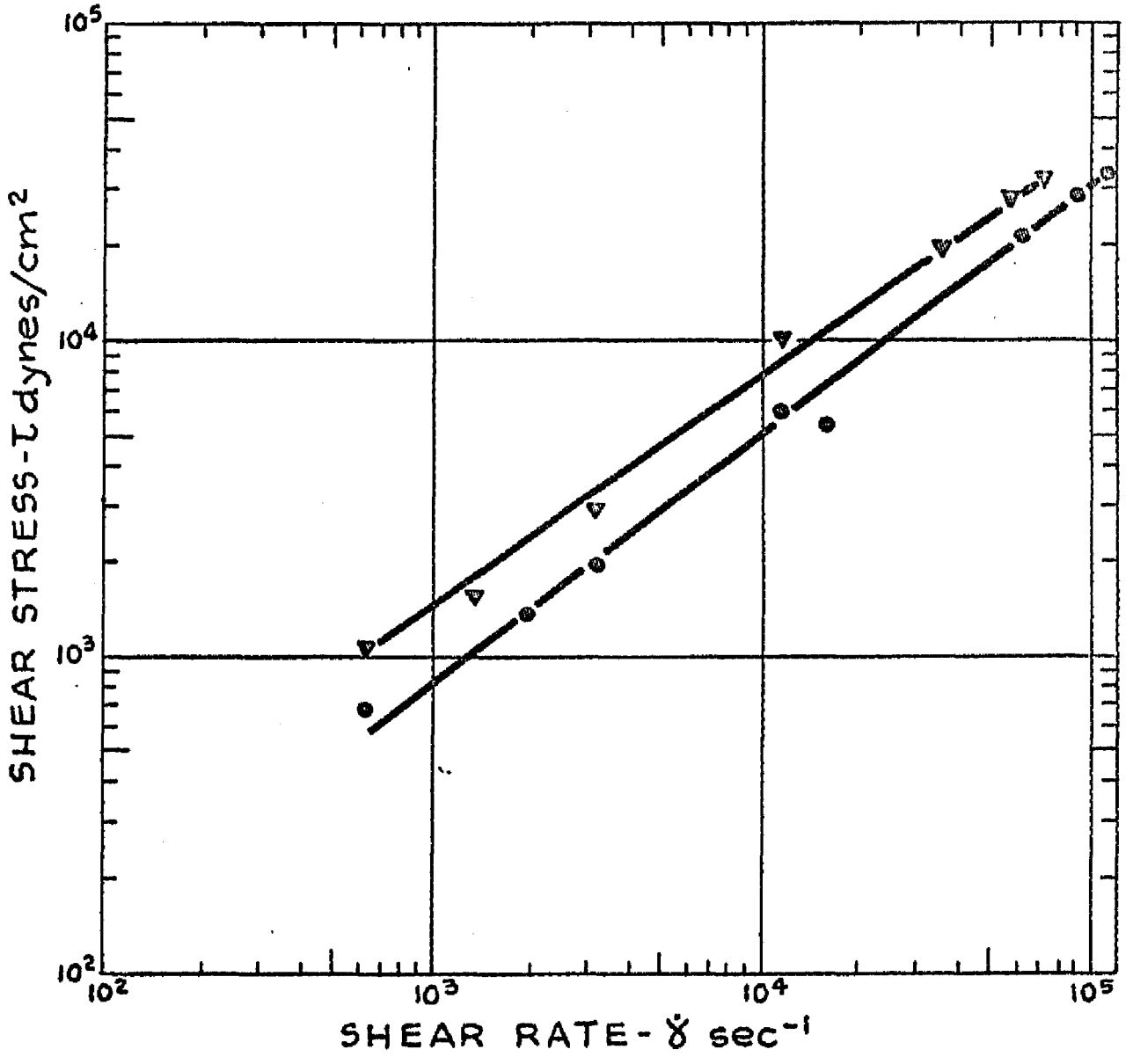

Figure 4-8. Shear stress - shear rate relations for test fluids;
▼-24% MPA 60 in xylene, ●-24% MPA 60 in mineral spirits, ◆-12.4% silica in water, O-0.1% Carbopol, Δ:▲-0.2% Carbopol, □:■-0.6% Carbopol, unfilled symbols for coaxial cylinder data, filled symbols for capillary viscometer data;
continued on next page.

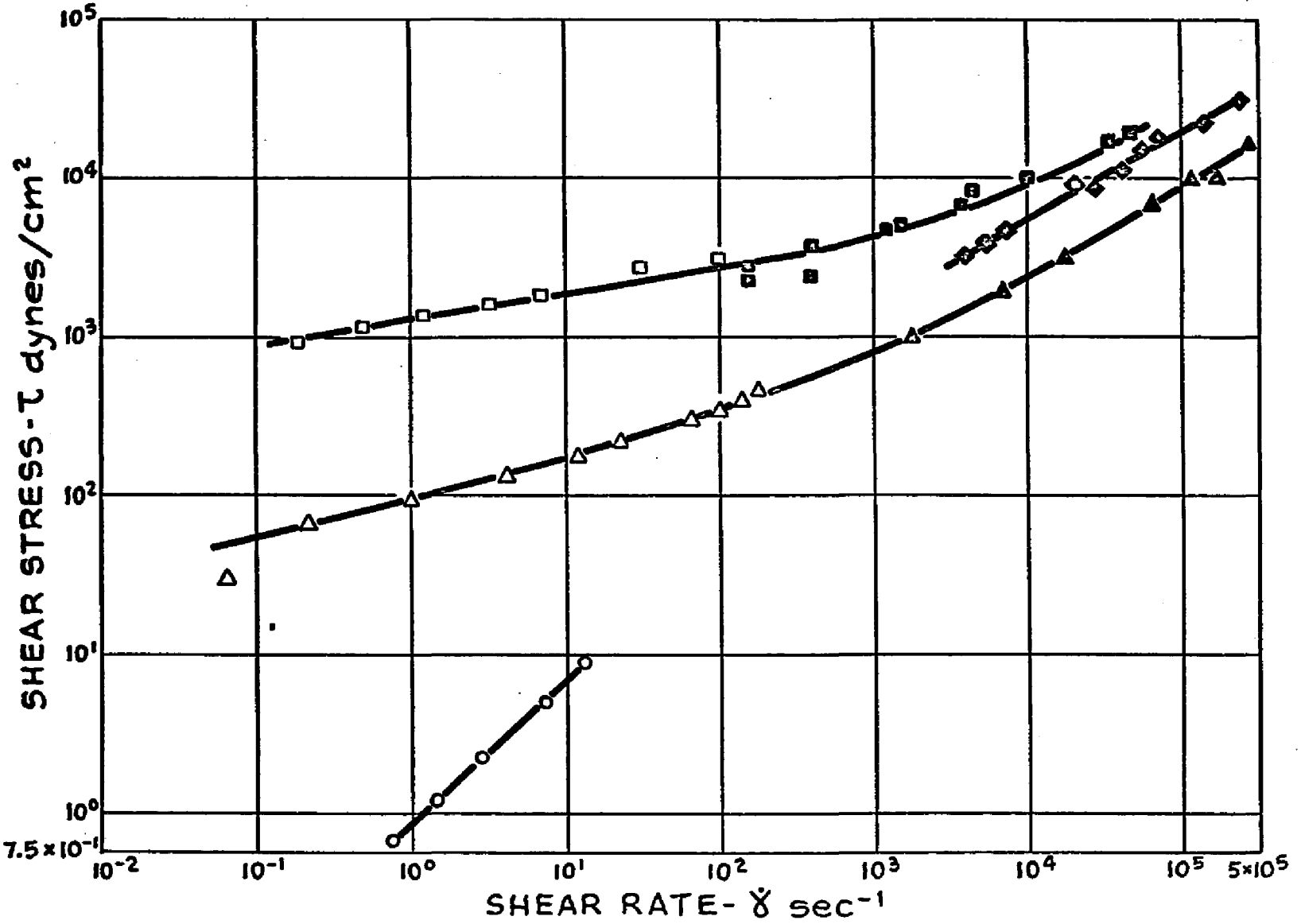

Figure 4-8. continued.

CHAPTER 5

PROFILE RELAXATION OF A LAMINAR CAPILLARY JET OF A NON-NEWTONIAN LIQUID

When a laminar capillary jet of liquid emerges from the nozzle into ambient air, it experiences a sudden removal of the confining wall. As a consequence of this, all stresses resulting from the previous shear flow will decay with increasing axial distance and the velocity profile will tend towards a uniform flow. Whether or not, the capillary jet is ever completely relaxed within its life-time depends upon the rate of stress relaxation. This in turn is a function of the rheological character of the fluid and the flow velocity.

Stress relaxation results in a diameter change which may be larger, smaller or unchanged from the nozzle bore. Experimentally, a jet diameter which remains constant with increasing axial distance is taken as evidence that the stress relaxation is complete.

The mechanism of profile decay in non-Newtonian jets is complicated by the fact that these fluids possess a three dimensional structure whose spatial configuration depends upon the local rate of shear. For example, polymer molecules in solution are believed to exist as a randomly entangled network of chains bound together by secondary chemical bonds. Under shear, these macromolecules tend to elongate and orient themselves with their major axes

parallel to the flow direction.

At the high shear rates of capillary flow, the three dimensional, 'zero shear' structure of the fluid is largely destroyed and a finite time is required outside of the capillary before it is regained. If the liquid possesses a structural formation time which is short compared to the time required for stress relaxation, then profile decay should occur at a rate corresponding to the liquid's zero shear viscosity. At the other extreme, a fluid with an 'infinite' structural formation time will relax at a rate corresponding to its apparent viscosity at the exit plane of the capillary.

This chapter investigates profile relaxation in capillary jets of non-Newtonian inelastic fluids and in viscoelastic liquids.

5.1 THE RATE OF PROFILE RELAXATION

The prediction of the rate of profile decay in Newtonian jets is facilitated by separating the analysis into two parts. A boundary layer approach is taken at large Reynolds numbers for short axial distances where the periphery of the liquid column does not interact with the core (30). At large axial distances, a linear perturbation approach is applied about the final relaxed state (32). Goren and Wronski present experimental results that are in fair agreement with their theoretical predictions.

The present effort extends the theory at large axial

distances to a capillary jet of a linear viscoelastic fluid.

5.1-1 SOLUTION OF THE DYNAMIC EQUATIONS

At some distance 'infinitely far' from the nozzle tip, the jet will have completely relaxed and attained its final values of diameter, velocity and pressure, as shown in figure 5-1. The rate of profile decay at large axial distances will be determined by performing a small perturbation analysis about the final state in a manner paralleling the development of Goren and Wronski. Frictional drag from the surroundings and gravity effects are assumed negligible. The flow is steady and the decay progresses in an axisymmetric pattern.

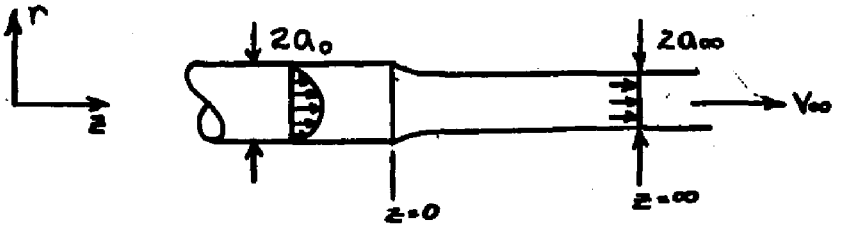

Figure 5-1 Profile relaxation of a laminar capillary jet.

In the usual notation, at $z = \infty$

$$V_r = 0 \; ; \; V_z = V_\infty \; ; \; a = a_\infty$$
$$p = p_\infty = \frac{\Sigma}{a_\infty} \; ; \; \tau_{ij} = 0 \qquad (5.1)$$

Just before $z = \infty$

$$V_r = \tilde{V}_r ; \; V_z = V_\infty + \tilde{V}_z \; ; \; a = a_\infty + \tilde{a}$$

$$p = p_\infty + \tilde{p} \; ; \; \tau_{ij} = 0 + \tilde{\tau}_{ij} \tag{5.2}$$

The perturbation quantities, designated as $\tilde{(\;)}$, are regarded as being infinitesimally small. Thus, quantities which are second order in magnitude, such as the inertial terms in the equations of motion or other non-linearities in the rheological constitutive equation, can be neglected.

The linearized equations of continuity and motion in a cylindrical coordinate system can be written as

$$\frac{1}{r}\frac{\partial}{\partial r}(r\tilde{V}_r) + \frac{\partial \tilde{V}_z}{\partial z} = 0 \tag{5.3}$$

$$\rho V_\infty \frac{\partial \tilde{V}_r}{\partial z} = -\frac{\partial \tilde{p}}{\partial r} + \frac{1}{r}\frac{\partial}{\partial r}(r\tilde{\tau}_{rr}) - \frac{\tilde{\tau}_{\theta\theta}}{r} + \frac{\partial \tilde{\tau}_{rz}}{\partial z} \tag{5.4a}$$

$$\rho V_\infty \frac{\partial \tilde{V}_z}{\partial z} = -\frac{\partial \tilde{p}}{\partial z} + \frac{1}{r}\frac{\partial}{\partial r}(r\tilde{\tau}_{rz}) + \frac{\partial \tilde{\tau}_{rz}}{\partial z} \tag{5.4b}$$

The boundary conditions state that the shear stress at the jet surface is zero since ambient effects are neglected and the radial component of the stress tensor at the periphery is balanced by the pressure due to surface tension forces. However, the position of the jet surface is unknown. Since the radius-a_∞ is much larger than the perturbation quantity-$\tilde{a}$, the boundary conditions are evaluated at

$r \approx a_\infty$. The location of this surface is given by the relation

$$\tilde{V}_r\Big|_{r\approx a_\infty} = \frac{D\tilde{a}}{Dt} \tag{5.5}$$

where the operator- $\frac{D}{Dt}$ is the usual substantial derivative. Thus, the boundary conditions are expressed as

B.C.1 $$\tilde{\tau}_{rz}\Big|_{r\approx a_\infty} = 0 \tag{5.6}$$

B.C.2 $$\left[-\tilde{p} + \tilde{\tau}_{rr}\right]_{r\approx a_\infty} = \tilde{p}_\sigma \tag{5.7}$$

where $\tilde{p}_\sigma$, the surface tension pressure is given by

$$\tilde{p}_\sigma = \frac{\sigma}{a_\infty^2}\left[\tilde{a} + a_\infty^2 \frac{\partial^2 \tilde{a}}{\partial z^2}\right] \tag{5.8}$$

B.C. 3 and 4 All velocities are finite at r=0.

The rheological properties of viscoelastic materials in the linear region are often expressed in operational form as

$$P\,\tau_{ij} = Q\,\Delta_{ij} \tag{5.9}$$

where P and Q are polynomials with constant coeficients in some convected derivative operator such as the Olydroyd (65) or Jaumann (67) derivative. Linearization of the convected derivative operator under steady flow conditions leads to polynomials in the operator $\frac{\partial}{\partial z}$. P and Q may then be written as

$$P = 1 + \lambda_1 V_\infty \frac{\partial}{\partial \bar{z}} + \lambda_2 V_\infty^2 \frac{\partial^2}{\partial \bar{z}^2} + \ldots + \lambda_M V_\infty^M \frac{\partial^M}{\partial \bar{z}^M} \tag{5.10}$$

$$Q = \eta_0 \left(1 + \mu_1 V_\infty \frac{\partial}{\partial \bar{z}} + \mu_2 V_\infty^2 \frac{\partial^2}{\partial \bar{z}^2} + \ldots + \mu_N V_\infty^N \frac{\partial}{\partial \bar{z}^N} \right. \tag{5.11}$$

The viscoelastic fluid has zero shear viscosity- η_0 and the $\lambda_1, \lambda_2, \ldots, \lambda_M, \mu_1, \mu_2, \ldots, \mu_N$ are properties of the material.

All variables are assumed to be expressible in the form

$$\tilde{f}(r, \bar{z}) = F(r) e^{-h\bar{z}/a_\infty} \tag{5.12}$$

By equation (5.12), the constitutive equation becomes

$$\tilde{\tau}_{ij} = \eta(h) \Delta_{ij} \tag{5.13}$$

$$\eta(h) = \eta_0 \frac{1 - \left(\frac{h V_\infty}{a_\infty}\right)\mu_1 + \left(\frac{h V_\infty}{a_\infty}\right)^2 \mu_2 - \ldots + (-1)^M \left(\frac{h V_\infty}{a_\infty}\right)^M \mu_M}{1 - \left(\frac{h V_\infty}{a_\infty}\right)\lambda_1 + \left(\frac{h V_\infty}{a_\infty}\right)^2 \lambda_1 - \ldots + (-1)^N \left(\frac{h V_\infty}{a_\infty}\right)^N \lambda_N} \tag{5.13a}$$

The equations of continuity and motion are similarly modified to

$$\frac{1}{r} \frac{\partial (r \tilde{V}_r)}{\partial r} - \frac{h \tilde{V}_z}{a_\infty} = 0 \tag{5.14}$$

$$-\rho \frac{V_\infty h}{a_\infty} \tilde{V}_r = -\frac{\partial \tilde{p}}{\partial r} + \eta(h) \left[\frac{\partial}{\partial r} \left(\frac{1}{r}\right) \frac{\partial}{\partial r} (r \tilde{V}_r) + \left(\frac{h}{a_\infty}\right)^2 \tilde{V}_r \right] \tag{5.15}$$

$$-\rho \frac{V_\infty h}{a_\infty} \tilde{V}_z = \frac{h}{a_\infty} \tilde{p} + \eta(h)\left[\frac{1}{r}\frac{\partial}{\partial r}\left(r \frac{\partial \tilde{V}_z}{\partial r}\right) + \left(\frac{h}{a_\infty}\right)\tilde{V}_z\right] = 0 \qquad (5.16)$$

Equations (5.15) and (5.16) are crossdifferentiated to eliminate the pressure term. A stream function $\tilde{\Psi}$ is defined as

$$\tilde{V}_r = \frac{1}{r}\frac{\partial \tilde{\Psi}}{\partial z} = -\frac{h}{a_\infty}\frac{\tilde{\Psi}}{r} \; ; \; \tilde{V}_z = \frac{1}{r}\frac{\partial \tilde{\Psi}}{\partial r} \qquad (5.17)$$

With the introduction of the stream function, a partial differential equation in $\tilde{\Psi}$ is obtained with the complex Reynolds number- $Re_\infty(h) = \frac{2a_\infty V_\infty \rho}{\eta(h)}$ as parameter.

$$D\left[D + \frac{h}{a_\infty^2} Re_\infty(h)\right]\tilde{\Psi} = 0 \qquad (5.18)$$

$$\text{where } D = \frac{\partial^2}{\partial r^2} - \frac{1}{r}\frac{\partial}{\partial r} + \frac{\partial^2}{\partial z^2} \qquad (5.18a)$$

The complete solution to (5.18) is

$$\tilde{\Psi} = [\tilde{\Psi}_1(r) + \tilde{\Psi}_2(r)]e^{-hz/a_\infty} \qquad (5.19)$$

where $\tilde{\Psi}_1(r)$ is the solution to $D\tilde{\Psi}_1(r)=0$ and
$\tilde{\Psi}_2(r)$ is the solution to $\left[D + \frac{h}{a_\infty^2} Re_\infty(h)\right]\tilde{\Psi}_2(r)=0$

The result is

$$\tilde{\Psi} = [\, AhJ_1(hr/a_\infty) + BhY_1(hr/a_\infty) + CmJ_1(mr/a_\infty) + \qquad (5.20)$$
$$+ EmY_1(mr/a_\infty)]e^{-hz/a_\infty}$$

where $m^2=h^2 + h*Re_\infty(h)/2$ (5.21)

J_n ( ) and Y_n( ) are modified Bessel functions of order n. The constants A,B,C,E are to be evaluated by the boundary conditions.

Insertion of the boundary conditions, after appropriate modification with the stream function, results in a characteristic equation for the damping coefficient-h as a function of the complex Reynolds number and a surface tension parameter-$S(h) = \sigma \rho a_\infty / \eta^2(h)$. The result is

$$4h^3 \left[\frac{mJ_0(m)}{J_1(m)} \right] + 2(m^2-h^2)h - (m^2+h^2)\frac{J_0(h)}{J_1(h)} = S(1+h^2)h \quad (5.22)$$

5.2 SOLUTION OF THE CHARACTERISTIC EQUATION

Equation (5.22) permits an infinite number of solutions and any perturbation quantity would be given by the sum of an infinite series. At large axial distances, the profile rearrangement should be controlled by the lowest eigenvalue since its decay rate is the slowest.

The lowest eigenvalue for the profile decay of a capillary jet of a Maxwell model fluid has been calculated by trial and error procedure and is given in figure 5-2 as a function of the final Reynolds number, with the Deborah number as parameter. For this viscoelastic fluid, the following definitions apply. The viscosity $\eta(h)$ is given by

$$\eta(h) = \frac{\eta_0}{1 - h\left(\frac{\lambda_1 V_m}{a_\infty}\right)} \quad (5.23)$$

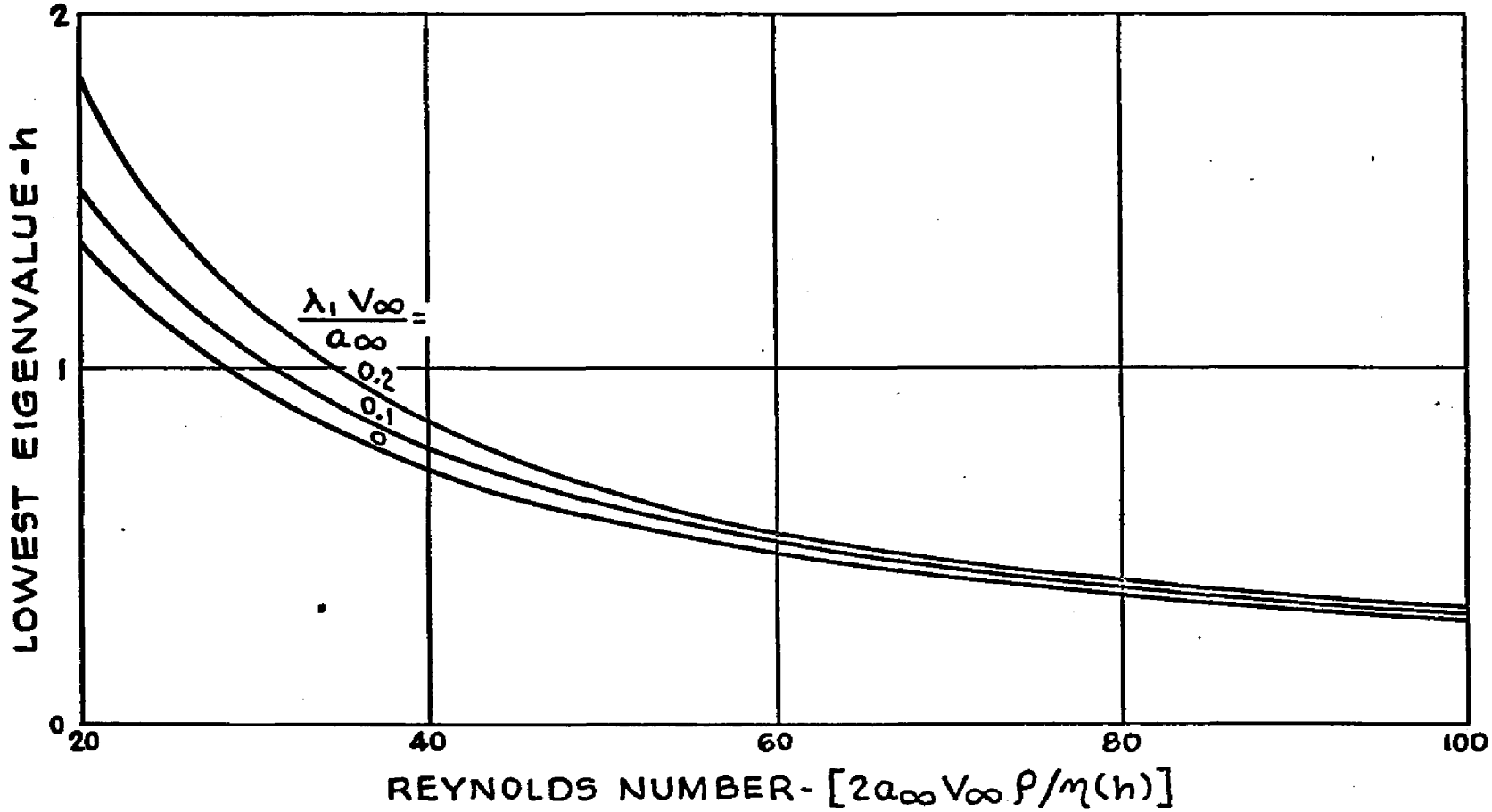

Figure 5-2 The lowest eigenvalue for a relaxing Maxwell model jet as a function of the final Reynolds number; surface tension parameter S = 0, complex viscosity - $\eta(h) = \eta_0 / \left[1 - \left(\frac{\lambda_1 V_\infty}{a_\infty}\right) h\right]$.

The final Reynolds number and Deborah number are expressed as

$$(Re_\infty) = \frac{2a_\infty V_\infty \rho}{\eta(h)} \quad ; (Deb_\infty) = \frac{\lambda_1 V_\infty}{a_\infty} \qquad (5.23a)$$

Over the range of Reynolds numbers investigated, variations in the surface tension parameter between S=0 and S=60 did not affect the eigenvalues shown in the figure to any significant extent.

The results of figure 5-2 show that a Maxwell model fluid relaxes faster than a Newtonian fluid of the same zero shear viscosity. This prediction is compared to experimental data in the next section. Under typical laboratory conditions of V_∞ = 200 cm/sec and $(2a_\infty)$ = 0.2 cm., a relaxation time of 10^{-4} seconds is required for a Deborah number of 0.2 . This value is in agreement with estimates of the relaxation time of polymer solutions at high shear rates as calculated from independent experimental data (55).

5.3 EXPERIMENTAL PROCEDURES

Photographs were taken of capillary jets of Newtonian, non-Newtonian inelastic and viscoelastic fluids along their length in the region immediately outside of the capillary. Measurements were then made of the jet diameter as a function of axial distance which will be related to the rate of decay of stresses generated during the previous

shear flow.

Photographic magnifications of approximately 10/1 were obtained on a 4"x5" bellows camera equipped with a Polaroid back. A reference rod of known diameter which was sized to fit snuggly within the nozzle bore was also photographed at each location. This provided absolute dimensions to correct for variations in the photographic magnification along the jet length due to the unavoidable non-parallelism between the plane of the jet and the plane of the camera. A profile projector equipped with a micrometer stage measured jets diameters from the photographs and the values reported are considered accurate to three significant figures. Chapter 3 provides a more detailed description of the procedures and equipment used.

5.4 EXPERIMENTAL MEASUREMENTS OF PROFILE DECAY

Measurements of the jet diameter as a function of axial distance from the nozzle exit were obtained for Newtonian, viscoinelastic and viscoelastic liquids. A single nozzle diameter was used and data were taken over a range of fluid velocities.

Newtonian fluids were included in order to verify the procedures and measuring techniques used in this investigation with published results. For this purpose, mixtures of glycerin and water were employed as test fluids. Their properties are given in standard handbooks and have been summarized in figure 4-1.

The shapes of capillary jets of glycerin-water mixtures are shown in figure 5-3 as a function of the axial distance from the nozzle for a series of Reynolds numbers. All the jets are seen to undergo contraction within the range of variables explored. The length required for complete profile relaxation is seen to increase with the Reynolds number.

The diameter ratio- $\chi = a_\infty/a_o$, is plotted in figure 5-4 and is seen to be a decreasing function of the Reynolds number. Only at the highest Reynolds number does χ approach the theoretical limit (35) of $\chi = \sqrt{3}/2$. Data points from this investigation fall smoothly within the dotted lines representing the scatter in published data (26,32,60).

The prediction of exponential decay at large axial distances was tested by plotting $\ln(\frac{a-a_\infty}{a_\infty})$ vs. $\ln(z/a_\infty)$ as in figure 5-5 and the resulting straight lines confirm this expectation. From the slope of the lines, the damping coefficient is obtained. These values are plotted in figure 5-6 as a function of the Reynolds number. Also included in this figure are the experimental results of Goren and Wronski, indicated by the shaded area, and the theoretical solution for the lowest eigenvalue with the surface tension parameter- S=0. The profile decay rates found in this research are somewhat higher than those reported by Goren and Wronski.

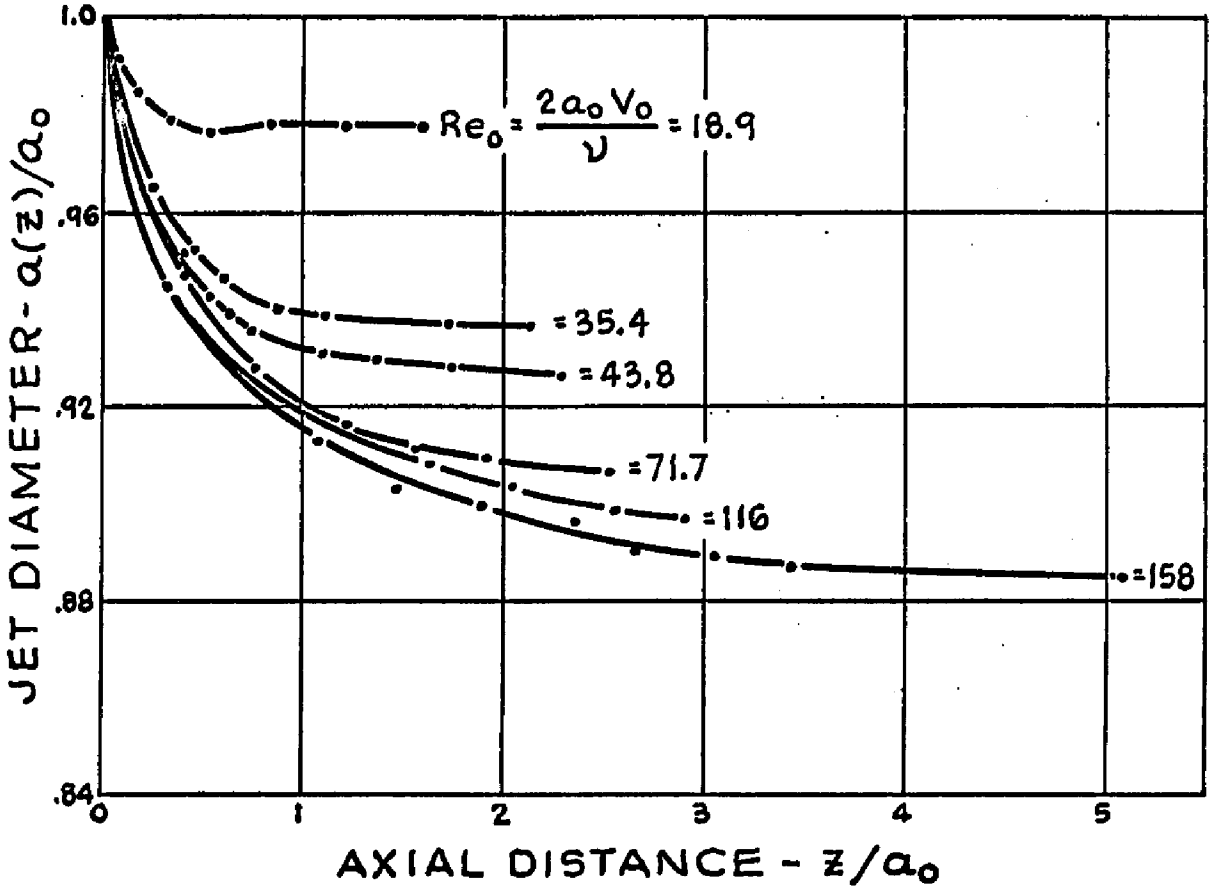

Figure 5-3 Diameter of capillary jets of glycerin-water as a function of the axial distance from the nozzle and the Reynolds number; nozzle diameter- 0.228 cm.

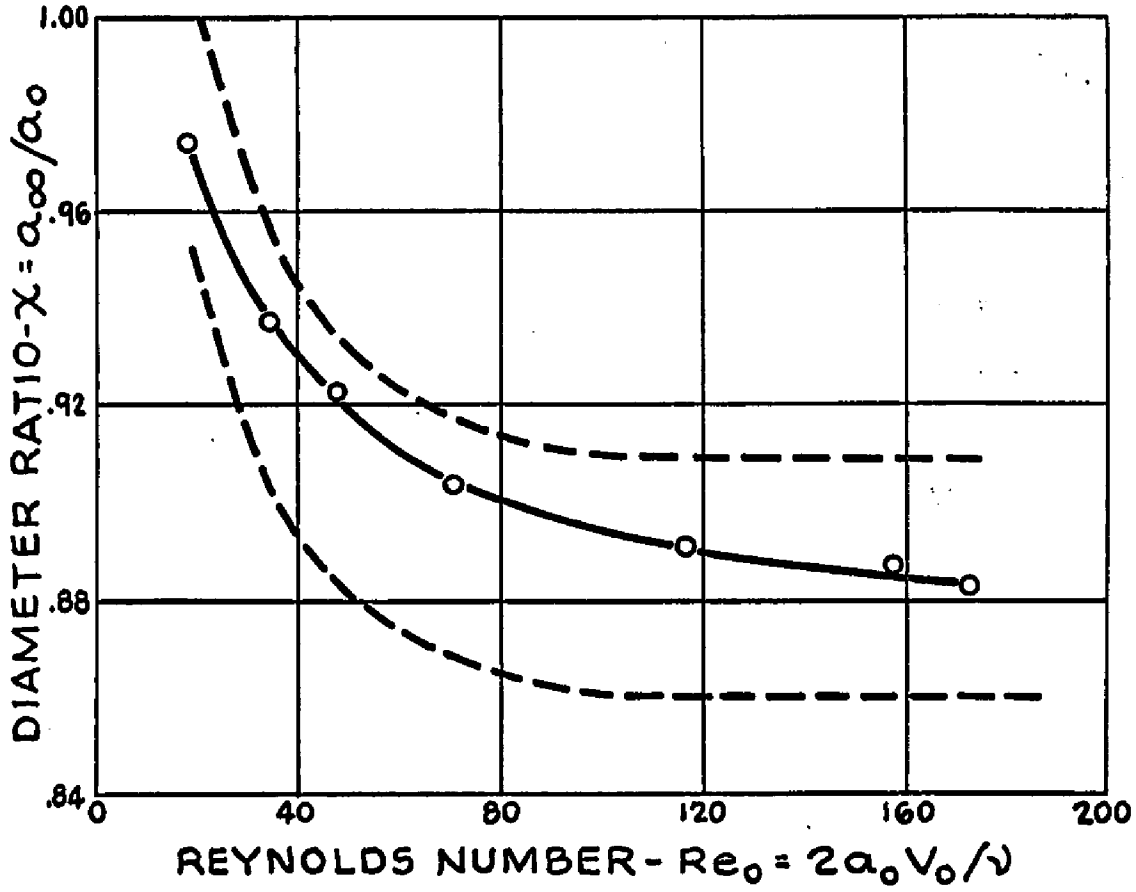

Figure 5-4 Diameter ratio of Newtonian jets as a function of the Reynolds number; ----scatter in published data (26,32,60), fluid: glycerin-water mixtures, nozzle diameter - 0.228 cm.

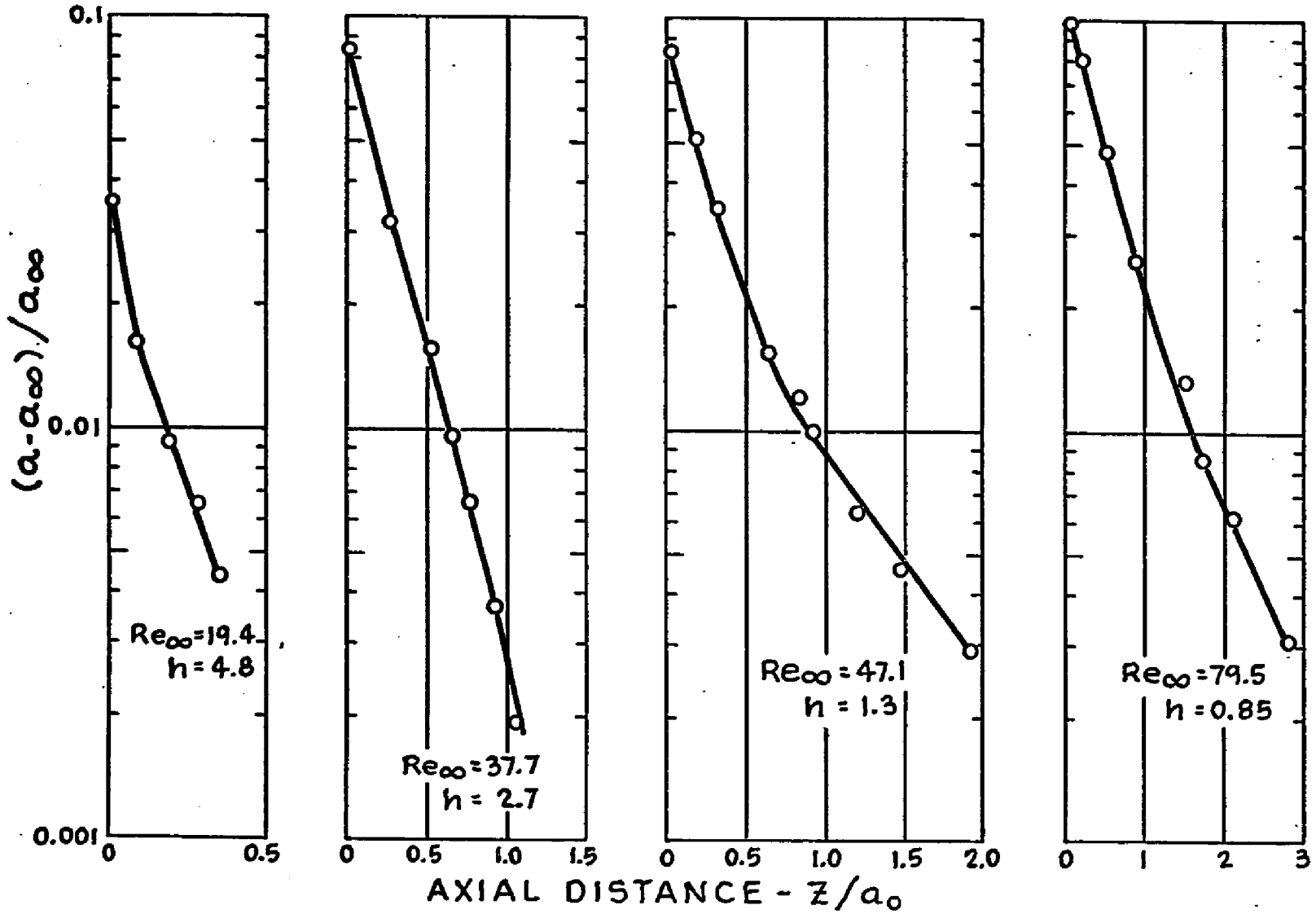

Figure 5-5 Exponential profile decay in capillary jets of glycerin-water for a series of Reynolds numbers; nozzle diameter-0.228 cm.

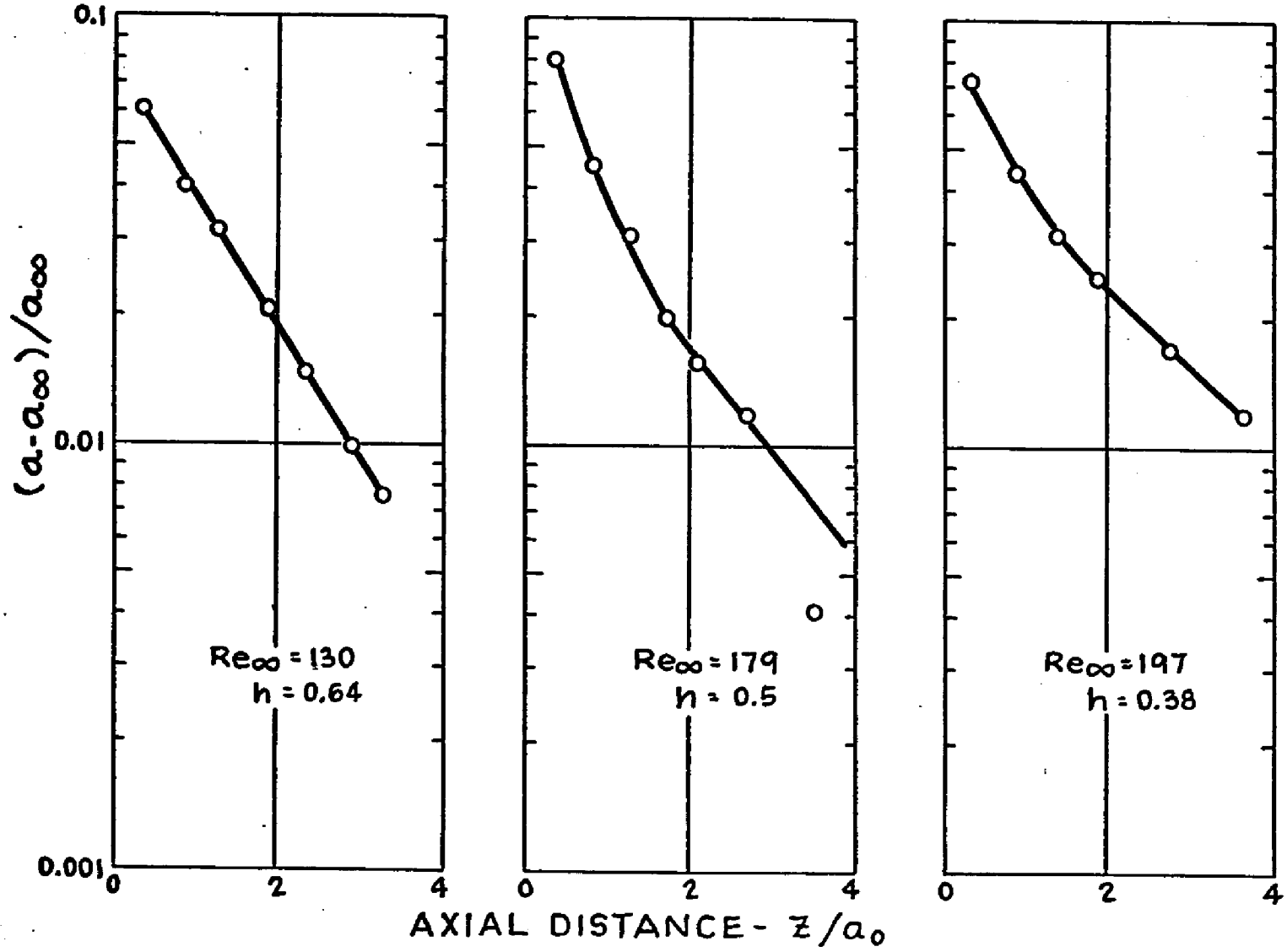

Figure 5-5 continued.

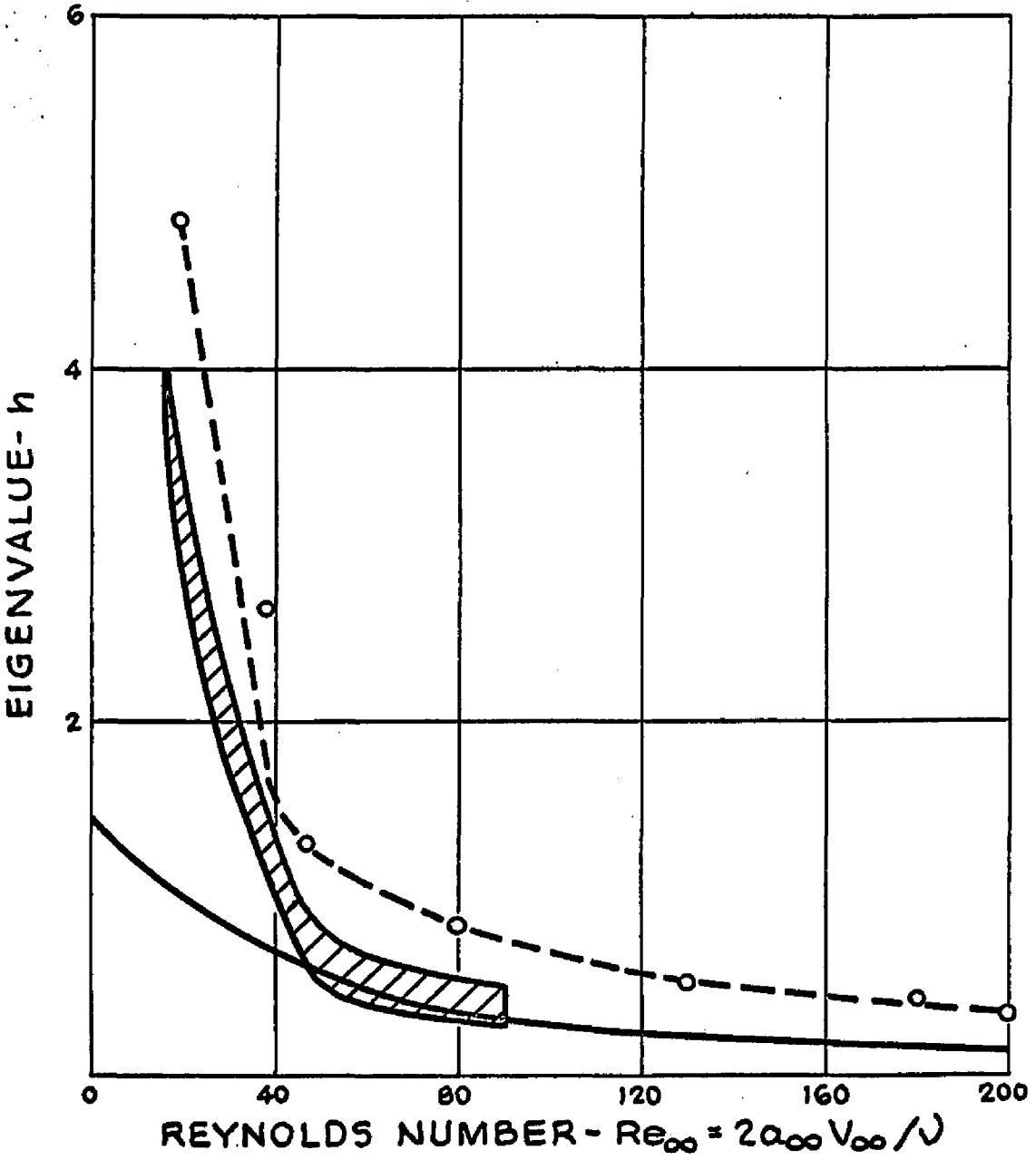

Figure 5-6 Damping coefficient for Newtonian jets as a function of the final Reynolds number; ——— Perturbation theory for S=0, shaded area - data of Goren and Wronski (32), ---- data of the current investigation.

The generally good agreement between the current measurements and published data, as typified by the comparisons in figures 5-3 through 5-6, are connotative of satisfactory techniques and procedures.

The behavior of a viscoinelastic fluid undergoing stress relaxation was investigated by obtaining profile measurements for a relaxing capillary jet of 0.6% Carbopol. Figure 5-7 shows the shape of the jet as a function of the axial distance from the nozzle for three different Reynolds numbers-Re_o', where Re_o' is the generalized non-Newtonian Reynolds number defined by Metzner and Park (53) as

$$Re_o' = \frac{(2a_o)^n (V_o)^{2-n} \rho}{K g_c 8^{n-1}} \qquad (5.24)$$

The constants K and n are the parameters in the power law constitutive equation (1.14)

The inclusion of the Reynolds number as the primary parameter influencing the profile decay rate in viscoinelastic jets is based on its similar significance for Newtonian jets. However, some commentary is necessary regarding the particular choice of Reynolds number. If it is assumed that the 0.6% Carbopol regains its structure instantly, then the Reynolds number based on its zero shear viscosity would be the correct correlating group. With such a choice, the calculated Reynolds numbers for all three flow rates would be less than unity and it is unlikely that the behavioral differences evidenced in figure 5-7 would

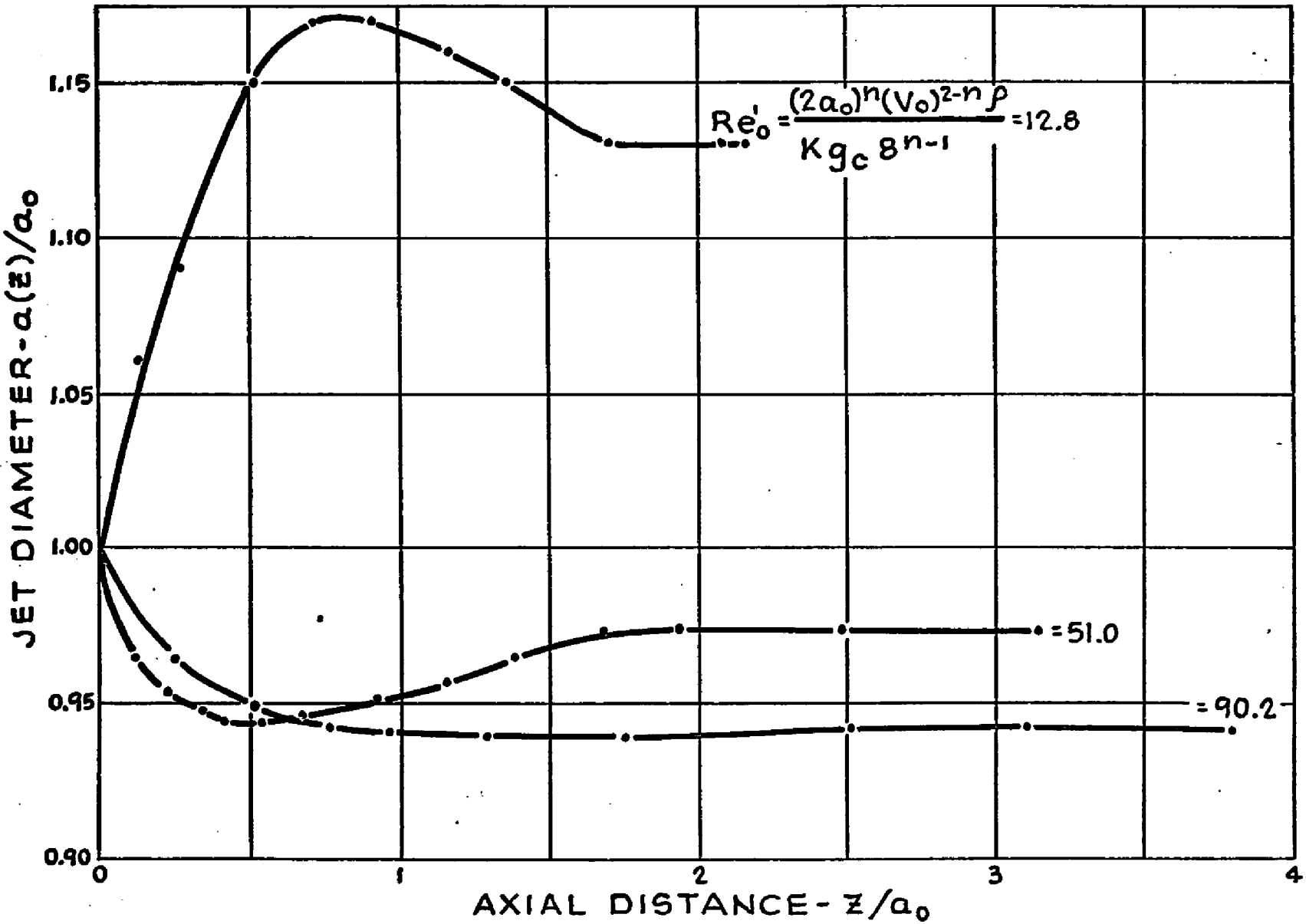

Figure 5-7 Diameter of capillary jets of 0.6% Carbopol as a function of the axial distance from the nozzle and the Reynolds number; nozzle diameter = 0.228cm.

occur within the narrow Reynolds number range of $0 < Re_o' < 1$. But the use of the generalized Reynolds number-Re_o' arranges the data into results that are similar to those published for Newtonian fluids in that expansion takes place for Re_o'=12.8 while contraction is obtained for Re_o'=51.0 and for Re_o'=90.2. . Since Re_o' is essentially a Reynolds number evaluated at the shear rate of capillary flow,, its usage implies that 0.6 % Carbopol does not exhibit any significant viscosity buildup above that possessed at the capillary exit. This could occur if the structural formation time was large compared to the time required for stress relaxation.

The jet diameter of 0.6 % Carbopol at a Reynolds number of Re_o'=12.8 initially increases and then decreases before finally achieving a constant value with increasing axial distance. At Reynolds numbers of Re_o'=51.0 and Re_o' = 90.2 an opposite behavior is observed. The latter response has been reported in Newtonian jets (32) at Reynolds numbers between Re_o= 12-17 .

The theory presented earlier in the chapter had predicted that a capillary jet of a linear viscoelastic fluid would relax faster than a Newtonian jet of the same zero shear viscosity. In attempting to verify this prediction experimentally, it is important that the test fluid satisfy the assumption of a linear viscoelastic fluid. Practically speaking, this requires the polymeric solution be sufficiently dilute so that the ratio of (normal stresses/shearing

stress) is low. However, it has been found that profile decay measurements cannot be performed satisfactorily with dilute, low viscosity fluids due to the rapid growth of disturbances on their surface.

The fluid chosen- 0.7% SCMC represents a compromise between these two requirements. Metzner et.al. (52) have reported that this fluid exhibits no measureable normal stresses at the shear rates encountered in a rheogoniometer although normal stress effects are evidenced at the higher shear rates of capillary flow.

The shapes of capillary jets of 0.7% SCMC are shown in figure 5-8 as a function of the axial distance from the nozzle exit and the Reynolds number. Next to each curve is the Reynolds number based on the zero shear viscosity of 0.7% SCMC and the generalized non-Newtonian Reynolds number evaluated at the capillary flow conditions. Only at the lowest Reynolds number did the jet diameter become constant within the axial distances measured. Contraction also occured at Re_o=13.6(with Re'_o=305) although these data are not shown due to gravity effects at the low flow velocity.

Comparison of this data with the Newtonian results presented in figure 5-3 shows that a longer axial distance is required to reach a constant column diameter for a 0.7 % SCMC jet than for a Newtonian jet of the same zero shear viscosity. This is in direct contradiction to the predict-

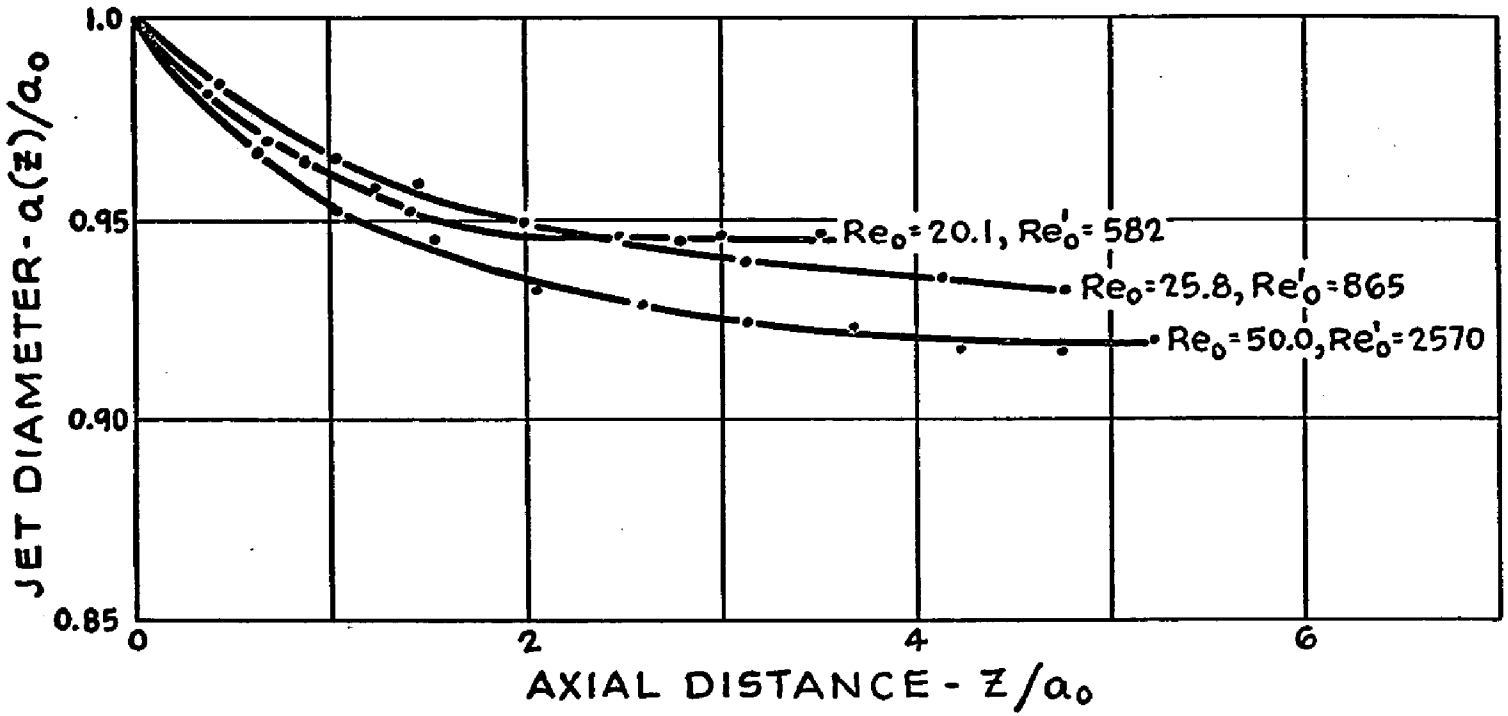

Figure 5-8 Diameter of capillary jets of 0.7% SCMC as a function of the axial distance from the nozzle and the Reynolds number; nozzle diameter - 0.228 cm.

ion from linear theory presented earlier. The comparison could not be made in terms of the damping coefficient-h as values for the final relaxed diameter were not available for the 0.7% SCMC jets.

If it is assumed that the structural formation time of 0.7% SCMC is large compared to the time required for stress relaxation, then the decay rate should be a function of some shear dependent Reynolds number such as Re_o' . At the values of Re_o' shown in figure 5-8, it is unlikely that this mechanism is followed since the jet surface would show the effects of air friction and turbulence.

The behavior evidenced by the 0.7 % SCMC jets would be consistent with a structural formation time which is intermediate between the two cases considered of 1. an 'instantaneous' regeneration of structure and 2. an 'infinite' time for viscosity buildup.

An alternate explanation, originally proposed by Gill and Gavis is that a slowly decaying axial tension exists along the jet. Continuity arguements show that this would cause the jet to expand. If such an effect is superimposed upon a jet contracting due to profile rearrangment, the net result would be to reduce the rate of profile decay. This explanation is in accord with the observed appearance of a viscoelastic jet undergoing breakup, which is discussed in chapter 6. It will be shown that axial tensile stresses are present that cause large axial deform-

ations.

5.5 SUMMARY OF EXPERIMENTAL RESULTS

Measurements were obtained for the shape of capillary jets of glycerin-water mixtures(Newtonian), 0.6 % Carbopol (viscoinelastic) and 0.7 % SCMC(viscoelastic) . The Newtonian results compared reasonably well with published data. Capillary jets of 0.6 % Carbopol expanded at low flow velocities and contracted at higher flow velocities. In order to explain the magnitude of this behavior, it was necessary to assume that the structural formation time of 0.6 % Carbopol was large compared to the time required for stress relaxation. Inelastic fluids may therefore possess a relaxation time in the manner of viscoelastic fluids and the effects of this property can be exhibited in an experiment where the relaxation time and the deformation time are of comparable magnitude.

Capillary jets of 0.7 % SCMC were found to decay slower than a Newtonian jet of the same zero shear viscosity. One possible explanation, which is in accord with the experimental data of chapter 6, is that a slowly decaying axial stress exists that serves to reduce the rate of profile decay.

The profile decay data for both the viscoinelastic and the viscoelastic jets have demonstrated that the relaxation of a long chain molecule is not necessarily in equilibrium with the relaxation of dynamic stresses.

CHAPTER 6

BREAKUP OF A LAMINAR CAPILLARY JET OF A NON-NEWTONIAN LIQUID

This chapter presents the experimental results obtained for the laminar breakup of capillary jets of Newtonian, non-Newtonian inelastic and viscoelastic liquids. A theoretical model developed by my colleague, Dr. J. Yerushalmi, for the stability of laminar viscoelastic jets is included and the use of his analysis is gratefully acknowledged.

6.1 SOLUTION OF THE DYNAMIC EQUATIONS

Consider an incompressible liquid jet emerging horizontally from a capillary and undergoing complete relaxation to a radius-a_∞ in a distance which may be neglected in comparison to the breakup length. The initially relaxed column then moves at a constant velocity-V_∞ and is unaffected by gravity or the presence of the surroundings. Due to the presence of external vibrations or microscopic burrs within the nozzle, an infinitesimal disturbance is superimposed upon the motion of the jet and propagates as an axisymmetric wave. Thus, the jet is circular in crossection at all times and either expands or contracts.

A cylindrical coordinate system is chosen (r, θ, z) which moves with a constant velocity-V_∞. Since the jet is taken to be initially relaxed, all components of the

velocity, stress tensor and pressure in the equations of motion and continuity represent small perturbation quantities only. Non-linear terms are therefore second order in magnitude and are omitted. In the usual notation, the linearized equations of continuity and motion are given by

$$\frac{1}{r}\frac{\partial(rV_r)}{\partial r} + \frac{\partial V_z}{\partial z} = 0 \qquad (6.1)$$

$$\rho\frac{\partial V_r}{\partial t} = -\frac{\partial p}{\partial r} + \frac{1}{r}\frac{\partial(r\tau_{rr})}{\partial r} - \frac{\tau_{\theta\theta}}{r} + \frac{\partial \tau_{rz}}{\partial z} \qquad (6.2a)$$

$$\rho\frac{\partial V_z}{\partial t} = -\frac{\partial p}{\partial z} + \frac{1}{r}\frac{\partial(r\tau_{rz})}{\partial z} + \frac{\partial \tau_{zz}}{\partial z} \qquad (6.2b)$$

The jet radius at any point may be expressed as

$$r = a_\infty + \xi \qquad (6.3)$$

where ξ (z,t) is the infinitesimal displacement of the free surface from the unperturbed radius.

At the jet surface, the shear stress- τ_{rz} is zero since ambient drag effects are neglected and the radial stress tensor is balanced by the pressure due to surface tension forces. The difficulty in applying the boundary conditions is that the position of the jet surface is unknown. If the displacement $\xi \ll a_\infty$, the boundary conditions may be approximated as

$$\text{B.C. 1} \quad (\tau_{rz})_{r\approx a_\infty} = 0 \qquad (6.4)$$

$$\text{B.C. 2} \quad (-p + \tau_{rr})_{r\approx a_\infty} = p_\sigma \qquad (6.5)$$

where the surface tension pressure-p_σ is given by

$$p_\sigma = \frac{\sigma}{a_\infty^2}\left[\xi + a_\infty^2 \frac{\partial^2 \xi}{\partial z^2}\right] \tag{6.6}$$

and σ is the coefficient of surface tension.

B.C. 3 and 4 All velocities are finite at r=0 .

Biot (2) and Bland (4) have shown that the rheological properties of any incompressible viscoelastic material in the region of very small deformations can be described by the following constitutive equation.

$$\tau_{ij} = E\,\gamma_{ij} + \eta_\infty \Delta_{ij} + \sum_{r=1}^{N} \int_{-\infty}^{t} C_r e^{-\phi_r(t-t')} \Delta_{ij}(t')\,dt' \tag{6.7}$$

where γ_{ij} and Δ_{ij} are the components of the strain and rate of deformation tensors, respectively, and E, η_∞, C_r and ϕ_r are all real and positive. The coefficients E and η_∞ account for the instantaneous elasticity and the long term viscous flow respectively. The summation represents a discrete spectrum of relaxation times- $1/\phi_r$.

Application of the Laplace time transform to equations (6.1) and (6.2a), and (6.7) results in

$$\frac{1}{r}\frac{\partial (r\hat{V}_r)}{\partial r} + \frac{\partial \hat{V}_z}{\partial z} = 0 \tag{6.8}$$

$$\rho \alpha \hat{V}_r = -\frac{\partial \hat{p}}{\partial r} + \hat{\eta}(\alpha)\left[\frac{\partial}{\partial r}\left(\frac{1}{r}\right)\frac{\partial}{\partial r}(r\hat{V}_r) + \frac{\partial^2 \hat{V}_z}{\partial z^2}\right] \tag{6.9a}$$

$$\rho \alpha \hat{V}_z = -\frac{\partial \hat{\rho}}{\partial z} + \hat{\eta}(\alpha)\left[\frac{1}{r}\frac{\partial}{\partial r}\left(r\frac{\partial \hat{V}_z}{\partial r}\right) + \frac{\partial^2 \hat{V}_z}{\partial z^2}\right] \tag{6.9b}$$

where α is the transform variable and $\hat{\eta}(\alpha)$ complex viscosity of eq. (6.7) . The complex viscosity represents the linear response of any viscoelastic meterial and is given by

$$\hat{\eta}(\alpha) = \frac{E}{\alpha} + \eta_\infty + \sum_{r=1}^{N} \frac{C_r}{\phi_r + \alpha} \tag{6.10}$$

The boundary conditions are similarly transformed to

$$\text{B.C. 1'} \quad \left(\frac{\partial \hat{V}_r}{\partial z} + \frac{\partial \hat{V}_z}{\partial r}\right)_{r \approx a_\infty} = 0 \tag{6.11}$$

$$\text{B.C. 2'} \quad \left(-\hat{p} + 2\hat{\eta}(\alpha)\frac{\partial \hat{V}_r}{\partial r}\right)_{r \approx a_\infty} = \frac{\sigma}{a_\infty^2}\left(\hat{\xi} + a_\infty^2 \frac{\partial^2 \hat{\xi}}{\partial z^2}\right) \tag{6.12}$$

$$\alpha \hat{\xi} = (\hat{V}_r)_{r \approx a_\infty} \tag{6.13}$$

Hereafter, the solution is identical to the method of Weber with the constant Newtonian viscosity η_0 replaced by the complex viscosity $\hat{\eta}(\alpha)$.

A stream function $\hat{\psi}$ is defined as

$$\hat{V}_r = \frac{1}{r}\frac{\partial \hat{\psi}}{\partial z} \; ; \; \hat{V}_z = -\frac{1}{r}\frac{\partial \hat{\psi}}{\partial r} \tag{6.14}$$

If equations (6.9a) and (6.9b) are crossdifferentiated to eliminate the pressure and the stream function is introduced,

a linear differential equation in $\hat{\psi}$ is obtained as

$$\left[D - \frac{\alpha \rho}{\hat{\eta}(\alpha)}\right] D\hat{\psi} = 0 \qquad (6.15)$$

where D is a linear operator given as

$$D = \frac{\partial^2}{\partial r^2} - \frac{1}{r}\frac{\partial}{\partial r} + \frac{\partial^2}{\partial z^2} \qquad (6.16)$$

The stream function $\hat{\psi}$ is assumed to be of the form

$$\hat{\psi}(r,z) = \left[\hat{\psi}_1(r) + \hat{\psi}_2(r)\right] e^{ikz} \qquad (6.17)$$

where k, the wave number, is related to the wavelength by $k = 2\pi/\delta$.

$\hat{\psi}_1$ is the solution to $D\hat{\psi}_1 = 0$
and $\hat{\psi}_2$ is the solution to $\left[D - \alpha\rho/\hat{\eta}(\alpha)\right]\hat{\psi}_2 = 0$

The complete formal solution for $\hat{\psi}$ is given by

$$\hat{\psi}(r,z) = r\left[C_1 I_1(kr) + C_2 I_1(gr) + C_3 K_1(kr) + C_4 K_1(gr)\right] x \qquad (6.18)$$
$$x\ e^{ikz}$$

where $g^2 = k^2 + \alpha\rho/\hat{\eta}(\alpha)$

$I_n(\ )$ and $K_n(\ )$ are modified Bessel functions of order n and the C_1, C_2, C_3, C_4 are constants to be determined from the boundary conditions.

Application of the boundary conditions leads to the

characteristic equation relating α and k .

$$\alpha^2 + \frac{2\hat{\eta}(\alpha)k^2}{\rho I_o(ka_\infty)}\left[I_1'(ka_\infty) - \frac{2kg}{k^2+g^2}\frac{I_1(ka_\infty)I_1'(ga_\infty)}{I_1(ga_\infty)}\right]\alpha = \tag{6.19}$$

$$= \frac{\sigma k}{2\rho a_\infty^2}(1-k^2a_\infty^2)\frac{I_1(ka_\infty)}{I_o(ka_\infty)}\frac{g^2-k^2}{g^2+k^2}$$

where $I_n'(\ )$ denotes differentiation of $I_n(\ )$ with respect to the arguement.

The solution to the characteristic equation determines the stability of the capillary jet. Depending upon whether the real part of α is positive, zero or negative, the initial disturbances will be amplified, neutrally stable, or dampened, respectively.

6.2 SOLUTION OF THE CHARACTERISTIC EQUATION

A considerable simplification of eq. (6.19) results when the wavelength is much greater than the jet radius, $\delta \gg a_\infty$ or, equivalently, when $(ka_\infty) \ll 1$ and when $(ga_\infty) \ll 1$. This condition is fufilled by low speed capillary jets of Newtonian liquids. Under these circumstances, the Bessel functions may be approximated by the first term of their series expansions and can be written as

$$I_o(ka_\infty) \sim 1 \quad ; \quad I_1'(ka_\infty) = I_1'(ga_\infty) \sim \tfrac{1}{2}$$
$$I_1(ka_\infty) \sim ka_\infty/2 \quad ; \quad I_1(ga_\infty) \sim ga_\infty/2 \tag{6.20}$$

With these simplifications, the characteristic equation

becomes

$$\alpha^2 + \frac{3K^2\hat{\eta}(\alpha)}{\rho}\alpha - \frac{\sigma K^2}{2\rho a_\infty}(1 - K^2 a_\infty^2) = 0 \qquad (6.21)$$

The capillary jet will be destroyed by the fastest growing wave- α^* which is obtained from the solution of $\frac{d\alpha}{dK} = 0$ and is given by

$$\alpha^* = \frac{\sqrt{\frac{\sigma}{2\rho a_\infty^3}}}{2 + \frac{3\hat{\eta}(\alpha)}{\rho}\sqrt{\frac{2\rho}{\sigma a_\infty}}} \qquad (6.22)$$

The highest growth rate of any fluid will be for an inviscid liquid in which $\hat{\eta}(\alpha) = 0$. Corresponding to α^* is the wave number-k^*

$$K^* = \alpha^* \sqrt{\frac{2\rho}{\sigma a_\infty}} \qquad (6.23)$$

The stability of a capillary jet will now be considered in relation to the properties of the complex viscosity. For the convenience of the reader, the general form of $\hat{\eta}(\alpha)$ is repeated.

$$\hat{\eta}(\alpha) = -\frac{E}{\alpha} + \eta_\infty + \sum_{r=1}^{N} \frac{C_r}{\phi_r + \alpha} \qquad (6.10)$$

CASE 1 NEWTONIAN LIQUID

For a Newtonian liquid of constant viscosity - η_0 , equations (6.22) and (6.23) become

$$\alpha_o^* = \frac{\sqrt{\frac{\sigma}{2\rho a_\infty^3}}}{2 + \frac{3\eta_o}{\rho}\sqrt{\frac{2\rho}{\sigma a_\infty}}} \tag{6.24}$$

$$K_o^* = \left[3\eta_o a_\infty \sqrt{\frac{2a_\infty}{\sigma\rho}} + 2a_\infty^2\right]^{-1/2} \tag{6.25}$$

where the subscript zero in α_o^* and K_o^* denotes Newtonian values. Equations (6.24) and (6.25) are identical to the results of Weber.

The dimensionless wavelength for a capillary jet of a Newtonian liquid is given by

$$\frac{\delta}{2a_\infty} = \pi\sqrt{2}\left[1 + \frac{3\eta_o}{\sqrt{2\rho a_\infty \sigma}}\right]^{1/2} \tag{6.26}$$

If the breakup time is assumed to be inversely proportional to the growth rate, then the breakup length of a Newtonian jet can be written as

$$L = C V_\infty / \alpha_o^* \tag{6.27}$$

where L is the breakup length and C is a constant of proportionality which must be determined experimentally. By virtue of equation (6.24) the dimensionless breakup length is obtained as

$$\frac{L}{2a_\infty} = C\left[We_\infty^{1/2} + 3\frac{We_\infty}{Re_\infty}\right] \tag{6.28}$$

where We_∞, the Weber number is given by $We_\infty = 2\rho a_\infty V_\infty^2/\sigma$, and Re_∞, the Reynolds number is defined as $Re_\infty = 2a_\infty V_\infty \rho/\eta_0$.

CASE 2 VISCOELASTIC FLUID WITHOUT STRUCTURE

The relative stability of a capillary jet of a viscoelastic fluid can be compared to that of a Newtonian liquid by dividing eq. (6.22) with eq. (6.24) to give

$$\frac{2 + \frac{3\hat{\eta}(\alpha)}{\rho}\sqrt{\frac{2\rho}{\sigma a_\infty}}}{2 + \frac{3\eta_0}{\rho}\sqrt{\frac{2\rho}{\sigma a_\infty}}} = \frac{\alpha_0^*}{\alpha^*} \qquad (6.29)$$

The ratio (α_0^*/α^*) thus depends upon the relative magnitude of $\hat{\eta}(\alpha^*)$ with respect to $\hat{\eta}(0)=\eta_0$. Since the complex viscosity of a viscoelastic fluid with E=0 is bounded by $\hat{\eta}(\infty) < \hat{\eta}(\alpha^*) < \hat{\eta}(0)$ it follows from eq. (6.29) that $\alpha_0^*/\alpha^* < 1$ and, therefore, a capillary jet of such a fluid is less stable than a Newtonian jet of the same zero shear viscosity- $\hat{\eta}(0) = \eta_0$.

A plot of α vs. k^2, derived from eq. (6.21) for a viscoelastic fluid with finite $\hat{\eta}(0)$, yields a curve which lies above the curve corresponding to a Newtonian fluid of the same zero shear viscosity and below the curve corresponding to an inviscid fluid $\hat{\eta}(0)=0$. All three curves cross the k^2 axis at the same points.

CASE 3 ELASTIC SOLID

When E is finite with η_∞ and all the ϕ_r equal to zero, the material behaves as an elastic solid for which

$$\hat{\eta}(\alpha) = \frac{E}{\alpha} \tag{6.30}$$

It can be shown that if

$$E < \frac{\sigma(1-K^2a_\infty^2)}{6a_\infty} \tag{6.31}$$

there will always be a real positive eigenvalue of α^* causing instability while if inequality (6.31) is reversed, the jet is unconditionally stable.

CASE 4 VISCOELASTIC FLUID WITH STRUCTURE ($E \neq 0$)

The same criteria governing the stability of a jet of an elastic solid, case 3, can also be shown to be applicable to the case of a viscoelastic fluid with structure.

The interested reader may consult the thesis of Dr. Yerushalmi (94) or the paper by Goldin et.al. (29) for details of this development.

6.3 DISCUSSION OF THEORETICAL RESULTS

In summary, it has been shown that a laminar capillary jet of a viscoelastic liquid whose complex viscosity is bounded by $\hat{\eta}(0) = \eta_0$, is more unstable that a Newtonian jet

of the same zero shear viscosity- η_0 . If, however, $\hat{\eta}(\alpha)$ is unbounded the jet may become unconditionally stable.

It is worthwhile to discuss some of the assumptions leading to these conclusions. Firstly, the liquid column was taken to be completely relaxed. As noted in the previous chapter, the jet, upon emerging from the capillary, undergoes a relaxation in which the stresses and velocity profile (of the capillary shear flow) decay with increasing axial distance. The rearrangement results in a relaxed jet diameter that is different from the capillary bore. For laminar Newtonian jets, it has been shown (32,57) by measuring the axial distance required for the jet to reach constant diameter, that the length required for complete relaxation may be neglected in comparison to the breakup length. Middleman and Gavis (61,62) and Metzner et.al. (52) have obtained similar data for jets of viscoelastic liquids but only report the ratio of the final relaxed diameter to the nozzle diameter. It may be inferred from their lack of comment as to the relaxation length that this distance was not unusual and was of the same order as for Newtonian jets. However, Gill and Gavis (27) interpret their experimental results to mean that a slowly decaying tensile stress exists in jets of viscoelastic liquids even at considerable axial distances.

For viscoelastic fluids consisting of dissolved polymers, there is also a structural relaxation time for the

long chain molecule to achieve an equilibrium, spatial configuration with the locally changing shear rate. If the molecular relaxation time is of the same order as the jet breakup time, about 10^{-2} to 10^{-3} seconds, the jet may never be fully relaxed.

The linear stability analysis just described had assumed that the propagating disturbance was infinitesimally small. On that basis, terms which were second order in magnitude were discarded from both the equations of motion and the rheological constitutive equation of the fluid. There is justification for neglecting the inertial terms in the equations of motion as the same assumption in the treatment of Newtonian jet breakup has produced theoretical predictions in good agreement with experimental data. However, the use of a linear constitutive equation for viscoelastic fluids which exhibit measureable non-linearities such as shear dependent viscosities and normal stresses is a much more restrictive approximation. The analysis may be applicable to very dilute viscoelastic fluids although Oliver (68) has measured normal stresses at concentrations down to the 0.01% level in jet thrust experiments. In the end, experimental data must be used to access the validity of the assumptions. As the photographs in the experimental section will show, marked non-linear phenomena are present at large axial distances even for jets of very dilute viscoelastic liquids.

6.4 EXPERIMENTAL RESULTS - QUALITATIVE OBSERVATIONS

Marked differences were found to exist between the behavior of capillary jets of Newtonian, non-Newtonian inelastic and viscoelastic fluids. The distinctions are summarized by the photographs of figure 6-1, which shows typical appearances of the jets formed by each class of fluids.

In laminar jets of Newtonian liquids, an infinitesimal disturbance generated within the capillary is propagated as an exponentially growing wave with a constant wavelength, according to equations (6.24) and (6.26). Capillary jets of low viscosity liquids such as 75% glycerin-water and ethylene glycol, which are seen in photographs (a) and (b) respectively, clearly illustrate this mode of instability. Viscous Newtonian jets are also broken up by the regular growth of a disturbance wave but, as shown in photograph (c) for a 97% glycerin-water jet, the wave character is not as uniform. Just before breakup, these high viscosity jets may also form fine threads over relatively short lengths.

The non-Newtonian, inelastic test fluids possessed certain rheological similarities. They all displayed a yield stress and a shear dependent viscosity but did not exhibit any of the phenomena normally associated with viscoelasticity, e.g. a Weissenberg effect.

Laminar capillary jets of 0.1% Carbopol and the MPA

NEWTONIAN

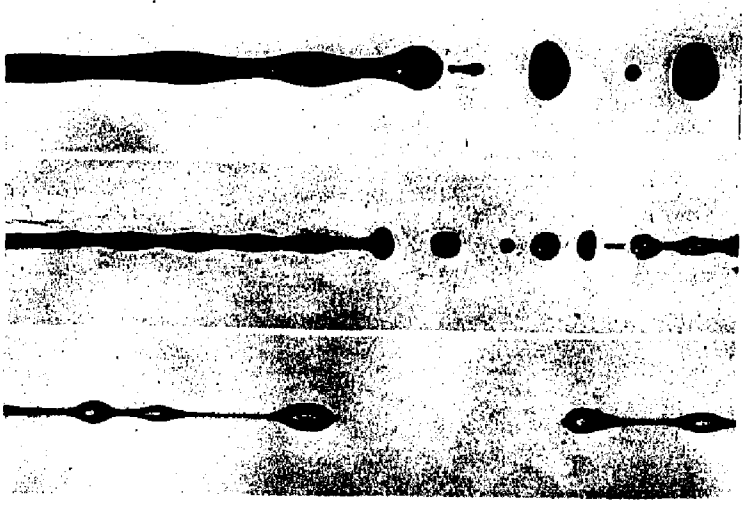

(a) 75% Glycerin-Water
(b) Ethylene Glycol
(c) 97% Glycerin-Water

VISCOINELASTIC

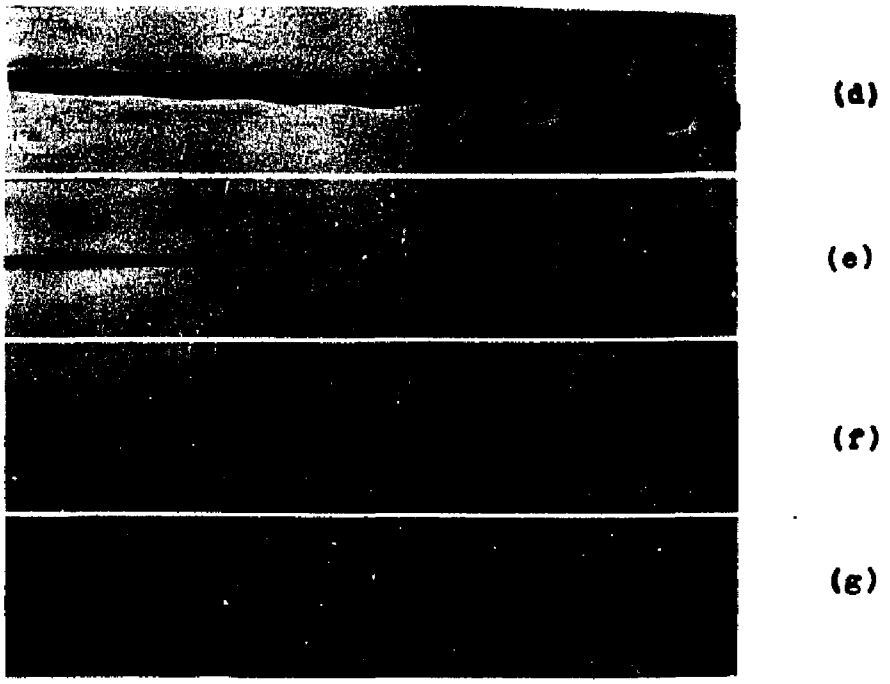

(d) 0.1% Carbopol
(e) MPA 60 in xylene
(f) MPA 60 in mineral spirits
(g) 0.2% Carbopol

Figure 6-1 Comparison of Capillary Jets of Newtonian, Viscoinelastic and Viscoelastic Liquids

VISCOINELASTIC

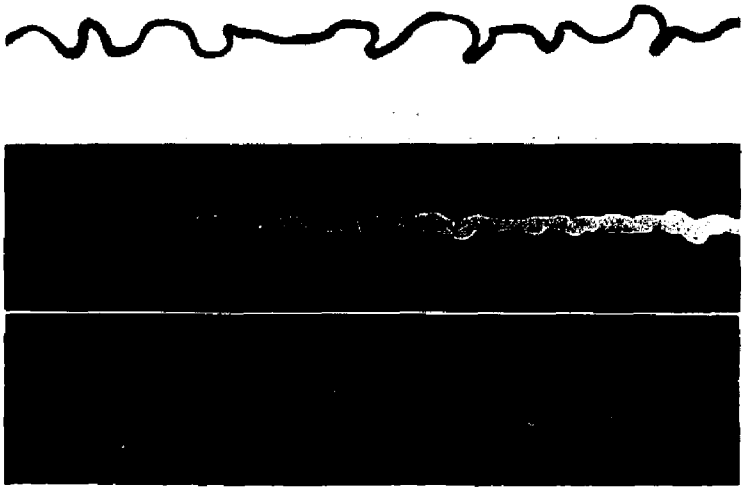

(h) 0.6% Carbopol
(i) 12.4% Silica at low velocity
(j) 12.4% Silica at high velocity

VISCOELASTIC

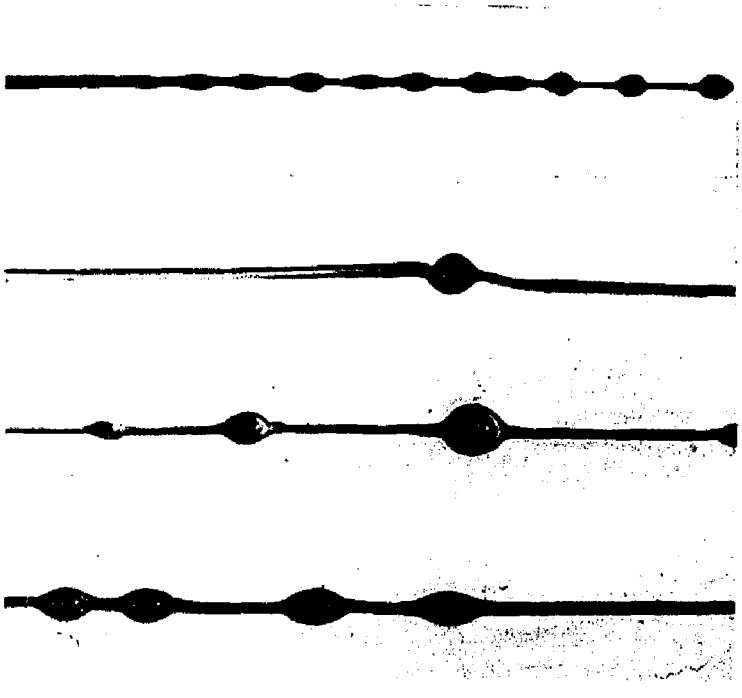

(k) 0.25% SCMC
(l) 0.25% Separan
(m) 0.25% Polyox
(n) 0.05% Separan

Figure 6-1 Comparison of Capillary Jets of Newtonian, Viscoinelastic and Viscoelastic Jets

60 dispersions, photographs (d), (e) and (f) respectively, appear to have characteristics similar to those of Newtonian jets in that they break up due to the growth of a disturbance wave. When the Carbopol concentration has increased to 0.2% from 0.1%, the fluid becomes considerably more viscous and the capillary jet formed by 0.2% Carbopol, shown in photograph (g), shows a barely perceptible wave propagation.

A 0.6% Carbopol solution has the consistency of a semirigid gell and the capillary jet of this fluid, seen in photograph (h), is unstable but only at very high velocities. No wave characteristics are apparent on the liquid column. The drag force of the surrounding air is no longer negligible under these high velocity flow conditions and imparts an irregular motion to the capillary jet.

An aqueous dispersion of silica at a 12.4% concentration is an inelastic liquid with a high yield stress. It forms capillary jets that show no regular wave pattern. At the intermediate velocity at which photograph (i) was taken, the column is stable and the "screw-like" disturbance pattern that is seen on the liquid column does not grow. The appearance of the capillary jet is remindful of melt fracture in polymer extrudates. When high velocities are reached, the jet becomes turbulent and breaks up rapidly due to the growth of non-axisymmetric disturbances, as shown in photograph (j). The high velocity silica jet

resembles the turbulent breakup of a low viscosity Newtonian liquid despite the fact that, at rest, the 12.4% silica dispersion is a stiff gel.

The viscoelastic test liquids used in these experiments all possess shear dependent viscosities, normal stresses (68,77) and show marked drag reduction at very low levels of polymer (23,36,76,84). At the same concentration, Separan and Polyox solutions display stronger viscoelastic effects than those of SCMC.

Dilute viscoelastic solutions of SCMC in water form jets which initially display a growing wave with a clearly defined wavelength, as in photograph (k). The growth of the wave is, however, arrested before breakup occurs and a series of droplets connected by threads appears. These threads thin with distance and eventually lead to the breakup of the liquid column.

In moderately elastic jets such as 0.25% Separan in water, shown in photograph (l), no wave motion is discernible and the first visible disturbance appears as a large droplet, isolated in space from any systematic growth pattern. At greater axial distances, the jet is composed of a series of random sized droplets connected by random lengths of threads, as illustrated by photograph (m) of 0.25% Polyox.

Dilute viscoelastic jets of 0.05% Separan, seen in photograph (n), exhibit an intermediate behavior between

0.25% SCMC and 0.25% Separan or 0.25% Polyox. The disturbance initially propagates as a wave of irregular amplitude with a wavelength that increases with distance. Gradually, the waves form a string of droplets connected by threads as in the case of the more elastic jets. The droplet distribution, while not completely random, is less regular than in 0.25% SCMC.

Capillary jets of viscoelastic liquids are thus distinguished by the formation of droplets connected by threads which thin with distance and ultimately break. Though threads have been observed near breakup for viscous Newtonian jets, they exist only over relatively short distances. The large axial lengths over which the droplet-thread configuration is propagated appears to be a characteristic peculiar to viscoelastic jets.

Since both non-Newtonian inelastic and viscoelastic liquids have shear dependent viscosities, the considerable difference in the appearances of their respective jets undoubtedly is associated with the presence or lack of elastic properties.

The complete breakup of a capillary jet of ethylene glycol is shown in the sequence of photographs of figure 6-2. The distances quoted in the legend represent the length from the nozzle tip to the midpoint of the photograph. Photograph (c) of this figure clearly shows the wave character of the propagating disturbance and also

depicts the well defined wavelength. The uniform distance between free droplets is an additional indication of the wave character of the propagating disturbance.

Figure 6-3 shows the breakup sequence for a jet of 97% glycerin-water and is illustrative of the behavior of a high viscosity, Newtonian liquid. As shown in photograph (c), the disturbance initially propagates in the form of a growing wave. However, near breakup, photograph (d) shows how the uniformity of the wave is altered. Fine liquid threads often appear in this region but only over relatively short distances.

The wave propagation of disturbances seen on capillary jets of 0.1% Carbopol and of 24% MPA 60 in xylene, figures 6-4 and 6-5 respectively, is strikingly similar to the appearance of low viscosity Newtonian jets. A related behavior is shown by 0.2% Carbopol jets in figure 6-6 even though the amplitude of the disturbance wave is considerably diminished. The Carbopol solutions and the MPA 60 dispersions exhibit definite yield stresses and show high apparent viscosities at low rates of shear. Yet all atomize readily and the breakup lengths are not indicative of any appreciable stability.

Solutions of 0.6% Carbopol are semi-rigid gells when at rest with a moderate yield stress. Capillary jets formed by these solutions are unstable, but only at very high velocities. Figure 6-7 shows the complete breakup

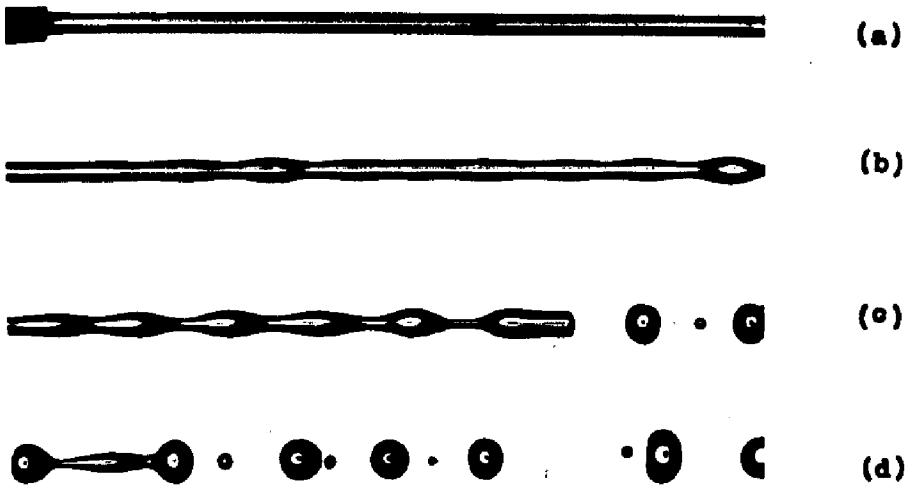

Figure 6-2 Breakup of a Laminar Capillary Jet of Ethylene Glycol
Magnification-3.3X; Nozzle diameter-0.0868 cm; Average fluid velocity-250 cm/sec; Distance from nozzle tip to midpoint of photograph- (a) 1.2 cm, (b) 11.6 cm, (c) 14.7 cm, (d) 17.3 cm.

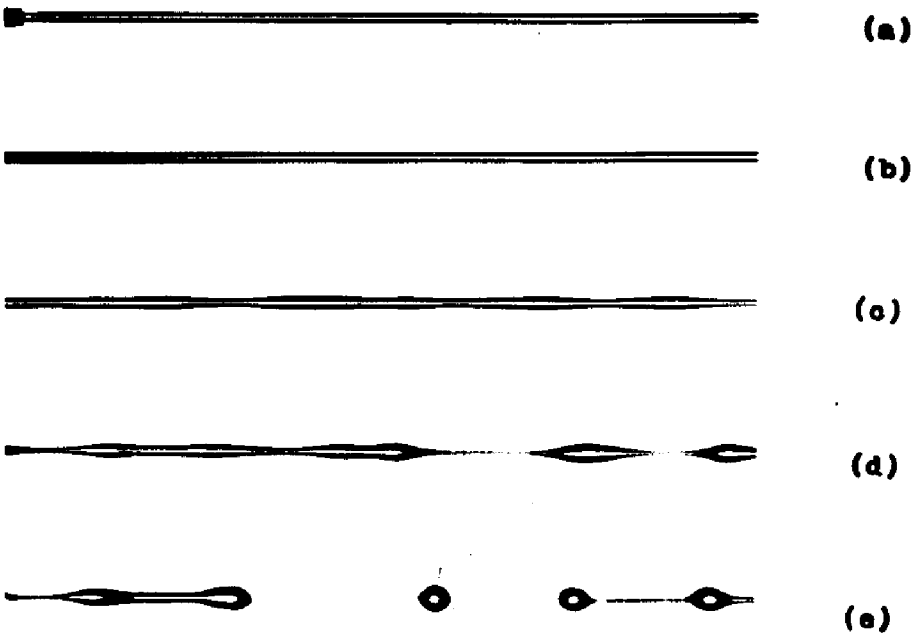

Figure 6-3 Breakup of a Laminar Capillary Jet of 97% Glycerin-Water
Magnification-3.3X; Nozzle diameter-0.0868 cm; Average jet velocity-708 cm/sec; Distance from nozzle tip to midpoint of photograph- (a) 1.3 cm, (b) 31.2 cm, (c) 46.7 cm, (d) 52.1 cm, (e) 56.2 cm

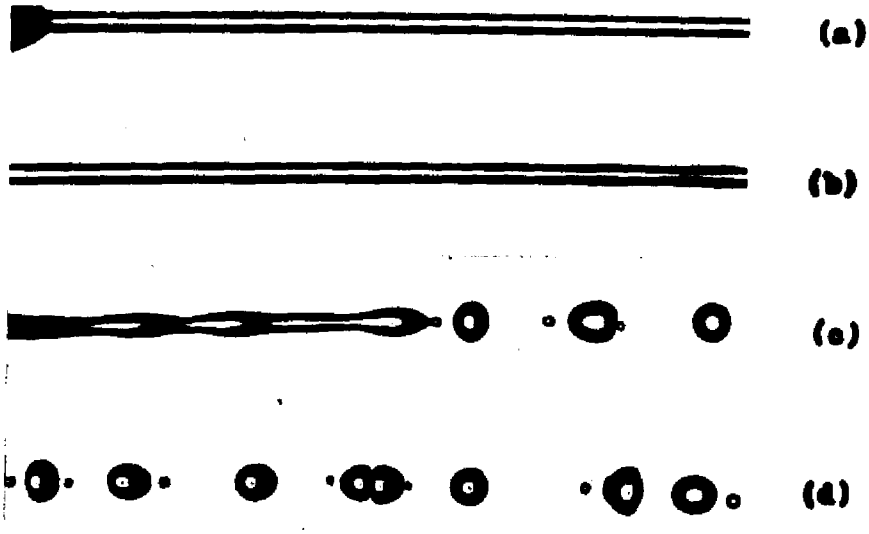

Figure 6-4 Breakup of a Laminar Capillary Jet of 0.1% Carbopol
Magnification-3.3X; Nozzle diameter-0.0868 cm; Average jet velocity-282 cm/sec; Distance from nozzle tip to midpoint of photograph- (a) 1.4 cm, (b) 4.7 cm, (c) 9.6 cm, (d) 11.8 cm

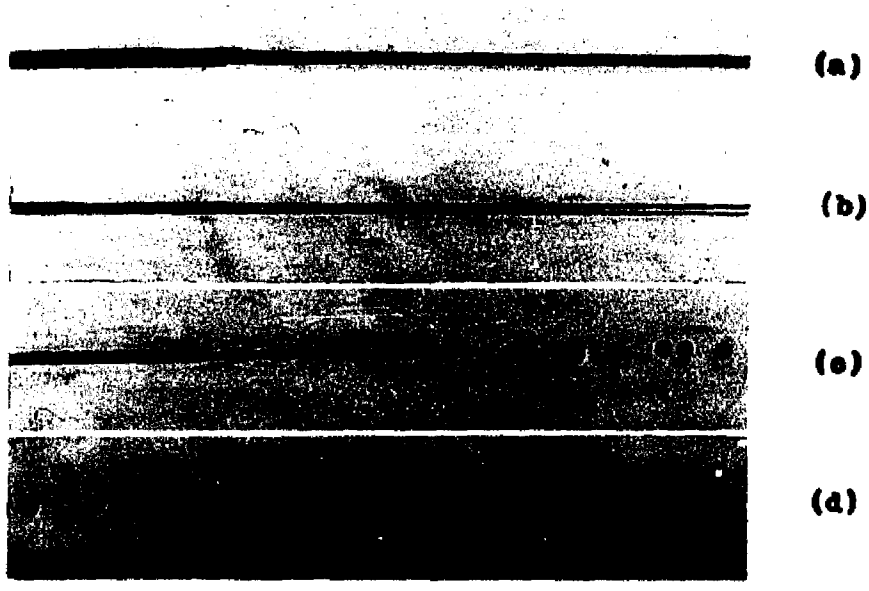

Figure 6-5 Breakup of a Laminar Capillary Jet of MPA 60 in Xylene
Magnification-2.8X; Nozzle diameter-0.0414 cm; Average jet velocity-258 cm/sec; Distance from nozzle tip to midpoint of photograph- (a) 1.8 cm, (b) 3.8 cm, (c) 6.8 cm, (d) 9.4 cm

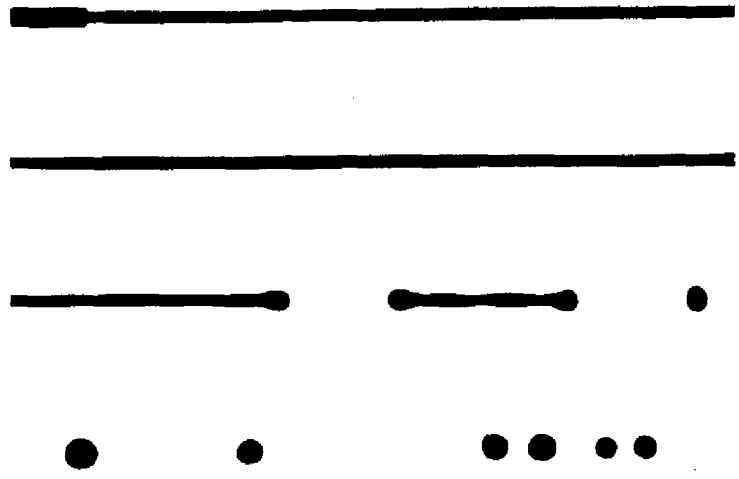

Figure 6-6 Breakup of a Laminar Capillary Jet of 0.2% Carbopol
Magnification-3.2X; Nozzle diameter-0.0414 cm; Average jet velocity-438 cm/sec; Distance from nozzle tip to midpoint of photograph- (a) 1.2 cm; (b) 7.3 cm, (c) 13.0 cm, (d) 17.3 cm

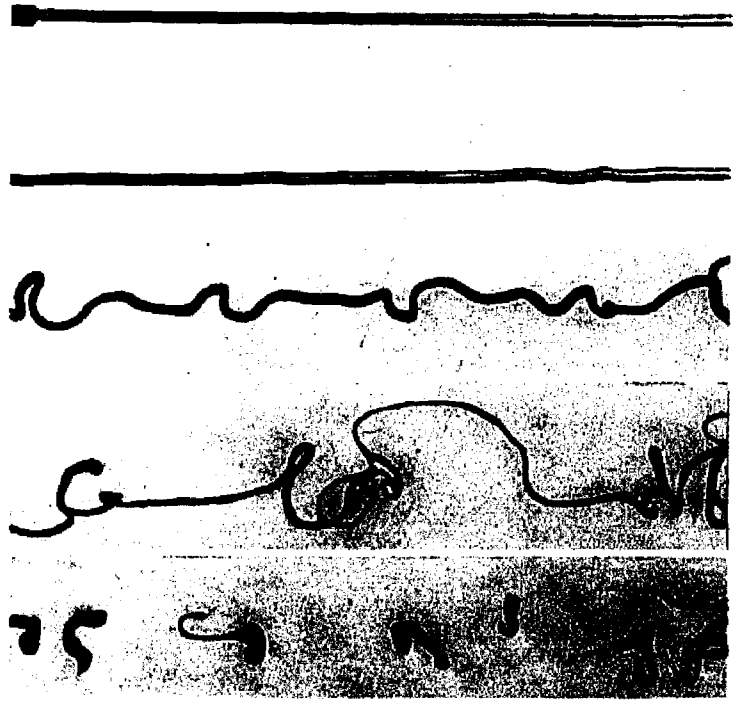

Figure 6-7 Breakup of a Capillary Jet of 0.6% Carbopol
Magnification-3.2X; Nozzle diameter- 0.0414 cm; Average fluid velocity- 4710 cm/sec; Distance from nozzle tip to midpoint of photograph- (a) 1.4 cm, (b) 26.1 cm, (c) 56.6 cm, (d) 61.6 cm, (d) 67.2 cm.

sequence for a capillary jet of 0.6% Carbopol moving with an average velocity of 4710 cm/sec. Air resistance at these high velocities produces the non-axisymmetric motion of the liquid column that is evident in photographs (c) and (d). The wave propagation which characterized the capillary jets of 0.1% Carbopol, 0.2% Carbopol and the MPA 60 dispersions is absent with 0.6% Carbopol. This is also confirmed by the random nature of the particles formed after breakup, as shown in photograph (e).

The sequence of photographs appearing in figures 6-8 through 6-10 shows the changing behavior of a capillary jet of a 12.4% silica dispersion. Photograph (a) of figure 6-8 depicts the formation of a non-axisymmetric disturbance on the liquid column as it emerges from the nozzle at an average velocity of 1080 cm/sec. The amplitude of the disturbance at a distance of 20.3 cm from the nozzle, photograph (b), does not appear to have increased over that at the capillary exit and actually seems to have dampened at a distance of 35.6 cm., as in photograph (c). The jet was stable within the 5 foot length available for photography. When the jet velocity has reached 1950 cm/sec, the montage pictured in figure 6-9 shows large amplitude disturbances visible on the surface of the jet which eventually result in its destruction. The growth of these disturbances appears to be random and this is further evidenced by the non-uniform nature of the

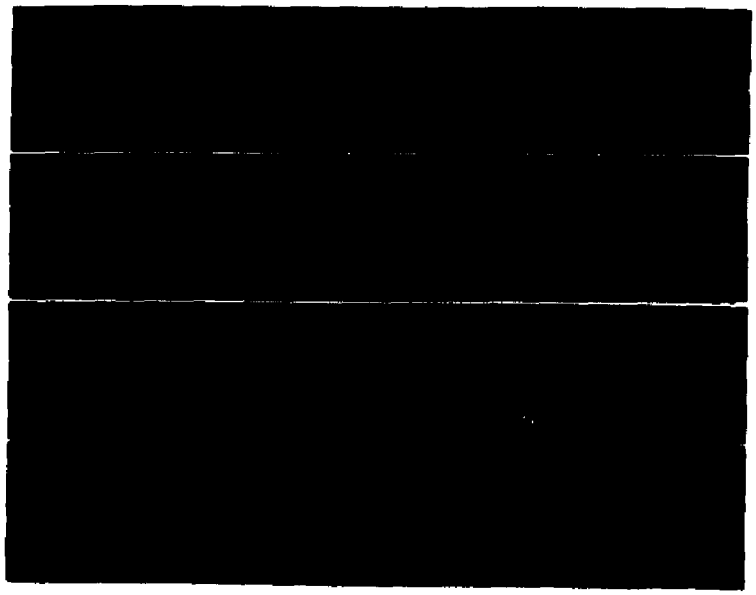

Figure 6-8 Breakup of a Capillary Jet of 12.4% Silica in Water
Magnification-1.4X; Nozzle diameter-0.180 cm; Average jet velocity-1080 cm/sec; Distance from nozzle tip to midpoint of photograph- (a) 2.7 cm, (b) 20.3 cm, (c) 35.6 cm, (d) 65.6 cm

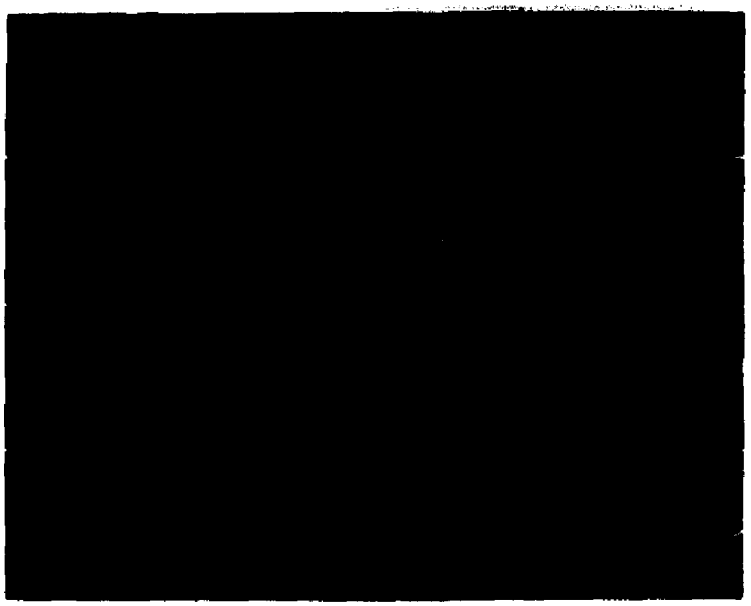

Figure 6-9 Breakup of a Capillary Jet of 12.4% Silica in Water
Magnification-1.4X; Nozzle diameter-0.180 cm; Average jet velocity-1950 cm/sec; Distance from nozzle tip to midpoint of photograph- (a) 1.9 cm, (b) 14.6 cm, (c) 24.2 cm, (d) 32.5 cm

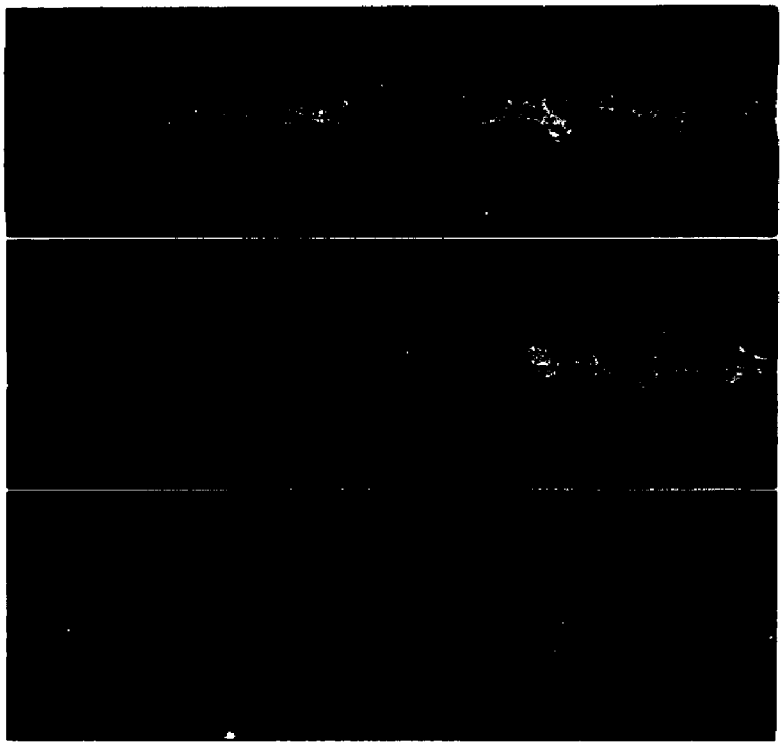

Figure 6-10 Breakup of a Capillary Jet of 12.4% Silica in Water
Magnification-1.4X; Nozzle diameter-0.180 cm; Average jet velocity-2850 cm/sec; Distance from nozzle tip to midpoint of photograph- (a) 3.1 cm, (b) 11.8 cm, (c) 23.2 cm

particles formed at breakup, as shown in photograph (d). At the highest jet velocity, 2850 cm/sec, the 12.4% silica jet, seen in the sequence of figure 6-10, undergoes turbulent breakup and is completely fragmented into individual particles within a relatively short distance. In none of this series of photographs is there evidence of the wave propagation which characterized the capillary jets of Newtonian liquids, 0.1% and 0.2% Carbopol solutions and the MPA 60 dispersions.

It is surprising to observe that 12.4% silica jets atomize so readily especially when one considers that this inorganic dispersion is a stiff gel, when at rest, with a high yield stress. Anotherinteresting observation is that the lowest velocity silica jet is stable whereas the higher velocity jets are unstable. These phenomena will be examined at greater length in the discussion of experimental results, section 6-6.

Solutions of 0.25% SCMC are very slightly elastic and the jets formed by this fluid initially show a growing wave with a clearly defined wavelength. The growth of the wave ceases before breakup occurs and a string of droplets connected by thin threads is formed. The droplets are found at regular distances from one another indicating their development from a wave of constant wavelength. This behavior is indicated in the sequence of photographs of figure 6-11. Secondary instabilities in the form of very

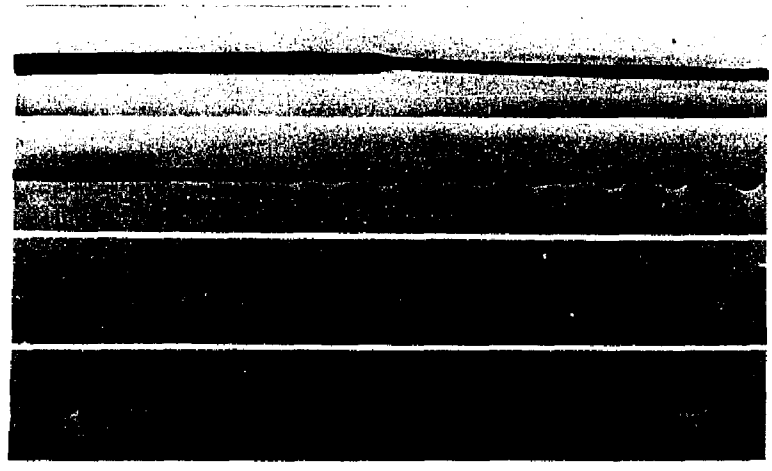

Figure 6-11 Breakup of a Laminar Capillary Jet of 0.25% SCMC
Magnification-3.6X; Nozzle diameter-0.0414 cm; Photographs (a)-(c):average jet velocity -306 cm/sec; Photograph (d):average jet velocity-606 cm/sec; Distance from nozzle tip to midpoint of photograph- (a) 0.2 cm, (b) 3.6 cm, (c) 6.4 cm, (d) 12.5 cm

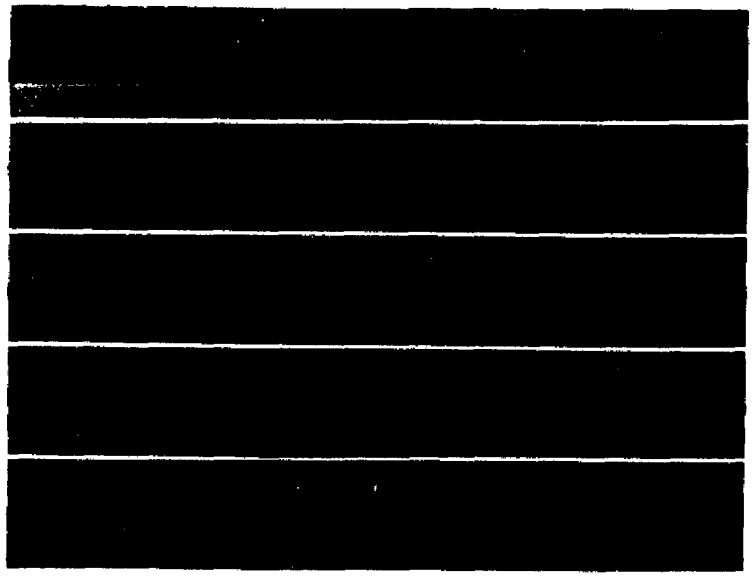

Figure 6-12 Breakup of a Laminar Capillary Jet of 0.25% Separan
Magnification-4.2X; Nozzle diameter-0.0414 cm; Average jet velocity-792 cm/sec; Distance from nozzle tip to midpoint of photograph- (a) 0.7 cm, (b) 60.5 cm, (c) 80.9 cm, (d) 115.7 cm, (e) 145 cm

small droplets may also be generated on the threads, as demonstrated in the last photograph of this figure.

In capillary jets of 0.25% Separan and 0.25% Polyox, which are considerably more elastic than 0.25% SCMC, wave characteristics are absent and the first visible disturbance appears as a large droplet, isolated in space from any systematic growth pattern. The thread lengths connecting the droplets are randomly distributed and thin with distance, eventually leading to the breakup of the column. A series of photographs taken along with the length of a 0.25% Separan jet illustrates these phenomena and is presented in figure 6-12. The behavior of a 0.25% Polyox jet is similar to that shown by 0.25% Separan. At high velocities, the threads are able to undergo large amplitude, three dimensional disturbances without breaking, as shown in photograph (a) of figure 6-14. At a concentration level of 0.5% Separan, no observable disturbances were detected within the limits of the 5 foot distance which could be conveniently photographed.

The photographs of figure 6-13 show how a 0.05% Separan jet changes in appearance from an initial wave-like contour to a configuration of droplets connected by threads. The threads are seen to thin with increasing distance from the nozzle and, at the same time, the droplet diameter increases. Jet breakup results from disruption of a thinning thread. In this dilute viscoelastic jet, there is a

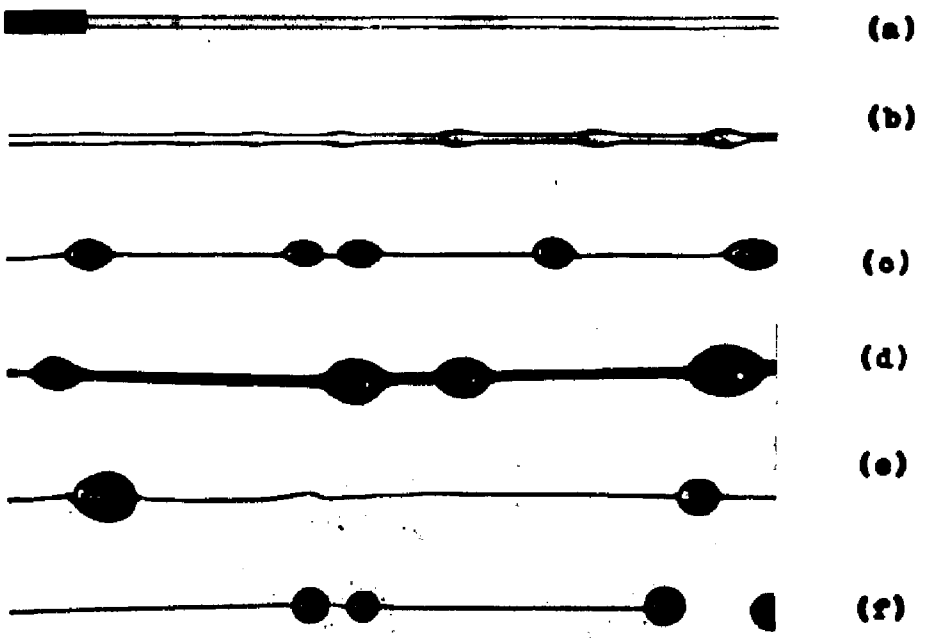

Figure 6-13 Breakup of a Laminar Capillary Jet of 0.05% Separan
Magnification-3.8X; Nozzle diameter-0.0414 cm; Average jet velocity-412 cm/sec; Distance from nozzle tip to midpoint of photograph- (a) 0.9 cm, (b) 12.7 cm, (c) 21.3 cm, (d) 21.3 cm (magnified view of (c)), (e) 31.6 cm, (f) 35.6 cm

preponderance of 'twin' droplets in juxtaposition and separated from the rest by long threads. Photograph (d) of this figure illustrates the interesting symmetry of the 'twin' droplets.

Another type of instability in which the liquid column possesses a screw orientation has been observed with dilute viscoelastic jets. There is only a narrow range where this phenomena is distinctly visible. Photographs (b) and (c) of figure 6-14 shows a 0.05% Guar Gum jet traveling at an average velocity of 350 cm/sec and forming a stable helix whose pitch increases with distance from the nozzle. Near breakup, a disturbance wave with an irregular, but identifiable wavelength can be seen superimposed upon the helix. Another example of a screw instability can be seen in photographs (d) through (i) for a 0.05% Separan jet moving with an average velocity of 690 cm/sec. The disturbance forms close to the nozzle but later dampens out and finally reverts to the droplet-thread configuration which has characterized the viscoelastic jets studied in this investigation. The screw instabilities observed for the capillary jets of 0.05% Guar Gum, 0.05% Separan and the 12.4% aqueous silica dispersion resemble the shapes assumed by molten polymers undergoing melt fracture.

6.5 SUMMARY OF QUALITATIVE EXPERIMENTAL RESULTS

A short summary will be present in order to provide a concise description of the qualitative phenomena just

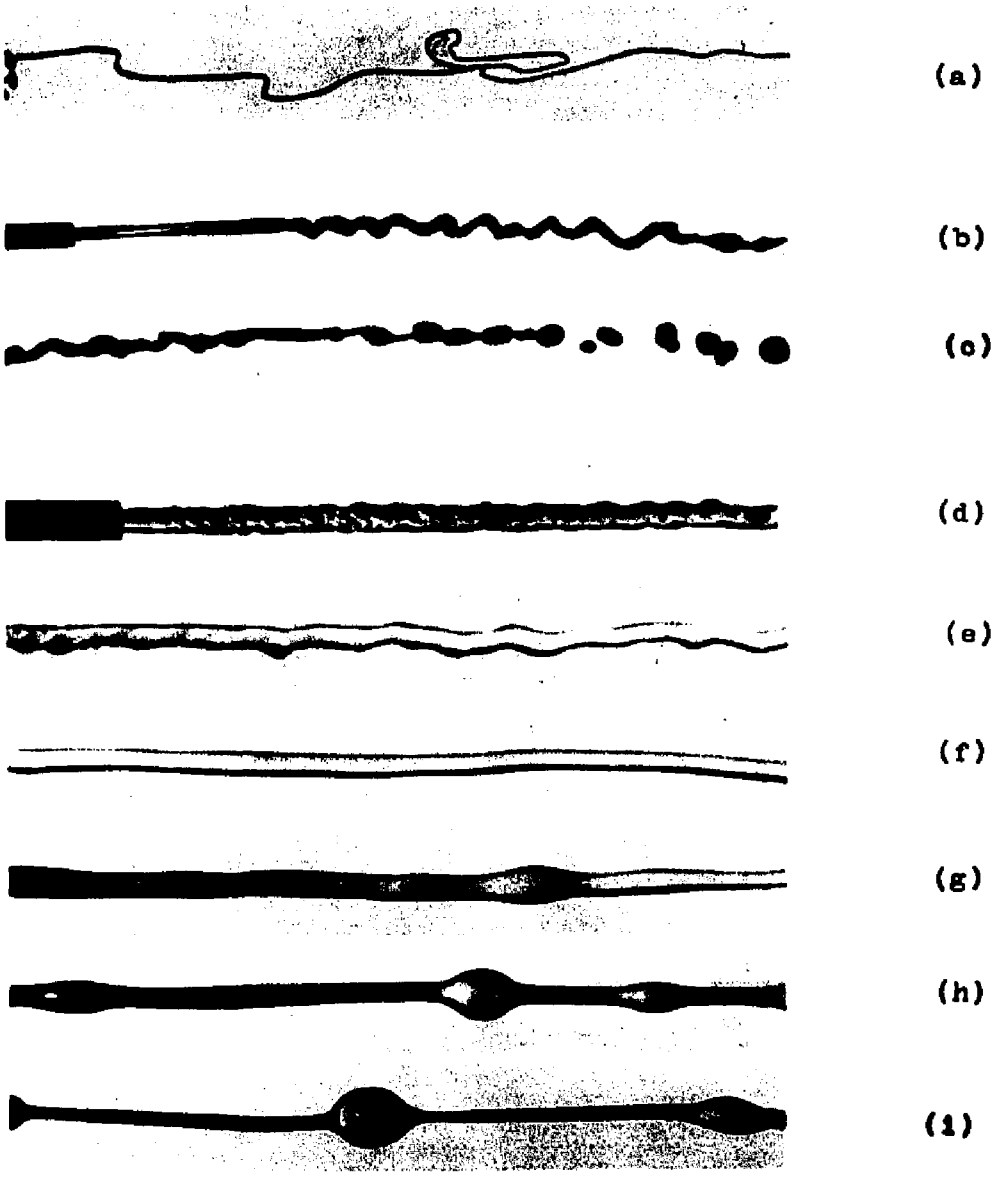

Figure 6-14 Unusual Phenomena Exhibited by Capillary Jets of Viscoelastic Fluids
Photograph (a)-0.25% Separan; Magnification 2.3X; Nozzle diameter-0.0216 cm; Average jet velocity-2810 cm/sec
Photographs (b)-(c) -0.05% Guar Gum; Magnification-0.8X; Nozzle diameter-0.158 cm; Average jet velocity-350 cm/sec; Distance from nozzle tip to midpoint of photograph-(b) 5.1 cm, (c) 11.0 cm
Photographs (d)-(i) -0.05% Separan; Magnification-4X; Nozzle diameter-0.0868 cm; Average jet velocity-690 cm/sec; Distance from nozzle tip to midpoint of photograph- (d) 0.8 cm, (e) 2.3 cm, (f) 7.3 cm, (g) 13.3 cm, (h) 20.0 cm, (i) 26.3 cm

described.

In capillary jets of low viscosity Newtonian liquids, disturbances are propagated as a growing wave with a constant wavelength. The free droplets formed after break-up are uniformly spaced and are an additional indication of their creation from a wave pattern. High viscosity Newtonian jets behave similarly except that, at breakup, the regularity of the wave is altered. Fine threads of liquid often appear in this region but only over relatively short distances.

The less gellified, viscoinelastic fluids formed capillary jets which resembled the appearance of Newtonian jets in that a disturbance was propagated as a growing wave with a constant wavelength. Capillary jets of the highly gellified, viscoinelastic fluids were unstable only at high velocities and displayed no wave characteristics. The instability of all liquids in this category is surprising since, at the low shear rates associated with the growth of symmetric disturbances, the viscoinelastic test fluids show high apparent viscosities. Viscosity is a stabiliz-ing influence and yet the breakup lengths of capillary jets of viscoinelastic liquids were not indicative of any exceptional stability.

Capillary jets of viscoelastic liquids are character-ized by the formation of droplets connected by threads which thin with distance and ultimately break. Even for

very dilute viscoelastic jets, which initially show a disturbance wave, the droplet-thread configuration is ultimately formed. Concentrated solutions of the more elastic polymers form capillary jets which show no wave characteristics. The first visible disturbance appears as a large droplet, isolated in space from any systematic growth pattern.

The photographs in figures 6-1 through 6-14 have served to qualitatively demonstrate the differences between the capillary jets of Newtonian, non-Newtonian inelastic and viscoelastic liquids. Section 6-6 is devoted to a more detailed and quantitative presentation of the data.

6.6 QUANTITATIVE EXPERIMENTAL RESULTS

The experimental data to be presented in this section involves measurements of the jet breakup length and the wavelength of the propagating disturbance wave, as obtained from still photographs and motion pictures. Results for capillary jets of Newtonian, non-Newtonian inelastic and viscoelastic liquids are given in subsections 6.6-1, 6.6-2 and 6.6-3 respectively.

Either pressurized nitrogen or the crosshead of an Instron mechanical tester moved the piston of a cylinder containing the test fluid and forced the liquid through hypodermic needle tubing. Further details on the equipment and procedures used to obtain jet breakup data are provided in chapter 3. Fluid properties are discussed in chapter 4.

6.6-1 CAPILLARY JETS OF NEWTONIAN LIQUIDS

In an experimental investigation of hydrodynamic stability, it is important that the apparatus introduce a low level of disturbances into the liquid. Data were obtained with Newtonian fluids in order to ascertain whether the equipment and procedures used in this work produced results which were comparable to those of previous investigators. The test fluids consisted of water, ethylene glycol, 75% glycerin-water, 97% glycerin-water and pure glycerin.

The dimensionless breakup length- $L/2a_o$, based on the capillary diameter, was measured for the capillary jets formed by each of the test liquids and, in the laminar range, was found to increase with velocity and nozzle diameter. These results are plotted in figures 6-15 through 6-19. Where the velocity range is sufficiently wide, as in the case of the water jet, the L vs. V curve goes through a maximum as air resistance becomes significant. Further increases in velocity bring about a decreased breakup length.

As noted in chapter 5, profile relaxation causes the diameter of the initially relaxed liquid column to change from that of the capillary bore. The experimental measurements were converted to values based on the relaxed diameter using published data (26,32,60) for $\chi = a_\infty / a_o$ as a function of the capillary Reynolds number. By continuity arguements,

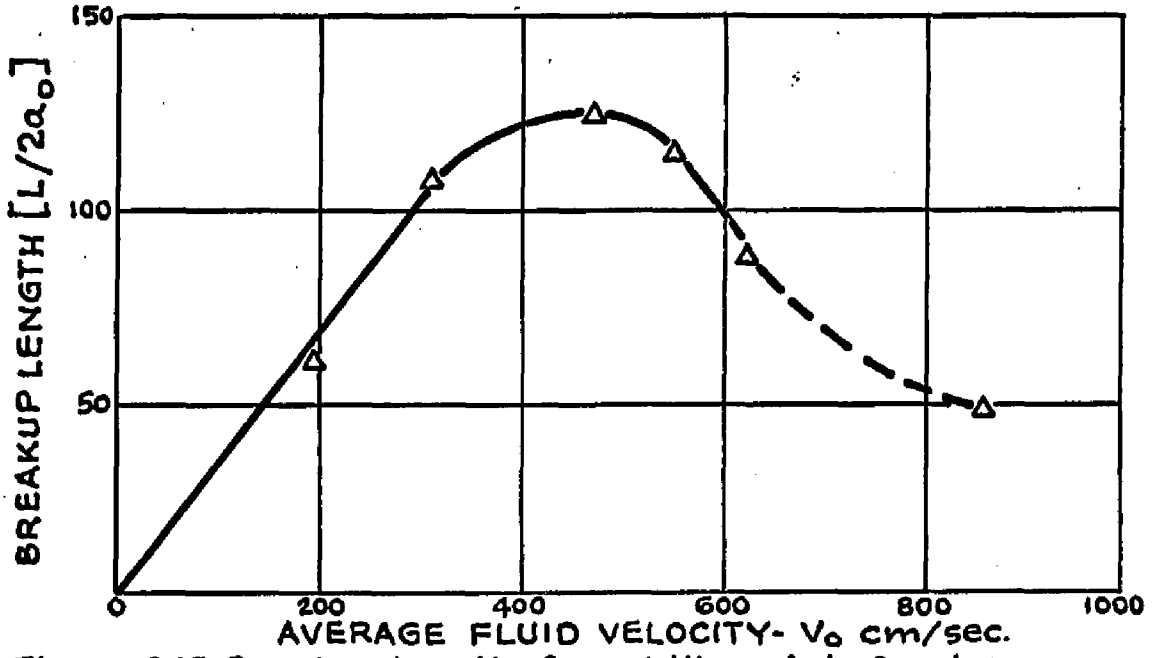

Figure 6-15 Breakup length of a capillary jet of water as a function of fluid velocity; fluid temperature- 25°C, nozzle diameter- 0.0263 cm.

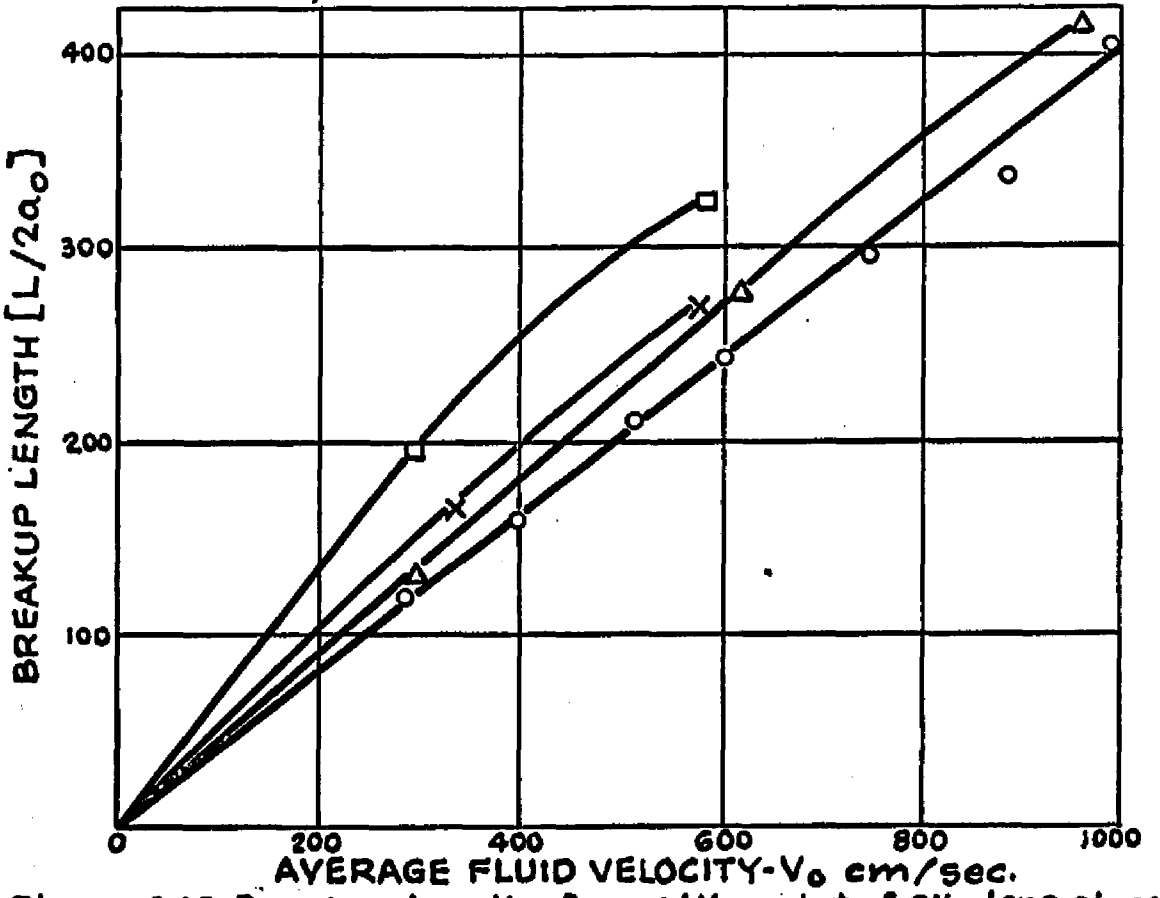

Figure 6-16 Breakup length of a capillary jet of ethylene glycol as a function of fluid velocity and nozzle diameter; fluid temperature-25°C, nozzle diameter: o-0.0216 cm., Δ-0.0263 cm., X-0.0414 cm., □-0.0868 cm.

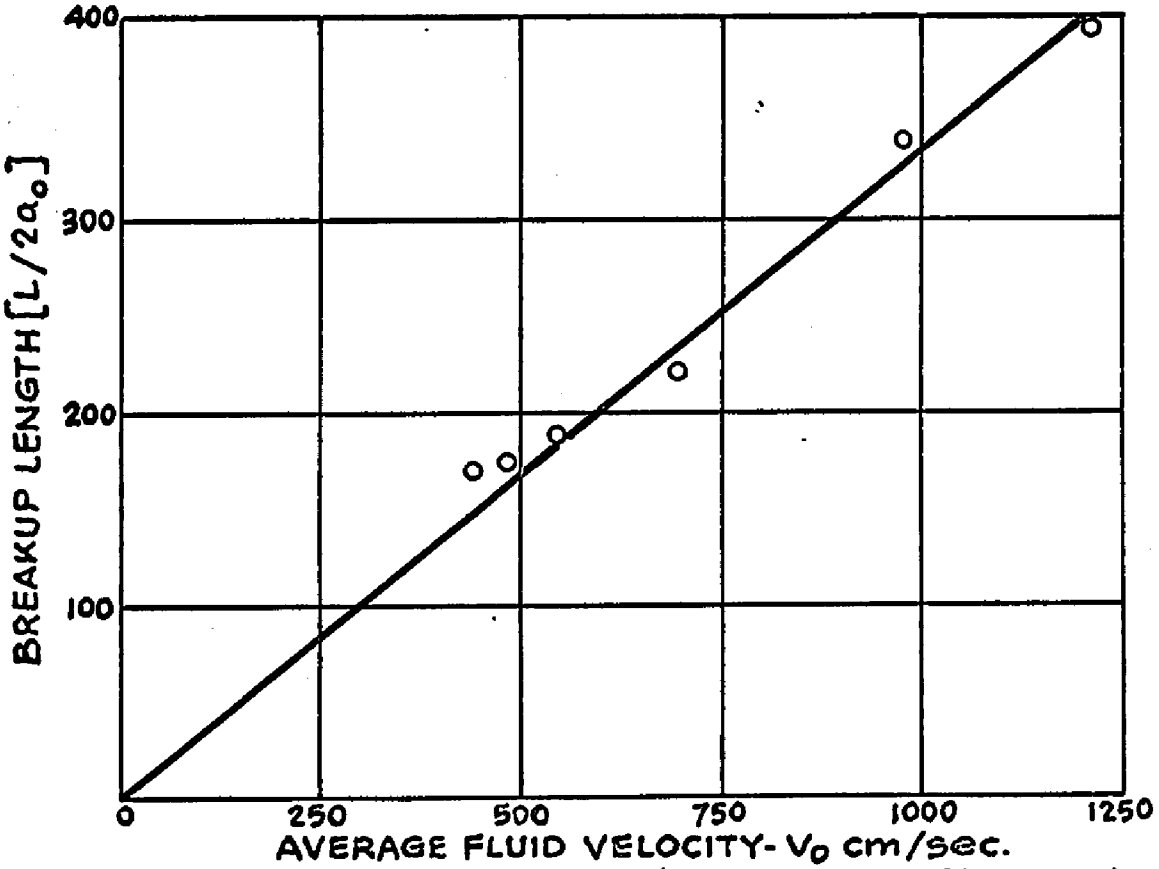

Figure 6-17 Breakup length of a capillary jet of 75% glycerin-water as a function of fluid velocity; fluid temperature-25°C, nozzle diameter-0.0190 cm.

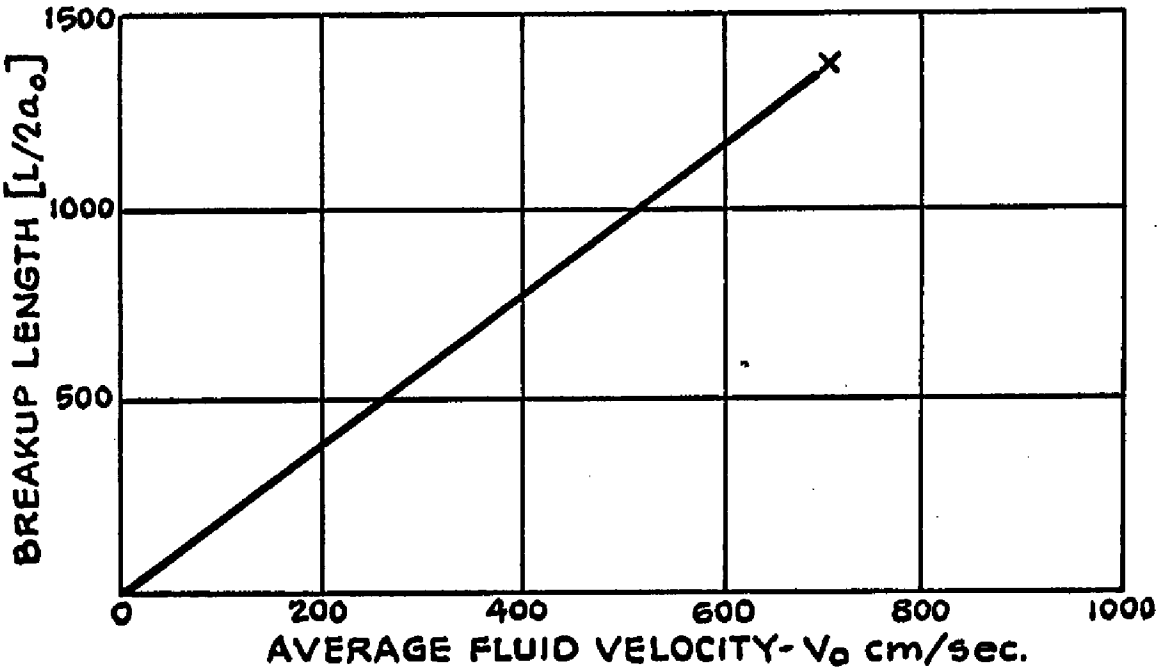

Figure 6-18 Breakup length of a capillary jet of 97% glycerin-water as a function of fluid velocity; fluid temperature-25°C, nozzle diameter-0.0414 cm.

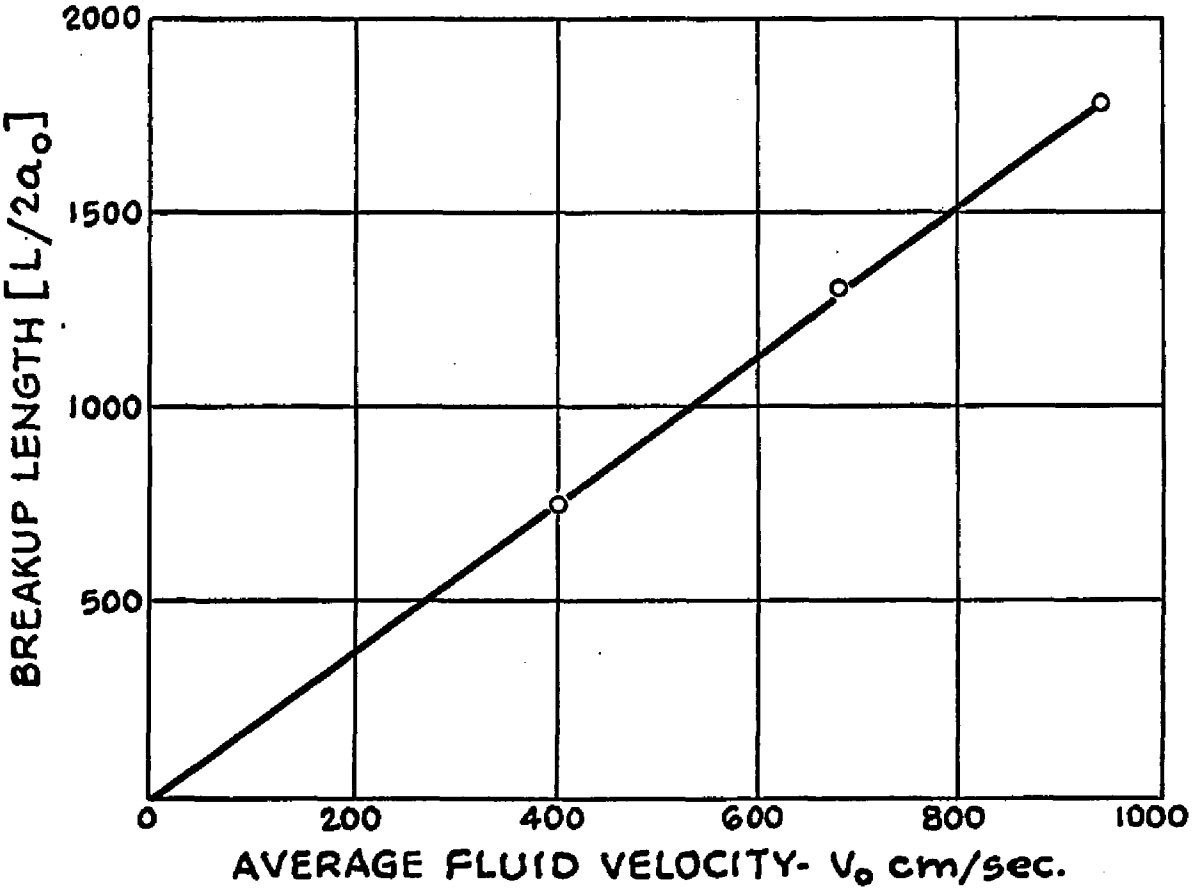

Figure 6-19 Breakup length of a capillary jet of glycerin as a function of fluid velocity; fluid temperature - 31°C, nozzle diameter - 0.0190 cm.

the following relationships apply

$$V = V_o/\chi^2 \quad ; \quad Re_\infty = Re_o/\chi \; ; \quad We_\infty = We_o/\chi^3 \qquad (6.32)$$

where a_∞ , V_∞ , $(Re)_\infty = 2a_\infty V_\infty /\nu$ and $(We)_\infty = 2 a_\infty V_\infty^2 /\sigma$ are the relaxed jet diameter, velocity, Reynolds number and Weber number, respectively. The corresponding quantities relative to the capillary diameter are designed by the subscript zero.

The converted data were compared to the extensive results of Kroesser (39) and Grant (33), as correlated by Kroesser, for the breakup length of a laminar Newtonian jet. As shown in figure 6-20, the agreement is excellent, indicating that the equipment and techniques are satisfactory.

The wave length of the propagating disturbance was measured directly from still photographs of the capillary jets near breakup over a range of nozzle diameters and fluid velocities. It is compared to the prediction of equation (6.26) in table 6-1. This relation, rewritten below for the convenience of the reader, shows that the wavelength will be a weak function of the velocity because of the dependence of the relaxed diameter- $2a_\infty$ on the velocity. The good agreement obtained between experimental and theoretical values is an additional confirmation of the linear stability theory.

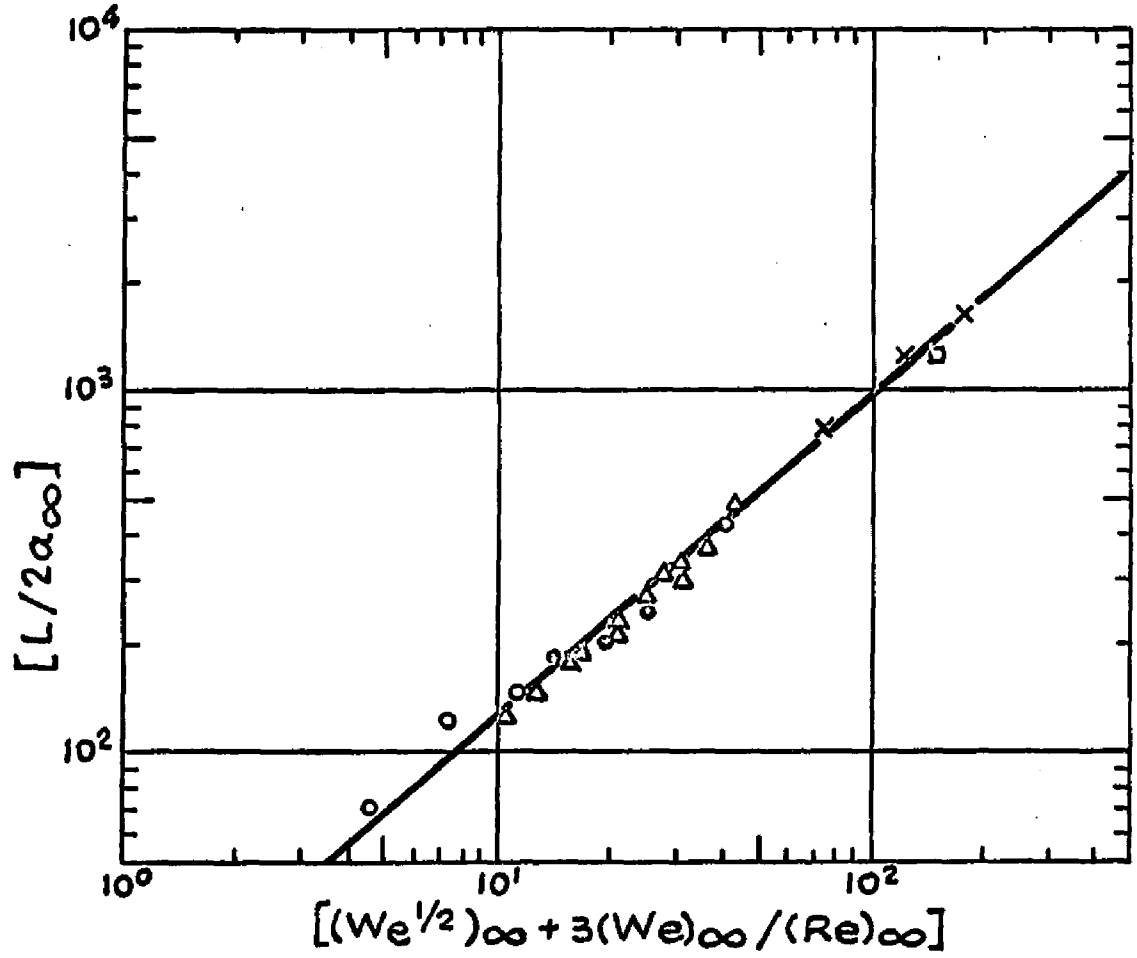

Figure 6-20 Correlation of Newtonian jet breakup data; O-water, Δ-ethylene glycol, ⊙-75% glycerin-water, □-97% glycerin-water, x-pure glycerin, ——Correlation of Kroesser and Middleman (39)

Table 6-1. Wavelengths of Disturbance Waves in Laminar Capillary Jets of Newtonian Liquids

Fluid	Nozzle Diameter	Average Fluid Velocity	Experimental Wavelength	Theoretical Wavelength-Eq. (6-26)
Water	0.0263 cm.	190 cm./sec.	0.08-0.10 cm.	0.10 cm.
		310	0.10	0.10
		522	0.10	0.10
Ethylene Glycol	0.0216	283	0.10-0.12	0.11
		515	0.10-0.12	0.11
		888	0.10-0.12	0.11
	0.0263	622	0.11	0.13
	0.0414	318	0.20	0.20
		590	0.18	0.19
	0.0868	250	0.38	0.39
		290	0.35	0.39
		590	0.35	0.38
		820	0.35-0.40	0.38
75% Glycerin-Water	0.0868	270	0.49	0.45
97% Glycerin-Water	0.0414	708	0.47	0.50

$$\frac{\delta}{2a_o} = \pi\sqrt{2}\left[1 + \frac{3\eta_o}{\sqrt{2\rho a_o \sigma}}\right]^{1/2} \qquad (6.26)$$

6.6-2 CAPILLARY JETS OF VISCOINELASTIC LIQUIDS

The breakup length of 0.1% Carbopol is shown in figure 6-21 as a function of the average fluid velocity and the nozzle diameter. As the jet passes from laminar to turbulent flow, the L vs. V curve exhibits the same characteristic shape as for a Newtonian liquid. For laminar jets, the breakup length increases with both the average fluid velocity and the nozzle diameter. However, as air resistance becomes significant, the L vs. V curve goes through a maximum and further increases in velocity result in a decreased breakup length. When the jet becomes turbulent, the breakup length again increases.

The stability of 0.1% Carbopol was compared to that of water, which behaves as an inviscid liquid under these conditions, by plotting the breakup length against the average fluid velocity for a 0.0263 cm nozzle. Figure 6-22 shows that when both curves are linear, the stability of the ideal fluid is greater than that of the 0.1% Carbopol. This result is surprising since the linear theory presented earlier predicts that viscosity is a stabilizing factor; yet the viscosity of 0.1% Carbopol is higher than that of water at all shear rates and their surface tensions are

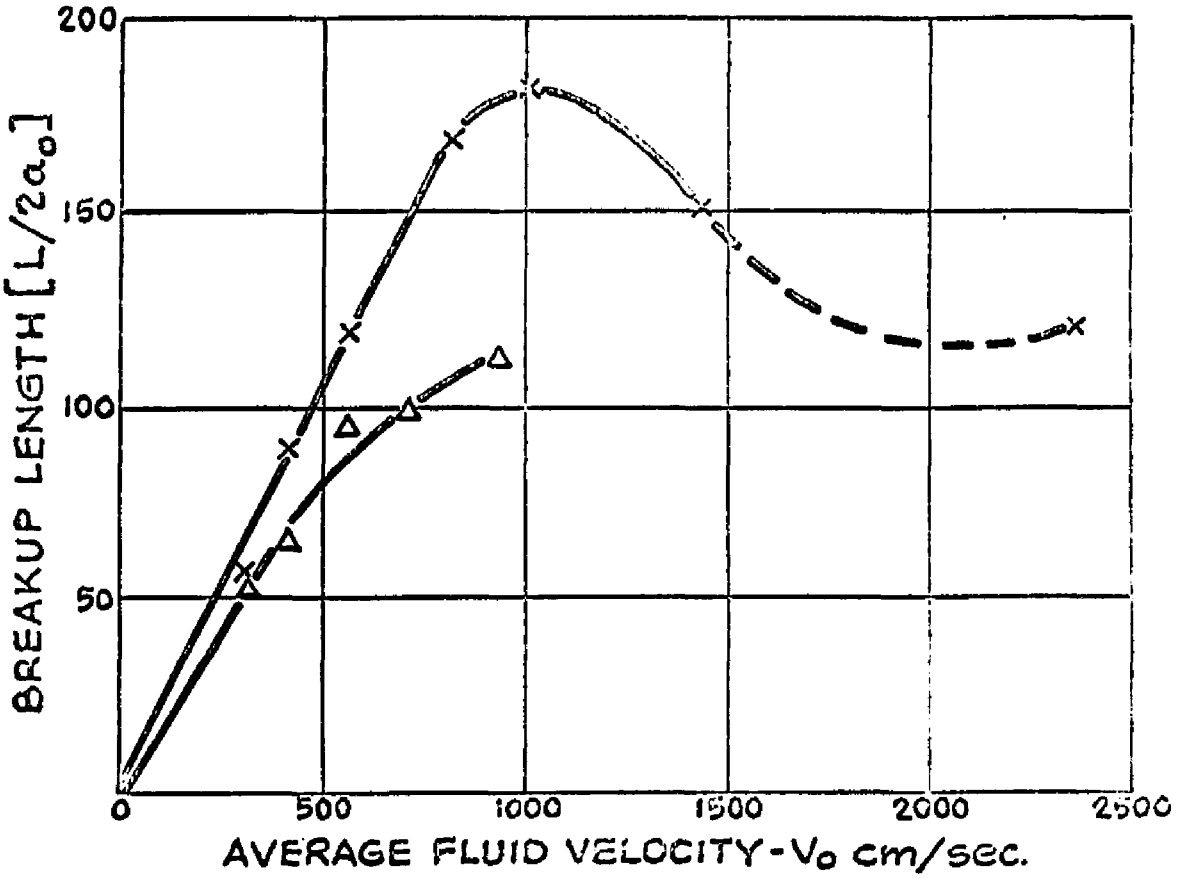

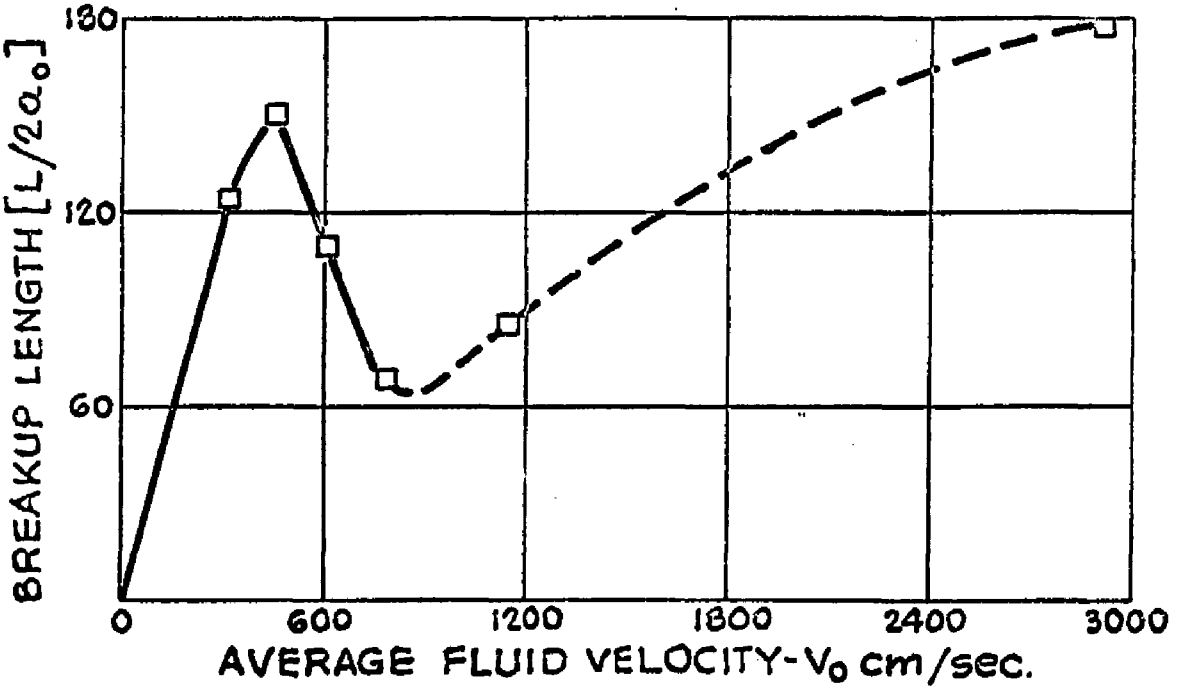

Figure 6-21 Breakup length of a capillary jet of 0.1% Carbopol as a function of fluid velocity and nozzle diameter; nozzle diameter: Δ-0.0263 cm., X-0.0414 cm., □-0.0868 cm.

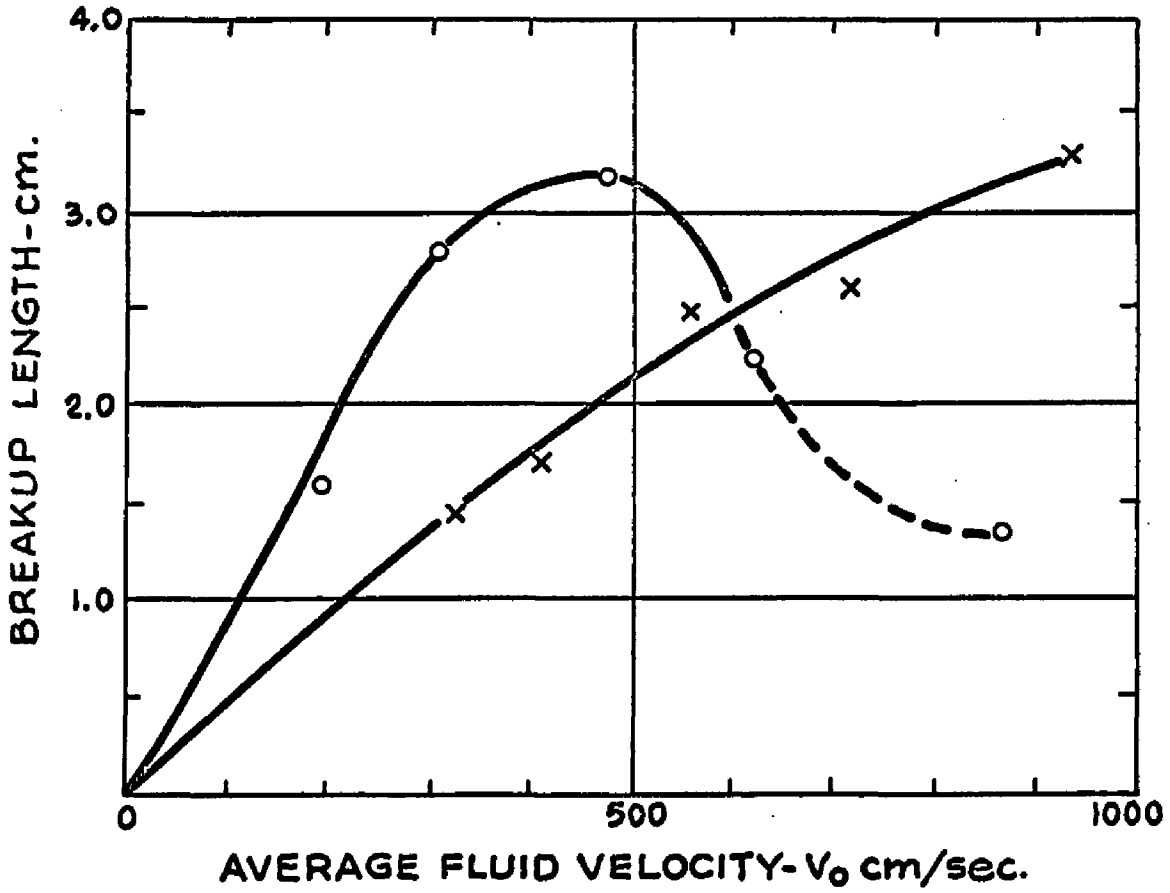

Figure 6-22 Breakup length of capillary jets of water and 0.1% Carbopol as a function of fluid velocity; O-water, X-0.1% Carbopol, nozzle diameter-0.0263 cm.

roughly equivalent. A more dramatic comparison is shown in figure 6-23 where the breakup length of a laminar capillary jet of water is seen to be 2½ times greater than that for 0.1 % Carbopol at the same average fluid velocity and nozzle diameter. However, as shown in figure 6-22, the viscous consistency of the 0.1 % Carbopol does inhibit breakup due to air resistance. The maximum in the L vs. V curve occurs at much higher velocities than for water.

The dimensionless breakup length- $L/2a_\infty$ for a capillary jet of a Newtonian liquid is predicted from equation (6.28) to be proportional to $(2a_\infty)^{\frac{1}{2}}$ for a low viscosity fluid and to be independent of $(2a_\infty)$ for a high viscosity liquid. This result was confirmed by the experimental data of figure 6-20. In order to test the diameter dependence for 0.1 % Carbopol jets, the figure 6-21 data at an average velocity of 300 cm/sec, which is within the laminar range, were replotted as $(L/2a_o)$ vs. $(2a_o)^{\frac{1}{2}}$ in figure 6-24. The nozzle diameter, rather than the relaxed jet diameter, was used since no correlations for the diameter change are available for 0.1 % Carbopol. Based on the analagous Newtonian data, a maximum error of 13.4 % would be expected. The linear dependence shown in figure 6-24 displays the inviscid nature of the 0.1% Carbopol jet.

If the fluid jet is assumed to completely regain its zero shear viscosity after profile relaxation, the disturbance wave will grow at a rate corresponding to this

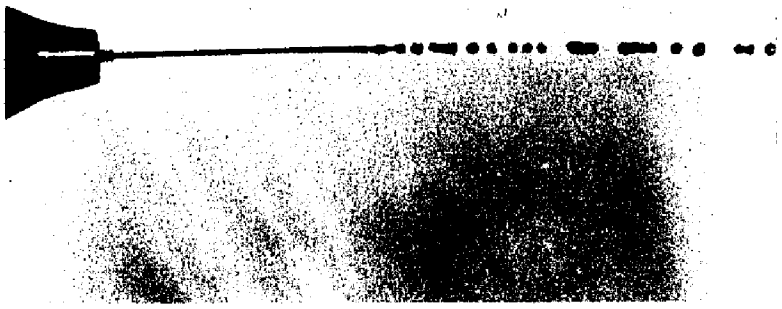

Water Jet

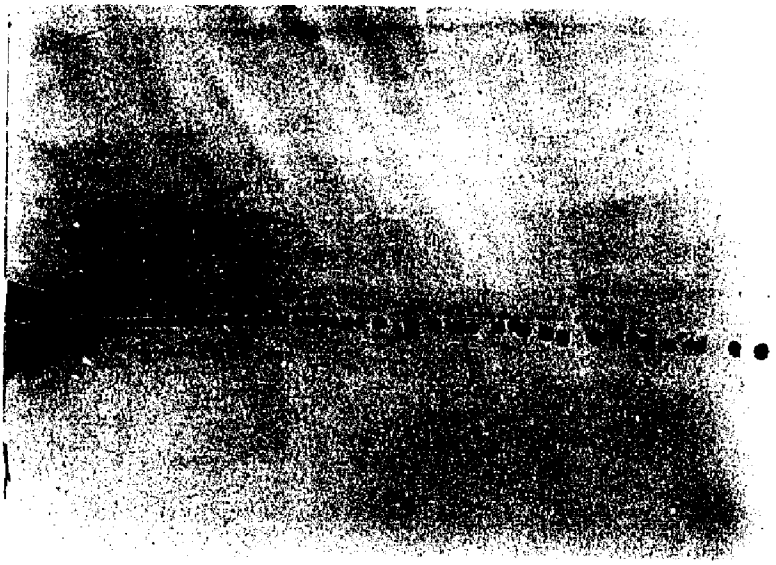

Figure 6-23 Comparison of breakup lengths for capillary jets of water and 0.1% Carbopol; Average fluid velocity-224 cm/sec, nozzle diameter-0.0216 cm.

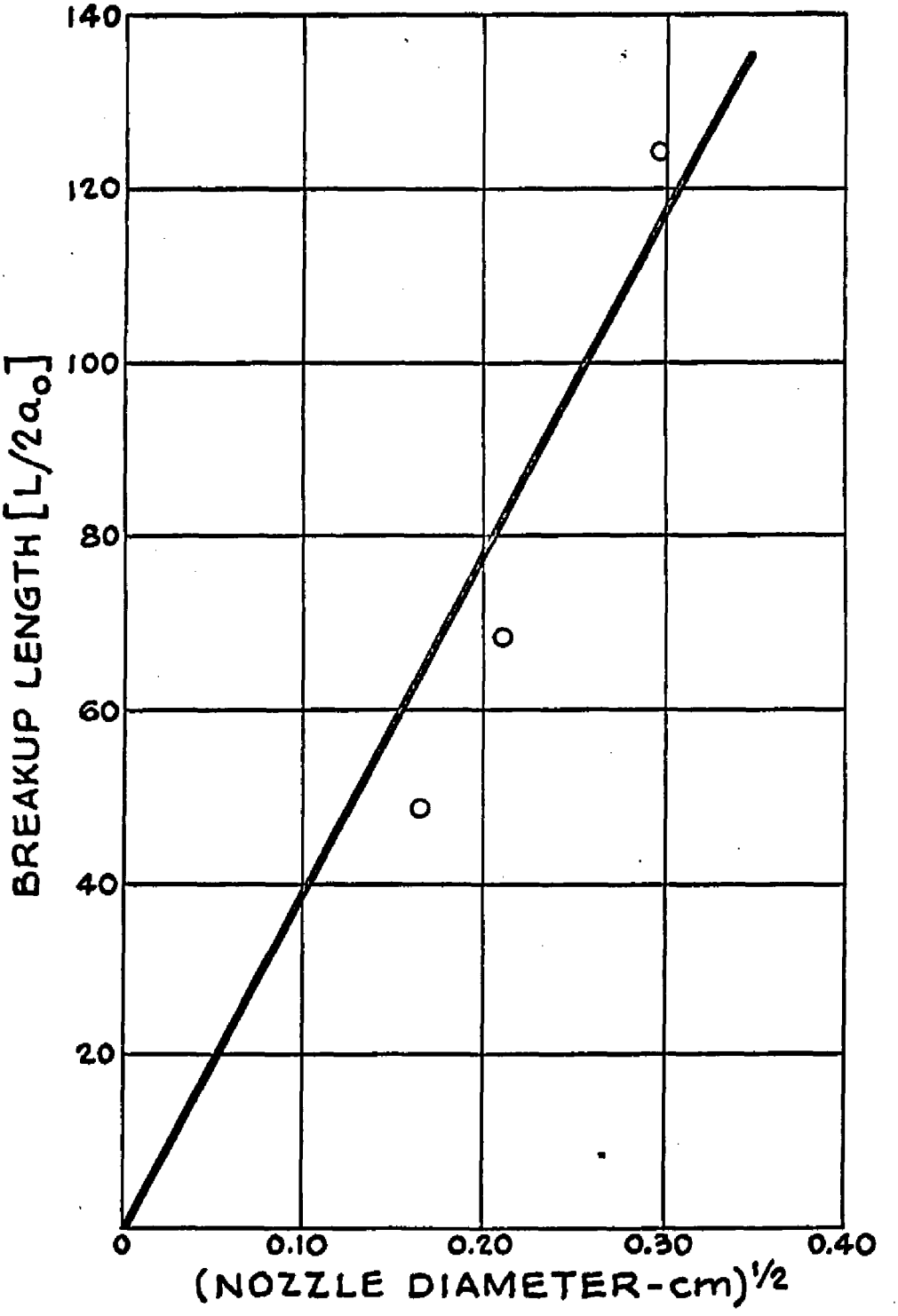

Figure 6-24 Effect of nozzle diameter on breakup length of capillary jets of 0.1% Carbopol; average fluid velocity = 300 cm/sec.

viscosity since the shear rates of wave propagation are quite small. A solution of 0.1% Carbopol shows moderate viscosities at low shear rates and yet the capillary jet of this fluid behaves as an inviscid liquid. This response is possible if the jet initially relaxes of all stresses originating from the previous capillary flow, but does not regain its zero shear viscosity because its structural relaxation time exceeds the jet breakup time. In that case, the behavior of the jet would correspond to that for a liquid having a radially varying viscosity roughly equivalent to that existing at the exit shear rate. This prospect will be explored in the presentation of data for the other viscoinelastic jets.

The breakup length of capillary jets of 24% MPA 60 in xylene and 24% MPA 60 in mineral spirits increases with the average fluid velocity and with the nozzle diameter, as shown in figure 6-25 and 6-26, respectively. All data points have been omitted for clarity because of the considerable scatter amongst them. Due to the thixotropic nature of the fluids, time dependent procedures such as the period spent in the hydraulic cylinder prior to a run may have an effect on the jet behavior. However, the tortuous path taken by the liquids through the fine pore filters, prior to entering the capillary, should have homogenized them. Another possibility for the variation is the presence of air bubbles introduced during the mixing that is required

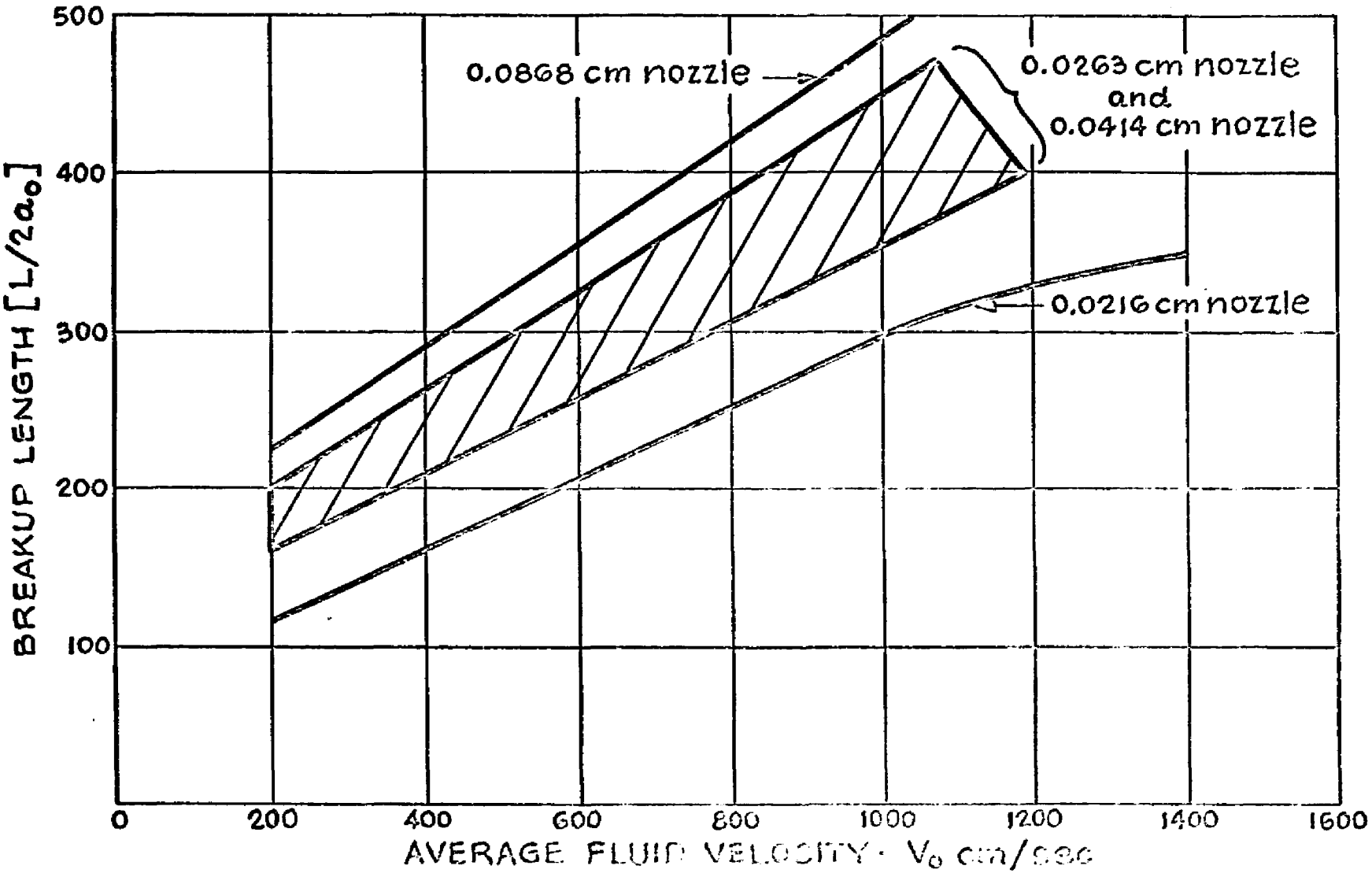

Figure 6-25 Breakup length of a capillary jet of 24% MPA 60 in xylene as a function of fluid velocity and nozzle diameter.

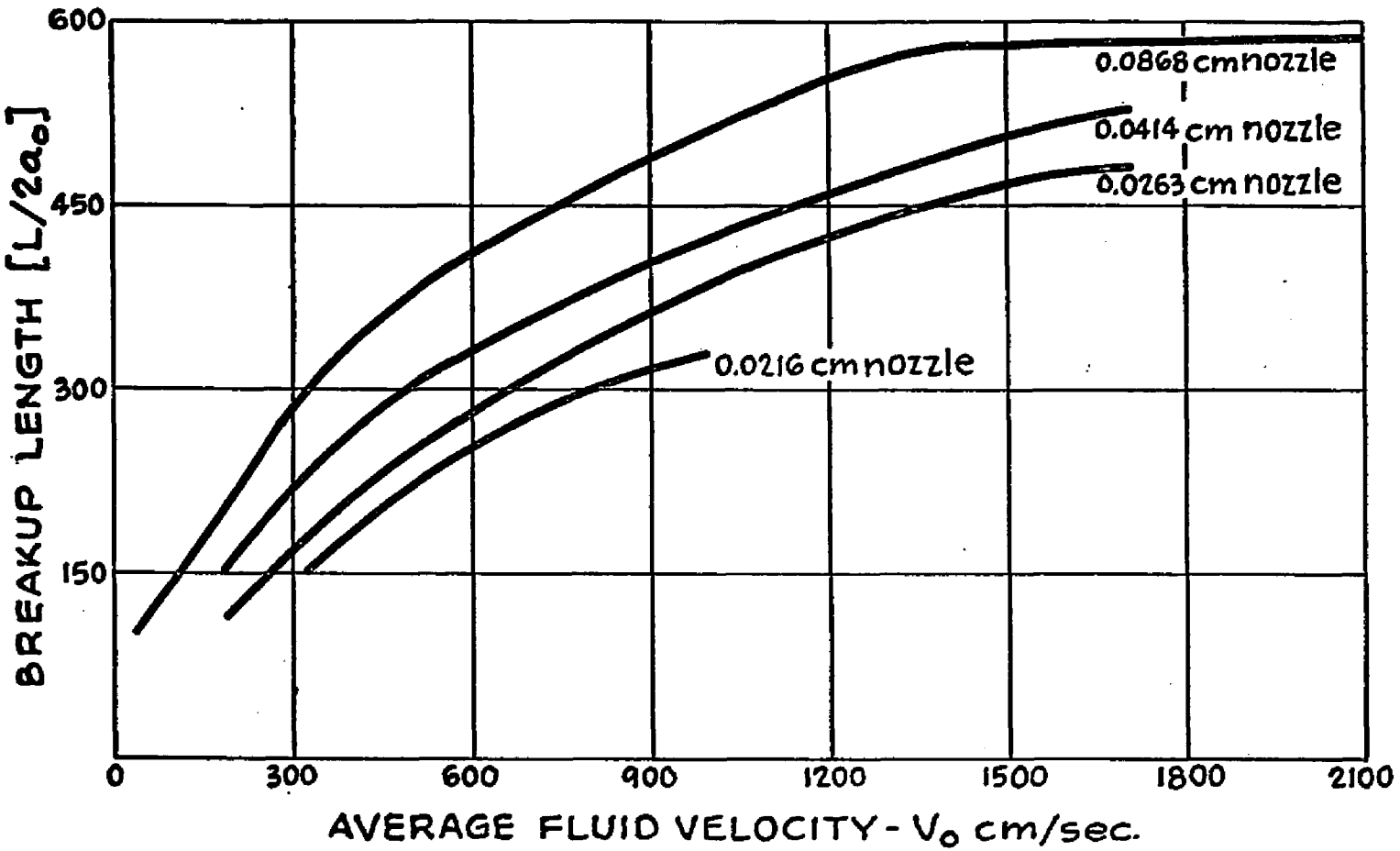

Figure 6-26 Breakup length of a capillary jet of 24% MPA 60 in mineral spirits as a function of fluid velocity and nozzle diameter.

to initially break the gel and pump the fluid into the hydraulic cylinder.

There is no maximum observed in the L vs. V curves within the experimental range of velocities considered. Another difference from previously described phenomena is that the curves do not appear to pass through the origin as with Newtonian and 0.1% Carbopol data. This is consistent with the hypothesis that the fluid has not regained its zero shear viscosity after profile relaxation but instead maintains a viscosity of the same magnitude and distribution as at the capillary exit. The explanation may be made clearer by recourse to the illustration of figure 6-27. The dotted lines represent the linear portion of the L vs. V curves for capillary jets of three Newtonian liquids of viscosities $\eta_a < \eta_b < \eta_c$, respectively. At velocity- V_a, the non-Newtonian inelastic fluid has an apparent viscosity $\eta \approx \eta_a$ and the breakup length- L_a corresponds to that of a Newtonian jet with constant viscosity- η_a. At some lower fluid velocity- V_b, the average apparent viscosity of the viscoinelastic fluid increases to $\eta \approx \eta_b$ and the breakup length L_b is approximately that for a Newtonian jet of constant viscosity- η_b. If the argument is continued in like fashion, the extrapolated L vs. V line does not pass through the origin.

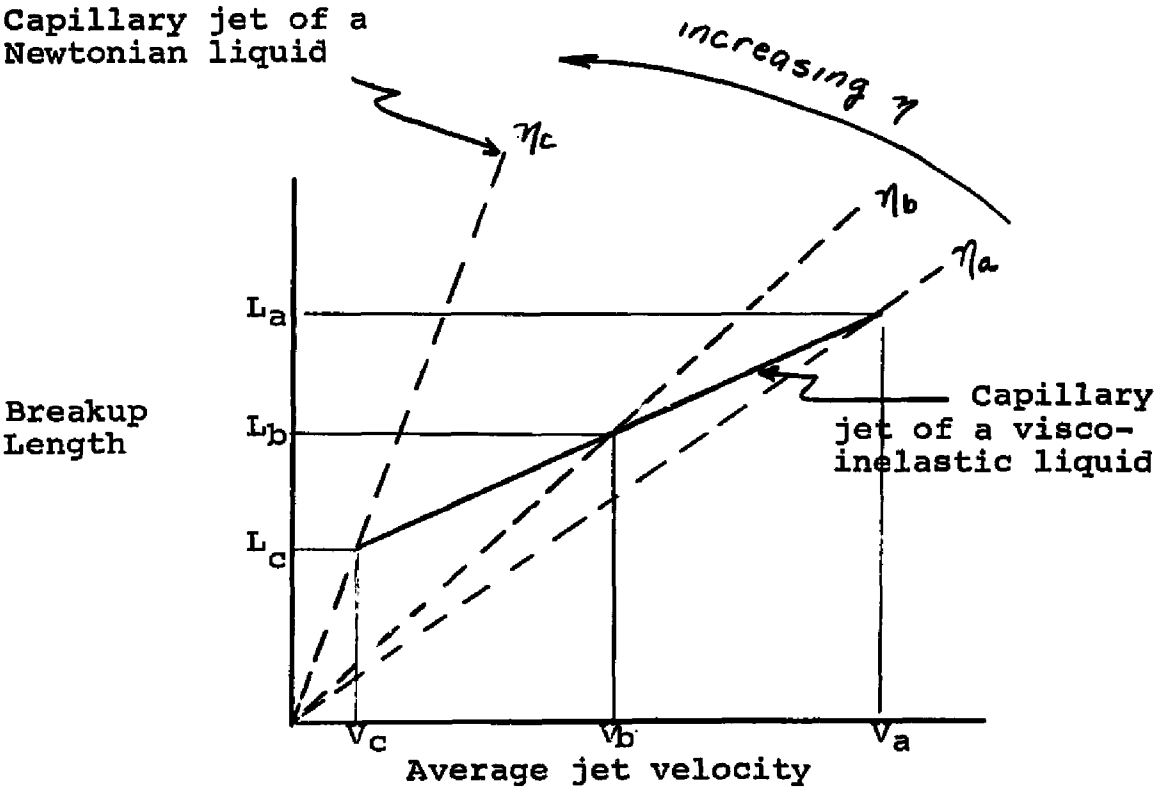

Figure 6-27. The behavior of a capillary jet of a viscoinelastic liquid.

A crossplot of the linear data in figures 6-25 and 6-26, taken at a constant velocity of 500 cm/sec, is given in figure 6-28 and shows $(L/2a_o)$ to be proportional to $(2a_o)^{\frac{1}{2}}$ for both fluids. As with the 0.1% Carbopol data, the nozzle diameters rather than the relaxed jet diameters were used. This linear dependence corresponds to the prediction for a low viscosity liquid and yet their apparent viscosities at low rates of shear are not indicative of such behavior. If, however, the MPA dispersions have a structural relaxation time which exceeds the lifetime of the jet then the apparent viscosity maintained in the jet will be approximately that existing at the capillary exit. Such a fluid would propagate

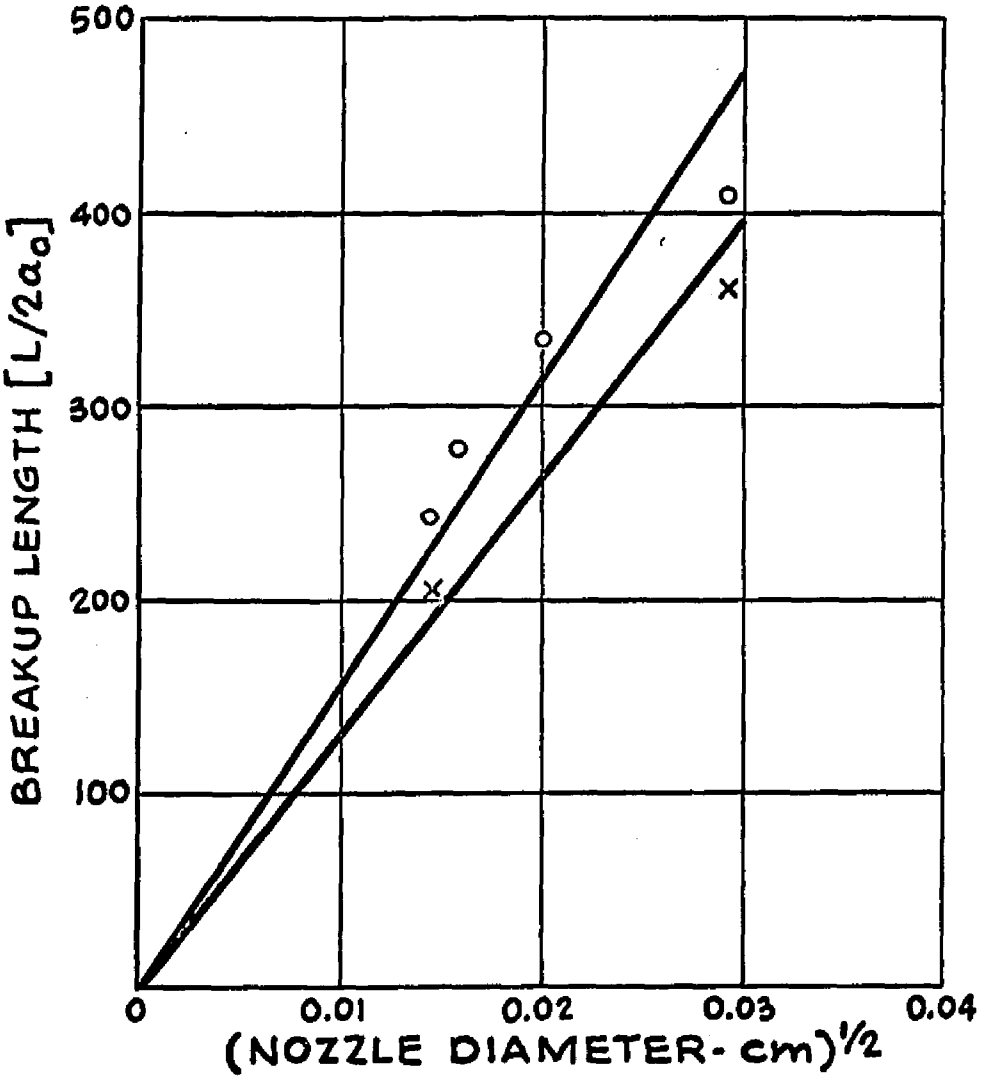

Figure 6-28 Effect of nozzle diameter on breakup length for jets of MPA 60 dispersions at constant fluid velocity; o- 24% MPA 60 in mineral spirits, x- 24% MPA 60 in xylene, average fluid velocity- 500 cm/sec.

disturbance waves for an ideal liquid.

The breakup length of capillary jets of 0.2 % Carbopol increases with the nozzle diameter and with the average fluid velocity, as shown in figure 6-29. At high velocities, data for the 0.0216 cm. nozzle indicate that the breakup length becomes independent of the nozzle diameter. No maximum is observed in the curves within the experimental range of velocities investigated, as is seen for Newtonian and 0.1 % Carbopol jets. The breakup length data do not appear to pass through the origin and the reason for this is felt to be due to the unrelaxed molecular structure as explained previously for the MPA 60 dispersions (figure 6-27). Similarly, the breakup lengths are not indicative of any exceptional stability which would be expected if the 0.2% Carbopol had regained its 'at rest' gel structure after profile relaxation.

A crossplot of the figure 6-29 data, taken at a laminar velocity of 500 cm/sec is given in figure 6-30 and shows the dimensionless breakup length- $L/2a_o$ to vary linearly with the nozzle diameter. This dependence does not correspond to either of the Newtonian predictions for low and high viscosity liquids and this behavior is not yet understood.

Solutions of 0.6% Carbopol are semi-rigid gells with very high apparent viscosities at low rates of shear, as may be seen from the data of figure 4-8 . The classical

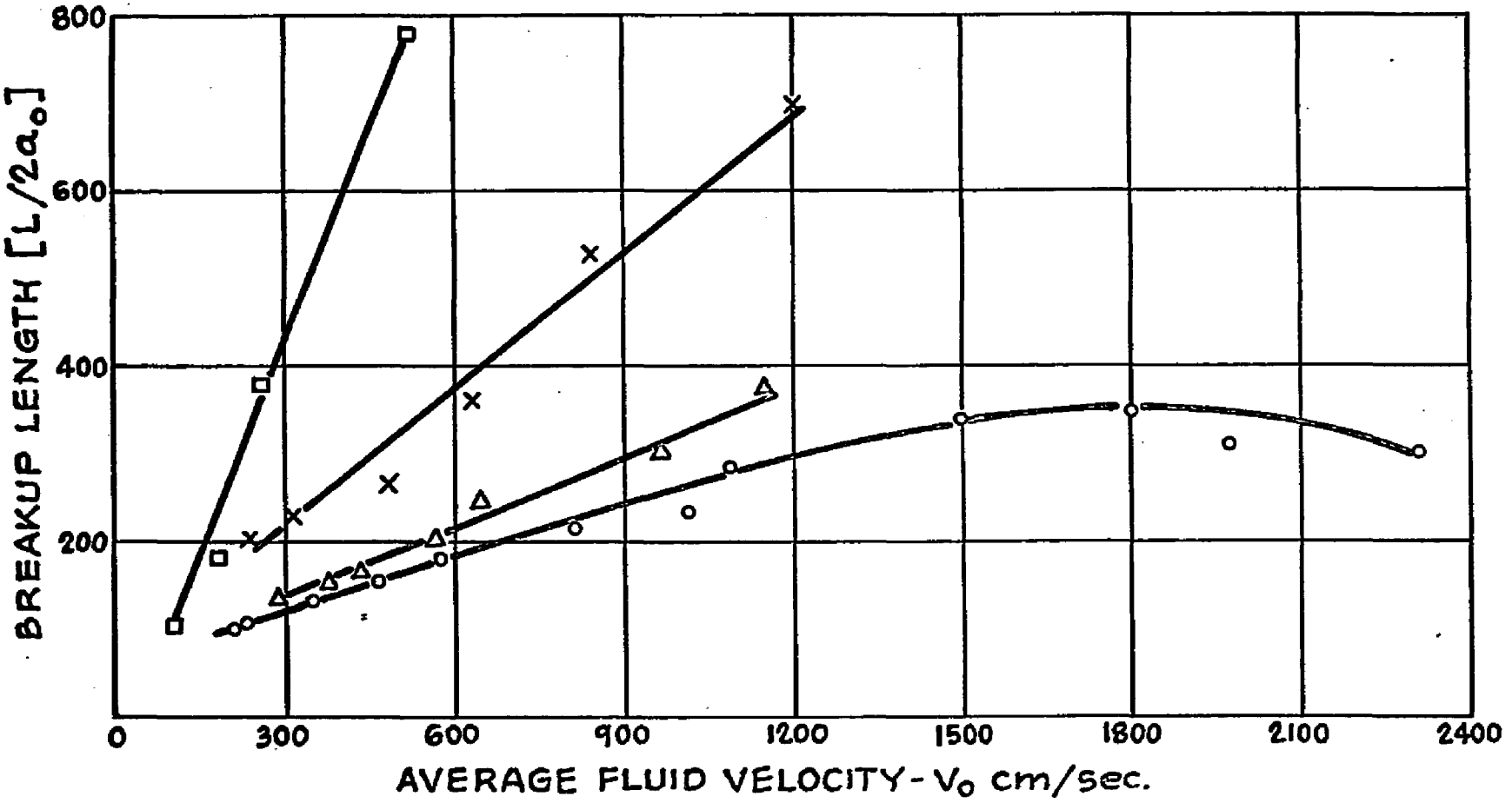

Figure 6-29 Breakup length of a capillary jet of 0.2% Carbopol; nozzle diameter: o - 0.0216 cm., Δ - 0.0263 cm., X - 0.0414 cm., □ - 0.0868 cm.

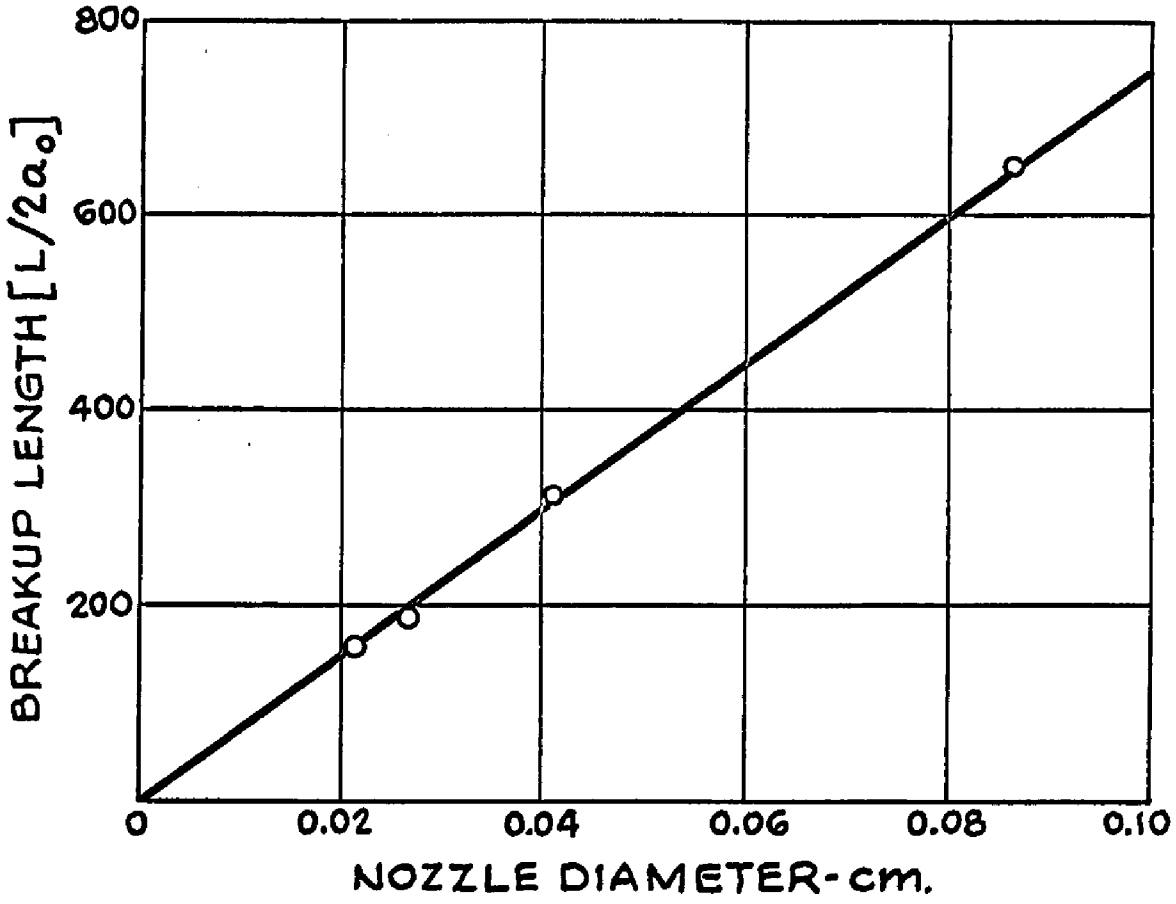

Figure 6-30 Effect of nozzle diameter on breakup length of a 0.2% Carbopol jet at constant fluid velocity; average fluid velocity = 500 cm/sec.

stability theory of Weber, which assumes an initially relaxed liquid column at its zero shear viscosity, would predict complete stability for capillary jets of 0.6% Carbopol. Figure 6-31 shows that 0.6% Carbopol jets are stable at low velocities but are increasingly unstable at high velocities. This behavior is reminiscent of capillary jets of 12.4% silica dispersions (see figures 6-8 through 6-10). Again, in order to explain the data it must be assumed that the liquid column is not initially relaxed at its zero shear viscosity, but instead is substantially at the apparent viscosity possessed at the capillary exit. Thus, only at the very high velocities used to obtain the figure 6-31 data is the apparent viscosity low enough for the 0.6% Carbopol jet to be destroyed.

The specific dependence exhibited in figure 6-31 cannot be explained in terms of a shear dependent viscosity whose power law exponent is less than unity. However, at these very high velocities, air resistance is significant and it has been shown for Newtonian and 0.1% Carbopol jets under similar conditions that a decreased stability with increasing velocity is also displayed. It is likewise possible that, at these very high shear rates, some irreversible structural degradation might be occurring.

In order to give some interpertation to the experimental data, the breakup lengths for capillary jets of 0.2% and 0.6% Carbopol solutions were compared to the Newtonian expectation that

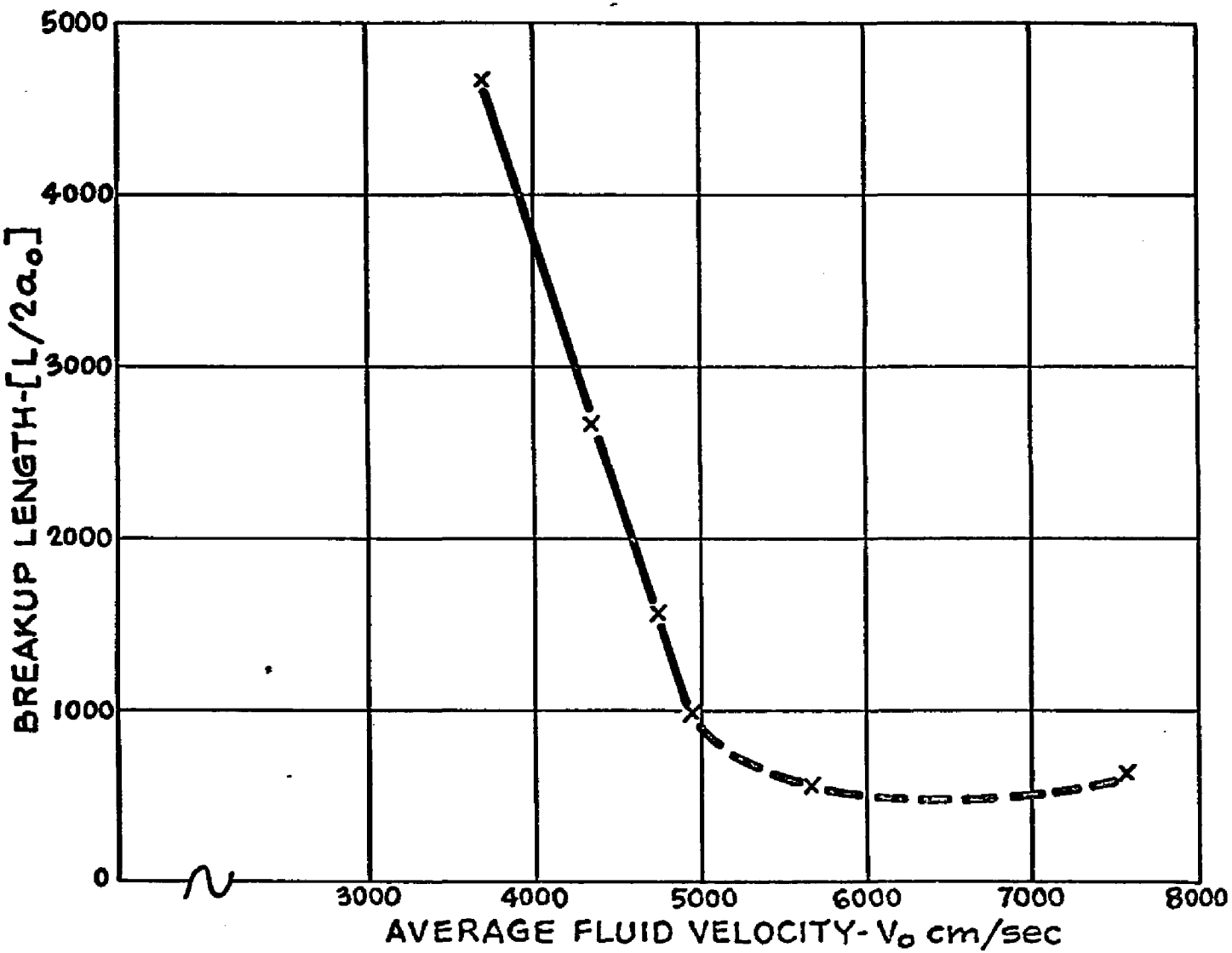

Figure 6-31 Breakup length of a capillary jet of 0.6% Carbopol as a function of fluid velocity; nozzle diameter- 0.0414 cm.

$$L/2a_{\infty} = C(We_{\infty}^{\frac{1}{2}} + 3\ We_{\infty}/Re_{\infty}) \qquad (2.9)$$

Two extreme cases were considered for the propagation of disturbance waves in viscoinelastic jets. The differences in the models will be reflected in the numerical value of the Reynolds number used in equation (2.9) . The first assumes that, outside the capillary, the fluid 'instantly' relaxes from all stresses generated during the capillary flow and also 'instantly' regains the gellified structure possessed under zero shear conditions. Since the shear rates associated with the growth of small, symmetrical disturbances are insufficient to cause significant departure from Newtonian behavior, the disturbance waves are assumed to propagate at a rate corresponding to the zero shear viscosity. However, the viscoinelastic test fluids have a yield stress and do not display any clearly defined zero shear viscosity. For comparitive purposes, the apparent viscosity at a shear rate of 0.1 sec^{-1} will be used to approximate the zero shear viscosity. This may be obtained from figure 4-8.

In the other case considered, it was assumed that the time required to reform the zero shear structure of the fluid is of the same order as or larger than the lifetime of the jet. The liquid column, in this instance, is also taken to be initially relaxed from all prior stresses.

However, because of the long structural formation time, the viscoinelastic fluid behaves as a Newtonian fluid with an average apparent viscosity approximately equivalent to that possessed at the nozzle exit. This behavior would be reflected in the use of a generalized non-Newtonian Reynolds number such as that defined by Metzner and Park (53), $Re_o' = (2a_o)^n (V_o)^{2-n} \rho / K \cdot 8^{n-1}$. The choice of this particular Reynolds number is not unique. All quantities are evaluated at the capillary flow conditions. The constants K and n are fluid parameters in the power law relation

$$\tau_{12} = K \Delta_{12}^n \qquad (1.14)$$

Table 6-2 compares the breakup lengths predicted for each of these two proposed models with representative experimental data for capillary jets of 0.2 % Carbopol and 0.6 % Carbopol. It is evident from the results that the assumption of a viscoinelastic jet propagating disturbances at a rate corresponding to its zero shear viscosity is totally inadequate for these fluids. The predicted breakup lengths for this model are many orders of magnitude higher than the experimental values. But the hypothesis that the viscosity possessed in the capillary is maintained throughout the lifetime of the jet provides results that are generally consistent with those measured.A similar comparison with the MPA 60 dispersions was not considered

feasible because the thixotropic nature of these fluids precluded the determination of the apparent viscosity at low shear rates. Data obtained with capillary jets of 0.1 % Carbopol was also excluded because of its unexplainable enhanced instability compared to inviscid jets.

Encouraged by the general agreement of the experimental data for the Carbopol solutions in table 6-2 with the assumption of a structural formation time which is large compared to the jet breakup time, breakup length measurements for all the Carbopol solutions and MPA 60 dispersions are plotted in the form of

$$\frac{L}{2a_o} = C\left[We_o^{1/2} + 3\frac{We}{Re'_o}\right] \qquad (6.32)$$

where Re'_o is given by

$$Re'_o = \frac{(2a_o)^n (V_o)^{2-n} \rho}{K \cdot 8^{n-1}} \qquad (6.32a)$$

The results are shown in figure 6-32 where the solid lines indicate the range of the Newtonian breakup length data determined from this work and the measurments of Grant (33) and Kroesser (39). General agreement is indicated between the viscoinelastic and the Newtonian data when plotted in the form of equation (6.32) . This accord represents a strong statement for the belief that the gel structure is not formed to any significant extent

Table 6-2. Comparison of calculated breakup lengths based on assumed viscosities with experimental values for viscoinelastic jets.

Fluid	Nozzle Diameter	Average Fluid Velocity-Vo	$(L/2a_o)$ based on η at $\dot{\gamma}_w$	$(L/2a_o)$ expt'l.	$(L/2a_o)$ based on η at $\dot{\gamma}=0.1$ sec^{-1}
0.2% Carbopol	0.0216 cm	300 cm/sec	120	120	45,000
	0.0263	300	111	137	45,000
	0.0414	300	133	215	45,000
	0.0868	300	182	380	45,000
0.6% Carbopol	0.0414	3700	1610	4700	$\sim 10^7$
		4900	1880	1000	$\sim 10^7$

within the lifetime of the jet. The same conclusion was reached from an examination of the profile relaxation data presented in chapter 5. Had the zero shear viscosity been used, instead of the apparent viscosity at the shear rate within the capillary, the data points would have fallen several orders of magnitude away from the Newtonian data.

The experimental data for the viscoinelastic jets should not be expected to correlate to a high degree for a variety of reasons. Undoubtedly, there is some viscosity buildup during the lifetime of the jet so that the use of the average apparent viscosity at the nozzle exit represents an idealization. Secondly, the use of equation (6.32) was not derived from any fundamental consideration of the equations of motion but is merely an arbitrary modification of the Newtonian relation, equation (2.9). Considerations as to the effect of the radially varying, apparent viscosity actually existing at the nozzle exit have been omitted from the arguement. The constants K and n , determined from the capillary viscometer measurements, are not known with the same degree of accuracy as is a Newtonian viscosity. It is not uncommon that literature values for these constants, determined by different investigators , differ by $\pm$ 30 % . The magnitude of the generalized non-Newtonian Reynolds number- Re_o' is especially sensitive to the value of the exponent- n .

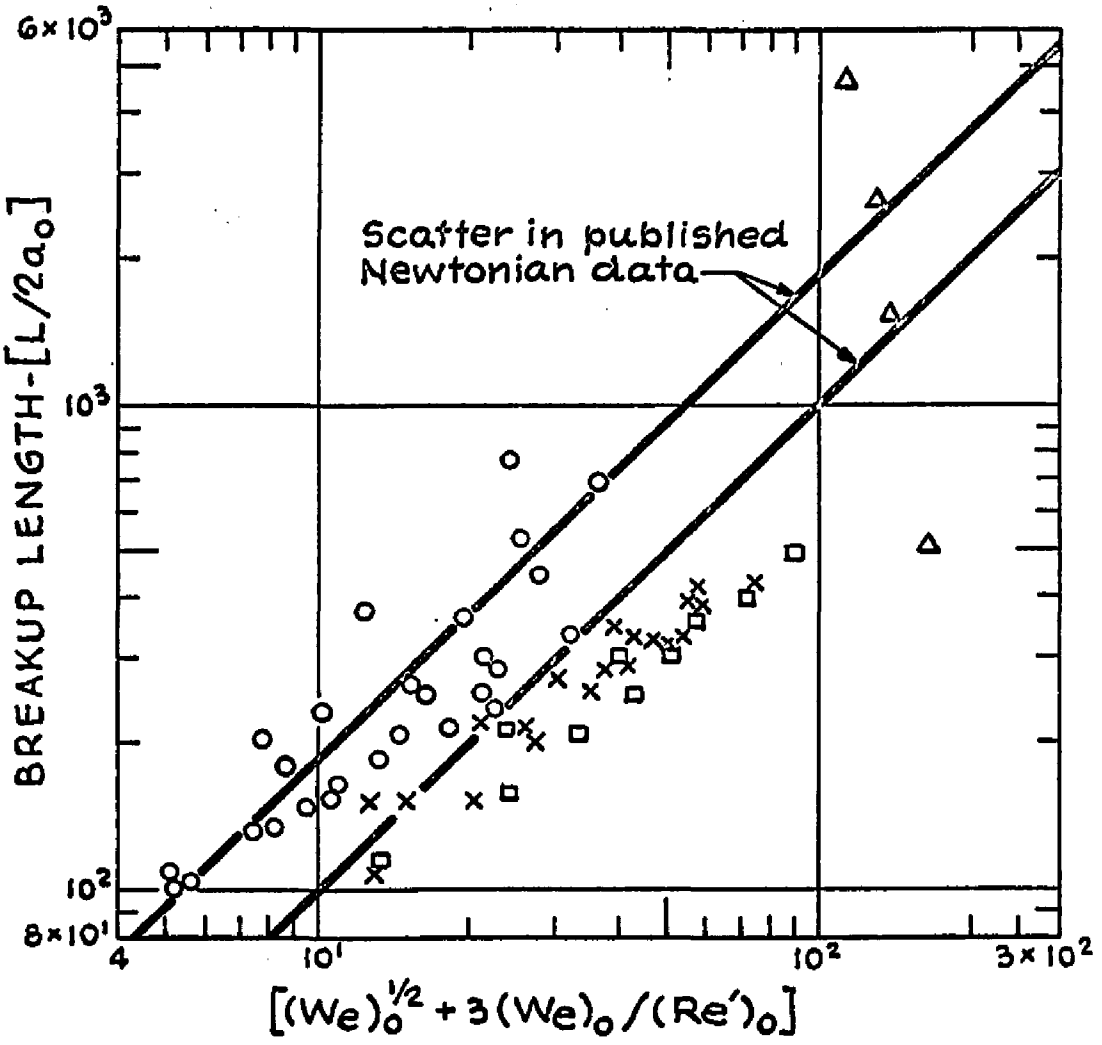

Figure G-32 Correlation of non-Newtonian jet breakup data based on a structural formation time which exceeds the jet breakup time; O-0.2% Carbopol, Δ-0.6% Carbopol, □-MPA 60 in xylene, X-MPA 60 in mineral spirits.

Finally, the possibility of shear degradation or of ultraviolet light deterioration between the time of property measurement and the determination of jet breakup lengths is unaccounted for.

The wavelength of the disturbance wave was measured from photographs in the region just prior to breakup. An apparent viscosity at that point was calculated from the Newtonian relation, equation (6.26), using the nozzle diameter instead of the relaxed jet diameter. Table 6-3 compares this calculated viscosity at breakup with the apparent viscosity based on the average shear rate within the capillary. Differences between the two values should be indicative of structural formation within the liquid.

The results are consistent with the findings of the breakup length data just presented that the structural relaxation time is of the same order as or exceeds the lifetime of the jet. Thus, the apparent viscosity for 0.1% Carbopol based on wavelength calculations displays the same inviscid nature as the apparent viscosity determined from capillary viscometer measurements. Capillary jets of 0.2% Carbopol exhibit disturbance wavelengths which denote a limited viscosity buildup from that possessed at the nozzle exit. The apparent viscosities calculated from wavelength data for 24% MPA 60 in xylene are generally below the apparent viscosities computed at the average shear rate within the capillary. Wavelength measurements taken from photographs for this fluid were not consistent and since

Table 6-3. Comparison of apparent viscosities calculated from wave length data at breakup with apparent viscosities at the capillary wall shear rate for viscoinelastic jets.

Fluid	Nozzle diameter	Average Fluid Velocity-Vo	Wave length at breakup	Apparent Viscosity from eq. (6.26)	Apparent Viscosity at $\dot{\gamma}_w$
MPA60 in xylene	0.0216 cm	328 cm/sec	0.11 cm	0.10 poise	0.35 poise
		474	0.12	0.15	0.31
		630	0.12	0.15	0.29
	0.0263	382	0.25	1.7	0.35
	0.0414	286	0.23	0.21	0.43
		448	0.19	0.03	0.38
		562	0.20	0.07	0.37
0.2% Carbopol	0.0216	228	0.17	0.79	0.08
	0.0263	645	0.20	0.75	0.058
	0.0414	472	0.30	0.85	0.08
0.1% Carbopol	0.0414	300	.15	0	$\sim$0.01-0.03
		440	.15	0	$\sim$0.01-0.03
	0. 0868	310	.35	0	$\sim$0.01-0.03
		410	.35	0	$\sim$0.01-0.03

changes of only 0.1 cm. significantly affect the calculated viscosities, the results are not considered accurate. However, all the viscoinelastic test fluids showed terminal viscosity values that were of the same order as the apparent viscosities possessed at the capillary exit. The model of a viscoinelastic jet propagating disturbances at a rate corresponding to its zero shear viscosity is clearly invalid since the wavelengths demanded by this model are several orders of magnitude larger than the experimental values.

6.6-3 CAPILLARY JETS OF VISCOELASTIC LIQUIDS

In Newtonian jets, a disturbance is propagated as an exponentially growing wave with a constant wavelength. There is almost no difference between the place where the wave is strongly evident and the place of final breakup. Capillary jets of 0.25% SCMC, a very slightly viscoelastic liquid, initially propagate disturbances in a similar manner but, as seen in figure 6-11, the growth of the wave is arrested and a string of droplets connected by threads, which thin with distance, is formed. Thread formation will be seen to be a characteristic of all viscoelastic jets used in this investigation and the reasons for its presence are not yet known. Final breakup occurs much later and, in this region of non-linear disturbances, the predictions of linear theory are inapplicable.

The breakup length for 0.25% SCMC jets is therefore

defined as the distance from the nozzle where the disturbance wave amplitude is comparable to the original jet radius, a definition which would give satisfactory results for Newtonian jets. Using this criterion, the breakup length and wavelength are found to lie between those predicted for an inviscid jet and those for a Newtonian fluid of the same zero shear viscosity, as shown in figures 6-33 and 6-34 respectively. This result is in agreement with the theoretical predictions. The nozzle diameter, rather than the relaxed jet diameter, was used in the calculations as information on the latter is not available for capillary jets of 0.25% SCMC.

Viscoelastic jets of 0.25% Separan and 0.25% Polyox, shown in figures 6-1 and 6-12, possess a unique initial disturbance distance, which represents the distance from the nozzle to the sudden appearance of a large droplet. Values for this distance are not as reproducible as for the Newtonian jet breakup length and were found to vary by $\pm$ 30%. The initial disturbance distance for a capillary jet of 0.25% Separan increases with the fluid velocity and the nozzle diameter, as shown in figure 6-35. A crossplot of the data, taken at a fluid velocity of 400 cm/sec, which is within the linear range, is given in figure 6-36 and illustrates the strong dependence of the (initial disturbance length/nozzle diameter) ratio on the nozzle diameter. As the nozzle diameter increases, the fluid becomes less sheared

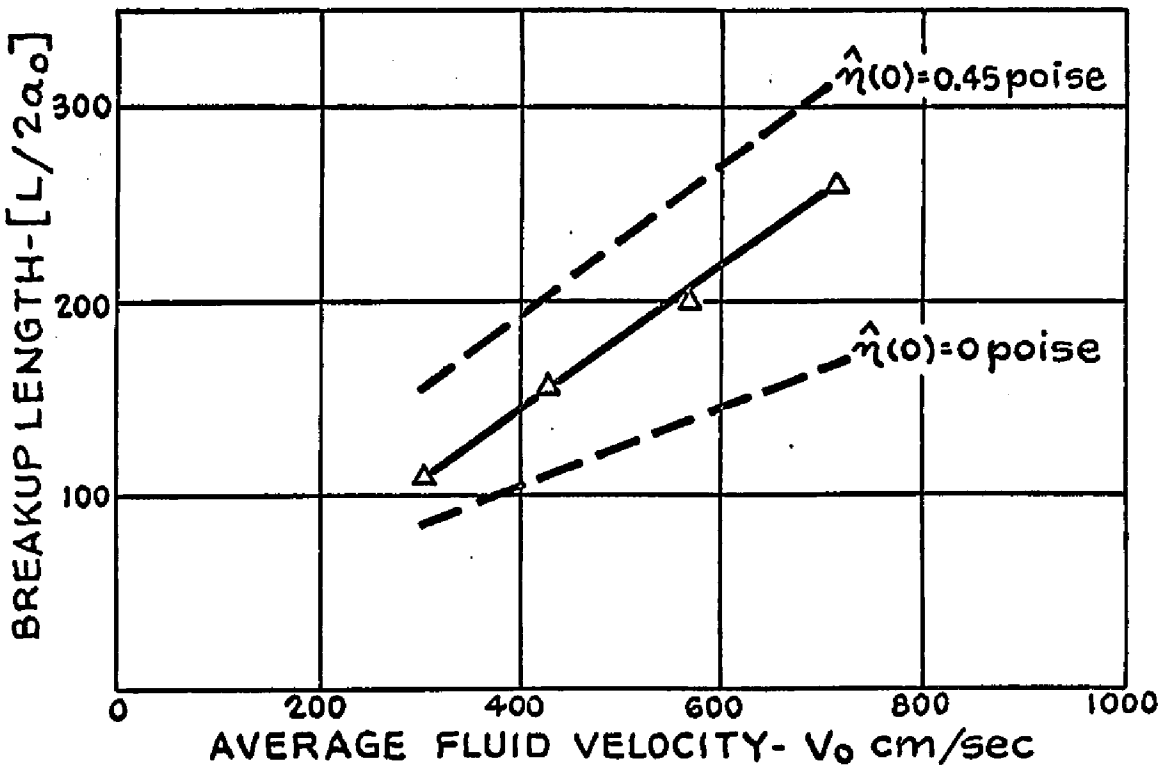

Figure 6-33 Breakup length of a capillary jet of 0.25% SCMC, based on wave amplitude, as a function of fluid velocity; nozzle diameter-0.0216 cm.

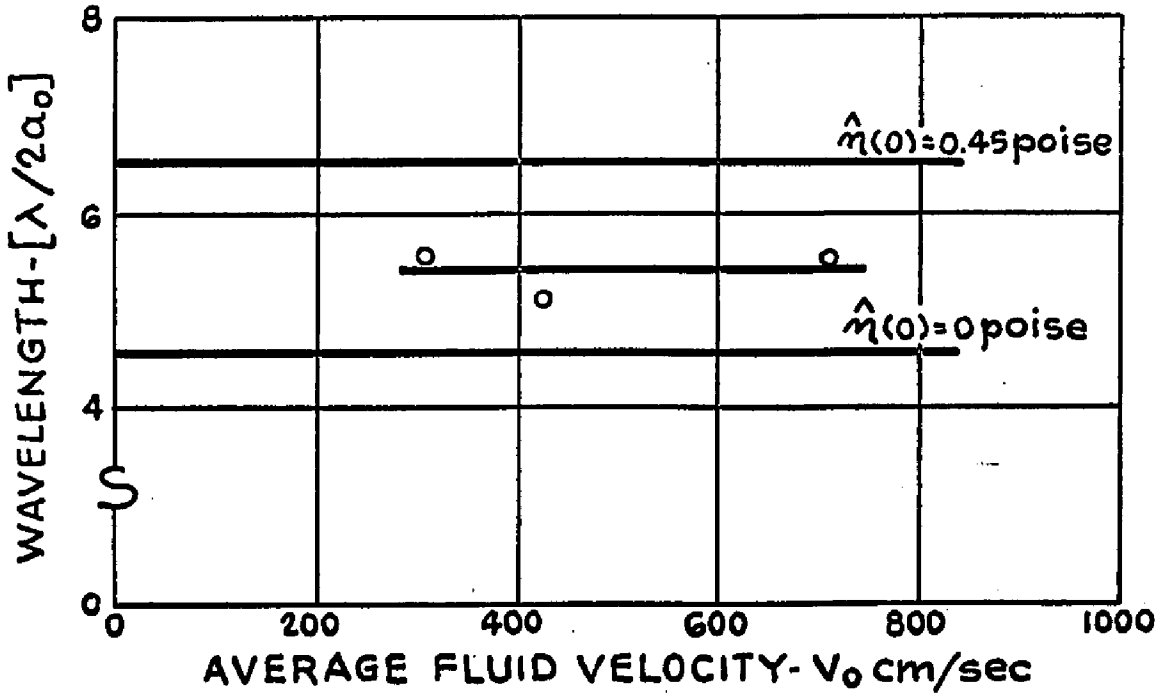

Figure 6-34 Wavelength of disturbance wave for a capillary jet of 0.25% SCMC; nozzle diameter- 0.0216 cm.

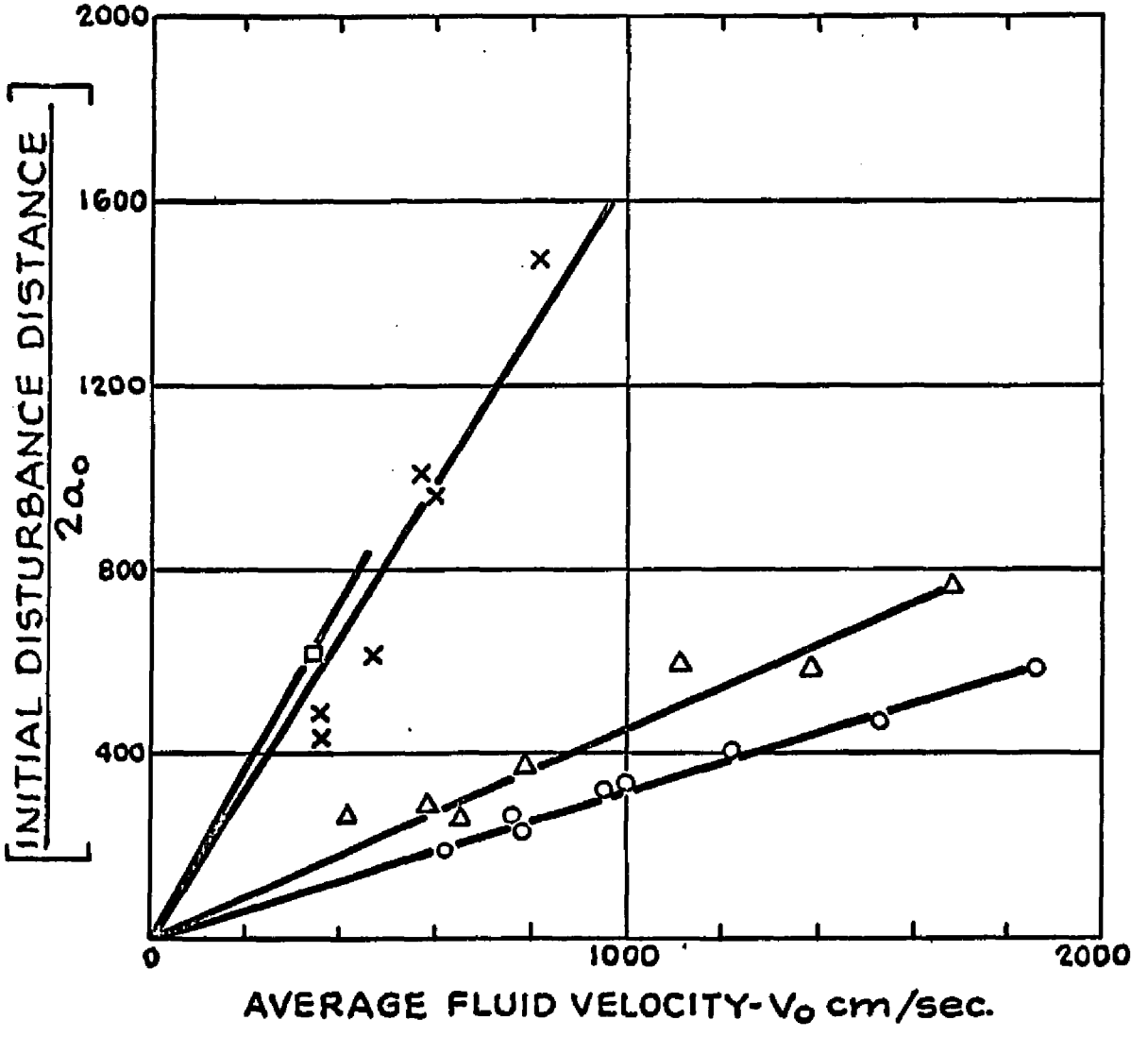

Figure 6-35 Initial disturbance distance for a capillary jet of 0.25% Separan; nozzle diameter: O-0.0216 cm., Δ-0.0263 cm., X-0.0414 cm., □-0.0868 cm.

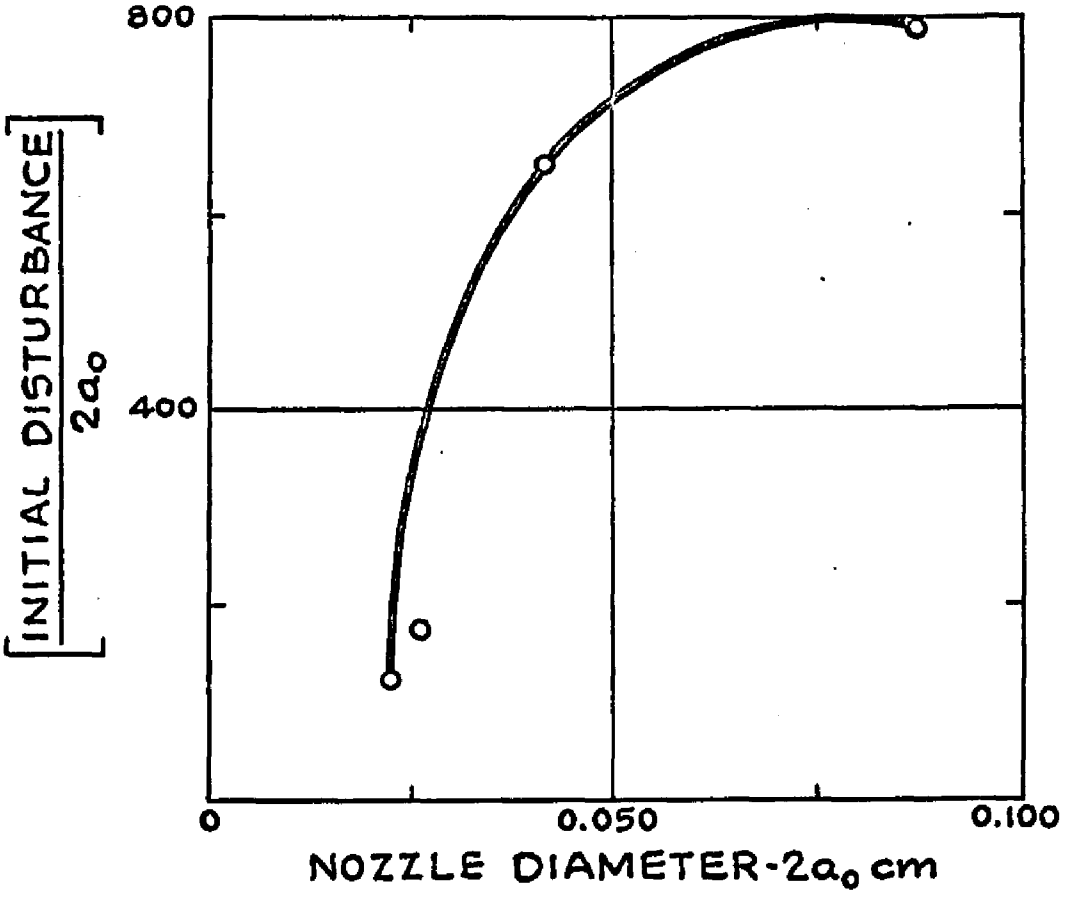

Figure G-36 Effect of the nozzle diameter on the initial disturbance length at constant fluid velocity for a capillary jet of 0.25% Separan; average fluid velocity- V_0 = 400 cm/sec.

and the (initial disturbance length/nozzle diameter) ratio becomes independent of diameter. This result would be expected for a highly shear sensitive liquid.

The breakup length of capillary jets of dilute (0.05%) and moderately concentrated (0.25%) Separan, based on the point where the threads break, is shown in figure 6-37 as a function of the fluid velocity and the nozzle diameter. Determination of this distance was made by visual observation of the liquid column under stroboscopic light and the accuracy of these measurements therefore depends upon the ability to detect the finest threads. Values are found to be reproducible to $\pm$ 10%. The breakup length of 0.05% Separan jets increases linearly with velocity and, at high velocities, becomes independent of it. Data points for all three nozzle diameters form a single continuous curve indicating that the breakup length- $L/2a_o$ is not a function of the capillary diameter. The breakup length of 0.25% Separan jets is seen to increase with fluid velocity and nozzle diameter. At sufficiently high fluid velocities, the breakup length also becomes independent of fluid velocity. This behavior was exhibited for several of the viscoinelastic jets.

The 'droplet-thread' configuration is the form eventually assumed by both the dilute and the moderately concentrated viscoelastic jets. Threads are seen to thin with increasing distance from the nozzle while the droplet

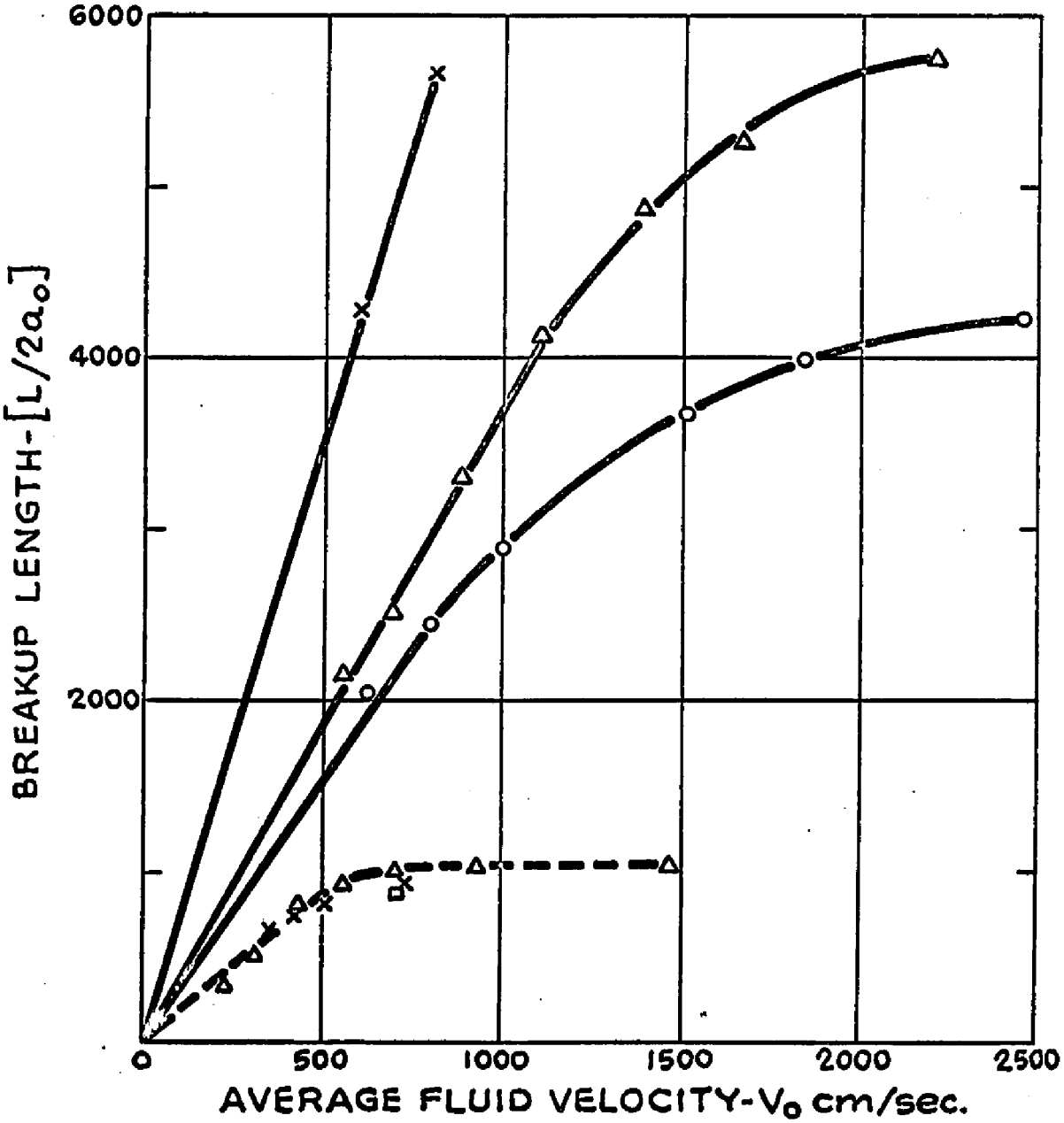

Figure G-37 Breakup length of a capillary jet of 0.05% Separan and 0.25% Separan as a function of the average fluid velocity and the nozzle diameter; nozzle diameter- O-0.0216 cm., Δ-0.0263 cm., X-0.0414 cm., □-0.0868cm., ---- 0.05% Separan, —— 0.25% Separan.

diameter increases. By photographing a 0.25% Separan jet along its length until breakup occurred, the droplet diameter and thread length were determined as a function of distance along the liquid column. The computed results are based on 20-30 droplets and thread lengths at each location. Original data may be found in appendix B .

Figure 6-38 is a plot of the length mean droplet diameter vs. distance from the nozzle and shows that the mean diameter increases until about halfway through its flight and thereafter remains constant. Also shown in the same figure are the Sauter mean diameter and the weight mean diameter which are defined as follows

$$D_s = \sum D_i^3 / \sum D_i^2 \qquad (6.33)$$

$$D_w = \sum D_i^4 / \sum D_i^3 \qquad (6.34)$$

where D_s and D_w are the Sauter mean diameter and the weight mean diameter, respectively. The fact that all three measures of average diameter show the same trend indicates that the distribution remains similar. The standard deviation at each location is between 25-35%.

The thread lengths between droplets were found to be widely distributed and showed no discernible pattern with increasing axial distance. At any one location, the values ranged from fractions of a centimeter to 6 cm. with an average of 2.5 cm. Thread lengths for 0.05% Separan jets

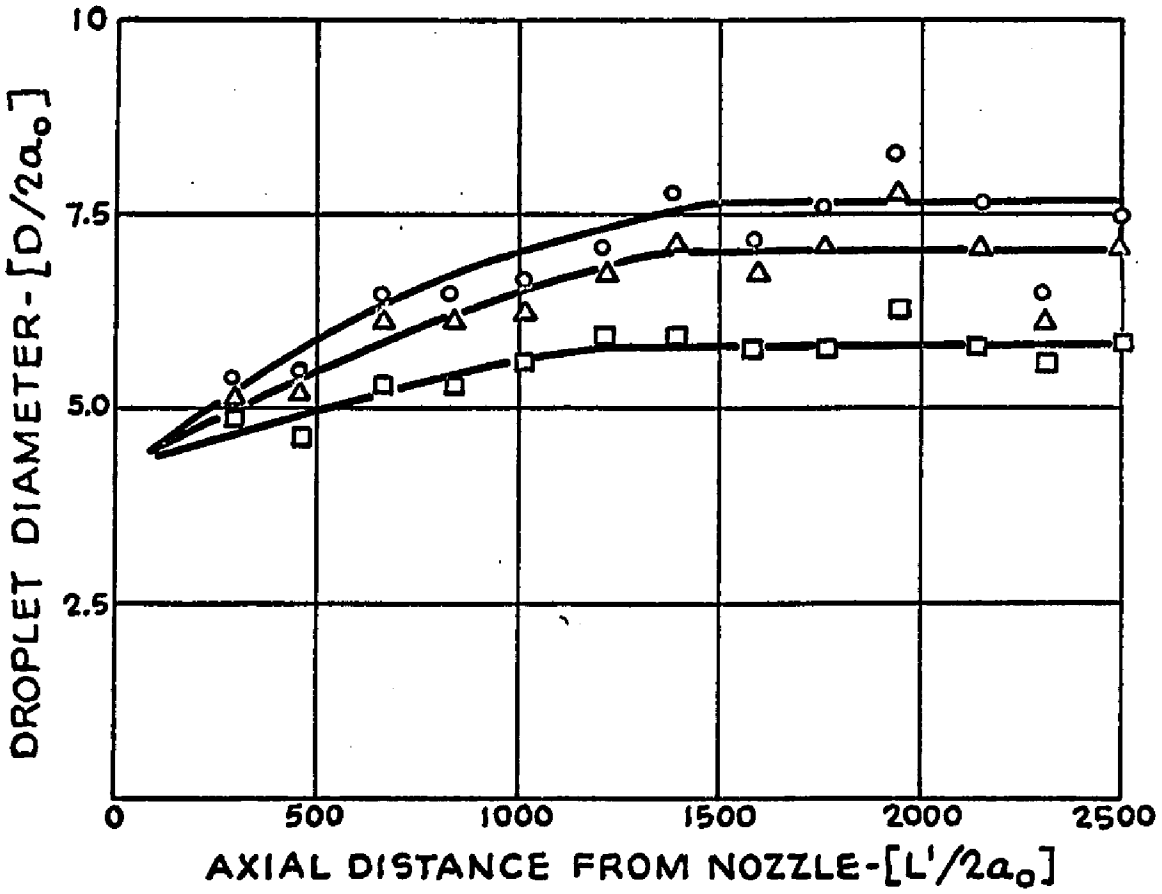

Figure 6-38 Growth of droplets on a capillary jet of 0.25% Separan as a function of the axial distance from the nozzle; nozzle diameter - 0.0216 cm., average fluid velocity - 1050 cm/sec., □ - length mean diameter, Δ - Sauter mean diameter, O - weight mean diameter.

varied in a similar manner except that the threads are shorter.

The change in droplet diameter with increasing axial distance and the random nature of the thread length at any one location both indicate that dynamic phenomena are occurring along the liquid column. Through the use of high speed motion pictures, taken at 3000-7000 pictures per second in the region where the droplet diameter is still increasing, the nature of these changes was investigated.

Selected frames are shown in figure 6-39 for a capillary jet of 0.05% Separan and in figure 6-40, photographs (a)-(f), for a 0.25% Separan jet. The droplets are seen to move at different velocities along the threads which create collisions in which new droplets of larger diameter are formed. Smaller particles decelerate more rapidly than larger particles due to frictional drag and this would lead to collisions of the type observed. However, this does not explain why the viscoelastic jet prefers the 'droplet-thread' configuration in the first place. One significant observation resulting from an analysis of the motion pictures is that the liquid column, far from being relaxed, continually undergoes large amplitude, axial deformations which require the existence of tensile stresses for their propagation. Photographs (g)-(j) of figure 6-40 show an instance where a whole section of the jet overtakes another section which was previously in front of it and then passes it. This phenomena is not as yet understood.

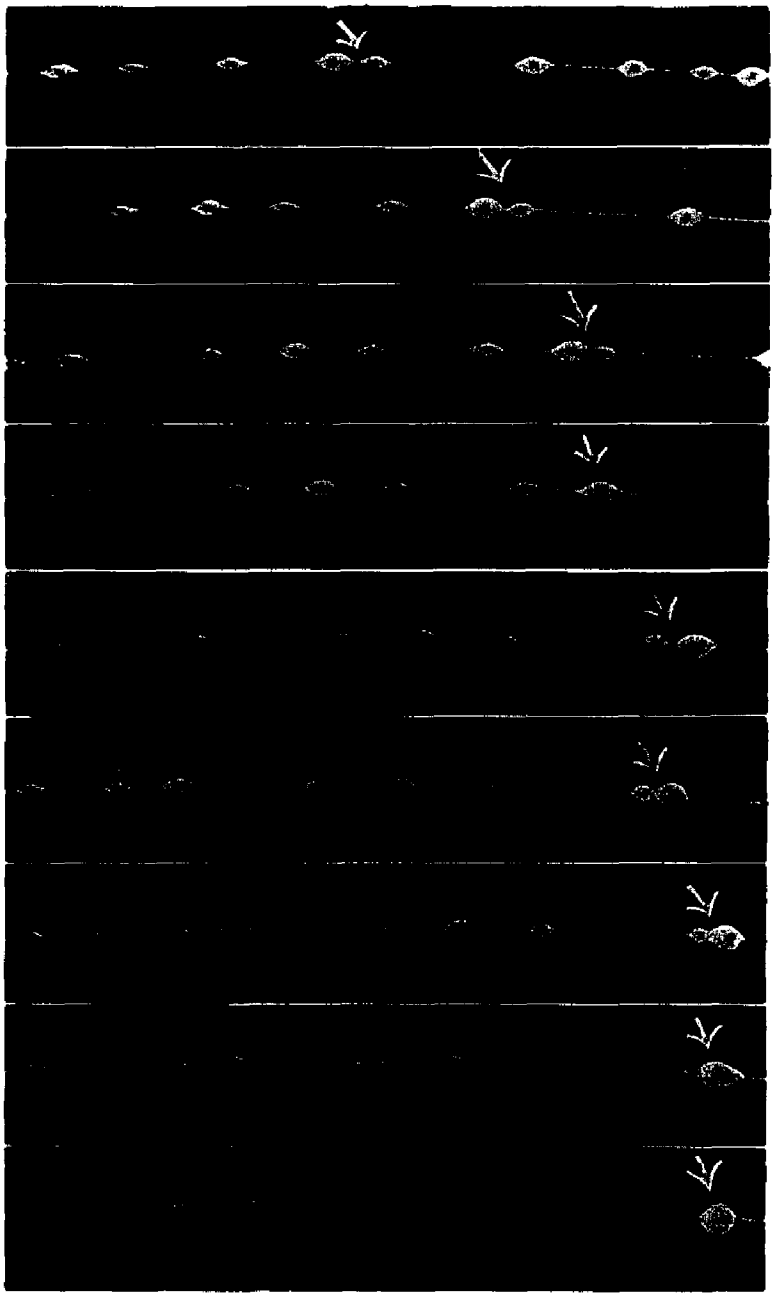

Figure 6-39 High speed motion pictures of a capillary jet of 0.05% Separan magnification-3X, nozzle diameter-0.0414 cm., average fluid velocity-224 cm/sec, distance from nozzle tip to midpoint of photograph-12 cm., frame speed:4500 pictures per second.

Figure 6-40 High speed motion pictures of a capillary jet of 0.25% Separan; magnification-1X, nozzle diameter-0.0414 cm., average fluid velocity-1120 cm/sec, distance from nozzle tip to midpoint of photograph-62 cm., frame speed:3000-4000 pictures per second

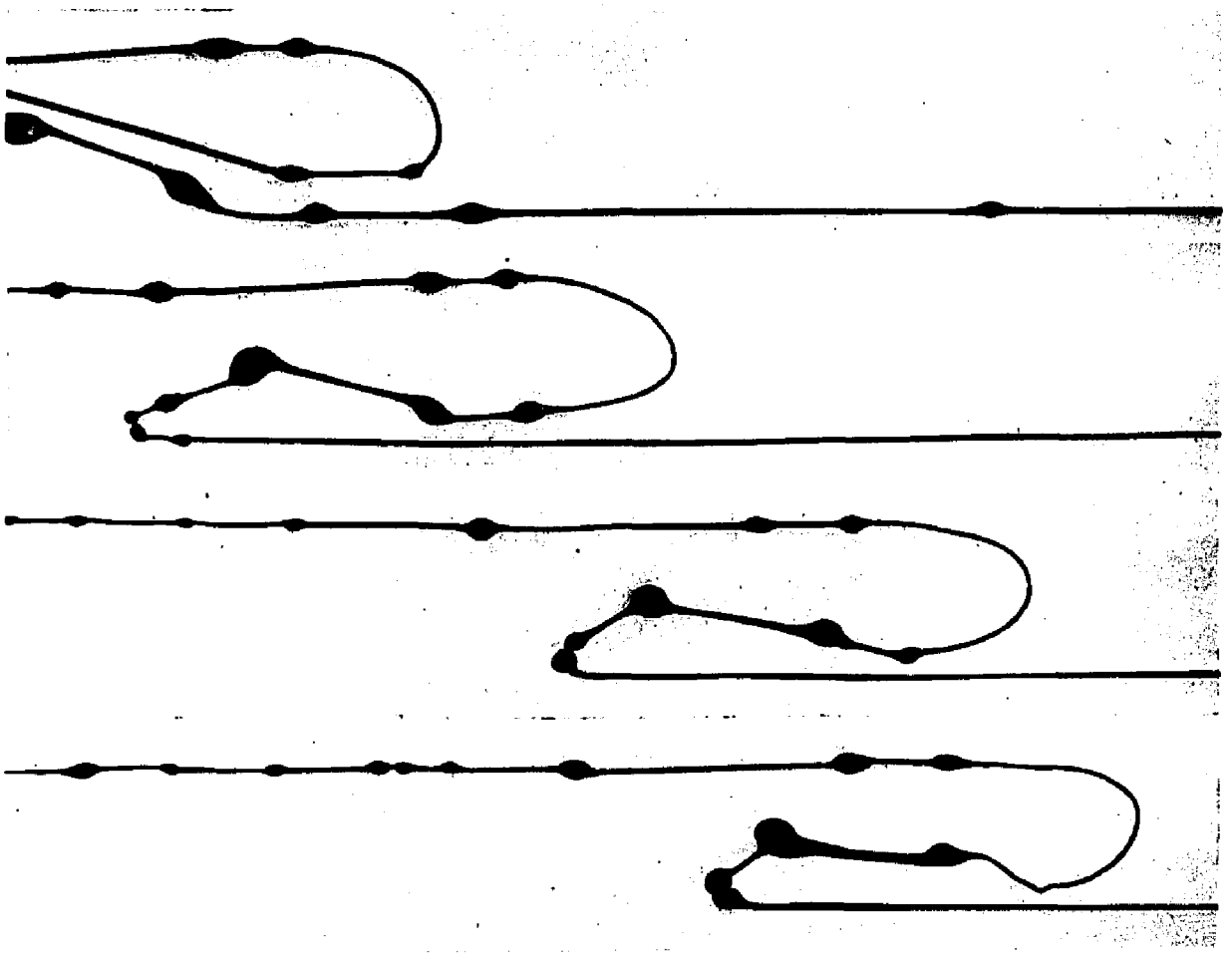

Figure 6-40 continued

While thread thinning data for all the viscoelastic jets as a function of axial distance show considerable scatter, a dimensionless plot of the fraction of the original radius- a'/a_o vs. the fraction of the breakup length- L'/L has the form shown in figure 6-41. Thus, breakup of the jet by disruption of the thinnest thread is imminent when the thread diameter is approximately ¼ of the original diameter. Just before breakup occurs, the threads thin quite rapidly. In this region, the stability of the threads is quite remarkable. For example, in the portion of the liquid column immediately proceeding the breakup point, the threads connecting a series of droplets in a 0.05% Separan jet (with $2a_0$=0.0216 cm and V_o=460 cm/sec) decreases in thickness to 0.004 cm from 0.01 cm. over a length of 8 cm. A Newtonian liquid of the same zero shear viscosity would breakup in only 1-2 cm. under these conditions.

The average diameter of the droplets formed after breakup as well as the size distribution was determined for capillary jets of glycerin, 0.05% Separan and 0.25% Separan. Data for the Newtonian fluid was obtained in order to compare the accuracy of the measuring technique with published correlations for these liquids. Glycerin, in particular, was chosen because its Newtonian viscosity is approximately the same as the zero shear viscosity of 0.25% Separan.

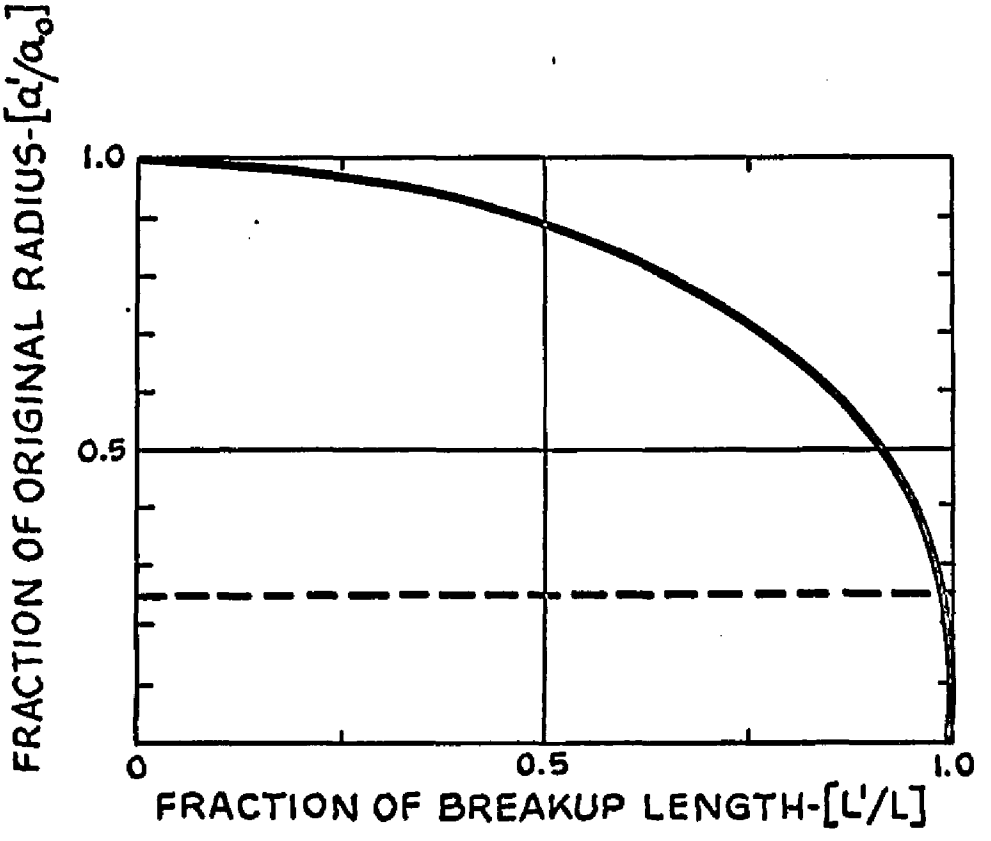

Figure 6-41 Correlation of all viscoelastic test data for the decrease in jet radius with increasing axial distance; ---- critical radius at inception of breakup.

Duffie and Marshall (17) investigated the droplet size distribution to be expected from the breakup of low speed, low viscosity Newtonian jets using capillary diameters and fluid velocities similar to those employed in this study. They found that the average, geometric mean diameter-D_g for all fluids investigated could be correlated by the empirical equation

$$D_g = 36(2a_o)^{0.56}(Re_o)^{-0.10} \qquad (6.35)$$

where D_g and a_o are in microns. D_g is defined as

$$Ln(D_g) = \sum Ln(D_i) / N \qquad (6.36)$$

and N is the number of observations. There is some uncertainty whether equation (6.30), which was obtained with low viscosity liquids, can be extended to high viscosity fluids such as glycerin.

The experimental data for glycerin droplets at 30°C are compared to the predictions of equation (6.35) in table 6-4 and the generally good agreement between the two indicates that the accuracy of the measuring technique is comparable to those of other investigators. Data taken at a point 4 cm. past breakup shows a larger droplet diameter than the corresponding data taken at breakup and is due to droplet collisions and subsequent coalescence. A significant discrepancy does exist from the predicted value for

droplets measured at the lowest fluid velocity. This resulted from the jet's tendency to break into segments, rather than discrete droplets, with an accompanying increase in the particle size eventually formed.

Table 6-4. Comparison of experimental droplet diameters for glycerin with the predicted values from equation (6.35).

nozzle diameter-0.0216 cm.
fluid temperature- 30°C.

Average fluid velocity	Experimental geometric mean droplet diameter at breakup	4 cm. from breakup	Predicted values - eq. (6.35)
403 cm/sec	0.089 cm.	0.094 cm.	0.070 cm.
678	0.069	0.075	0.066
937	0.071	0.072	0.064

The results for the average droplet diameter of the viscoelastic jets and of glycerin are summarized in table 6-5. Data taken for the glycerin and 0.05% Separan droplets showed a coefficient of dispersion (standard deviation/length mean diameter) of 14-21% while that of the 0.25% Separan was 39%. The disparity arises from differences in the nature of their breakup. From photographs taken at the point of breakup, it was observed that, in the dilute viscoelastic fluids, the fine connecting threads are absorbed into the droplets and a relatively uniform size distribution is produced. The comparatively small separation between the length mean diameter, the Sauter mean

Table 6-5. Droplet diameters produced from the breakup of Newtonian and viscoelastic jets.

Fluid	Nozzle diameter	V_o	D_L	D_s	D_w	Coefficient of Dispersion
0.05% Separan	0.0263 cm	222 cm/sec	0.106 cm.	0.115 cm.	0.119 cm.	19.8 %
		312	0.094	0.104	0.111	22.3
		435	0.090	0.100	0.105	24.4
		490	0.083	0.091	0.095	21.6
		715	0.083	0.088	0.090	16.8
		937	0.084	0.088	0.090	15.5
		1473	0.080	0.087	0.091	21.3
	0.0414	349	0.113	0.121	0.125	17.8
		420	0.125	0.130	0.133	14.4
		505	0.121	0.126	0.129	14.1
		722	0.122	0.130	0.133	17.2
	0.0868	723	0.222	0.238	0.245	18.9
0.25% Separan	0.0216	1066	0.133	0.166	0.174	39.0
Glycerin	0.0216	403*	0.090	0.096	0.099	17.8
		403**	0.096	0.103	0.106	18.8
		678*	0.070	0.076	0.078	20.0
		678**	0.076	0.082	0.086	21.0
		937*	0.073	0.078	0.080	20.6
		937**	0.073	0.078	0.081	19.2

* Data taken at breakup

** Data taken 4 cm. past breakup

diameter and the weight mean diameter reflect the homogeneity of the dispersion. However, the threads in a 0.25% Separan jet collapse and form small satellite droplets which widens the droplet size distribution. This is also apparent from the larger standard deviation and from the increased differences between the three measures of droplet diameter.

It is seen from the table that the droplet diameter resulting from the breakup of a capillary jet of 0.05% Separan, issuing from a 0.0263 cm. nozzle initially decreases with increasing fluid velocity and then becomes independent of it. A comparison with figure 6-37 shows that both the breakup length and the droplet diameter reach constant values over the same range of fluid velocity. A constant diameter region is also exhibited in the data taken with the 0.0414 cm. nozzle. In this constant diameter regime, figure 6-42 shows that the dimensionless droplet diameter- $D_L/2a_o$, where D_L is the length mean diameter, is proportional to $(2a_o)^{-0.2}$.

Equation(6.30) predicts droplet diameters for the Separan solutions which are substantially below the experimentally observed values. This is expected since the high speed movies given in figures 6-39 and 6-40 have shown that the droplets formed on the intact capillary jet are continually colliding and coalescing to create larger diameter droplets.

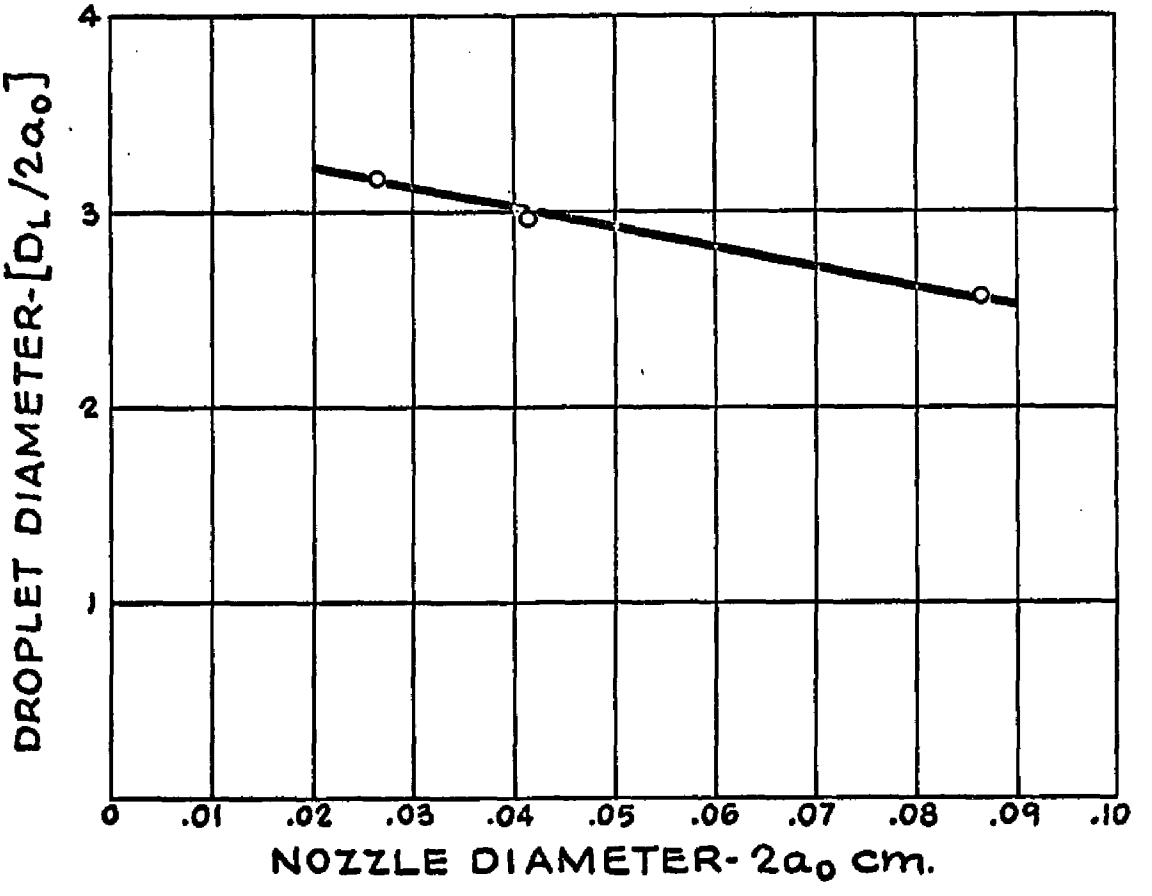

Figure 6-42 The effect of nozzle diameter on the droplet diameter for a capillary jet of 0.05% Separan; average fluid velocity-722 cm/sec.

The droplet size distribution of glycerin and of 0.05% Separan follow a normal distribution as shown in figures 6-43 and 6-44, respectively, whereas the results of 0.25% Separan, given in figure 6-45, deviate from this pattern. As explained previously, this occurs because the capillary jets of 0.25% Separan form small satellite droplets at breakup along with the main droplets. Thus, there will be a preponderance of these small droplets included and the size distribution will assume the shape of a bimodal distribution. This is more easily seen in the histograms of figure 6-46, which were constructed from representative droplet data for each of the three test fluids.

6.6-4 DISCUSSION OF EXPERIMENTAL RESULTS

Fluids which exhibit a yield stress or a shear dependent viscosity possess a three dimensional structure that requires some finite time to form or break down upon removal or application of shearing stresses. This relaxation time, in some cases, could be longer than the time for the velocity profile and the shear stresses to reach equilibrium. Thus, the hydrodynamic behavior of such a non-Newtonian fluid should be related to at least two different relaxation times, a structural relaxation time and a stress relaxation time. Whether or not these relaxation times are significant depends upon the time scale of the experiment. A jet breakup experiment is ideally suited to

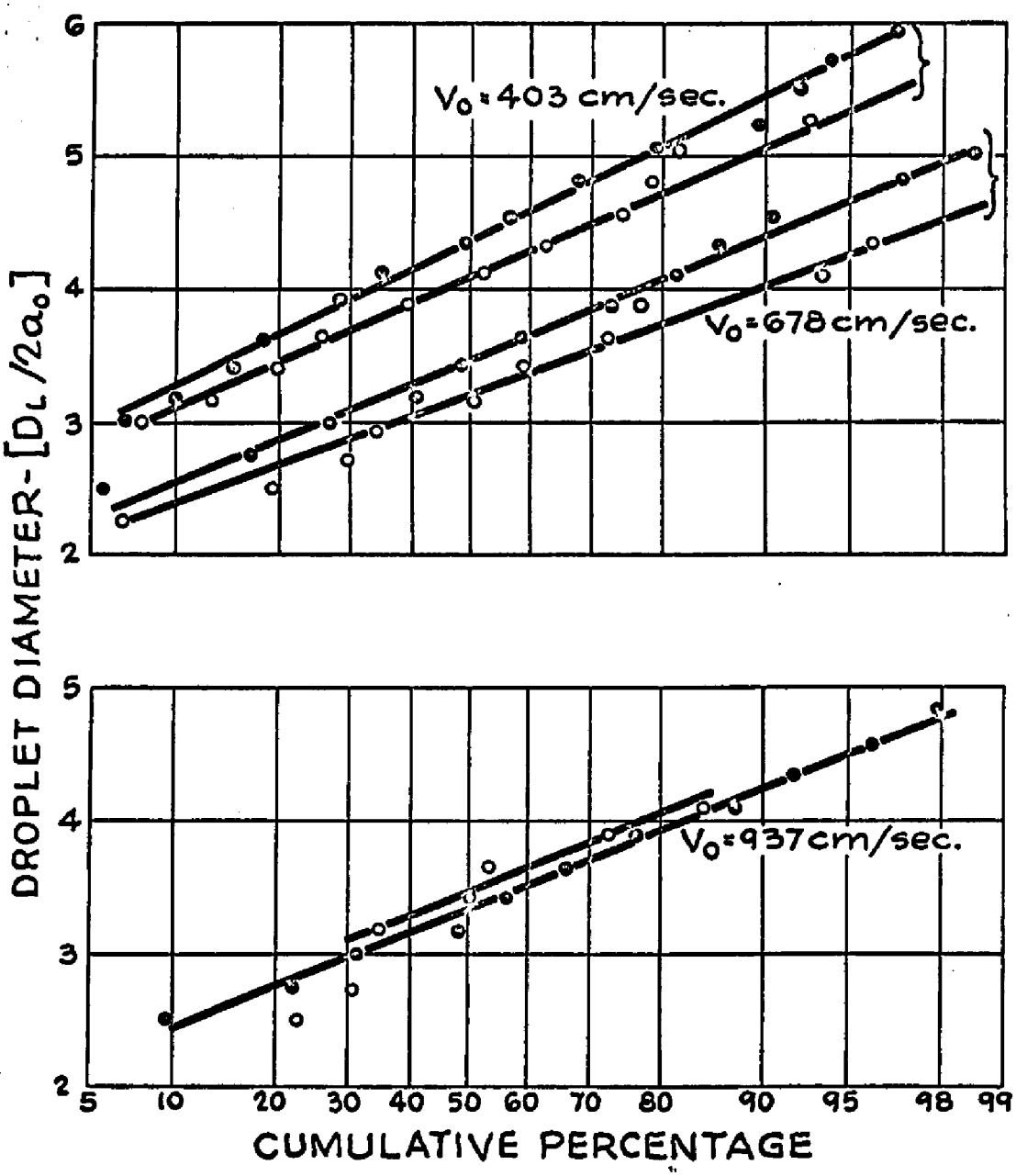

Figure 6-43 Droplet size distribution for a capillary jet of glycerin; nozzle diameter - 0.0216 cm., O-data taken 36 cm. from nozzle, ⊕-data taken 40 cm. from nozzle.

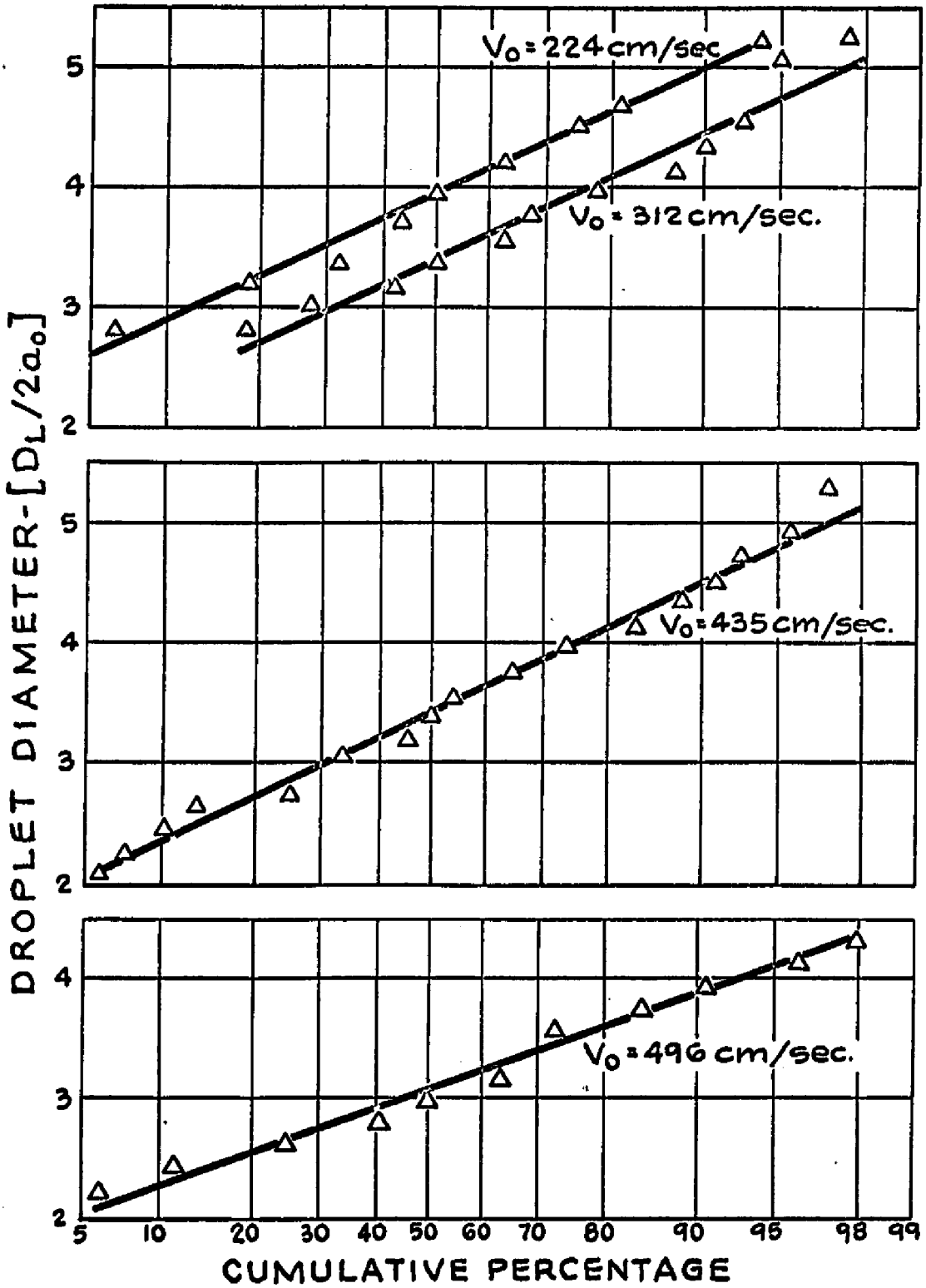

Figure 6-44 Droplet size distribution for a capillary jet of 0.05% Separan as a function of the average fluid velocity and the nozzle diameter; nozzle diameter-Δ-0.0263 cm, X-0.0414 cm, □- 0.0868 cm.

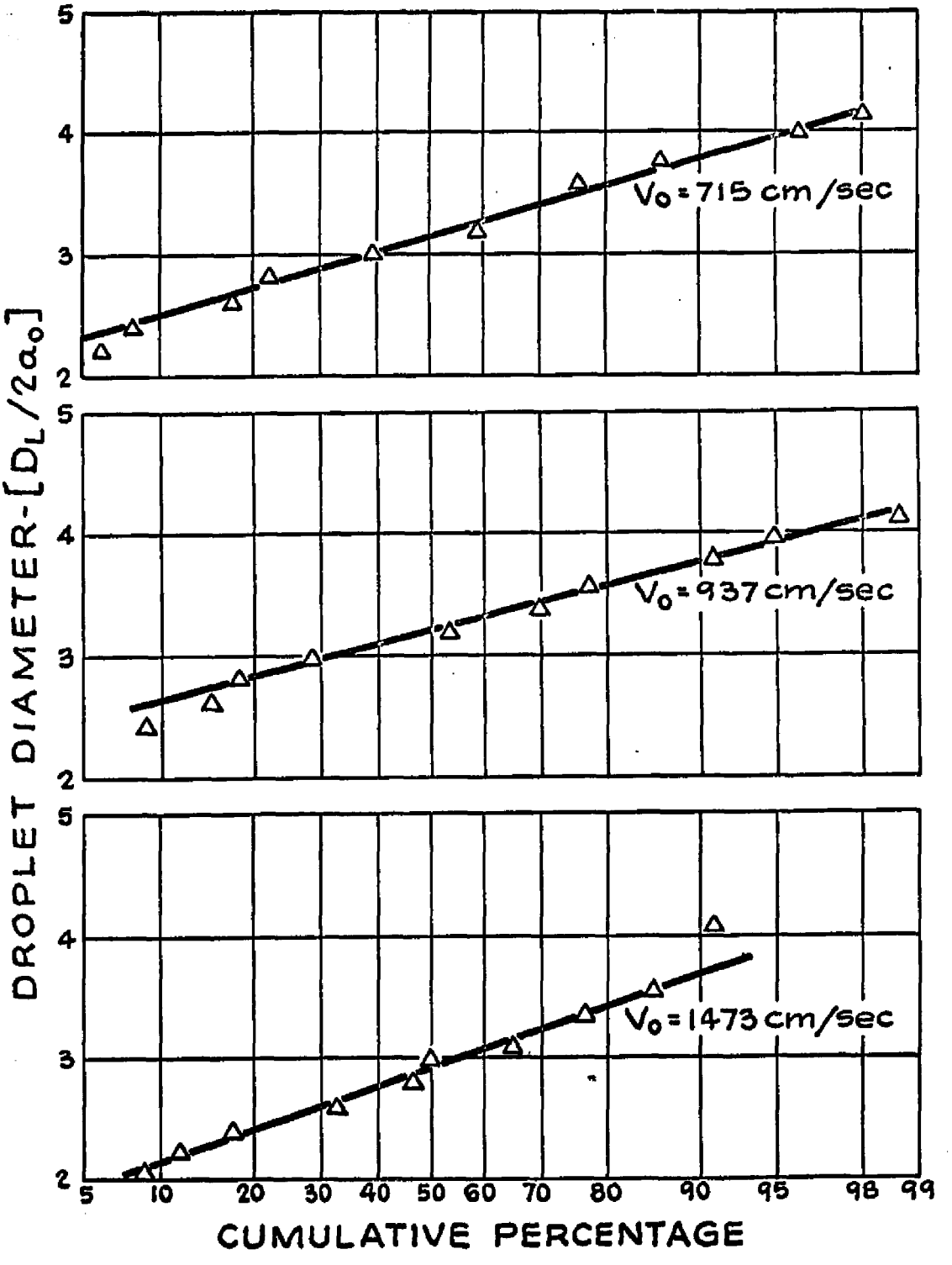

Figure 6-44 continued

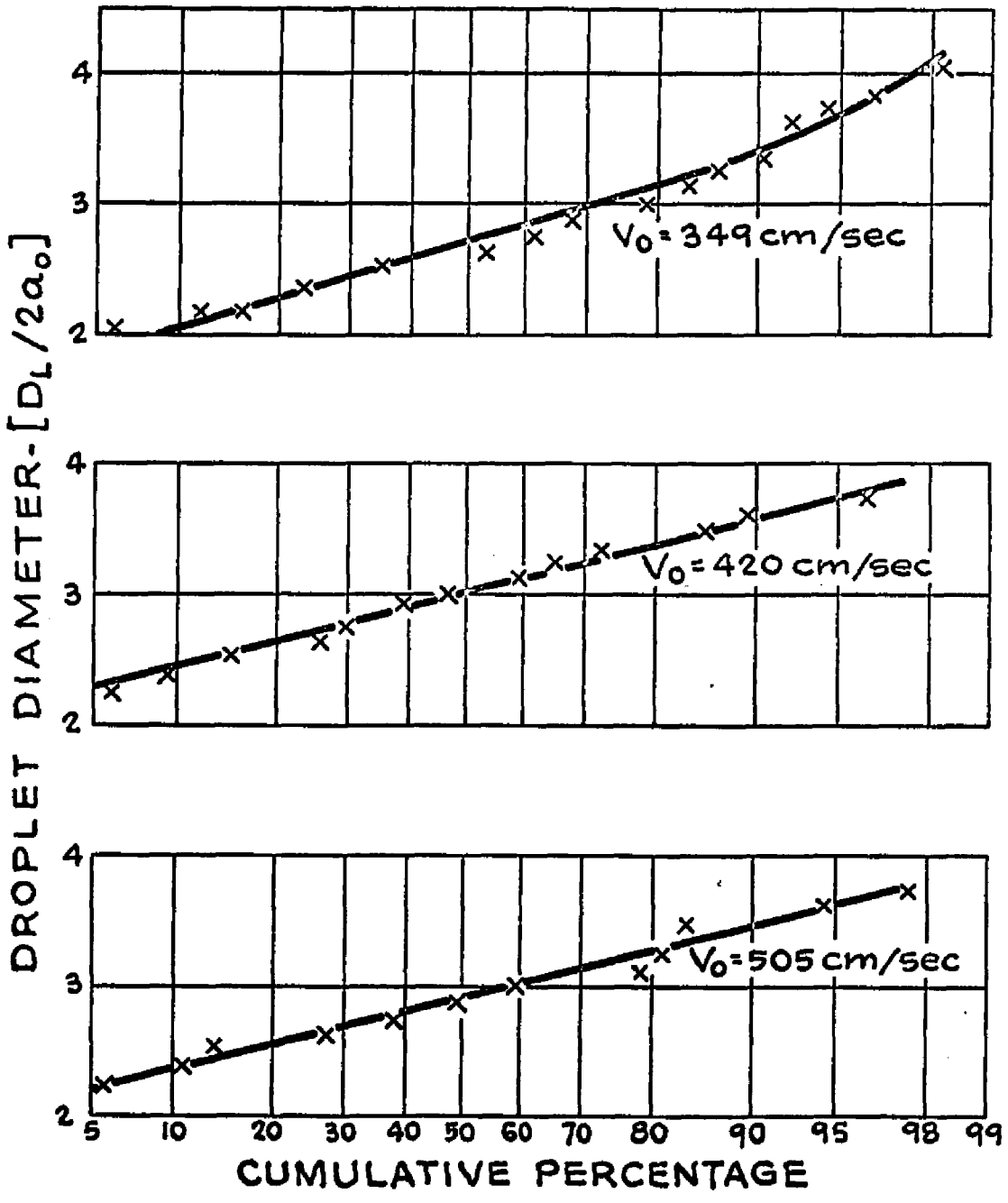

Figure 6-44 continued

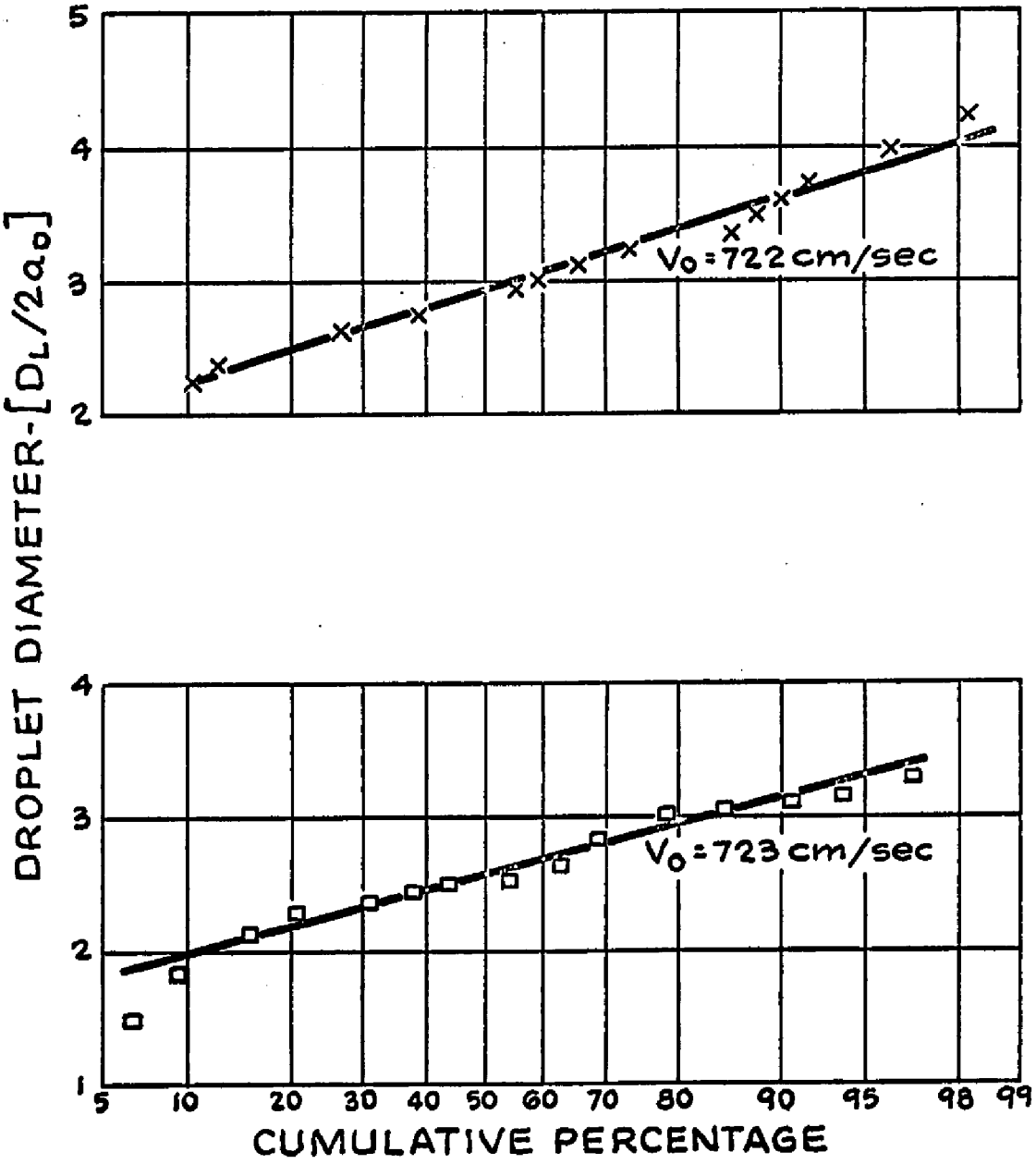

Figure 6-44 continued

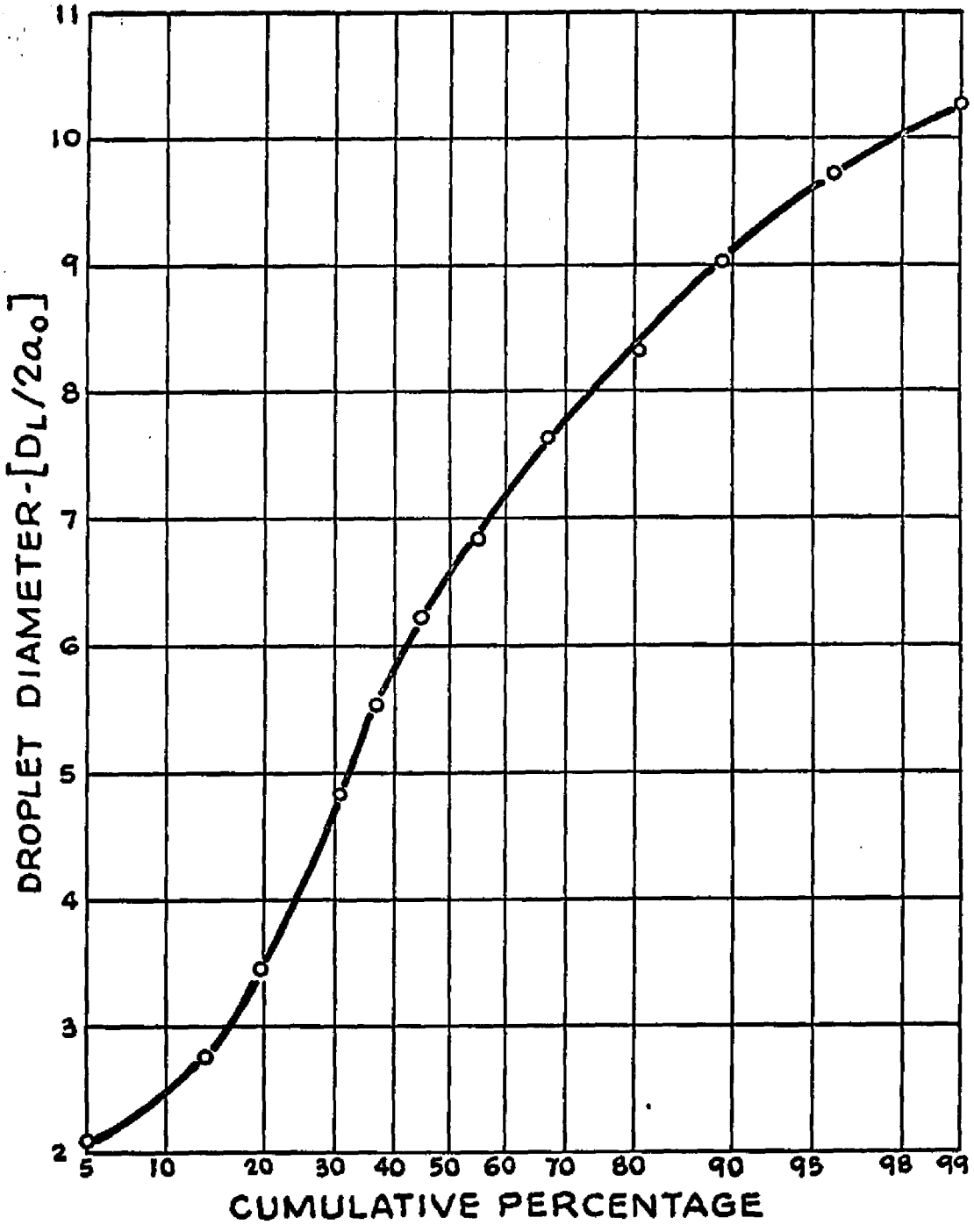

Figure G-45 Droplet size distribution for a capillary jet of 0.25% Separan; nozzle diameter-0.0216 cm, average fluid velocity-1045 cm/sec.

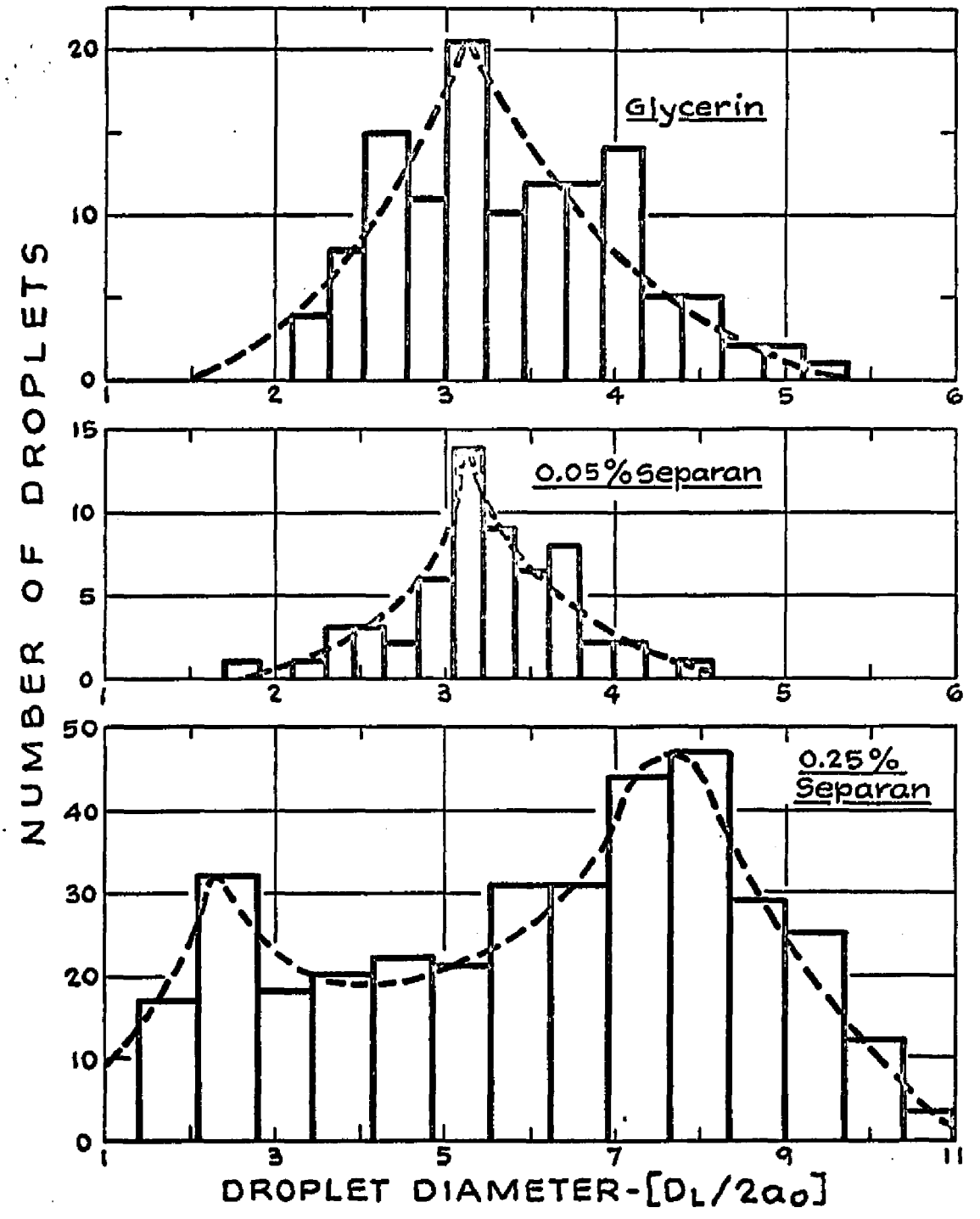

Figure 6-46 Comparison of droplet size distribution for capillary jets of glycerin, 0.05% Separan and 0.25% Separan;

fluid	nozzle diameter	average fluid velocity
glycerin	0.0216 cm	937 cm/sec
0.05% Separan	0.0263	937
0.25% Separan	0.0216	1045

demonstrate the effects of relaxation phenomena which are of the same order as the lifetime of the liquid column, about 0.001-0.01 seconds.

The experimental results of this paper showed that the viscoinelastic test fluids could all be atomized readily. This is surprising since several of them- the 0.6% Carbopol, the MPA 60 dispersions and the aqueous silica dispersion are highly gellified fluids when at rest. In particular, the silica dispersion, whichhas a relatively high yield stress, broke up in a manner similar to a low viscosity capillary jet in turbulent flow. With the exception of 0.6% Carbopol and the silica dispersion, the disturbance in the non-Newtonian inelastic fluids was propagated as a growing wave with a well defined wavelength. The two aforementioned fluids broke up only at very high velocities and, under these conditions, had an irregular, non-axisymmetric appearance.

Classical Newtonian theory assumes the capillary jet to be initially relaxed from all prior stresses and at its zero shear viscosity. This model predicts complete stability for the viscoinelastic test fluids since the small shear rates associated with the growth of infinitesimal, symmetrical disturbances would not cause significant departure from Newtonian behavior. In the theory outlined earlier in the paper, a capillary jet of an initially relaxed viscoelastic liquid with a yield stress could be stable,

if the elastic modulus were such as to make the complex viscosity unbounded.

For either of these theories to be applicable, the structure which gives rise to the yield stress or the shear dependent viscosity would have to be formed within a time period which was short compared to the jet breakup time. It has been shown in the literature, e.g. Carver and Van Wazer (7), that certain fluids require several minutes or hours to completely regain their 'at rest' structure. Fischer et.al. (21) have presented data that demonstrates how the level of shear, to which the material was previously subjected, also influences the structural formation time. This latter point might explain why the silica jet was stable at the lower velocities or shear rates and atomized readily at the higher velocities.

The breakup length and wavelength data for the visco-inelastic jets cannot be explained in terms of a liquid column that relaxes instantly to regain its structure and then propagates disturbances at a rate corresponding to its zero shear viscosity. Such a model predicts results that are several orders of magnitude higher than experimentally observed values.

The measurements are reasonably consistent, however, if it is assumed that all prior stresses relax shortly beyond the capillary exit but the time required to reform the gellified structure is of the same order or exceeds the

lifetime of the jet. In this model, the liquid column behaves as a Newtonian liquid whose viscosity is approximately the same as the apparent viscosity of the visco-inelastic fluid, evaluated at the average shear rate within the capillary. The proposed behavior is also in agreement with the experimental observation that the breakup length vs. fluid velocity curves do not appear to pass through the origin. However, no explanation is available for the increased instability of capillary jets of 0.1% Carbopol over an inviscid fluid, when both are in laminar flow.

The linearized stability analysis has shown that the growth rate of axisymmetric disturbances for any visco-elastic fluid, whose complex viscosity is bounded, is higher than that of a Newtonian fluid of the same zero shear viscosity. If the complex viscosity could readily be measured, then one could predict the growth rate as a function of the wavelength, assuming that the liquid column is completely relaxed initially. However, for the dilute solutions used in these experiments, the complex viscosity cannot be determined and only a qualitative prediction can be made.

In the experiments, growth rates were not measured directly and comparisons of jet stability were made on the basis of the breakup length. This approach gives good agreement with Weber's theoretical predictions for Newtonian liquids. In the region of linear wave propagation, the breakup length and the wavelength of a capillary

jet of 0.25% SCMC were found to be shorter than a Newtonian liquid of the same zero shear viscosity but greater than for an inviscid liquid. This result is in agreement with the predictions of the linear theory.

Contrary to what occurs in Newtonian liquids, the growth of the disturbance wave in 0.25% SCMC solutions does not lead to immediate breakup and the droplets remain connected for a considerable distance by thin threads. This thread formation seems to be typical of elastic liquids. No wave formation has been observed in highly elastic fluids such as 0.25% Separan and 0.25% Polyox. Even in relatively dilute solutions(0.05% Separan), the waves which do appear initially are damped out. Instead, disturbances propagate as isolated droplets connected by random lengths of threads. In many cases, the threads are longer than any reasonable wavelength that could be associated with the droplet. These non-linear disturbances occur at a distance which is shorter than the breakup length of a Newtonian liquid of comparable zero shear viscosity. Thus, one cannot conclude that the viscoelastic jet is more stable with respect to the growth of axisymmetric waves.

It has been observed for all the viscoelastic jets that the droplets which are formed are connected by threads which continually thin and lead to the eventual breakup of the jet. Two questions arise: why do the threads form and what causes their remarkable stability? While the original

jet does not show any increased stability as compared to a Newtonian jet, the connecting threads have a lifetime several fold higher than expected. Viscoelastic jets extruded from a nozzle which is of the same order of thickness as the threads do not exhibit this increased stability.

Two reasons might explain this difference. First, a viscoelastic jet extruded from a nozzle which is of similar thickness as the threads has just experienced a high shear rate. If the breakup time and the structural relaxation time are of comparable magnitude, the jet will break up before the fluid has regained its zero shear viscosity. However, the thin thread at a distance from the nozzle is derived from a much thicker jet, which was less severely sheared in the capillary and which has also had time to partially regain its zero shear viscosity. The second and more important difference is that the thread is under some stress, as shown by the fact that it continues to thin. This stress might be caused by either the surface tension forces at the connection to a droplet or by the relative motion of two droplets. Looking at photograph (a) of figure 6-14, one might question this explanation as the liquid column looks quite relaxed. However, the high speed movies indicate that the threads and droplets are constantly changing their configuration and are undergoing large scale deformations, as seen in figures 6-39 and 6-40.

The stability of a viscoelastic thread has similarities

to the unique ability of viscoelastic liquids to be spun into fibers. During thread thinning, the fluid undergoes a flow which is characterized as a stretching or extrusion flow. It is well known that the behavior of elastic liquids under tension is completely different from that in shear flow in the sense that viscoelastic liquids possess an elongational viscosity which increases with the stretching rate. Thus, elastic liquids of low viscosity can be spun into fibers whereas Newtonian liquids are spinnable only at high viscosities.

6.6-5 CONCLUDING REMARKS

The results presented in this chapter have shown the limitations inherent in using assumptions, which are valid for capillary jets of Newtonian liquids, in the analysis of non-Newtonian fluids without prior experimental verification. In particular, it is evident that stress relaxation phenomena occuring outside the capillary exit can play a significant role in the ultimate behavior of the liquid column. The atomization of a non-Newtonian jet thus involves considerations of the fluid's transient and steady state flow properties.

A very practical result of this research is the finding that highly gellified liquids are unstable if their structural relaxation time is of the same order as or exceeds the lifetime of the jet, about 0.001-0.01 seconds. Additives such as Carbopol, in a 0.1% concentration, have

the ability to thicken a solution yet are able to enhance the atomization. The classical notion that viscosity always increases the stability of a jet must be re-examined in light of these data.

CHAPTER 7

SUMMARY AND CONCLUSIONS

The objective of this research has been to carry out an experimental program which would provide an initial understanding into the behavior of capillary jets of non-Newtonian liquids.

Two categories of fluids were chosen for study: visco-inelastic materials and viscoelastic liquids. The viscoinelastic fluids were comprised of a wide variety of substances and included organic polymer solutions, an inorganic dispersion and organic polymer dispersions. They ranged in consistency from relatively thin liquids to stiff gels and could be characterized as possessing a shear dependent viscosity, a yield stress and an absence of elastic phenomena. The viscoelastic solutions were all composed of organic polymer solutions of a class which exhibits marked drag reduction in turbulent flow.

The experiments concentrated on profile decay measurements and on jet breakup studies. Data were obtained through high speed still and motion picture photographs taken along the length of the jet.

Profile decay measurements refer to the change in jet diameter with axial distance as the emerging jet relaxes from the stresses generated during the previous shear flow. A linear perturbation analysis taken about the final relaxed

state showed that a Maxwell model fluid would relax faster than a Newtonian jet of the same zero shear viscosity.

Experimental profile decay data obtained for Newtonian liquids confirmed the theoretical prediction that , within the range of variablesinvestigated, the damping coefficient is a function only of the Reynolds number. Values of the damping coefficient were in fair agreement with the analytical solution.

Profile decay data taken for a typical viscoinelastic fluid- 0.6 % Carbopol could be satisfactorily correlated only by assuming that the structural formation time was large compared to the time required for stress relaxation. This model assumed that no viscosity buildup occured above that possessed at the capillary exit. This proposed explanation was found to be consistent with wavelength and breakup length data for the viscoinelastic jets . For most of the test liquids, the breakup lengths corresponded to those for a Newtonian fluid of the same apparent viscosity as that possessed within the capillary. One notable exception was 0.1 % Carbopol which displayed an enhanced instability compared to water, when both were in the laminar range. Wavelength data taken near the point of breakup also confirmed the lack of any significant structural formation. All these observations lend support to the theory that the behavior of a capillary jet of a viscoinelastic liquid can be explained in terms of a

structural formation time which is large compared to the lifetime of the jet.

A theoretical analysis due to Yerushalmi (94) had predicted that a fluid with a sufficiently high yield stress could lead to a completely stable jet. However, the development assumed that the jet was initially relaxed at its zero shear structure. Such a conclusion would be inapplicable to the viscoinelastic liquids of this investigation which never reform their 'at rest' structure within the breakup time of the jet.

A practical application of these experimental results is that highly gellified viscoinelastic fluids can be readily atomized. The stiffest liquid studied, 12.4 % silica in water, had the appearance of a low viscosity jet in turbulent flow. It also appears that certain additives such as 0.1 % Carbopol are able to thicken a solution and yet enhance its atomization.

Profile decay data for a typical viscoelastic fluid-0.7 % SCMC showed decay rates slower than for a Newtonian jet of the same zero shear viscosity but faster than that for one of the same apparent viscosity. This is in direct contradiction to the theory of profile relaxation discussed earlier. The results can be interperted as showing that some structural formation had occurred. Another possibility which can not be resolved by these data alone is that a slowly decaying axial tensile stress exists along

the jet length which serves to retard the diameter change on a contracting column. However, high speed movies taken for several of the viscoelastic test fluids showed that large scale axial deformations are continually occuring and these require the existence of axial tensile stresses . The viscoelastic jets were seen to propagate disturbances by means of a droplet-thread configuration and the preference for this unusual configuration is not yet understood. While the evidence can not be regarded as conclusive, the data do point towards a limited viscosity or structural buildup within the lifetime of the jet and do demonstrate vividly the effects of axial normal stresses.

The linearized stability analysis for the breakup of a viscoelastic jet had predicted a higher growth rate of disturbances than for a Newtonian liquid of the same zero shear viscosity. This was partially confirmed for jets of 0.25 % SCMC. But even in the most dilute fluids studied, the initial wave propagation of disturbances was arrested and evolved into the unique droplet-thread configuration of these fluids.

While these studies have proposed some tentative theories to explain the behavior of capillary jets of visco-inelastic and viscoelastic liquids, they have also raised many questions and indicated the need for continued research in this area.

BIBLIOGRAPHY

1. Ballman, R.L., Extensional flow of polystyrene melts, Rheol. Acta. 4, 137 (1965).

2. Biot, M.A., Theory of stress-strain relations in anisotropic viscoelasticity and relaxation phenomena, J. Appl. Phys. 25, 1385 (1954).

3. Bird, R.B., Experimental tests of generalized non-Newtonian models containing a zero shear viscosity and a characteristic time, Canad. J. Chem. Eng. 43, 161 (1965).

4. Bland, D.R., "The Theory of Linear Viscoelasticity," Pergamon Press, New York 1960.

5. Bogue, D.C. and J.O. Doughty, Comparison of constitutive equations for viscoelastic fluids, Ind. and Eng. Chem. Fund. 5, 243 (1966).

6. Borodin, V.A. and Y.F. Dityakin, Unstable capillary waves on surface of separation of two viscous liquids, NACA Tech Memo 1281 (1951).

7. Carver, E.K. and J.R. Van Wazer, The sudden application of a constant shearing motion to anomalous fluids, J. Phys. and Colloid Chem. 51, 751 (1947).

8. Chandresakar, S., "Hydrodynamic and Hydromagnetic Stability," Oxford Univ. Press, London and New York, 1961.

9. Clegg, P.L., in "Rheology of Elastomers" ed. by P. Mason and N. Wookey, p. 174, Pergamon Press, London, 1958.

10. Coleman, B.D. and W. Noll, Steady extension of incompressible simple fluids, Phys. Fluids 5, 840 (1962).

11. Coleman, B.D., H. Markovitz and W. Noll, "Viscometric Flows of non-Newtonian Fluids," p. 75-83, Springer-Verlag, New York, 1966.

12. Davies, C.N. Proc. Int'l Rheol. Cong., vol. II, p. 152, vol. III, p. 52 (1948).

13. Denn, M.M. and J.J. Roisman, Rotational stability and measurement of normal stress functions in dilute polymer solutions, A.I.Ch.E. J. 15, 454 (1969).

14. Dodge, D.W. and A.B. Metzner, Turbulent flow of non-Newtonian systems, A.I.Ch.E. J. 5, 189 (1959).

15. Dombrowsky, N., P. Eisenklam and R.P. Fraser, Flow and disintegration of thin sheets of viscoelastic liquids J. Fuel Inst. London, 30, 399 (1957).

16. Donnelly, R.J. and W. Glaberson, Experiments on the capillary instability of a liquid jet, Proc. Roy. Soc. London, A290, 547 (1957) .

17. Duffie, J.A. and W.R. Marshall, Jr., Factors influencing the properties of spray dried materials, Chem. Eng. Prog. 49, 417,480 (1953).

18. Eckhaus, W., "Studies in Non-Linear Stability Theory", Springer-Verlag, New York, 1965 .

19. Fenn, R.W. III and S. Middleman, Newtonian jet stability: the role of air resistance, A.I.Ch.E. J. 15, 379 (1969).

20. Ferry, J.D., "Viscoelastic Properties of Polymers", John Wiley, London and New York, 1961 .

21. Fischer, W.H., W.H. Bauer and S.E. Wiberly, Yield stresses and flow properties of carboxypolymethylene-water systems, Trans. Soc. Rheol. 5, 221 (1961).

22. Fredrickson, A.G. , "Principles and Applications of Rheology", Prentice-Hall, New Jersey, 1964 .

23. Gadd, G.E., Turbulence damping and drag reduction produced by certain additives in water, Nature 206, 463 (1965) .

24. Gaskins, F.H. and W. Phillipoff, The behavior of jets of viscoelastic fluids, Trans. Soc. Rheol. 3, 181 (1959).

25. Gavis, J., Contribution of surface tension to expansion and contraction of capillary jets , Phys. Fluids 7, 1097 (1964) .

26. Gavis, J. and M. Modan, Expansion and contraction of jets of Newtonian liquids in air: effect of tube length, Phys. Fluids 10, 487 (1967).

27. Gill, S.J. and J. Gavis, Tensile stresses in jets of viscoelastic fluids, I- J.Poly. Sci. 20, 287 (1956) .
II- J.Poly. Sci. 21, 353 (1956) .

28. Ginn, R.F. and M.M. Denn, Rotational stability in viscoelastic liquids: theory, A.I.Ch.E. J. 15, 451 (1969).

29. Goldin, M., J. Yerushalmi. R. Pfeffer and R. Shinnar, Breakup of a laminar capillary jet of a viscoelastic fluid, J. Fluid Mech. 38, 689 (1969) .

30. Goren, S.L., Development of the boundary layer at a free surface from a uniform shear flow, J. Fluid Mech. 25, 87 (1966) .

31. Goren, S.L. and J. Gavis, Transverse wave motion on a thin capillary jet of a viscoelastic liquid, Phys. Fluids 4, 575 (1961) .

32. Goren, S.L. and S. Wronski, The shape of low speed capillary jets of Newtonian liquids, J. Fluid Mech. 25, 185 (1966) .

33. Grant, R.P. and S. Middleman, Newtonian jet stability, A.I.Ch.E. J. 12, 669 (1966) .

34. Haenlein, A., Disintegration of a liquid jet, NACA Tech. Memo No. 659 (1932) .

35. Harmon, D.B. Jr., Drop sizes from low speed jets, J. Franklin Inst. 259, 519 (1955) .

36. Hoyt, J.W. and A.G. Fabula, The effect of additives on fluid friction ,Fifth Symp. Naval Hydrodynamics, Bergen, Norway (1964), Office of Naval Research, Wash., D.C.

37. Huppler, J.D., The secondary normal stress difference, Ph.D. thesis in chem. eng. , Univ. of Wisconsin (1965) .

38. Hurd, R.E., B.Ch.E. thesis in chem. eng., Univ. of Delaware (1962).

39. Kroesser, F.W. and S.Middleman, Viscoelastic jet stability, A.I.Ch.E. J. 15, 383 (1969).

40. Kapoor, N.N., Unpublished M.S. thesis in chem. eng., Univ. of Minnesota (1963), reported in Fredrickson (22), pp. 120,178 .

41. Lee, D.W. and R.C. Spencer, Photomicrographic studies of fuel sprays, NACA Report no. 454 (1932) .

42. Lin, C.C., "The Theory of Hydrodynamic Stability", Cambridge Univ. Press, London and New York, 1955.

43. Lodge, A.S., "Elastic Liquids", pp. 114-118, Academic Press, 1964 .

44. Lodge, A.S., Colloque, Intn'l. de Rheol., Paris, France, 1960.

45. Markovitz, H., Normal stress effect in polyisobutylene solutions II. Classification and application of rheological theories, Trans. Soc. Rheol. 1, 37 (1957) .

46. Marshall, W.R. Jr., Atomization and spray drying, Chem. Eng. Prog. Symp. Ser. no. 50 (1954).

47. Meksyn, D. and J.T. Stuart, Stability of viscous motion between parallel flows for finite disturbances, Proc. Roy. Soc. (London) A208, 517 (1951).

48. Merrill, E.W., Viscometric classification of polymer solutions, Ind. and Eng. Chem. 51, 868 (1959) .

49. Merrill, E.W., H.S. Mickley and A.M. Ram, Instability in Couette flow of solutions of macromolecules, J. Fluid Mech. 13, 86 (1962).

50. Merrington, R.C. and E.G. Richarson, The breakup of liquid jets, Proc. Phys. Soc. 59, 1 (1947).

51. Metzner, A.B., in "Handbook of Fluid Dynamics" ed. by V.L. Streeter, Chap. 7, McGraw-Hill, New York, 1961 .

52. Metzner, A.B., W.T. Houghton, R.A. Sailor and J.L. White, A method for the measurement of normal stresses in simple shearing flow, Trans. Soc. Rheol. 5, 133 (1961).

53. Metzner, A.B. and M.G. Park, Turbulent flow characteristics of viscoelastic fluids, J. Fluid Mech. 20, 291 (1964).

54. Metzner, A.B., J.L. White and M.M. Denn, Constitutive equations for viscoelastic fluids for short deformation periods and for rapidly changing flows: significance of the Deborah number, A.I.Ch.E. J. 12, 863 (1966).

55. Metzner, A.B., J.L. White and M.M. Denn, Behavior of viscoelastic materials in short time processes, Chem. Eng. Prog. 62,81 (1966) .

56. Metzner, A.B. and M. Whitlock, Flow behavior of concentrated solutions, Trans. Soc. Rheol. 2, 239 (1958) .

57. Middleman, S. Profile relaxation in Newtonian jets, Ind. and Eng. Chem. Fund. 3, 118 (1964) .

58. Middleman, S., Stability of a viscoelastic jet, Chem. Eng. Sci. 20, 1037 (1965).

59. Middleman, S. , "The Flow of High Polymers", Interscience, New York, 1968 .

60. Middleman, S. and J. Gavis, Expansion and contraction of capillary jets of Newtonian liquids, Phys. Fluids 4, 355 (1961) .

61. Middleman,S. and J. Gavis, Expansion and contraction of capillary jets of viscoelastic liquids, Phys. Fluids 4, 963 (1961) .

62. Middleman, S. and J. Gavis, Errata, Phys. Fluids 4, 1450 (1961) .

63. Miesse, C.C., Correlation of experimental data on the disintegration of liquid jets, Ind. and Eng. Chem. 47, 1690 (1955).

64. Nitschmann, H. and J. Schrade, On the ability to draw threads from liquids of anomalous viscosity, Helv. Chim. Acta, 31, 297 (1948).

65. Oldroyd, J.G., On the formulation of rheological equations of state, Proc. Roy. Soc. (London) A200, 523 (1950) .

66. Oldroyd, J.G., The motion of an elastico-viscous liquid contained between coaxial cylinders. I, Quart. J. Mech. Appl. Math. 4, 271 (1951) .

67. Oldroyd, J.G., Non-Newtonian effects in steady motion of some idealized elastico-viscous liquids, Proc. Roy. Soc. (London) A295, 278 (1958) .

68. Oliver, D.R., Expansion/contraction behavior of laminar liquid jets, Canad. J. Chem. Eng. 44, 100 (1966).

69. Powell, R.L., Transient and steady state behavior of normal stresses in capillary flow of viscoelastic liquids, Ph.D thesis in chem. eng., Univ. of Rochester, 1967 .

70. Rayleigh, Lord, On the instability of jets, Proc. London Math. Soc. 10, 4 (1879) .

71. Rayleigh, Lord, On the capillary phenomena of jets, Proc. Roy. Soc. (London) A29, 71 (1879) .

72. Rayleigh, Lord, On the instability of a cylinder of viscous liquid under capillary forces, Phil. Mag. 34, 145 (1892) .

73. Rayleigh, Lord, On the instability of cylindrical fluid surfaces, Phil. Mag. 34, 177 (1892).

74. Rubin, H. and C. Elata, Stability of Coeutte flow of dilute polymer solutions, Phys. Fluids 4, 1929 (1966) .

75. Savart, F., Notes on the behavior of liquid jets ejected from thin walled circular orifices, Ann. Chim. 53, 337 (1833).

76. Savins, J.G., Some comments on the pumping requirements for non-Newtonian fluids, J. Inst. Petrol. 47, 329 (1961).

77. Schwarz, W.H. and C. Bruce, Rheological properties of ionic and non-ionic polyacrylamide solutions, submitted for publication, Standford Univ.

78. Seyer, F.A. and A.B. Metzner, Turbulent flow properties of viscoelastic fluids, Canad. J. Chem. Eng. 45, 121 (1967) .

79. Slattery, J.C. and W.R. Schowalter, Effect of surface tension on the measurement of the average normal stress at the exit of a capillary tube through an analysis of the capillary jet, J. Appl. Poly. Sci. 8, 1941 (1964) .

80. Smith, S.W.J. and H.Moss, Experiments with mercury jets, Proc. Roy. Soc. (London) A93, 373 (1917) .

81. Spriggs, T.W., J.D. Huppler and R.B. Bird, An experimental appraisal of viscoelastic models, Trans. Soc. Rheol. 10, 191 (1966).

82. Stuart, J.T., On the non-linear mechanics of hydrodynamic stability, J. Fluid Mech. 4, 1 (1958) .

83. Taylor, G.I., Stability of a viscous liquid contained between two rotating cylinders, Phil. Trans. Roy. Soc. A223, 289 (1923) .

84. Toms, B.A., Some observations on the flow of linear polymer solutions through straight tubes at large Reynolds numbers, Proc. Int'l. Cong. Rheol., Holland, 1948, North-Holland Publ. Co., Amsterdam, 1949 .

85. Tyler, E., Instability of liquid jets, Phil. Mag. 16, 504 (1933).

86. Tyler, E. and E.G. Richardson, The characteristic curves of liquid jets, Proc. Phys. Soc. London 37, 297 (1925) .

87. Tyler, E. and F. Watkin, Experiments with capillary jets, Phil. Mag. 14, 849 (1932).

88. Van Wazer, J.R., J.W. Lyons, K.Y. Kim and R.E. Colwell, "Viscosity and Flow Measurement", Interscience, New York, 1966 .

89. Weber, C., Disintegration of a liquid jet, Z. angew. Math. Mech. 11, 136 (1931) .

90. Weissenberg, K., A continuum theory of rheological phenomena, Nature 159, 310 (1947) .

91. Wells, C.S. Jr., Anomalous turbulent flow of non-Newtonian fluids, AIAA J. 3, 1800 (1965) .

92. White, J.L., Dynamics of viscoelastic fluids; melt fracture and rheology of fiber spinning, J. Appl. Poly. Sci. 8, 2339 (1964) .

93. Wilcox, J.D., R.K. June, H.A. Brown Jr. and R.C. Kelly, Retardation of drop breakup in high velocity air stream by polymeric modifiers, J. Appl. Poly. Sci. 5, 1 (1961) .

94. Yerushalmi, J., The stability of a filament of a viscoelastic fluid, Ph.D. thesis in chem. eng., City Univ. of New York, 1969.

95. Ziabicki, A. and K. Kedzierska, Mechanical aspects of fiber spinning process in molten polymers - I. stream diameter and velocity distribution along the spinning way. Kolloid Z. 171, 51 (1960) .

APPENDIX A

CAPILLARY VISCOMETER DATA

Fluid	Instron speed- in./sec.	Nozzle diameter - cm.	Nozzle length - in.	Transducer output- millivolts
24 % MPA 60 in xylene	$3.3(10^{-4})$	0.0414	2.690	3.00
			4.168	4.60
	$1.0(10^{-3})$	0.0414	2.690	6.88
			4.168	9.25
	$1.7(10^{-3})$	0.0414	2.690	9.25
			4.168	12.75
	$3.3(10^{-3})$	0.0868	1.552	1.60
			5.842	3.90
	$1.0(10^{-2})$	0.0868	1.552	3.20
			5.842	7.63
	$1.7(10^{-2})$	0.0868	1.552	4.25
			5.842	10.63
	$2.3(10^{-2})$	0.0868	1.552	4.90
			5.842	12.37
	$3.3(10^{-3})$	0.228	18.0	0.45
			36.0	0.84
	$6.6(10^{-3})$	0.228	18.0	0.76
			36.0	1.35
	$1.7(10^{-2})$	0.228	18.0	1.50
			36.0	2.60
24 % MPA 60 in mineral spirits	$1.3(10^{-3})$	0.0414	2.690	5.50
			4.168	7.25
	$2.0(10^{-3})$	0.0414	2.690	7.25
			4.168	10.63
	$2.7(10^{-3})$	0.0414	2.690	9.00
			4.168	13.25
	$3.3(10^{-3})$	0.0868	1.552	0.64
			5.842	1.95

Fluid	Instron speed- in./sec.	Nozzle diameter - cm.	Nozzle length - in.	Transducer output- millivolts
24 % MPA 60 in mineral spirits	$1.0(10^{-2})$	0.0868	1.552	1.60
			5.842	4.85
	$1.7(10^{-2})$	0.0868	1.552	2.35
			5.842	7.35
	$2.7(10^{-2})$	0.0868	1.552	3.50
			5.842	10.13
	$3.3(10^{-2})$	0.0868	1.552	4.25
			5.842	12.00
	$3.3(10^{-2})$	0.228	18.0	0.25
			36.0	0.50
	$1.0(10^{-2})$	0.228	18.0	0.44
			36.0	0.95
	$1.7(10^{-2})$	0.228	18.0	0.65
			36.0	1.38
	$2.7(10^{-2})$	0.228	18.0	0.95
			36.0	1.63
	$8.3(10^{-2})$	0.228	18.0	2.60
			36.0	4.55
12.4 % silica- water	$2.0(10^{-2})$	0.228	18.0	1.55
			36.0	2.80
	$2.7(10^{-2})$	0.228	18.0	1.70
			36.0	3.20
	$3.8(10^{-2})$	0.228	18.0	1.90
			36.0	3.80
	0.10	0.228	18.0	3.43
			36.0	6.95
	0.14	0.228	18.0	4.00
			36.0	7.50
	0.20	0.228	18.0	5.30
				12.00

Fluid	Instron speed- in./sec.	Nozzle diameter - cm.	Nozzle length - in.	Transducer output- millivolts
12.4 % silica-water	0.27	0.228	18.0	6.50
			36.0	12.75
	0.38	0.228	18.0	7.63
			36.0	14.75
	$3.8(10^{-2})$	0.0868	1.552	4.00
			5.842	10.15
	$6.7(10^{-2})$	0.0868	1.552	5.75
			5.842	12.75
0.2 % Carbopol	$5.0(10^{-4})$	0.0868	1.552	0.13
			5.842	0.37
	$1.9(10^{-3})$	0.0868	1.552	0.24
			5.842	0.72
	$5.0(10^{-4})$	0.0414	3.386	1.35
			4.148	1.62
	$1.9(10^{-3})$	0.0414	3.386	3.09
			4.148	3.73
	$5.0(10^{-4})$	0.0263	1.445	2.08
			1.916	2.70
	$8.3(10^{-4})$	0.0263	1.445	3.10
			1.916	3.88
	$1.2(10^{-3})$	0.0263	1.445	3.91
			1.916	4.78
	$1.7(10^{-3})$	0.0263	1.445	5.14
			1.916	6.74
0.6 % Carbopol	$3.2(10^{-5})$	0.0868	1.552	0.32
			5.842	0.87
	$3.2(10^{-5})$	0.0868	1.552	0.32
			5.842	0.96

Fluid	Instron speed- in./sec.	Nozzle diameter - cm.	Nozzle length - in.	Transducer output- millivolt
0.6 % Carbopol	$8.3(10^{-5})$	0.0868	1.552	0.40
			5.842	1.24
	$8.3(10^{-5})$	0.0868	1.552	0.44
			5.842	1.30
	$3.2(10^{-5})$	0.0414	2.690	1.48
			4.148	2.28
	$2.5(10^{-4})$	0.0868	1.552	0.59
			5.842	1.78
	$8.3(10^{-5})$	0.0414	3.368	3.10
			4.148	3.69
	$9.3(10^{-4})$	0.0868	1.552	0.89
			5.842	2.71
	$2.5(10^{-4})$	0.0414	2.690	3.35
			4.148	4.90
	$2.5(10^{-4})$	0.0414	2.690	3.45
			4.148	5.15
	$7.5(10^{-4})$	0.0414	2.690	5.60
			4.148	8.55
	$8.3(10^{-5})$	0.0263	1.444	3.53
			1.916	5.02
	$9.1(10^{-4})$	0.0414	3.368	7.88
			4.148	9.45
	$8.3(10^{-5})$	0.0263	1.444	3.82
			1.916	5.35
	$1.0(10^{-3})$	0.0414	2.690	6.63
			4.148	9.80
	$1.7(10^{-4})$	0.0263	1.444	5.22
			1.916	6.92

Fluid	Instron speed- in./sec.	Nozzle diameter - cm.	Nozzle length - in.	Transducer output- millivolts
0.6 % Carbopol	$2.5(10^{-4})$	0.0263	1.444	6.08
			1.916	8.28
	$3.3(10^{-4})$	0.0263	1.444	7.15
			1.916	9.45
	$4.2(10^{-4})$	0.0263	1.444	7.92
			1.916	10.30
	$2.5(10^{-4})$	0.0263	1.444	5.90
			1.916	8.50
	$4.2(10^{-4})$	0.0263	1.444	8.00
			1.916	10.75
	$6.7(10^{-4})$	0.0263	1.444	10.00
			1.916	13.13
	$9.3(10^{-4})$	0.0263	1.444	11.63
			1.916	16.00

The diameter of the hydraulic cylinder containing the test fluid was 4.000 inches I.D. Therefore, the volumetric flow rate is obtained as the crossectional area of the hydraulic cylinder multiplied by the Instron speed.

APPENDIX B

DROPLET DISTRIBUTION DATA

The following data was taken along the length of a capillary jet of 0.25 % Separan and represents the change in the droplet diameter with increasing axial distance. A volumetric flow rate of 23 ml./min. passed through a 0.0263 cm. capillary.

Distance from nozzle	Droplet number	Droplet length	Droplet width	Droplet diameter
2.0 cm.	1	0.111 cm.	0.078 cm.	0.093 cm.
	2	0.111	0.090	0.100
	3	0.094	0.103	0.099
6.1	1	0.145	0.055	0.089
	2	0.128	0.078	0.100
	3	0.137	0.077	0.103
	4	0.137	0.101	0.118
	5	0.159	0.138	0.148
	6	0.124	0.065	0.090
	7	0.141	0.065	0.096
	8	0.156	0.100	0.125
	9	0.111	0.086	0.098
	10	0.111	0.067	0.087
	11	0.111	0.108	0.110
	12	0.100	0.054	0.074
	13	0.139	0.113	0.125
	14	0.117	0.119	0.118
10.1	1	0.119	0.067	0.089
	2	0.140	0.110	0.124
	3	0.137	0.077	0.102
	4	0.103	0.058	0.078
	5	0.128	0.082	0.103
	6	0.142	0.101	0.120
	7	0.121	0.076	0.096
	8	0.097	0.052	0.071
	9	0.089	0.045	0.063
	10	0.098	0.056	0.074
	11	0.156	0.115	0.134
	12	0.141	0.102	0.120
	13	0.115	0.065	0.086

Distance from nozzle	Droplet number	Droplet length	Droplet width	Droplet diameter
10.1 cm.	14	0.108 cm.	0.044 cm.	0.068 cm.
	15	0.132	0.094	0.111
	16	0.160	0.128	0.143
	17	0.179	0.095	0.131
	18	0.133	0.067	0.094
	19	0.112	0.047	0.073
	20	0.157	0.120	0.137
14.1	1	0.095	0.037	0.060
	2	0.111	0.243	0.164
	3	0.133	0.098	0.114
	4	0.164	0.122	0.141
	5	0.147	0.111	0.128
	6	0.108	0.036	0.062
	7	0.108	0.036	0.062
	8	0.182	0.109	0.120
	9	0.167	0.140	0.153
	10	0.103	0.045	0.068
	11	0.127	0.064	0.091
	12	0.128	0.084	0.104
	13	0.160	0.116	0.136
	14	0.176	0.140	0.157
	15	0.141	0.113	0.126
	16	0.088	0.046	0.063
	17	0.183	0.149	0.165
	18	0.149	0.100	0.122
	19	0.125	0.087	0.104
	20	0.127	0.072	0.096
	21	0.127	0.131	0.129
	22	0.155	0.128	0.141
	23	0.132	0.067	0.094
	24	0.149	0.104	0.124
	25	0.210	0.129	0.164
18.1	1	0.161	0.151	0.156
	2	0.173	0.154	0.163
	3	0.102	0.063	0.080
	4	0.190	0.126	0.155
	5	0.074	0.059	0.066
	6	0.128	0.046	0.077
	7	0.195	0.133	0.161
	8	0.167	0.126	0.145
	9	0.129	0.043	0.074

Distance from nozzle	Droplet number	Droplet length	Droplet width	Droplet diameter
18.1 cm.	10	0.139 cm.	0.072 cm.	0.100 cm.
	11	0.139	0.090	0.112
	12	0.122	0.074	0.095
	13	0.146	0.103	0.123
	14	0.200	0.130	0.161
	15	0.113	0.063	0.085
	16	0.111	0.066	0.085
	17	0.146	0.102	0.122
	18	0.115	0.072	0.091
22.1	1	0.171	0.137	0.153
	2	0.181	0.153	0.167
	3	0.085	0.059	0.071
	4	0.111	0.080	0.094
	5	0.176	0.145	0.159
	6	0.130	0.095	0.111
	7	0.124	0.100	0.112
	8	0.177	0.167	0.172
	9	0.100	0.065	0.081
	10	0.141	0.148	0.144
	11	0.144	0.117	0.130
	12	0.151	0.115	0.132
	13	0.126	0.096	0.110
	14	0.183	0.155	0.168
	15	0.108	0.048	0.072
	16	0.150	0.111	0.129
	17	0.132	0.109	0.120
	18	0.192	0.126	0.156
	19	0.140	0.086	0.110
	20	0.078	0.042	0.057
	21	0.156	0.133	0.144
	22	0.122	0.089	0.104
	23	0.122	0.085	0.102
	24	0.132	0.111	0.121
	25	0.117	0.090	0.103
26.1	1	0.176	0.111	0.140
	2	0.128	0.127	0.128
	3	0.133	0.112	0.122
	4	0.133	0.097	0.114
	5	0.150	0.154	0.152
	6	0.132	0.104	0.117
	7	0.164	0.114	0.137

Distance from nozzle	Droplet number	Droplet length	Droplet width	Droplet diameter
26.1 cm.	8	0.203 cm.	0.151 cm.	0.175 cm.
	9	0.072	0.055	0.063
	10	0.103	0.064	0.081
	11	0.162	0.125	0.142
	12	0.158	0.113	0.133
	13	0.163	0.120	0.140
	14	0.144	0.088	0.112
	15	0.186	0.154	0.169
	16	0.101	0.058	0.076
	17	0.131	0.110	0.120
	18	0.209	0.155	0.180
	19	0.178	0.140	0.158
	20	0.093	0.056	0.072
	21	0.086	0.055	0.069
	22	0.192	0.146	0.168
	23	0.232	0.146	0.185
30.1	1	0.080	0.029	0.049
	2	0.144	0.096	0.118
	3	0.181	0.171	0.176
	4	0.078	0.045	0.059
	5	0.197	0.178	0.187
	6	0.178	0.137	0.156
	7	0.128	0.080	0.101
	8	0.097	0.061	0.077
	9	0.201	0.165	0.182
	10	0.152	0.132	0.141
	11	0.175	0.146	0.160
	12	0.089	0.059	0.072
	13	0.123	0.077	0.097
	14	0.146	0.093	0.116
	15	0.194	0.171	0.182
	16	0.202	0.142	0.169
	17	0.222	0.159	0.188
	18	0.086	0.041	0.060
	19	0.155	0.109	0.130
	20	0.164	0.123	0.142
34.1	1	0.200	0.193	0.196
	2	0.104	0.067	0.083
	3	0.104	0.070	0.085
	4	0.179	0.151	0.164
	5	0.091	0.063	0.076

Distance from nozzle	Droplet number	Droplet length	Droplet width	Droplet diameter
34.1 cm.	6	0.145 cm.	0.114 cm.	0.129 cm.
	7	0.126	0.083	0.102
	8	0.169	0.147	0.157
	9	0.128	0.085	0.104
	10	0.104	0.070	0.085
	11	0.115	0.090	0.102
	12	0.128	0.069	0.094
	13	0.104	0.060	0.079
	14	0.158	0.129	0.143
	15	0.166	0.139	0.152
	16	0.151	0.126	0.138
	17	0.150	0.118	0.133
	18	0.154	0.122	0.137
	19	0.160	0.122	0.140
	20	0.174	0.149	0.161
	21	0.078	0.046	0.060
	22	0.212	0.182	0.197
	23	0.173	0.152	0.162
	24	0.165	0.136	0.150
	25	0.106	0.094	0.100
38.1	1	0.106	0.067	0.084
	2	0.098	0.065	0.080
	3	0.080	0.035	0.053
	4	0.082	0.072	0.077
	5	0.188	0.232	0.209
	6	0.120	0.113	0.117
	7	0.221	0.166	0.192
	8	0.116	0.098	0.107
	9	0.130	0.113	0.121
	10	0.112	0.056	0.079
	11	0.189	0.171	0.180
	12	0.177	0.164	0.171
	13	0.116	0.151	0.132
	14	0.076	0.068	0.072
	15	0.103	0.065	0.082
	16	0.200	0.175	0.187
	17	0.114	0.099	0.106
	18	0.158	0.110	0.132
	19	0.110	0.144	0.126
	20	0.184	0.144	0.163
	21	0.133	0.134	0.134
	22	0.157	0.144	0.150

Distance from nozzle	Droplet number	Droplet length	Droplet width	Droplet diameter
42.1 cm.	1	0.109 cm.	0.089 cm.	0.099 cm.
	2	0.179	0.178	0.178
	3	0.088	0.058	0.071
	4	0.170	0.212	0.190
	5	0.082	0.051	0.064
	6	0.143	0.122	0.132
	7	0.136	0.119	0.127
	8	0.165	0.280	0.215
	9	0.240	0.173	0.204
	10	0.146	0.130	0.138
	11	0.164	0.159	0.161
	12	0.127	0.121	0.124
	13	0.183	0.209	0.196
	14	0.151	0.138	0.144
	15	0.081	0.068	0.075
	16	0.156	0.237	0.192
	17	0.186	0.188	0.187
	18	0.113	0.096	0.105
	19	0.121	0.107	0.114
	20	0.079	0.055	0.066
	21	0.081	0.071	0.076
46.1	1	0.104	0.075	0.088
	2	0.162	0.141	0.151
	3	0.169	0.286	0.220
	4	0.040	0.051	0.045
	5	0.162	0.160	0.161
	6	0.101	0.093	0.097
	7	0.054	0.036	0.044
	8	0.164	0.190	0.177
	9	0.137	0.108	0.122
	10	0.152	0.145	0.149
	11	0.093	0.079	0.086
	12	0.122	0.121	0.121
	13	0.154	0.128	0.140
	14	0.157	0.157	0.157
	15	0.116	0.094	0.105
	16	0.171	0.161	0.166
	17	0.122	0.105	0.113
	18	0.080	0.066	0.072
	19	0.143	0.139	0.141
	20	0.185	0.176	0.180
	21	0.257	0.124	0.179

Distance from nozzle	Droplet number	Droplet length	Droplet width	Droplet diameter
46.1 cm.	22	0.089 cm.	0.064 cm.	0.076 cm.
	23	0.053	0.032	0.041
	24	0.119	0.099	0.108
	25	0.119	0.099	0.108
	26	0.119	0.102	0.110
	27	0.129	0.110	0.119
	28	0.198	0.194	0.196
	29	0.100	0.097	0.098
	30	0.167	0.167	0.167
50.1	1	0.119	0.117	0.118
	2	0.153	0.150	0.151
	3	0.116	0.111	0.113
	4	0.105	0.100	0.103
	5	0.111	0.114	0.113
	6	0.121	0.120	0.120
	7	0.149	0.154	0.151
	8	0.147	0.147	0.147
	9	0.119	0.120	0.120
	10	0.180	0.170	0.175
	11	0.085	0.139	0.109
	12	0.156	0.078	0.110
	13	0.076	0.151	0.107
	14	0.108	0.047	0.072
	15	0.057	0.095	0.073
	16	0.138	0.059	0.091
	17	0.183	0.126	0.152
	18	0.162	0.188	0.174
	19	0.094	0.150	0.119
	20	0.118	0.079	0.097
	21	0.164	0.112	0.136
54.1	1	0.157	0.146	0.151
	2	0.089	0.091	0.090
	3	0.096	0.078	0.086
	4	0.102	0.095	0.099
	5	0.045	0.036	0.040
	6	0.161	0.152	0.157
	7	0.080	0.082	0.081
	8	0.148	0.146	0.147
	9	0.169	0.154	0.161
	10	0.094	0.088	0.091
	11	0.219	0.186	0.202

Distance from nozzle	Droplet number	Droplet length	Droplet width	Droplet diameter
54.1 cm.	12	0.158 cm.	0.149 cm.	0.153 cm.
	13	0.159	0.147	0.153
	14	0.185	0.173	0.179
	15	0.221	0.145	0.179
	16	0.137	0.128	0.133
	17	0.116	0.111	0.114
	18	0.114	0.111	0.113
	19	0.040	0.028	0.033
	20	0.146	0.146	0.146
	21	0.127	0.107	0.117
	22	0.087	0.062	0.074
	23	0.115	0.103	0.109
	24	0.188	0.188	0.188
	25	0.176	0.163	0.169

The following data was taken along the length of a capillary jet of 0.25 % Separan. It represents the length between the droplets described on pages 230-237 as a function of the axial distance from the nozzle. The volumetric flow rate was 23 ml./min. through a 0.0263 cm. capillary.

Distance from nozzle	Picture number	Thread number	Thread length	Average thread length
10.1 cm.	1	1	4.3 cm.	2.9 cm.
	1	2	3.1	
	2	1	6.0	
	3	1	5.4	
	3	2	1.1	
	4	1	4.8	
	4	2	1.1	
	4	3	1.2	
	4	4	0.3	
	5	1	4.8	
	6	1	2.2	
	6	2	1.1	
	6	3	2.3	
	7	1	4.3	
	7	2	3.4	
	8	1	2.2	
	8	2	0.5	
	8	3	3.5	
14.1	1	1	2.6	2.7
	1	2	2.8	
	2	1	5.6	
	3	1	3.6	
	3	2	0.3	
	3	3	2.2	
	3	4	0.6	
	4	1	2.0	
	4	2	1.6	
	4	3	4.1	
	5	1	1.1	

Distance from nozzle	Picture number	Thread number	Thread length	Average thread length
14.1 cm.	5	2	5.1 cm.	2.7 cm.
	6	1	5.7	
	6	2	0.6	
	7	1	4.8	
	8	1	0.9	
	8	2	3.0	
	8	3	1.7	
18.1	1	1	2.3	2.0
	1	2	2.4	
	1	3	0.5	
	1	4	2.5	
	2	1	3.1	
	2	2	0.0	
	2	3	4.6	
	3	1	3.6	
	3	2	3.5	
	4	1	0.4	
	4	2	1.6	
	4	3	1.3	
	4	4	0.2	
	4	5	0.7	
	4	6	2.6	
	5	1	3.2	
	5	2	0.2	
	5	3	3.7	
22.1	1	1	4.1	2.6
	1	2	1.5	
	2	1	3.2	
	2	2	4.5	
	3	1	2.9	
	3	2	4.1	
	3	3	0.1	
	4	1	1.4	
	4	2	2.4	
	4	3	3.7	
	5	1	1.8	
	5	2	4.3	
	5	3	0.8	
	6	1	3.2	
	6	2	0.9	
	6	3	2.5	
	7	1	4.2	

Distance from nozzle	Picture number	Thread number	Thread length	Average thread length
22.1 cm.	7	2	1.4 cm.	2.6 cm.
	8	1	4.6	
	8	2	0.4	
	8	3	1.5	
	9	1	4.5	
	9	2	2.1	
26.1	1	1	2.9	2.7
	1	2	0.7	
	1	3	3.8	
	2	1	2.1	
	2	2	3.6	
	2	3	0.9	
	3	1	4.1	
	3	2	1.8	
	3	3	1.5	
	4	1	3.7	
	4	2	4.0	
	5	1	1.8	
	5	2	1.9	
	5	3	3.4	
	6	1	3.9	
	6	2	3.1	
	7	1	5.8	
	8	1	4.3	
	8	2	0.3	
	8	3	2.3	
	8	4	0.5	
	9	1	5.1	
	9	2	0.6	
30.1	1	1	3.1	2.6
	1	2	4.6	
	2	1	3.4	
	2	2	1.5	
	3	1	5.6	
	3	2	2.1	
	4	1	2.8	
	4	2	0.3	
	4	3	0.4	
	4	4	2.6	
	4	5	1.5	
	5	1	3.6	

Distance from nozzle	Picture number	Thread number	Thread length	Average thread length
30.1 cm.	5	2	0.9 cm.	2.6 cm.
	5	3	3.2	
	6	1	2.2	
	6	2	1.2	
	6	3	4.2	
	7	1	2.6	
	7	2	1.4	
	8	1	3.3	
	8	2	3.4	
34.1	1	1	1.3	2.4
	1	2	0.7	
	1	3	1.4	
	1	4	1.0	
	1	5	2.9	
	2	1	1.3	
	2	2	4.9	
	3	1	2.2	
	3	2	1.9	
	3	3	3.6	
	4	1	1.5	
	4	2	6.2	
	5	1	0.3	
	5	2	0.6	
	5	3	2.8	
	5	4	1.8	
	6	1	2.0	
	6	2	3.2	
	7	1	5.1	
	7	2	0.7	
	8	1	2.2	
	8	2	4.4	
38.1	1	1	2.0	2.6
	1	2	0.4	
	1	3	4.2	
	2	1	3.1	
	3	1	1.0	
	3	2	2.0	
	3	3	3.3	
	4	1	7.7	
	5	1	0.5	
	5	2	2.9	

Distance from nozzle	Picture number	Thread number	Thread length	Average thread length
38.1 cm.	5	3	4.0 cm.	2.6 cm.
	6	1	4.9	
	7	1	1.5	
	7	2	3.6	
	8	1	3.1	
	8	2	0.3	
	8	3	2.8	
	8	4	0.5	
42.1	1	1	0.6	2.5
	1	2	1.6	
	1	3	5.4	
	2	1	3.2	
	2	2	0.5	
	2	3	3.2	
	3	1	5.6	
	4	1	4.6	
	4	2	0.2	
	4	3	2.8	
	5	1	5.2	
	5	2	0.4	
	5	3	0.3	
	6	1	0.3	
	6	2	2.2	
	6	3	3.4	
	7	1	0.2	
	7	2	4.2	
	7	3	2.9	
	8	1	2.7	
	8	2	2.4	
	8	3	2.5	
46.1	1	1	1.2	2.0
	1	2	0.5	
	2	1	4.3	
	3	1	2.2	
	3	2	2.4	
	3	3	2.3	
	4	1	4.0	
	4	2	0.2	
	4	3	0.7	
	4	4	2.9	
	5	1	5.9	
	6	1	2.3	

Distance from nozzle	Picture number	Thread number	Thread length	Average thread length
46.1 cm.	6	2	1.8 cm.	2.0 cm.
	6	3	1.2	
	6	4	0.4	
	7	1	0.8	
	7	2	1.6	
	7	3	2.0	
	7	4	2.7	
	8	1	2.4	
	8	2	0.1	
	8	3	0.3	
	8	4	1.2	
	9	1	5.3	
50.1	1	1	1.1	2.5
	1	2	4.6	
	2	1	5.8	
	2	2	0.2	
	2	3	0.2	
	3	1	0.5	
	3	2	6.0	
	4	1	4.5	
	4	2	1.4	
	5	1	3.3	
	5	2	2.4	
	5	3	0.4	
	6	1	4.6	
	6	2	1.8	
	7	1	4.6	
	7	2	2.1	
	8	1	2.6	
54.1	1	1	2.5	2.4
	1	2	2.9	
	2	1	6.7	
	3	1	2.4	
	3	2	0.1	
	3	3	1.8	
	4	1	1.7	
	4	2	4.9	
	5	1	4.5	
	5	2	2.6	
	6	1	1.5	
	6	2	0.3	

Distance from nozzle	Picture number	Thread number	Thread length	Average thread length
54.1 cm.	6	3	4.4 cm.	2.4 cm.
	7	1	3.1	
	7	2	3.6	
	8	1	4.9	
	8	2	0.4	
	8	3	0.4	
	8	4	0.4	
	8	5	0.6	
	8	6	1.9	
58.1	1	1	2.7	2.5
	1	2	0.5	
	2	1	4.1	
	2	2	2.4	
	3	1	4.6	
	3	2	0.5	
62.1	1	1	0.5	0.4
	1	2	0.3	

The data tabulated below are the droplet diameters after breakup for a capillary jet of 0.05 % Separan. The volumetric flow rate was 7.25 ml./min. through a 0.0263 cm. nozzle.

Droplet number	Droplet length	Droplet width	Average droplet diameter
1	0.087 cm.	0.087 cm.	0.087 cm.
2	0.087	0.087	0.087
3	0.145	0.127	0.136
4	0.118	0.118	0.118
5	0.166	0.132	0.148
6	0.108	0.108	0.108
7	0.122	0.122	0.122
8	0.072	0.072	0.072
9	0.113	0.110	0.112
10	0.100	0.096	0.098
11	0.083	0.083	0.083
12	0.100	0.100	0.100
13	0.083	0.083	0.083
14	0.149	0.129	0.139
15	0.109	0.109	0.109
16	0.099	0.099	0.099

The data tabulated below are the droplet diameters after breakup for a capillary jet of 0.05 % Separan. The volumetric flow rate was 10.2 ml./min. through a 0.0263 cm. nozzle.

Droplet number	Droplet length	Droplet width	Average droplet diameter
1	0.076 cm.	0.076 cm.	0.076 cm.
2	0.086	0.079	0.083
3	0.138	0.138	0.138
4	0.075	0.075	0.075

Droplet number	Droplet length	Droplet width	Average droplet diameter
5	0.081 cm.	0.081 cm.	0.081 cm.
6	0.073	0.073	0.073
7	0.095	0.095	0.095
8	0.108	0.108	0.108
9	0.094	0.094	0.094
10	0.078	0.078	0.078
11	0.073	0.073	0.073
12	0.094	0.094	0.094
13	0.073	0.073	0.073
14	0.083	0.083	0.083
15	0.095	0.095	0.095
16	0.072	0.072	0.072
17	0.157	0.110	0.131
18	0.076	0.076	0.076
19	0.096	0.096	0.096
20	0.096	0.093	0.095
21	0.118	0.097	0.107
22	0.088	0.066	0.076
23	0.084	0.084	0.084
24	0.104	0.104	0.104
25	0.112	0.112	0.112
26	0.082	0.082	0.082
27	0.115	0.102	0.109
28	0.088	0.088	0.088
29	0.067	0.067	0.067
30	0.090	0.090	0.090
31	0.101	0.101	0.101
32	0.182	0.168	0.175
33	0.090	0.090	0.090
34	0.121	0.115	0.118
35	0.085	0.085	0.085
36	0.103	0.099	0.101
37	0.127	0.093	0.109
38	0.112	0.092	0.102
39	0.098	0.098	0.098
40	0.076	0.070	0.073

The data tabulated below are the droplet diameters after breakup for a capillary jet of 0.05 % Separan. The volumetric flow was 14.2 ml./min. through a

0.0263 cm. nozzle.

Droplet number	Droplet length	Droplet width	Average droplet diameter
1	0.118 cm.	0.118 cm.	0.118 cm.
2	0.075	0.075	0.075
3	0.106	0.095	0.101
4	0.077	0.077	0.077
5	0.087	0.087	0.087
6	0.102	0.095	0.099
7	0.105	0.107	0.111
8	0.155	0.132	0.143
9	0.141	0.109	0.124
10	0.143	0.120	0.131
11	0.074	0.078	0.076
12	0.072	0.072	0.072
13	0.137	0.104	0.119
14	0.104	0.093	0.099
15	0.051	0.051	0.051
16	0.073	0.073	0.073
17	0.126	0.126	0.126
18	0.085	0.085	0.085
19	0.100	0.090	0.095
20	0.095	0.090	0.093
21	0.103	0.103	0.103
22	0.136	0.136	0.136
23	0.111	0.106	0.109
24	0.104	0.104	0.104
25	0.080	0.080	0.080
26	0.080	0.080	0.080
27	0.110	0.110	0.110
28	0.097	0.097	0.097
29	0.074	0.074	0.074
30	0.079	0.070	0.074
31	0.113	0.095	0.104
32	0.123	0.092	0.106
33	0.118	0.097	0.107
34	0.065	0.065	0.065
35	0.116	0.078	0.095
36	0.086	0.086	0.086
37	0.052	0.052	0.052
38	0.067	0.067	0.067
39	0.064	0.064	0.064
40	0.056	0.056	0.056

Droplet number	Droplet length	Droplet width	Average droplet diameter
41	0.075 cm.	0.075 cm.	0.075 cm.
42	0.077	0.067	0.072
43	0.082	0.082	0.082
44	0.053	0.053	0.053
45	0.076	0.076	0.076
46	0.099	0.067	0.081
47	0.075	0.075	0.075
48	0.086	0.076	0.081
49	0.066	0.066	0.066
50	0.081	0.081	0.081
51	0.118	0.097	0.107
52	0.083	0.083	0.083
53	0.085	0.085	0.085
54	0.135	0.097	0.114
55	0.083	0.067	0.075
56	0.120	0.102	0.111
57	0.102	0.102	0.102
58	0.102	0.102	0.102
59	0.110	0.110	0.110
60	0.130	0.130	0.130
61	0.081	0.081	0.081
62	0.094	0.094	0.094
63	0.094	0.090	0.092
64	0.096	0.096	0.096
65	0.094	0.094	0.094
66	0.105	0.105	0.105
67	0.088	0.088	0.088
68	0.021	0.017	0.019

The data tabulated below are the droplet diameters after breakup for a capillary jet of 0.05 % Separan. The volumetric flow was 16.2 ml./min. through a 0.0263 cm. nozzle.

Droplet number	Droplet length	Droplet width	Average droplet diameter
1	0.063 cm.	0.063 cm.	0.063 cm.
2	0.112	0.094	0.103
3	0.098	0.098	0.098
4	0.106	0.086	0.096
5	0.068	0.068	0.068
6	0.103	0.090	0.096
7	0.094	0.094	0.094
8	0.065	0.065	0.065
9	0.171	0.128	0.148
10	0.067	0.067	0.067
11	0.074	0.074	0.074
12	0.085	0.075	0.080
13	0.100	0.085	0.092
14	0.104	0.068	0.084
15	0.078	0.078	0.078
16	0.082	0.082	0.082
17	0.061	0.061	0.061
18	0.087	0.082	0.084
19	0.079	0.079	0.079
20	0.084	0.084	0.084
21	0.127	0.088	0.105
22	0.099	0.092	0.095
23	0.068	0.068	0.068
24	0.083	0.069	0.076
25	0.058	0.058	0.058
26	0.082	0.082	0.082
27	0.076	0.076	0.076
28	0.072	0.072	0.072
29	0.112	0.096	0.103
30	0.105	0.089	0.096
31	0.095	0.095	0.095
32	0.093	0.093	0.093
33	0.061	0.061	0.061
34	0.102	0.102	0.102
35	0.037	0.037	0.037
36	0.109	0.109	0.109
37	0.109	0.109	0.109
38	0.073	0.073	0.073
39	0.073	0.073	0.073
40	0.068	0.068	0.068
41	0.100	0.100	0.100
42	0.080	0.080	0.080
43	0.080	0.080	0.080

Droplet number	Droplet length	Droplet width	Average droplet diameter
44	0.068 cm.	0.068 cm.	0.068 cm.
45	0.054	0.054	0.054
46	0.071	0.071	0.071
47	0.111	0.111	0.111
48	0.071	0.071	0.071
49	0.071	0.071	0.071
50	0.073	0.073	0.073
51	0.067	0.067	0.067
52	0.100	0.087	0.093

The data tabulated below are the droplet diameters after breakup for a capillary jet of 0.05 % Separan. The volumetric flow was 23.3 ml./min. through a 0.0263 cm. nozzle.

Droplet number	Droplet length	Droplet width	Average droplet diameter
1	0.063 cm.	0.063 cm.	0.063 cm.
2	0.076	0.076	0.076
3	0.089	0.089	0.089
4	0.074	0.074	0.074
5	0.077	0.077	0.077
6	0.116	0.088	0.101
7	0.095	0.074	0.084
8	0.082	0.082	0.082
9	0.091	0.091	0.091
10	0.083	0.083	0.083
11	0.152	0.083	0.112
12	0.095	0.095	0.095
13	0.082	0.082	0.082
14	0.089	0.089	0.089
15	0.076	0.076	0.076
16	0.085	0.085	0.085
17	0.060	0.060	0.060
18	0.068	0.068	0.068
19	0.082	0.082	0.082
20	0.078	0.078	0.078

Droplet number	Droplet length	Droplet width	Average droplet diameter
21	0.068 cm.	0.068 cm.	0.068 cm.
22	0.066	0.066	0.066
23	0.066	0.066	0.066
24	0.072	0.072	0.072
25	0.079	0.079	0.079
26	0.079	0.079	0.079
27	0.147	0.070	0.101
28	0.073	0.073	0.073
29	0.093	0.093	0.093
30	0.119	0.080	0.097
31	0.085	0.085	0.085
32	0.098	0.098	0.098
33	0.081	0.081	0.081
34	0.097	0.097	0.097
35	0.105	0.105	0.105
36	0.105	0.105	0.105
37	0.100	0.100	0.100
38	0.081	0.081	0.081
39	0.085	0.085	0.085
40	0.066	0.066	0.066
41	0.090	0.090	0.090
42	0.051	0.051	0.051
43	0.086	0.086	0.086
44	0.083	0.073	0.078
45	0.056	0.056	0.056
46	0.078	0.078	0.078
47	0.119	0.071	0.192
48	0.088	0.088	0.088
49	0.108	0.108	0.108
50	0.104	0.104	0.104
51	0.084	0.084	0.084

The data tabulated below are the droplet diameters after breakup for a capillary jet of 0.05 % Separan. The volumetric flow rate was 30.5 ml./min. through a 0.0263 cm. nozzle.

Droplet number	Droplet length	Droplet width	Average droplet diameter
1	0.121 cm.	0.083 cm.	0.100 cm.
2	0.075	0.075	0.075
3	0.096	0.082	0.089
4	0.092	0.078	0.085
5	0.091	0.072	0.081
6	0.088	0.079	0.083
7	0.101	0.083	0.091
8	0.113	0.099	0.106
9	0.091	0.081	0.086
10	0.089	0.089	0.089
11	0.083	0.083	0.083
12	0.101	0.079	0.089
13	0.104	0.079	0.091
14	0.090	0.090	0.090
15	0.098	0.068	0.082
16	0.112	0.103	0.107
17	0.088	0.077	0.083
18	0.085	0.085	0.085
19	0.094	0.072	0.082
20	0.062	0.057	0.060
21	0.064	0.064	0.064
22	0.127	0.106	0.116
23	0.088	0.088	0.088
24	0.104	0.074	0.088
25	0.119	0.080	0.097
26	0.095	0.095	0.095
27	0.095	0.095	0.095
28	0.076	0.076	0.076
29	0.067	0.067	0.067
30	0.088	0.088	0.088
31	0.047	0.047	0.047
32	0.066	0.066	0.066
33	0.097	0.069	0.082

Droplet number	Droplet length	Droplet width	Average droplet diameter
34	0.083 cm.	0.083 cm.	0.083 cm.
35	0.065	0.073	0.069
36	0.078	0.078	0.078
37	0.065	0.065	0.065
38	0.076	0.076	0.076
39	0.063	0.063	0.063
40	0.102	0.092	0.097
41	0.097	0.097	0.097
42	0.090	0.079	0.084
43	0.083	0.079	0.081
44	0.097	0.092	0.095
45	0.092	0.084	0.088
46	0.099	0.099	0.099
47	0.098	0.098	0.098
48	0.100	0.100	0.100
49	0.081	0.077	0.079
50	0.071	0.071	0.071
51	0.076	0.076	0.076
52	0.093	0.093	0.093
53	0.084	0.084	0.084
54	0.084	0.084	0.084
55	0.100	0.094	0.097
56	0.075	0.075	0.075

The data tabulated below are the droplet diameters after breakup for a capillary jet of 0.05 % Separan. The volumetric flow rate was 48.0 ml./min. through a 0.0263 cm. nozzle.

Droplet number	Droplet length	Droplet width	Average droplet diameter
1	0.116 cm.	0.097 cm.	0.107 cm.
2	0.109	0.078	0.092
3	0.088	0.088	0.088
4	0.130	0.095	0.111
5	0.077	0.061	0.069
6	0.053	0.053	0.053

Droplet number	Droplet length	Droplet width	Average droplet diameter
7	0.072 cm.	0.072 cm.	0.072 cm.
8	0.047	0.047	0.047
9	0.094	0.077	0.085
10	0.071	0.069	0.070
11	0.087	0.087	0.087
12	0.068	0.068	0.068
13	0.068	0.068	0.068
14	0.106	0.079	0.091
15	0.079	0.079	0.079
16	0.071	0.071	0.071
17	0.074	0.068	0.071
18	0.114	0.114	0.114
19	0.081	0.081	0.081
20	0.087	0.079	0.083
21	0.086	0.086	0.086
22	0.068	0.068	0.068
23	0.061	0.061	0.061
24	0.053	0.053	0.053
25	0.064	0.064	0.064
26	0.059	0.059	0.059
27	0.084	0.084	0.084
28	0.114	0.099	0.106
29	0.092	0.092	0.092
30	0.084	0.084	0.084
31	0.125	0.105	0.115
32	0.091	0.084	0.087
33	0.066	0.066	0.066
34	0.075	0.075	0.075

The data tabulated below are the droplet diameters after breakup for a capillary jet of 0.05% Separan. The volumetric flow rate was 28.2 ml./min. through a 0.0414 cm. nozzle.

Droplet number	Droplet length	Droplet width	Average droplet diameter
1	0.166 cm.	0.166 cm.	0.166 cm.
2	0.098	0.088	0.093
3	0.109	0.097	0.103
4	0.113	0.113	0.113
5	0.096	0.096	0.096
6	0.111	0.111	0.111
7	0.095	0.095	0.095
8	0.073	0.073	0.073
9	0.137	0.137	0.137
10	0.146	0.103	0.123
11	0.103	0.103	0.103
12	0.103	0.103	0.103
13	0.078	0.078	0.078
14	0.126	0.116	0.121
15	0.101	0.101	0.101
16	0.121	0.121	0.121
17	0.121	0.121	0.121
18	0.123	0.088	0.104
19	0.123	0.090	0.105
20	0.127	0.110	0.118
21	0.111	0.094	0.102
22	0.234	0.126	0.172
23	0.118	0.107	0.113
24	0.125	0.125	0.125
25	0.184	0.114	0.145
26	0.108	0.108	0.108
27	0.108	0.108	0.108
28	0.108	0.108	0.108
29	0.102	0.102	0.102
30	0.088	0.088	0.088
31	0.137	0.121	0.129
32	0.098	0.098	0.098
33	0.108	0.108	0.108
34	0.109	0.109	0.109

Droplet number	Droplet length	Droplet width	Average droplet diameter
35	0.109 cm.	0.109 cm.	0.109 cm.
36	0.086	0.086	0.086
37	0.108	0.108	0.108
38	0.157	0.117	0.136
39	0.168	0.142	0.154
40	0.083	0.083	0.083
41	0.133	0.133	0.133
42	0.119	0.119	0.119
43	0.129	0.129	0.129
44	0.110	0.110	0.110
45	0.170	0.141	0.155
46	0.126	0.112	0.119
47	0.097	0.097	0.097
48	0.120	0.120	0.120
49	0.125	0.125	0.125
50	0.090	0.090	0.090
51	0.107	0.107	0.107

The data tabulated below are the droplet diameters after breakup for a capillary jet of 0.05 % Separan. The volumetric flow rate was 33.9 ml./min. through a 0.0414 cm. nozzle.

Droplet number	Droplet length	Droplet width	Average droplet diameter
1	0.163 cm.	0.127 cm.	0.144 cm.
2	0.094	0.085	0.089
3	0.130	0.118	0.124
4	0.126	0.126	0.126
5	0.113	0.113	0.113
6	0.133	0.119	0.126
7	0.133	0.115	0.123
8	0.153	0.124	0.138
9	0.166	0.139	0.152
10	0.117	0.117	0.117
11	0.146	0.129	0.137
12	0.141	0.141	0.141

Droplet number	Droplet length	Droplet width	Average droplet diameter
13	0.126 cm.	0.126 cm.	0.126 cm.
14	0.129	0.115	0.122
15	0.163	0.121	0.141
16	0.116	0.116	0.116
17	0.120	0.112	0.116
18	0.169	0.105	0.133
19	0.087	0.087	0.087
20	0.101	0.101	0.101
21	0.118	0.118	0.118
22	0.145	0.137	0.141
23	0.106	0.106	0.106
24	0.167	0.118	0.141
25	0.106	0.106	0.106
26	0.101	0.101	0.101
27	0.183	0.119	0.148
28	0.129	0.129	0.129
29	0.107	0.107	0.107
30	0.148	0.113	0.129
31	0.141	0.141	0.141
32	0.111	0.111	0.111
33	0.097	0.097	0.097
34	0.181	0.128	0.152
35	0.176	0.137	0.155
36	0.128	0.128	0.128
37	0.147	0.120	0.133
38	0.149	0.126	0.137
39	0.108	0.108	0.108
40	0.095	0.095	0.095
41	0.097	0.097	0.097
42	0.103	0.103	0.103
43	0.128	0.128	0.128
44	0.109	0.109	0.109
45	0.119	0.119	0.119
46	0.159	0.140	0.149
47	0.185	0.138	0.159
48	0.137	0.137	0.137
49	0.108	0.108	0.108
50	0.141	0.124	0.133
51	0.122	0.122	0.122
52	0.154	0.154	0.154
53	0.188	0.129	0.155
54	0.160	0.130	0.144

The data tabulated below are the droplet diameters after breakup for a capillary jet of 0.05 % Separan. The volumetric flow rate was 40.8 ml./min. through a 0.0414 cm. nozzle.

Droplet number	Droplet length	Droplet width	Average droplet diameter
1	0.180 cm.	0.124 cm.	0.149 cm.
2	0.111	0.111	0.111
3	0.114	0.103	0.108
4	0.154	0.087	0.115
5	0.109	0.109	0.109
6	0.136	0.126	0.131
7	0.160	0.136	0.147
8	0.137	0.112	0.124
9	0.147	0.145	0.146
10	0.145	0.114	0.128
11	0.125	0.125	0.125
12	0.095	0.095	0.095
13	0.112	0.112	0.112
14	0.144	0.110	0.125
15	0.109	0.109	0.109
16	0.109	0.109	0.109
17	0.162	0.136	0.148
18	0.096	0.096	0.096
19	0.140	0.115	0.127
20	0.128	0.075	0.098
21	0.113	0.113	0.113
22	0.113	0.113	0.113
23	0.123	0.123	0.123
24	0.090	0.090	0.090
25	0.193	0.125	0.155
26	0.126	0.126	0.126
27	0.153	0.110	0.130
28	0.125	0.107	0.116
29	0.120	0.111	0.115
30	0.155	0.135	0.144
31	0.135	0.115	0.124
32	0.126	0.126	0.126
33	0.121	0.121	0.121
34	0.102	0.102	0.102

Droplet number	Droplet length	Droplet width	Average droplet diameter
35	0.116 cm.	0.116 cm.	0.116 cm.
36	0.218	0.118	0.161
37	0.109	0.109	0.109

The data tabulated below are the droplet diameters after breakup for a capillary jet of 0.05 % Separan. The volumetric flow rate was 58.3 ml./min. through a 0.0414 cm. nozzle.

Droplet number	Droplet length	Droplet width	Average droplet diameter
1	0.138 cm.	0.128 cm.	0.133 cm.
2	0.129	0.129	0.129
3	0.084	0.084	0.084
4	0.139	0.106	0.121
5	0.118	0.118	0.118
6	0.118	0.118	0.118
7	0.110	0.110	0.110
8	0.093	0.093	0.093
9	0.111	0.104	0.107
10	0.160	0.130	0.144
11	0.092	0.092	0.092
12	0.114	0.101	0.107
13	0.135	0.135	0.135
14	0.084	0.084	0.084
15	0.155	0.097	0.123
16	0.166	0.104	0.131
17	0.114	0.114	0.114
18	0.114	0.114	0.114
19	0.114	0.114	0.114
20	0.224	0.139	0.176
21	0.184	0.139	0.160
22	0.149	0.123	0.135
23	0.163	0.143	0.153
24	0.133	0.133	0.133
25	0.155	0.123	0.138
26	0.118	0.118	0.118

Droplet number	Droplet length	Droplet width	Average droplet diameter
27	0.118 cm.	0.118 cm.	0.118 cm.
28	0.118	0.118	0.118
29	0.118	0.118	0.118
30	0.139	0.114	0.126
31	0.203	0.152	0.176
32	0.136	0.136	0.136
33	0.196	0.136	0.163
34	0.096	0.096	0.096
35	0.116	0.116	0.116
36	0.119	0.119	0.119
37	0.105	0.105	0.105
38	0.111	0.111	0.111
39	0.109	0.109	0.109
40	0.137	0.137	0.137
41	0.109	0.109	0.109
42	0.136	0.136	0.136
43	0.110	0.110	0.110
44	0.166	0.133	0.149
45	0.129	0.129	0.129
46	01112	0.112	0.112
47	0.106	0.078	0.091
48	0.123	0.091	0.106
49	0.153	0.122	0.137

The data tabulated below are the droplet diameters after breakup for a capillary jet of 0.05 % Separan. The volumetric flow rate was 256.6 ml./min. through a 0.0868 cm. nozzle.

Droplet number	Droplet length	Droplet width	Average droplet diameter
1	0.288 cm.	0.276 cm.	0.282 cm.
2	0.219	0.189	0.204
3	0.230	0.228	0.229
4	0.267	0.267	0.267
5	0.222	0.182	0.201
6	0.219	0.219	0.219

Droplet number	Droplet length	Droplet width	Average droplet diameter
7	0.289 cm.	0.235 cm.	0.261 cm.
8	0.222	0.206	0.216
9	0.319	0.219	0.264
10	0.197	0.197	0.197
11	0.274	0.211	0.241
12	0.231	0.214	0.223
13	0.181	0.181	0.181
14	0.181	0.181	0.181
15	0.199	0.186	0.192
16	0.129	0.129	0.129
17	0.374	0.199	0.273
18	0.414	0.272	0.336
19	0.235	0.211	0.223
20	0.227	0.212	0.219
21	0.137	0.121	0.129
22	0.211	0.211	0.211
23	0.259	0.241	0.250
24	0.206	0.206	0.206
25	0.207	0.207	0.207
26	0.233	0.233	0.233
27	0.204	0.204	0.204
28	0.259	0.244	0.252
29	0.265	0.265	0.265
30	0.157	0.157	0.157
31	0.259	0.259	0.259
32	0.235	0.199	0.216

The data tabulated below are the droplet diameters after breakup for a capillary jet of 0.25 % Separan. The volumetric flow rate was 23.0 ml./min. through a 0.0214 cm. nozzle.

Droplet number	Droplet length	Droplet width	Average droplet diameter
1	0.165 cm.	0.165 cm.	0.165 cm.
2	0.171	0.174	0.173
3	0.145	0.144	0.145
4	0.131	0.139	0.135
5	0.140	0.153	0.146
6	0.032	0.050	0.040
7	0.029	0.051	0.038
8	0.151	0.149	0.150
9	0.190	0.181	0.186
10	0.050	0.060	0.055
11	0.102	0.102	0.102
12	0.164	0.164	0.164
13	0.144	0.159	0.151
14	0.167	0.163	0.165
15	0.171	0.156	0.163
16	0.165	0.157	0.161
17	0.128	0.128	0.128
18	0.155	0.157	0.156
19	0.061	0.081	0.070
20	0.193	0.193	0.193
21	0.142	0.186	0.162
22	0.118	0.131	0.125
23	0.123	0.127	0.125
24	0.106	0.099	0.103
25	0.057	0.057	0.057
26	0.039	0.042	0.041
27	0.061	0.054	0.057
28	0.071	0.081	0.076
29	0.048	0.037	0.042
30	0.069	0.069	0.069
31	0.055	0.057	0.056
32	0.181	0.181	0.181
33	0.197	0.213	0.205
34	0.092	0.085	0.088

Droplet number	Droplet length	Droplet width	Average droplet diameter
35	0.185 cm.	0.185 cm.	0.185 cm.
36	0.075	0.075	0.075
37	0.113	0.108	0.110
38	0.167	0.162	0.164
39	0.164	0.162	0.163
40	0.127	0.113	0.120
41	0.174	0.167	0.170
42	0.055	0.055	0.055
43	0.201	0.205	0.203
44	0.160	0.160	0.160
45	0.155	0.155	0.155
46	0.089	0.088	0.088
47	0.074	0.074	0.074
48	0.237	0.216	0.226
49	0.132	0.125	0.128
50	0.159	0.155	0.157
51	0.107	0.107	0.107
52	0.057	0.069	0.063
53	0.118	0.128	0.123
54	0.142	0.157	0.149
55	0.204	0.220	0.212
56	0.143	0.143	0.143
57	0.218	0.234	0.226
58	0.075	0.085	0.080
59	0.182	0.152	0.166
60	0.111	0.095	0.103
61	0.060	0.057	0.058
62	0.192	0.192	0.192
63	0.152	0.147	0.149
64	0.164	0.164	0.164
65	0.189	0.189	0.189
66	0.135	0.130	0.132
67	0.155	0.151	0.153
68	0.160	0.159	0.160
69	0.132	0.132	0.132
70	0.163	0.171	0.167
71	0.146	0.146	0.146
72	0.192	0.192	0.192
73	0.061	0.050	0.055
74	0.095	0.090	0.093
75	0.199	0.199	0.199
76	0.130	0.117	0.123
77	0.079	0.074	0.077

Droplet number	Droplet length	Droplet width	Average droplet diameter
78	0.097 cm.	0.097 cm.	0.097 cm.
79	0.037	0.037	0.037
80	0.086	0.086	0.086
81	0.084	0.084	0.084
82	0.052	0.057	0.054
83	0.033	0.033	0.033
84	0.178	0.178	0.178
85	0.100	0.107	0.104
86	0.066	0.066	0.066
87	0.175	0.181	0.178
88	0.101	0.104	0.102
89	0.140	0.140	0.140
90	0.219	0.203	0.211
91	0.157	0.168	0.162
92	0.171	0.187	0.179
93	0.074	0.074	0.074
94	0.167	0.167	0.167
95	0.148	0.148	0.148
96	0.104	0.104	0.104
97	0.086	0.086	0.086
98	0.154	0.154	0.154
99	0.152	0.152	0.152
100	0.146	0.146	0.146
101	0.192	0.202	0.197
102	0.169	0.182	0.175
103	0.189	0.189	0.189
104	0.219	0.219	0.219
105	0.052	0.052	0.052
106	0.175	0.175	0.175
107	0.138	0.144	0.141
108	0.173	0.173	0.173
109	0.060	0.055	0.057
110	0.080	0.080	0.080
111	0.060	0.060	0.060
112	0.060	0.060	0.060
113	0.159	0.159	0.159
114	0.091	0.091	0.091
115	0.194	0.201	0.197
116	0.094	0.094	0.094
117	0.203	0.203	0.203
118	0.098	0.098	0.098
119	0.087	0.087	0.087
120	0.124	0.115	0.119
121	0.171	0.171	0.171

Droplet number	Droplet length	Droplet width	Average droplet diameter
122	0.169 cm.	0.179 cm.	0.173 cm.
123	0.052	0.052	0.052
124	0.109	0.105	0.107
125	0.069	0.064	0.067
126	0.040	0.040	0.040
127	0.156	0.156	0.156
128	0.181	0.181	0.181
129	0.184	0.184	0.184
130	0.177	0.225	0.199
131	0.173	0.173	0.173
132	0.101	0.092	0.097
133	0.120	0.145	0.132
134	0.196	0.219	0.207
135	0.086	0.104	0.094
136	0.168	0.173	0.170
137	0.147	0.144	0.144
138	0.111	0.111	0.111
139	0.127	0.127	0.127
140	0.126	0.146	0.135
141	0.159	0.168	0.163
142	0.040	0.040	0.040
143	0.082	0.082	0.082
144	0.184	0.232	0.207
145	0.036	0.036	0.036
146	0.201	0.201	0.201
147	0.144	0.144	0.144
148	0.130	0.130	0.130
149	0.191	0.191	0.191
150	0.068	0.068	0.068
151	0.211	0.222	0.216
152	0.153	0.153	0.153
153	0.112	0.112	0.112
154	0.201	0.201	0.201
155	0.206	0.196	0.201
156	0.142	0.142	0.142
157	0.143	0.143	0.143
158	0.118	0.118	0.118
159	0.156	0.156	0.156
160	0.100	0.100	0.100
161	0.042	0.042	0.042
162	0.042	0.042	0.042
163	0.171	0.180	0.175
164	0.074	0.074	0.074

Droplet number	Droplet length	Droplet width	Average droplet diameter
165	0.054 cm.	0.054 cm.	0.054 cm.
166	0.123	0.123	0.123
167	0.206	0.213	0.210
168	0.170	0.170	0.170
169	0.193	0.193	0.193
170	0.192	0.192	0.192
171	0.110	0.115	0.112
172	0.212	0.223	0.217
173	0.175	0.175	0.175
714	0.075	0.083	0.079
175	0.171	0.171	0.171
176	0.058	0.058	0.058
177	0.103	0.103	0.103
178	0.058	0.058	0.058
179	0.075	0.075	0.075
180	0.199	0.199	0.199
181	0.186	0.186	0.186
182	0.187	0.187	0.187
183	0.146	0.146	0.146
184	0.171	0.171	0.171
185	0.162	0.160	0.161
186	0.168	0.321	0.232
187	0.150	0.150	0.150
188	0.190	0.190	0.190
189	0.103	0.103	0.103
190	0.173	0.195	0.184
191	0.049	0.049	0.049
192	0.070	0.070	0.070
193	0.152	0.152	0.152
194	0.190	0.190	0.190
195	0.039	0.039	0.039
196	0.046	0.056	0.050
197	0.068	0.076	0.072
198	0.069	0.069	0.069
199	0.201	0.201	0.201
200	0.085	0.085	0.085
201	0.109	0.109	0.109
202	0.141	0.146	0.144
203	0.165	0.165	0.165
204	0.148	0.306	0.213
205	0.181	0.181	0.181
206	0.121	0.121	0.121
207	0.046	0.046	0.046

Droplet number	Droplet length	Droplet width	Average droplet diameter
208	0.154 cm.	0.154 cm.	0.154 cm.
209	0.223	0.121	0.164
210	0.092	0.100	0.096
211	0.129	0.129	0.129
212	0.088	0.088	0.088
213	0.223	0.209	0.216
214	0.086	0.086	0.086
215	0.165	0.165	0.165
216	0.105	0.105	0.105
217	0.129	0.129	0.129
218	0.180	0.186	0.183
219	0.180	0.180	0.180
220	0.222	0.222	0.222
221	0.050	0.050	0.050
222	0.084	0.084	0.084
223	0.064	0.064	0.064
224	0.047	0.047	0.047
225	0.104	0.104	0.104
226	0.172	0.172	0.172
227	0.211	0.211	0.211
228	0.147	0.147	0.147
229	0.057	0.057	0.057
230	0.044	0.044	0.044
231	0.047	0.047	0.047
232	0.129	0.129	0.129
233	0.188	0.188	0.188
234	0.205	0.201	0.203
235	0.054	0.054	0.054
236	0.147	0.147	0.147
237	0.052	0.052	0.052
238	0.050	0.050	0.050
239	0.114	0.123	0.118
240	0.184	0.184	0.184
241	0.050	0.050	0.050
242	0.134	0.134	0.134
243	0.039	0.039	0.039
244	0.172	0.172	0.172
245	0.192	0.192	0.192
246	0.052	0.052	0.052
247	0.143	0.143	0.143
248	0.238	0.202	0.219
249	0.200	0.200	0.200
250	0.110	0.110	0.110

Droplet number	Droplet length	Droplet width	Average droplet diameter
251	0.159 cm.	0.159 cm.	0.159 cm.
252	0.159	0.159	0.159
253	0.170	0.170	0.170
254	0.150	0.150	0.150
255	0.117	0.126	0.121
256	0.217	0.220	0.218
257	0.074	0.084	0.079
258	0.086	0.096	0.091
259	0.048	0.048	0.048
260	0.133	0.133	0.133
261	0.187	0.184	0.185
262	0.201	0.201	0.201
263	0.175	0.161	0.168
264	0.136	0.136	0.136
265	0.127	0.127	0.127
266	0.147	0.147	0.147
267	0.206	0.026	0.206
268	0.053	0.061	0.057
269	0.146	0.154	0.150
270	0.098	0.098	0.098
271	0.159	0.159	0.159
272	0.155	0.155	0.155
273	0.172	0.172	0.172
274	0.160	0.160	0.160
275	0.126	0.123	0.124
276	0.113	0.113	0.113
277	0.175	0.175	0.175
278	0.138	0.138	0.138
279	0.174	0.179	0.177
280	0.151	0.137	0.144
281	0.144	0.156	0.150
282	0.172	0.178	0.175
283	0.083	0.083	0.083
284	0.207	0.197	0.202
285	0.158	0.142	0.150
286	0.207	0.179	0.192
287	0.115	0.126	0.120
288	0.168	0.168	0.168
289	0.145	0.145	0.145
290	0.055	0.055	0.055
291	0.154	0.154	0.154
292	0.077	0.077	0.077
293	0.179	0.179	0.179

Droplet number	Droplet length	Droplet width	Average droplet diameter
294	0.056 cm.	0.056 cm.	0.056 cm.
295	0.167	0.167	0.167
296	0.161	0.161	0.161
297	0.167	0.167	0.167
298	0.110	0.110	0.110
299	0.032	0.032	0.032
300	0.068	0.068	0.068
301	0.128	0.128	0.128
302	0.174	0.174	0.174
303	0.110	0.110	0.110
304	0.131	0.131	0.131
305	0.169	0.169	0.169
306	0.149	0.149	0.149
307	0.159	0.159	0.159
308	0.036	0.036	0.036
309	0.034	0.034	0.034
310	0.047	0.047	0.047
311	0.163	0.261	0.206
312	0.045	0.045	0.045
313	0.114	0.114	0.114
314	0.166	0.166	0.166
315	0.181	0.175	0.178
316	0.099	0.108	0.103
317	0.164	0.164	0.164
318	0.158	0.164	0.161
319	0.215	0.184	0.199
320	0.123	0.123	0.123
321	0.176	0.176	0.176
322	0.187	0.187	0.187
323	0.176	0.176	0.176
324	0.164	0.164	0.164
325	0.172	0.172	0.172
326	0.212	0.212	0.212
327	0.066	0.066	0.066
328	0.151	0.151	0.151
329	0.174	0.174	0.174
330	0.134	0.137	0.136
331	0.189	0.189	0.189
332	0.169	0.169	0.169
333	0.109	0.109	0.109
334	0.121	0.121	0.121
335	0.113	0.113	0.113
336	0.199	0.199	0.199
337	0.133	0.133	0.133

Droplet number	Droplet length	Droplet width	Average droplet diameter
338	0.211 cm.	0.201 cm.	0.206 cm.
339	0.135	0.135	0.135
340	0.135	0.135	0.135
341	0.109	0.109	0.109
342	0.167	0.167	0.167
343	0.185	0.185	0.185
344	0.131	0.131	0.131
345	0.169	0.169	0.169
346	0.156	0.156	0.156
347	0.108	0.108	0.108
348	0.164	0.170	0.167
349	0.205	0.205	0.205
350	0.135	0.135	0.135
351	0.099	0.099	0.099
352	0.162	0.162	0.162

The data tabulated below are the droplet diameters after breakup for a capillary jet of pure glycerin. The volumetric flow rate was 8.85 ml./min. through a 0.0216 cm. nozzle.

Droplet number	Droplet length	Droplet width	Average droplet diameter
1	0.114 cm.	0.114 cm.	0.114 cm.
2	0.083	0.083	0.083
3	0.099	0.099	0.099
4	0.059	0.059	0.059
5	0.109	0.090	[illegible]9
6	0.151	0.068	0.101
7	0.075	0.075	0.075
8	0.062	0.062	0.062
9	0.132	0.064	0.092
10	0.087	0.087	0.087
11	0.170	0.078	0.116
12	0.113	0.082	0.096
13	0.105	0.067	0.084
14	0.096	0.084	0.090
15	0.084	0.084	0.084
16	0.129	0.090	0.108
17	0.068	0.068	0.068
18	0.085	0.085	0.085
19	0.114	0.075	0.093
20	0.084	0.067	0.075
21	0.075	0.066	0.070
22	0.130	0.096	0.111
23	0.084	0.086	0.084
24	0.108	0.072	0.088
25	0.103	0.071	0.085
26	0.092	0.092	0.092
27	0.101	0.101	0.101
28	0.089	0.089	0.089
29	0.095	0.095	0.095
30	0.130	0.099	0.113
31	0.090	0.090	0.090
32	0.084	0.084	0.084
33	0.112	0.120	0.116
34	0.120	0.120	0.120

Droplet number	Droplet length	Droplet width	Average droplet diameter
35	0.134 cm.	0.096 cm.	0.114 cm.
36	0.063	0.059	0.061
37	0.066	0.066	0.066
38	0.080	0.080	0.080
39	0.101	0.081	0.090
40	0.086	0.072	0.079
41	0.123	0.076	0.097
42	0.132	0.092	0.110
43	0.106	0.094	0.100
44	0.070	0.070	0.070
45	0.080	0.080	0.080
46	0.085	0.085	0.085
47	0.133	0.112	0.122
48	0.062	0.062	0.062
49	0.129	0.101	0.114
50	0.082	0.082	0.082
51	0.098	0.080	0.088
52	0.102	0.082	0.092
53	0.143	0.089	0.112
54	0.071	0.071	0.071

The data tabulated below are the droplet diameters after breakup for a capillary jet of pure glycerin, photographed 4 cms. beyond the breakup point. The volumetric flow rate was 8.85 ml./min. through a 0.0216 cm. nozzle.

Droplet number	Droplet length	Droplet width	Average droplet diameter
1	0.093 cm.	0.093 cm.	0.093 cm.
2	0.094	0.094	0.094
3	0.094	0.094	0.094
4	0.085	0.085	0.085
5	0.127	0.127	0.127

Droplet number	Droplet length	Droplet width	Average droplet diameter
6	0.115 cm.	0.099 cm.	0.107 cm.
7	0.093	0.093	0.093
8	0.068	0.068	0.068
9	0.125	0.081	0.101
10	0.111	0.075	0.092
11	0.128	0.103	0.115
12	0.084	0.084	0.084
13	0.120	0.113	0.117
14	0.104	0.103	0.103
15	0.092	0.092	0.092
16	0.111	0.099	0.105
17	0.077	0.077	0.077
18	0.134	0.097	0.114
19	0.085	0.085	0.085
20	0.092	0.092	0.092
21	0.106	0.106	0.106
22	0.136	0.120	0.128
23	0.198	0.104	0.144
24	0.128	0.101	0.114
25	0.101	0.098	0.100
26	0.054	0.054	0.054
27	0.139	0.114	0.126
28	0.215	0.086	0.136
29	0.117	0.110	0.114
30	0.110	0.110	0.110
31	0.158	0.113	0.134
32	0.084	0.084	0.084
33	0.113	0.113	0.113
34	0.070	0.068	0.069
35	0.106	0.106	0.106
36	0.085	0.085	0.085
37	0.082	0.079	0.080
38	0.095	0.089	0.092
39	0.095	0.089	0.092
40	0.096	0.093	0.095
41	0.100	0.100	0.100
42	0.098	0.093	0.095
43	0.163	0.111	0.135
44	0.080	0.080	0.080
45	0.061	0.061	0.061
46	0.122	0.118	0.120
47	0.113	0.097	0.105
48	0.086	0.082	0.084

Droplet number	Droplet length	Droplet width	Average droplet diameter
49	0.122 cm.	0.110 cm.	0.116 cm.
50	0.190	0.104	0.141
51	0.096	0.096	0.096
52	0.057	0.056	0.056
53	0.109	0.109	0.109
54	0.113	0.109	0.111
55	0.100	0.096	0.098
56	0.105	0.094	0.099
57	0.064	0.064	0.064
58	0.089	0.089	0.089
59	0.080	0.080	0.080
60	0.084	0.084	0.084
61	0.073	0.073	0.073
62	0.117	0.066	0.088
63	0.081	0.081	0.081
64	0.113	0.109	0.111
65	0.097	0.092	0.094
66	0.099	0.095	0.097
67	0.106	0.104	0.105
68	0.103	0.075	0.088
69	0.106	0.101	0.103
70	0.088	0.088	0.088
71	0.106	0.082	0.093
72	0.118	0.103	0.110
73	0.107	0.107	0.107
74	0.102	0.102	0.102
75	0.139	0.107	0.122
76	0.094	0.094	0.094
77	0.110	0.110	0.110
78	0.128	0.128	0.128
79	0.084	0.080	0.082
80	0.063	0.063	0.063
81	0.091	0.091	0.091
82	0.073	0.070	0.071
83	0.074	0.074	0.074
84	0.091	0.091	0.091
85	0.063	0.063	0.063
86	0.059	0.059	0.059
87	0.067	0.067	0.067
88	0.103	0.099	0.101
89	0.116	0.103	0.109
90	0.080	0.080	0.080
91	0.061	0.061	0.061

Droplet number	Droplet length	Droplet width	Average droplet diameter
92	0.076 cm.	0.076 cm.	0.076 cm.
93	0.068	0.068	0.068
94	0.105	0.097	0.101
95	0.097	0.092	0.094
96	0.102	0.102	0.102
97	0.083	0.083	0.083
98	0.112	0.085	0.097
99	0.103	0.103	0.103
100	0.071	0.071	0.071
101	0.103	0.101	0.102
102	0.104	0.098	0.101
103	0.106	0.106	0.106
104	0.088	0.088	0.088
105	0.114	0.102	0.107
106	0.089	0.089	0.089
107	0.107	0.107	0.107
108	0.094	0.094	0.094
109	0.113	0.109	0.111
110	0.096	0.096	0.096
111	0.072	0.076	0.074
112	0.112	0.112	0.112
113	0.115	0.115	0.115
114	0.106	0.106	0.106
115	0.106	0.106	0.106
116	0.072	0.072	0.072

The data tabulated below are the droplet diameters after breakup for a capillary jet of pure glycerin. The volumetric flow rate was 14.9 ml./min. through a 0.0216 cm. nozzle.

Droplet number	Droplet length	Droplet width	Average droplet diameter
1	0.049 cm.	0.049 cm.	0.049 cm.
2	0.070	0.070	0.070
3	0.096	0.089	0.092
4	0.080	0.080	0.080
5	0.088	0.078	0.083
6	0.046	0.046	0.046
7	0.089	0.089	0.089
8	0.050	0.050	0.050
9	0.048	0.048	0.048
10	0.073	0.069	0.071
11	0.059	0.053	0.056
12	0.069	0.063	0.066
13	0.095	0.077	0.086
14	0.056	0.056	0.056
15	0.134	0.075	0.100
16	0.055	0.052	0.054
17	0.105	0.070	0.086
18	0.069	0.059	0.064
19	0.066	0.066	0.066
20	0.082	0.070	0.076
21	0.095	0.077	0.085
22	0.086	0.055	0.069
23	0.068	0.055	0.061
24	0.148	0.054	0.090
25	0.057	0.057	0.057
26	0.111	0.068	0.087
27	0.066	0.067	0.067
28	0.063	0.056	0.059
29	0.079	0.073	0.076
30	0.060	0.058	0.059
31	0.126	0.073	0.096
32	0.053	0.052	0.052
33	0.067	0.067	0.067

Droplet number	Droplet length	Droplet width	Average droplet diameter
34	0.097 cm.	0.075 cm.	0.085 cm.
35	0.054	0.051	0.053
36	0.094	0.061	0.076
37	0.056	0.051	0.053
38	0.107	0.068	0.085
39	0.068	0.068	0.068
40	0.120	0.052	0.079
41	0.086	0.050	0.066
42	0.085	0.061	0.072
43	0.109	0.064	0.083
44	0.056	0.047	0.052
45	0.120	0.046	0.075
46	0.078	0.066	0.072
47	0.092	0.063	0.076

The data tabulated below are the droplet diameters after breakup for a capillary jet of pure glycerin, photographed 4 cms. beyond the breakup point. The volumetric flow rate was 14.9 ml./min. through a 0.0216 cm. nozzle.

Droplet number	Droplet length	Droplet width	Average droplet diameter
1	0.082 cm.	0.064 cm.	0.072 cm.
2	0.080	0.080	0.080
3	0.054	0.054	0.054
4	0.099	0.079	0.088
5	0.056	0.056	0.056
6	0.084	0.081	0.083
7	0.062	0.056	0.059
8	0.087	0.087	0.087
9	0.087	0.087	0.087
10	0.095	0.095	0.095
11	0.095	0.072	0.083
12	0.072	0.068	0.070

Droplet number	Droplet length	Droplet width	Average droplet diameter
13	0.068 cm.	0.060 cm.	0.064 cm.
14	0.084	0.081	0.082
15	0.063	0.063	0.063
16	0.070	0.070	0.070
17	0.070	0.066	0.068
18	0.077	0.064	0.070
19	0.087	0.073	0.080
20	0.098	0.074	0.085
21	0.067	0.060	0.063
22	0.070	0.059	0.064
23	0.060	0.060	0.060
24	0.069	0.063	0.066
25	0.112	0.101	0.107
26	0.113	0.110	0.111
27	0.052	0.052	0.052
28	0.131	0.092	0.110
29	0.081	0.064	0.072
30	0.049	0.049	0.049
31	0.102	0.102	0.102
32	0.077	0.077	0.077
33	0.101	0.072	0.085
34	0.145	0.050	0.085
35	0.063	0.054	0.058
36	0.100	0.100	0.100
37	0.075	0.071	0.073
38	0.093	0.076	0.084
39	0.076	0.064	0.070
40	0.076	0.065	0.070
41	0.107	0.065	0.084
42	0.119	0.089	0.103
43	0.059	0.056	0.057
44	0.105	0.081	0.092
45	0.106	0.062	0.081
46	0.062	0.057	0.060
47	0.090	0.076	0.083
48	0.092	0.068	0.079
49	0.057	0.057	0.057
50	0.071	0.071	0.071
51	0.066	0.066	0.066
52	0.063	0.063	0.063
53	0.068	0.066	0.067
54	0.093	0.068	0.079
55	0.076	0.076	0.076

Droplet number	Droplet length	Droplet width	Average droplet diameter
56	0.061 cm.	0.058 cm.	0.059 cm.
57	0.058	0.058	0.058
58	0.057	0.057	0.057
59	0.067	0.067	0.067
60	0.073	0.073	0.073
61	0.079	0.079	0.079
62	0.051	0.051	0.051
63	0.093	0.088	0.090
64	0.070	0.070	0.070
65	0.057	0.057	0.057
66	0.092	0.092	0.092
67	0.062	0.062	0.062
68	0.074	0.074	0.074
69	0.056	0.056	0.056
70	0.068	0.068	0.068
71	0.088	0.073	0.080
72	0.064	0.057	0.060
73	0.112	0.061	0.083
74	0.099	0.068	0.082
75	0.062	0.062	0.062
76	0.084	0.084	0.084
77	0.086	0.082	0.084
78	0.122	0.087	0.103
79	0.101	0.087	0.094
80	0.051	0.051	0.051
81	0.168	0.102	0.131
82	0.071	0.063	0.067
83	0.090	0.073	0.081
84	0.062	0.062	0.062
85	0.064	0.064	0.064
86	0.068	0.068	0.068
87	0.104	0.076	0.089
88	0.066	0.066	0.066
89	0.101	0.062	0.079
90	0.076	0.070	0.073
91	0.090	0.085	0.088
92	0.065	0.065	0.065
93	0.085	0.085	0.085
94	0.054	0.054	0.054
95	0.094	0.094	0.094
96	0.079	0.079	0.079
97	0.118	0.090	0.103
98	0.116	0.087	0.101

Droplet number	Droplet length	Droplet width	Average droplet diameter
99	0.056 cm.	0.056 cm.	0.056 cm.
100	0.060	0.060	0.060
101	0.115	0.073	0.092
102	0.101	0.089	0.095
103	0.059	0.059	0.059
104	0.082	0.072	0.077
105	0.059	0.054	0.056
106	0.090	0.069	0.079
107	0.076	0.063	0.069
108	0.075	0.063	0.069
109	0.124	0.075	0.096
110	0.075	0.084	0.079
111	0.079	0.076	0.077
112	0.071	0.071	0.071
113	0.088	0.088	0.088
114	0.098	0.098	0.098
115	0.120	0.091	0.105
116	0.058	0.058	0.058
117	0.084	0.084	0.084
118	0.106	0.086	0.095
119	0.068	0.068	0.068
120	0.090	0.090	0.090
121	0.101	0.101	0.101
122	0.061	0.061	0.061
123	0.083	0.083	0.083
124	0.081	0.081	0.081
125	0.089	0.074	0.081
126	0.055	0.052	0.053
127	0.071	0.067	0.069
128	0.108	0.089	0.098

The data tabulated below are the droplet diameters after breakup for a capillary jet of pure glycerin. The volumetric flow rate was 20.6 ml./min. through a 0.0216 cm. nozzle.

Droplet number	Droplet length	Droplet width	Average droplet diameter
1	0.056 cm.	0.056 cm.	0.056 cm.
2	0.116	0.076	0.094
3	0.078	0.064	0.071
4	0.090	0.072	0.081
5	0.052	0.052	0.052
6	0.108	0.077	0.091
7	0.102	0.062	0.079
8	0.075	0.060	0.067
9	0.099	0.070	0.083
10	0.073	0.068	0.070
11	0.125	0.067	0.092
12	0.052	0.052	0.052
13	0.083	0.083	0.083
14	0.056	0.051	0.054
15	0.124	0.052	0.080
16	0.063	0.054	0.058
17	0.106	0.061	0.081
18	0.090	0.084	0.087
19	0.097	0.080	0.088
20	0.052	0.052	0.052
21	0.089	0.089	0.089
22	0.049	0.049	0.049
23	0.093	0.093	0.093
24	0.054	0.054	0.054
25	0.072	0.070	0.071
26	0.075	0.065	0.070

The data tabulated below are the droplet diameters after breakup for a capillary jet of pure glycerin, photographed 4 cms. beyond the breakup point. The volumetric flow rate was 20.6 ml./min. through a 0.0216 cm. nozzle.

Droplet number	Droplet length	Droplet width	Average droplet diameter
1	0.074 cm.	0.074 cm.	0.074 cm.
2	0.090	0.083	0.086
3	0.054	0.054	0.054
4	0.078	0.078	0.078
5	0.055	0.055	0.055
6	0.075	0.075	0.075
7	0.100	0.100	0.100
8	0.051	0.051	0.051
9	0.078	0.078	0.078
10	0.097	0.076	0.086
11	0.057	0.057	0.057
12	0.096	0.082	0.089
13	0.068	0.068	0.068
14	0.097	0.082	0.089
15	0.067	0.067	0.067
16	0.115	0.056	0.080
17	0.083	0.083	0.083
18	0.117	0.078	0.096
19	0.089	0.082	0.085
20	0.067	0.067	0.067
21	0.083	0.083	0.083
22	0.066	0.066	0.066
23	0.107	0.082	0.094
24	0.058	0.058	0.058
25	0.058	0.058	0.058
26	0.105	0.068	0.085
27	0.124	0.081	0.100
28	0.060	0.052	0.056
29	0.079	0.069	0.074
30	0.084	0.069	0.076
31	0.055	0.055	0.055
32	0.094	0.085	0.089

Droplet number	Droplet length	Droplet width	Average droplet diameter
33	0.086 cm.	0.073 cm.	0.079 cm.
34	0.053	0.053	0.053
35	0.077	0.077	0.077
36	0.055	0.055	0.055
37	0.063	0.063	0.063
38	0.120	0.076	0.096
39	0.078	0.060	0.068
40	0.072	0.060	0.066
41	0.079	0.065	0.072
42	0.077	0.064	0.070
43	0.064	0.062	0.063
44	0.097	0.062	0.077
45	0.080	0.061	0.070
46	0.077	0.064	0.070
47	0.101	0.086	0.093
48	0.077	0.063	0.069
49	0.089	0.082	0.086
50	0.060	0.060	0.060
51	0.083	0.079	0.081
52	0.068	0.068	0.068
53	0.046	0.046	0.046
54	0.116	0.097	0.106
55	0.068	0.068	0.068
56	0.076	0.071	0.073
57	0.064	0.061	0.062
58	0.083	0.072	0.077
59	0.050	0.050	0.050
60	0.101	0.101	0.101
61	0.060	0.060	0.060
62	0.060	0.060	0.060
63	0.096	0.070	0.082
64	0.064	0.065	0.065
65	0.065	0.065	0.065
66	0.096	0.096	0.096
67	0.070	0.070	0.070
68	0.096	0.080	0.087
69	0.070	0.070	0.070
70	0.084	0.066	0.074
71	0.065	0.065	0.065
72	0.055	0.055	0.055
73	0.085	0.085	0.085
74	0.049	0.049	0.049
75	0.120	0.100	0.109

Droplet number	Droplet length	Droplet width	Average droplet diameter
76	0.056 cm.	0.056 cm.	0.056 cm.
77	0.075	0.075	0.075
78	0.053	0.053	0.053
79	0.050	0.050	0.050
80	0.068	0.068	0.068
81	0.068	0.068	0.068
82	0.088	0.080	0.084
83	0.085	0.085	0.085
84	0.087	0.087	0.087
85	0.067	0.060	0.063
86	0.082	0.082	0.082
87	0.088	0.088	0.088
88	0.117	0.067	0.088
89	0.090	0.070	0.079
90	0.059	0.059	0.059
91	0.070	0.064	0.067
92	0.062	0.062	0.062
93	0.087	0.071	0.079
94	0.077	0.065	0.071
95	0.113	0.075	0.092
96	0.096	0.086	0.091
97	0.056	0.056	0.056
98	0.075	0.075	0.075
99	0.088	0.088	0.088
100	0.137	0.067	0.096
101	0.088	0.050	0.066
102	0.052	0.052	0.052
103	0.055	0.055	0.055
104	0.080	0.062	0.071
105	0.074	0.064	0.069
106	0.078	0.062	0.069
107	0.113	0.059	0.082
108	0.068	0.064	0.066
109	0.063	0.063	0.063
110	0.051	0.051	0.051
111	0.125	0.102	0.113
112	0.097	0.082	0.089
113	0.087	0.078	0.082
114	0.052	0.052	0.052
115	0.056	0.056	0.056
116	0.107	0.080	0.092
117	0.073	0.073	0.073
118	0.058	0.058	0.058

Droplet number	Droplet length	Droplet width	Average droplet diameter
119	0.097 cm.	0.077 cm.	0.086
120	0.061	0.061	0.061
121	0.057	0.057	0.057
122	0.066	0.066	0.066